

**DEEP ROW TRENCHING OF PIT LATRINE AND WASTE WATER
TREATMENT WORKS SLUDGE: WATER AND NUTRIENT FLUXES IN
FOREST PLANTATIONS**

Patrick Cudjoe Adadzi

A Thesis submitted to the School of Agricultural, Earth and Environmental Sciences

University of KwaZulu-Natal

In partial fulfilment of the requirements of the degree of

Master of Science (Hydrology)

Centre for Water Resources Research

School of Agricultural, Earth and Environmental Sciences

College of Agriculture, Engineering and Science

University of KwaZulu-Natal

Pietermaritzburg, South Africa

December 2012

DECLARATION

I hereby certify that the research reported in this thesis is the result of my own investigation, excepted as acknowledged herein, and that it has not been submitted for a higher degree at any other university or institution.

Signed: Date:

Patrick C. Adadzi

Signed: Date:

Prof S.A. Lorentz

(Supervisor)

Signed:..... Date:.....

Mr. D. Still

(Co-supervisor)

ACKNOWLEDGEMENT

First, to the Lord Almighty God for seeing me through the programme, I praise Him name.

I would sincerely like to thank my supervisor, Prof S.A. Lorentz of the School of Agricultural, Earth and Environmental Sciences (AEES) at the University of KwaZulu-Natal (UKZN) in Pietermaritzburg, for his expert advice and invaluable time for the completion of this dissertation. I also want to acknowledge the support of my co-supervisor, Mr. D. Still of Partners in Development and Prof C. Buckley of Pollution Research Group.

I also appreciate the technical and support staff of the discipline of Bioresources Engineering & Environmental Hydrology. You all contributed in a special way to this thesis. Just to mention a few, Cobus Pretorius, Sean Thornton-Dibb, Mark Horan, thanks so much. This work was made possible by the support from field assistant John Ngaleka as well as laboratory assistants Nhlakanipho Zondi.

I am especially grateful to my wife Sylvia, and my children for enduring three years of “hard times” and incessant offering of prayer and encouragement throughout the period.

To my brother, Ferdinand Adadzi for his moral support.

Dedicated to my parents:
Simon and Elizabeth Adadzi

ABSTRACT

The deep row trenching of ventilated improved pit-latrines (VIP) and waste water treatment works (WWTW) sludge is a unique alternative cost effective land application method that will prevent odour and health problems and may permit higher application rates than surface application. The goal of this research is to assess the environmental consequences of employing deep row incorporation of VIP and WWTW sludge to forest plantation lands for the production of *Eucalyptus dunnii*. The objectives are to monitor, define and quantify the fluxes of nutrients (nitrate and phosphorus) from the buried sludge to the surrounding soils, groundwater and surface water. The WWTW study was conducted on a forestry plantation located near the Shafton Karkloof Falls, about 10 km from Howick in the KwaZulu-Natal province of South Africa. The land for the research is owned by SAPPI, a timber plantation company. The trenching was done with stockpiled secondary sludge from Umgeni WWTW in Howick. VIP sludge trenching was done at the Umlazi E-ponds site in Durban owned by EThekweni Municipality. This site was formally used as a wastewater treatment plant sludge drying bed. The treatment works comprised three oxidation ponds and was operated until 1999, when it was decommissioned after a heavy flood, resulting in damage to the oxidation ponds. The sites were instrumented with wetting front detectors, piezometers and boreholes for collection and analysis of leachate from which were determined subsurface loss of nitrogen and phosphorus. Soil water status and groundwater levels were also monitored. Simulation of the process of water, nitrate and phosphorus transport was performed in order to aid the development of the sustainable management methodologies for land application and the trenching of VIP/WWTW sludge. The study focuses on the entrenched sludge to determine the concentration of pollutants, monitor changes in concentration over time and to monitor the movement of solutes and any change taking place in the surrounding soil water and groundwater. The results contribute to the development of guidelines and protocols for VIP/WWTW sludge handling and trenching in South Africa. It was demonstrated that the nutrient migration processes can be approximated with the conceptual simplifications of the inputs to the model based on field evidence, soil survey data and applicable literature. In the study, it was found that high concentrations of nutrients were evident in the water infiltrating into and through the sludge in all trench types. The nitrate concentration median values in the trenches were 234mg/l and 36mg/l for SAPPI and

Umlazi respectively, while the recorded median value for phosphorus was 1.0mg/l and 3.5mg/l for SAPPI and Umlazi respectively. However the effect of vertical seepage of nutrients, into the deep aquifer in fractured rock has not been observed in the deep borehole with the nitrate concentration median values at 5mg/l and 0.6mg/l for SAPPI and Umlazi respectively, while the phosphorus concentration median values were 0.03mg/l and 0.15mg/l for SAPPI and Umlazi sites respectively.

The study revealed significant differences between the sandy alluvial site at Umlazi and the shale dolorite site at the SAPPI forests. Where an unsaturated zone below the entrenched sludge existed at the Umlazi site, nutrient transport was retarded, whereas in the shales of the SAPPI site, preferential delivery flowpaths transported high concentrations of nutrients rapidly from the entrenched sludge to the base of the hillslope. These mechanisms needed to be treated differently in the simulation exercise.

TABLE OF CONTENTS

ABSTRACT.....	i
TABLE OF CONTENTS.....	iii
LIST OF FIGURES	vi
LIST OF TABLES	xi
1. INTRODUCTION.....	1
2. LITERATURE REVIEW	4
2.1 Types of Disposal of WWTW and VIP Sludge	4
2.1.1 Disposal of WWTW sludge into large water bodies.....	5
2.1.2 Landfilling.....	5
2.1.3 Incineration.....	6
2.1.4 Disposal on agricultural land.....	6
2.1.5 Composting	7
2.1.6 Vermi-composting of WWTW sludge	9
2.1.7 Treatment of VIP sludge at existing sewage treatment works	9
2.2 Impacts of On-site Sewage Disposal	9
2.2.1 Surface application.....	10
2.2.2 Burial	10
2.2.4 Trench drains/septic tanks	10
2.3 Regulations Governing Sludge Disposal	11
2.4 NO ₃ and P Movement from VIP and WWTW Sludge in Soils.....	12
2.5 Modelling and Simulation of Water and Nutrient Fluxes.....	13
2.6 HYDRUS-2D	15
2.7 Electrical Resistivity Tomography.....	21
2.7.1 ERT in hydrology.....	21
2.7.2 Basics of Electrical Resistivity Tomography	22
2.7.3 Electrode array	23
2.7.4 Tomography interpretation.....	25
2.8 Stable Isotopes in Hydrology.....	26

2.8.1	Fractionation during Precipitation.....	27
2.8.3	Temperature effect	28
2.8.4	Precipitation and equilibrium fractionation.....	28
2.8.5	Rainout effect	29
2.8.6	Fractionation during evaporation	31
2.8.7	Hydrological applications.....	33
3.	METHODOLOGY	34
3.1	WWTW Sludge Trenching and Instrumentation	35
3.1.1	Trench layout and instrumentation at the SAPPI site.....	35
3.1.2	Trench layout and instrumentation at the Umlazi site.....	42
3.2	Geophysical Electrical Resistivity Tomography (ERT) Characterisation	47
3.3	Soil Hydraulic Characterization.....	49
3.3.1	SAPPI site.....	49
3.3.2	Umlazi site.....	50
3.4	HYDRUS Application	53
3.4.1	SAPPI.....	53
3.4.2	Umlazi	54
3.5	Monitoring and Analysis.....	56
4.	RESULTS AND DISCUSSIONS	60
4.1	Electrical Resistivity Tomography (ERT) Survey	60
4.1.1	ERT at SAPPI site	60
4.1.2	ERT at Umlazi site	65
4.2	Soil Water Analysis for SAPP1 Site	70
4.2.1	Volumetric water contents at SAPPI site	70
4.2.2	Water sample analysis from WFD at the SAPPI site	72
4.2.3	Water sample analysis from piezometers, boreholes and stream at the SAPPI site	76
4.2.4	Stable isotopes of water samples for the SAPPI site.....	81
4.2.5	Soil properties at the SAPPI WWTW sludge trenching site	82
4.3	Soil Water and Properties for the Umlazi VIP Trenching Site	84
5.	MODELLING	95

5.1	SAPPI Karkloof WWTW Sludge Trenching Site.....	96
5.2	Umlazi VIP pit latrine sludge trenching site.....	119
6.	CONCLUSIONS.....	125
6.1	SAPPI.....	125
6.2	Umlazi.....	126
6.3	Comparison of Sites.....	126
7.	RECOMMENDATIONS.....	130
8.	REFERENCES.....	131
APPENDIX A Error! Bookmark not defined.	
APPENDIX B	155
APPENDIX C	169
APPENDIX D	189

LIST OF FIGURES

Figure 2.1	Sludge disposal in South Africa.....	11
Figure 2.2	Conceptual model for water, NO ₃ and P transport in trench to groundwater and stream.....	14
Figure 3.1	Location of SAPPI WWTW and Umlazi VIP pit latrine sludge burial sites .	35
Figure 3.2	Experimental layout at SAPPI, Karkloof site	36
Figure 3.3	Schematics of instrumentation at the SAPPI Karkloof site	37
Figure 3.4	Schematic layout of TDR probes in T1 at SAPPI.....	39
Figure 3.5	Schematic layout of TDR probes in T2 at SAPPI.....	39
Figure 3.6	Schematic layout of TDR probes in T3 at SAPPI.....	40
Figure 3.7	Schematic layout of TDR probes in T4 at SAPPI.....	40
Figure 3.8	Wetting Front Detector installation in trench at SAPPI.....	41
Figure 3.9	Trench layout at the Umlazi sludge burial site at SAPPI.....	42
Figure 3.10	Umlazi VIP sludge trenching in progress	42
Figure 3.11	Location of piezometer/Wetting Front Detector (WFD) at the Umlazi	43
Figure 3.12	Location of boreholes at Umlazi	44
Figure 3.13	Installation of wetting front monitors and monitoring of piezometers	44
Figure 3.14	Terrameter SAS 1000 instrument and Probe	47
Figure 3.15	Map of ERT transects, boreholes, piezometers and soil water sensing nests at the.....	48
Figure 3.16	Double ring infiltrometer and Guelph permeameter test at SAPPI.....	50
Figure 3.17	Sketch of the site at Umlazi, with indication of trenches and measurement spots.....	51
Figure 3.18	Conceptual model and boundary conditions for SAPPI	54
Figure 3.19	Conceptual model and boundary conditions for Umlazi.....	56
Figure 3.20	Spectroscopic instrument LGR DLT-100.	57
Figure 3.21	Calibration curve for P (left) and NO ₃ (right).....	59

Figure 4.2	Resistivity for transect near Borehole BH1 (12-18 July 2011) at SAPPI.....	61
Figure 4.3	Resistivity for transect near Borehole BH2 (12-18 July 2011) at SAPPI.....	62
Figure 4.4	Resistivity for transect near piezometer SP6 (12-18 July 2011) at SAPPI....	62
Figure 4.5	Resistivity for transect near piezometer SP7 (12-18 July 2011) at SAPPI....	63
Figure 4.6	Resistivity for transect of T1 plot (12-18 July 2011) at SAPPI.....	63
Figure 4.7	Resistivity for transect across T2 and T3 treatments (12-18 July 2011) at SAPPI.....	64
Figure 4.8	Resistivity for transect of T4 plot (12-18 July 2011) at SAPPI.....	65
Figure 4.9	Map of ERT transect at the Umlazi sludge burial site at SAPPI	66
Figure 4.10	ERT Transects 1 and Transect 2 before trenching in 2008 at Umlazi	66
Figure 4.11	Transect 1 inverse model resistivity a year later in August 2009 at Umlazi..	67
Figure 4.12	Transects Umlaz1-4 used for the ERT study in July 2011 Umlazi.....	68
Figure 4.13	ERT inverse resistivity section Umlaz1-4 from top to bottom (July, 2011) Umlazi	69
Figure 4.14	Water content and rainfall dynamics in T1 at the SAPPI site.....	70
Figure 4.15	Water content and rainfall dynamics in T2 at the SAPPI site.....	71
Figure 4.16	Water content and rainfall dynamics in T3 at the SAPPI site.....	71
Figure 4.17	Water content and rainfall dynamics in T4 at the SAPPI site.....	72
Figure 4.18	Observed nitrate concentrations in T1 at the SAPPI site	73
Figure 4.19	Observed nitrate concentrations in T2 at the SAPPI site	73
Figure 4.20	Observed nitrate concentrations in T3 at the SAPPI site	74
Figure 4.21	Observed phosphorus concentrations in T1 at the SAPPI site.....	75
Figure 4.22	Observed phosphorus concentrations in T2 the SAPPI site.....	75
Figure 4.23	Observed phosphorus concentrations in T3 at the SAPPI site.....	76
Figure 4.24	Groundwater depths in boreholes BH1 and BH2 at the SAPPI site	77
Figure 4.25	Perched groundwater depths in piezometers SP6 and SP7 at the SAPPI site	77
Figure 4.26	Observed nitrate concentration in boreholes and stream at the SAPPI site ...	79
Figure 4.27	Observed phosphorus concentrations in boreholes and stream at the SAPPI site	80
Figure 4.28	Observed phosphorus concentrations in piezometers and stream at the SAPPI site	80

Figure 4.29	Stable isotope responses in the boreholes, piezometers and stream at the.....	81
Figure 4.30	Stable isotope of ² H responses in the boreholes, piezometers and stream at the at SAPPI.....	82
Figure 4.31	Stable isotope of ¹⁸ O responses in the boreholes, piezometers and stream at the SAPPI site	82
Figure 4.32	van Genuchten Fitted Soil Water Retention curves in treatments at the SAPPI site	83
Figure 4.33	Surface topography, expected flow path and groundwater levels at the Umlazi site	85
Figure 4.34	Time series of borehole water levels at the Umlazi site.....	85
Figure 4.35	Nitrate concentration in piezometers and WFD before they were destroyed at the Umlazi site.....	86
Figure 4.36	Nitrate concentration in boreholes and the stream at the Umlazi site.....	87
Figure 4.37	Dissolved phosphorus concentration in piezometers and wetting front detectors at the Umlazi site	88
Figure 4.38	Phosphorus concentration in boreholes 2 and 5 and stream at the Umlazi site	89
Figure 4.39	pH of borehole water samples and stream at the Umlazi site	90
Figure 4.40	EC of borehole water samples and stream	91
Figure 4.41	Hydraulic conductivity and retention characteristics at Trench 2 100mm at the Umlazi site	93
Figure 4.42	Saturated hydraulic conductivity variation in trenched with depth at the Umlazi site.	94
Figure 5.1	Simulated water content in Treatment 1 for 4 characteristic times during the SAPPI site	99
Figure 5.2	Observed and simulated water contents in treatment 1 (T1) at SAPPI.....	100
Figure 5.3	Observed and simulated water contents in treatment 1 (T1) at SAPPI.....	100
Figure 5.4	Observed and simulated water contents in treatment 1 (T1) at SAPPI.....	101
Figure 5.5	Observed and simulated water contents in treatment 2 (T2) at SAPPI.....	101
Figure 5.6	Observed and simulated water contents in treatment 2 (T2) at SAPPI.....	102

Figure 5.7	Observed and simulated water contents in treatment 2 (T2) at SAPPI.....	102
Figure 5.8	Observed and simulated water contents in treatment 3 (T3) at SAPPI.....	103
Figure 5.9	Observed and simulated water contents in treatment 3 (T3) at SAPPI.....	103
Figure 5.10	Observed and simulated water contents in treatment 3 (T3) at SAPPI.....	104
Figure 5.11	Observed and simulated water contents in treatment 4 (T4) at SAPPI.....	104
Figure 5.12	Observed and simulated water contents in treatment 4 (T4) at SAPPI.....	105
Figure 5.13	Observed and simulated water contents in treatment 2 (T2) at SAPPI.....	105
Figure 5.14	Observed and simulated nitrate in treatment 1 (T1) at a depth of 0.5 m at the SAPPI site	106
Figure 5.15	Observed and simulated nitrate in treatment 1 (T1) at a depth of 1.2 m at the SAPPI site	107
Figure 5.16	Observed and simulated nitrate in treatment 2 (T2) at a depth of 0.5 m at the SAPPI site	107
Figure 5.17	Observed and simulated nitrate in treatment 2 (T2) at a depth of 1.2 m at the SAPPI site	108
Figure 5.18	Simulated nitrate transport in Treatments 3 (T3) for six characteristic times SAPPI site	109
Figure 5.19	Observed and simulated nitrate in treatment 3 (T3) at a depth of 0.5 m at the SAPPI site	110
Figure 5.20	Observed and simulated nitrate in Treatment 3 (T3) at a depth of 1.2 m at the.	110
Figure 5.21	Observed and simulated phosphorus in Treatment 1 (T1) at a depth of 0.5 m at the SAPPI site.....	111
Figure 5.22	Observed and simulated phosphorus in Treatment 1 (T1) at a depth of 1.2 m at the SAPPI site.....	112
Figure 5.23	Observed and simulated phosphorus in Treatment 2 (T2) at a depth of 0.5 m at the SAPPI site.....	112
Figure 5.24	Observed and simulated phosphorus in Treatment 2 (T2) at a depth of 1.2 m at the SAPPI site.....	113
Figure 5.25	Observed and simulated phosphorus in Treatment 3 (T3) at a depth of 0.5 m at the SAPPI site.....	113

Figure 5.26	Observed and simulated phosphorus in Treatment 3 (T3) at a depth of 1.2 m at the SAPPI site.....	114
Figure 5.27	SAPPI trial site schematic flow path, showing rainfall input, evapotranspiration, subsurface pathways and accumulation, boreholes (BH-) and piezometers (SP-) at SAPPI	116
Figure 5.28	Illustration of the near surface preferential flowpath cross-sectional areas at piezometers SP6 and SP7 at the SAPPI site.....	117
Figure 5.29	The catchment area of the stream on the southern edge of the trial.....	118
Figure 5.30	Cumulative loads of NO ₃ and P from the near surface source and in the stream at SAPPI	119
Figure 5.31	Material distributions in profile at Umlazi site	120
Figure 5.32	Simulated NO ₃ concentration distributions in the flow domain for eight characteristic times during the period from 1 January 2009 to 30 September 2011 at the Umlazi site.....	122
Figure 5.33	Observed (all boreholes) and simulated (node 3) NO ₃ concentration at the Umlazi site	123
Figure 5.34	Simulated phosphorus concentration distributions in the flow domain for four	124
Figure 5.35	Observed (all boreholes) and simulated phosphorus concentration at the Umlazi	124

LIST OF TABLE

Table 2.1	Characteristics of three types of water molecules (excerpted from Hoefs, 1997).	26
Table 3.1	Locations of Soil Characteristic Measurements at the Umlazi site	52
Table 4.1	Physical properties of soil in Treatment 1	83
Table 4.2	Physical properties of soil in Treatment 2	83
Table 4.3	Physical properties of soil in Treatment 3	84
Table 4.4	Physical properties of soil in Treatment 4	84
Table 4.5	Physical properties of sewage sludge	84
Table 4.6	Analysis of soil samples collected from pits in April 2008.....	91
Table 4.7	Summary of particle size fractions at the Umlazi site	92
Table 4.8	Summary of the saturated hydraulic conductivities at surface and trenched sites	94
Table 5.1	Hydraulic parameters for sewage sludge.....	95
Table 5.2	Van Genuchten parameters for hydraulic characteristics in Treatments 1-4 at SAPPI.....	95
Table 5.3	Solute transport and reaction parameters for Treatments T1-T4 at SAPPI97	
Table 5.4	Correlation between observed and simulated NO ₃ and P concentrations at the SAPPI site.....	114
Table 5.5	Fitted hydraulic characteristics (van Genuchten and Mualem) of different soil	
Table 5.6	Solute transport and reaction parameters for materials outside trench (adapted from Hassan et al., 2010).	121
Table 6.1	Comparison of the nutrient concentrations between the Umlazi and SAPPI site.....	127

1. INTRODUCTION

The land application of waste water treatment works (WWTW) sludge by deep trenching is an innovative method used to deal with stockpiles of secondary sludge accumulating at treatment plants in South Africa. The term “sludge” is used to describe the solid or semi-solid material produced by water and wastewater treatment processes, and includes industrial sludges. This method is a potential alternative to landfills, which are becoming difficult to site and costly to construct. The sludge provides plant nutrients, enhances soil productivity and improves soil properties; however, offensive odours and perceptions of health and environmental problems result in application restrictions. This is a unique alternative land application method that solves many of the problems associated with surface application techniques. The practice involves placement of sludge into trenches that are immediately covered with overburden, eliminating odour problems, reducing contact which could cause health problems and maintaining sludge in an anaerobic environment. The area is then planted with trees that have high water and nutrient consumption rate (e.g. Eucalyptus). The major environmental concern of deep row VIP and WWTW sludge application remains the potential for the contamination of groundwater and surface water by nitrate (NO_3) and phosphorus (P) leached from sludge.

The deep row incorporation of VIP and WWTW sludge establishes a soil rich in organic matter and with high water holding capacity, which may prevent risks of leaching of nutrients and deterioration of groundwater quality. VIP and WWTW sludge is applied to agricultural land as a conditioner and as a fertilizer, providing nitrogen, phosphorus and micronutrients. A total of 8% of South African sewage sludge is sold to farmers for use on agricultural lands and a further 20% is used for beneficial land application (Ekama, 1992). The use of VIP and WWTW sludge provides a means of supplying nutrients; however, it may also result in the contamination of soils, crops, atmosphere, groundwater and surface water. VIP and WWTW sludges also contain heavy metals, organic compounds and pathogens. Both nutrients and contaminants are subject to leaching through the soil into groundwater. Many researchers have studied the potential for the disposal of sewage sludge to agricultural and forest land (Costantini *et al.*, 1995; Dunigan and Dick, 1980; Loch *et al.*, 1995). Considerable attention has also been given to the leaching of nitrates from sludge amended soils (Shephard, 1996; Smith, 1996; Cooke *et al.*, 2001; Joshua *et*

al., 2001; McLaren *et al.*, 2003). Several models have been developed to simulate nitrate leaching, the uptake and mineralisation of organic matter, such as APSIM (McCown *et al.*, 1996) and LEACHM (Wagenet and Hudson, 1989).

The aim and objectives of this study are to evaluate the changes in the concentration and water content in the entrenched sludge; to understand the impact of the geology of entrenchment sites on water and nutrient fluxes through geophysical survey; and to quantify the fluxes of nutrients from the entrenched sludge to the surrounding soils, ground water and surface water. The estimation of the possible nutrient impact from the deep trench disposal of sewage sludge and pit latrine waste on water resources was carried out in four phases:

- The site was firstly characterised, so that the dominant flow pathways can be described. To do this, the surface topography survey, the subsurface geophysics and the subsurface hydraulic properties were determined. The geophysics comprises Electrical Resistivity Tomography, from which a 2-dimensional distribution of the electrical resistivity of the subsurface along selected transects is derived. The 2-D distribution of electrical resistivity is indicative of the soil and geological layering, as well as the water distribution in the subsurface. The interpretation of this geophysical data gives a first indication of the likely flow paths from the disposal site and enables the definition of the boundary conditions for later simulation of subsurface water and nutrient movement. ERT surveys later in the study are used to highlight local effects of water and salinity movement from the trenches. The measurement of soil hydraulic characteristics (water retention and hydraulic conductivity) is used in interpreting observed water and nutrient movement, as well as providing the hydraulic parameters for the simulation of water and nutrient fluxes;
- Secondly, the monitoring of the water and nutrient dynamics in the subsurface is aimed at quantifying the concentration, rates and prevalence of water and nutrients in the soil and groundwater. The monitoring also provides observations of soil water and nutrient status, which can be compared to the simulated status, to allow for the calibration of the simulation, so that accurate simulated discharges of water and nutrients (which cannot be directly observed) can be reported;

- The third phase of the estimation requires an assessment of the various observations and surveys to deduce flow pathways, the duration of discharges and the concentration of nutrients in the subsurface flow; and
- The fourth and final phase of the study requires the simulation of water and nutrient fluxes, including a water balance of rainfall, evapotranspiration and other subsurface fluxes and storage. From these results, the discharge of subsurface water and nutrients to either groundwater or stream can be estimated.

This document comprises eight chapters. Chapter one is the introduction of the study and the purpose for the study. Chapter two present the literature review, which highlighted the methods of disposal of VIP and WWTW sludge, their environmental implications and regulations governing sludge disposal in South Africa. Chapter three is the methodology which presents the aims and objectives of the study, methods, instrumentations and experimental setup at the sludge entrenchment sites. Results and discussions are presented in chapter four, while the modelling and simulation using HYDRUS 2-D is presented in chapter five. Chapter six is the conclusions made from the study and suggested recommendations are presented in chapter seven.

2. LITERATURE REVIEW

This section comprises a review of the types of disposal options available for WWTW sludge and VIP sludges and regulations governing their disposal and utilization in South Africa.

2.1 Types of Disposal of WWTW and VIP Sludge

The ultimate disposal of wastewater sludge (biosolids) continues to be one of the most difficult and expensive problems in the field of wastewater engineering (Tchobanoglous and Burton, 1991). Due to the large volumes of sludge generated during wastewater treatment and the potentially hazardous nature of the materials contained in it, the production and disposal of sewage sludge is a worldwide concern. Pit latrines are probably the oldest, and crudest method of sewage disposal that are used. Dating back to antediluvian times, the modern pit latrine can be quite a smart structure with ventilation, a moulded seat and ablution facilities contained in an air-conditioned man-made capsule. Pit latrine designs range from simple unimproved pit latrines, through to Ventilated Improved Pit latrines (VIPs), to alternating twin-pit systems. In a twin-pit system, the second pit is only used when the first pit is filled. The first pit is left sealed for a year or more before emptying, during which time disease-causing organisms are destroyed by natural processes. After such storage, without the addition of fresh wastes, the contents become safe to handle and may be used as compost. The basic components of a pit latrine are the pit, ideally 4-5 meters deep, a cover slab with a hole, through which users defaecate into the pit and a superstructure, sufficient to ensure privacy and provide protection from the weather. VIPs are pit latrines incorporating a vent pipe, designed to draw flies and odour away from the pit and cabin. When sludges are removed from pits, these must be managed in a hygienic and environmentally-safe way. Various approaches can be considered for disposing and/or treating the sludges, as described in this chapter. The following are the disposal methods used in South Africa.

According to, Still (2001), regarding faecal waste disposal, by far the most economical option is to bury the contents on the site where they are generated. Where the contents must be removed due to a lack of space for on-site disposal, then municipalities have essentially three options: i) the faecal waste can be disposed of at sewage treatment plants, although these plants must have

enough capacity to handle the extra load (the volume of pit latrine sludge dumped per day should be small relative to the volume of ordinary sewage sludge processed per day); ii) the waste can be composted by mixing with other organic waste and aerating; iii) the waste can be buried at dedicated landfill sites designed for this purpose. Of the above options, the most economical are (ii) and (iii), and the simplest to implement is (iii).

2.1.1 Disposal of WWTW sludge into large water bodies

The dumping of sludge is a major component of waste disposal to the ocean and is coming under increasingly close scrutiny because of possible adverse environmental effects. Disposal of sewage sludge to the marine environment is still permissible in South Africa and the majority of developing countries. The main advantage of the ocean disposal of sludge is its simplicity and consequent low cost, although the latter may be disregarded if deep-sea dumping is required (Kudo and Miyahara, 1991). The negative impact of sludge disposal into large water bodies is the excessive build-up of nitrogen and phosphorus compounds, which can lead to eutrophication. Eutrophication is a process by which pollution by organic and mineral nutrients from sources such as sewage effluent or leachate from fertilized fields causes lakes, ponds, or rivers to become over rich resulting in rapid algae, cyanobacteria and plants growth thereby depleting the oxygen supply.

2.1.2 Landfilling

WWTW sludge can also be co-disposed off to landfills, in alternate layers, with municipal solid waste. In South Africa, 4% of the sewage sludge produced annually is landfilled. Treatment prior to landfilling usually involves de-watering and possible anaerobic digestion (Marx *et al.*, 2004) and the minimum solids concentration required is often determined by local sanitary landfill regulations. The degradation within the landfill of organic matter in sludge produces landfill gas, mostly methane. For safety reasons, this must be collected and either flared or used as an energy source. The disposal of WWTW sludge to landfills, especially which have high water content, increases the volume of leachate that forms at the bottom of the landfill. The uncontrolled release of liquid leachate can cause severe damage to ground and surface waters. Landfills may be on

public land, such as a municipal-owned landfill, or on private land. The transport of large volumes of sludge by sealed truck or tanker from the Sewage Treatment Works to the landfill is costly and energy-intensive and it also poses the risk of accidental spillage. In addition, the landfilling of sludge has become expensive because of the high costs associated with burial in properly-constructed landfills. Landfilling also concentrates organic wastes and may result in point-source contamination for future generations to deal with. However, the biggest challenge facing the landfilling of WWTW sludge is the fact that there is increasing international pressure to discontinue the disposal of sludge on landfills, because of the space it takes up.

2.1.3 Incineration

Incineration of WWTW sludge is an expensive technology option and is currently only likely to be cost-effective for large cities in developed countries (Horan, 1990). Today, incineration technologies are highly developed (U.S.E.P.A., 1985), with the main types of equipment being multiple hearths and fluidized bed furnaces. Nevertheless, it does not have a high level of public acceptability, the concerns over gas emissions and the difficulty in gaining consent to construct new incinerators. The main pollution problems arise from gaseous emissions and ash disposal, the former of which can be greatly reduced by scrubbers. VIP pit latrine sludge can also be incinerated if there is an existing incinerator, usually at a sewage treatment facility. It is generally too costly to set up an incinerator specifically for this, but many sewage works have a facility that uses the digester gas as a fuel.

2.1.4 Disposal on agricultural land

The application of WWTW sludge directly to agricultural land promotes sludge decomposition, with subsequent benefits to soil and crop production. WWTW sludge application in agriculture (as fertilizer or irrigation water) has been recognized as both environmentally and economically feasible. Land application provides a feasible means of managing sewage sludge, while also providing farmers with organic matter to improve the physical conditions of the soil and to supplement conventional fertilizers, usually at little or no cost (Muse *et al.*, 1991). Organic matter in the sludge improves the structure and the workability (tilth) of most soils. In addition,

organic matter also improves water retention, permits easier root penetration and consequently reduces water runoff and soil erosion (Horan, 1990; Pescod, 1992).

There is enormous potential for disposing of sludge in ways that recover its nutrient value, contribute to food security and reduce the need to dedicated disposal sites. WWTW sludge contains many nutrients needed for plant growth, including nitrogen, phosphorus, potassium, zinc and copper. However, the amount of nutrients in sludge varies from source to source, based on the treatment process, origin, types and quantity and quality of wastewaters treated (Muse *et al.*, 1991). Nitrogen (N), phosphorus (P) and potassium (K) levels in sludge are about one-fifth of those found in typical chemical fertilizers, therefore larger amounts of sludge must be added, in order to achieve the same effects as commercial fertilizers. As a result, sludge can be considered a high volume, low analysis fertilizer (Jimenez *et al.*, 2002). Much of the nitrogen and phosphorous in sludge is in an organic form and not all readily available to plants. When applied to land, part of the organic nitrogen will be mineralized or biologically converted into ammonium, nitrate, or both, to become available to plants over time. Some nitrogen in the sludge may be lost to the air during this process because of ammonia volatilization (Conway and Pretty, 1991). To reduce the amount of nitrogen lost, sludge is often injected or ploughed into the soil directly after application. Incorporation also reduces any potential odour problems, which are sometimes associated with the land application sludge. However, excess nitrogen and potassium applied as plant nutrients have a tendency to seep into ground water and excess phosphorous may flow into surface water supplies with eroded sediment (Fatoki *et al.*, 2003). To prevent surface and ground water pollution, sludge nitrogen should be applied in amounts that will be utilized by actively growing plants (Muse *et al.*, 1991; Richards *et al.*, 2004).

2.1.5 Composting

The composting of WWTW sludge is an accelerated bio-oxidation of organic matter passing through a thermophilic stage, where micro-organisms (mainly bacteria, fungi and actinomycetes) liberate heat, carbon dioxide and water (Dominguez *et al.*, 1997). During the composting process, the heterogeneous organic material is transformed into a homogeneous and stabilized

humus-like product. Advantages of co-composting, as reported by Epstein (1997), based on experience in North Carolina, USA are:

- Reduced cost of sludge composting by using the solid waste as a bulking agent;
- Incorporation of diverse waste streams (sludge, septage, solid waste, yard waste, organic industrial waste);
- Lower capital costs than most alternative technologies;
- Combining the cost of sludge and solid waste disposal;
- Process flexibility through modular construction;
- Reduced volume of the mass of solid waste to landfills;
- Good environmental control;
- A usable, marketable product or products can be produced and
- Compatibility with recycling.

The process does, however, have certain disadvantages including:

- A composting facility takes up more space than combustion systems;
- Labour requirements are intensive;
- Landfill space for solid waste residuals is needed and
- Product(s) produced needs to be marketed or utilized.

Sludge from VIP pit latrines, mixed with other bulking materials, can be composted. The process is improved with forced aeration, which will also result in the pasteurization of the sludge when the windrow is properly prepared. This significantly reduces the risk of disease transmission from handling the mature compost and growing food in agricultural plots, using the compost. Guidelines are available for the composting of sludges. Where composting toilets have been used, the dry matter from the pits can be used directly as compost. However, this material will not have undergone the pasteurization process of an aerated compost heap, and hence it is recommended that the compost is first matured for several months before being used for growing edible crops.

2.1.6 Vermi-composting of WWTW sludge

The vermi-composting of WWTW sludge is also a bio-oxidation and stabilization process of organic material that, in contrast to conventional composting, involves the joint action of earthworms and micro-organisms and does not involve a thermophilic stage (Dominguez *et al.*, 1997). Thermophilic stage is a stage in the composting process characterized by active bacteria which favour a high temperature; it occurs early, before the mesophilic stage, and is associated with a high rate of decomposition. Phillips (1988) defines vermicomposting as “*a low-cost technology system for the processing and treatment of organic wastes*”. As with the composting process, vermi-composting provides a great reduction in waste bulk density, although it tends to take longer.

2.1.7 Treatment of VIP sludge at existing sewage treatment works

In urban areas, where there are existing sewage treatment works, the VIP pit latrine sludge can be added to the works, either at the inlet to the works, or directly to the sludge handling section of the works. In many cases, sludges are deposited in sewer manholes some distance from the works. Solid wastes, such as refuse, bottles, etc. should be removed from the sludge before it is added to sewage treatment works, because it causes a major handling problem which has precipitated the trenching option.

2.2 Impacts of On-site Sewage Disposal

Where on-site sewage and disposal systems are located on shallow ground water tables, there is the potential for contamination. The contaminants potentially affect human health and the environment. The impacts of the methods of application, such as surface application, burial, pit latrine and trench drains/septic tanks, are discussed in this section.

2.2.1 Surface application

A recent trend in the treatment and disposal of VIP and WWTW sludge is land application to agricultural and municipal lands. Many questions have arisen out of a concern for public health safety because of this practice. The application of sludge through spraying and other means, leads to the concern of how potential contaminants may affect the groundwater in the affected regions.

2.2.2 Burial

This is the incorporation of the VIP and WWTW sludge into soil, where it is covered without exposure to the environment as compared to surface spraying. Trenching is one of the methods for sludge burial. Entrenchment prevents the contamination of surface water, buries pathogens, permitting their demise during sludge decomposition, promotes slow nitrogen release and favours denitrification. Pit latrine sludges can be buried on-site, provided there is sufficient space and a suitable pit can be dug. The buried sludge must be covered with at least 500 mm of soil and the pit must not be within 50 m of a borehole used for drinking water purposes. Alternatively, the sludge can be transported to a prepared site, with larger pits for the burying of sludge from a number of latrines. Where there are concerns of groundwater pollution, the procedures outlined in the Groundwater Protocol, to assess the risks, should be followed.

2.2.4 Trench drains/septic tanks

Trench drains are type of floor drain containing a dominant channel-shaped body. It is used for the rapid evacuation of surface water or sewage for containment. Through, the trench drains sewage is transported to sewage treatment plants. Employing a solid cover or grating that is flush with the adjoining surface, this drain is commonly made of concrete in-situ and may utilize polymer- or metal-based liners or a channel former, to aid in channel crafting and slope formation. Characterized by its long length and narrow width, the cross-section of the drain is a function of the maximum flow volume anticipated from the surrounding surface. A septic tank is

basically a vessel buried underground, for the purpose of the collection, storage and, treatment of sewage.

2.3 Regulations Governing Sludge Disposal

The “Permissible Utilization and Disposal of Sewage Sludge, Edition 1” (1997) was developed to assist organizations involved in sewage treatment to promote the safe handling, disposal and utilization of sewage sludge. Sewage sludges are classified in four categories, according to the potential to cause odour nuisances, fly breeding and transmit pathogenic organisms to man and his environment. The ultimate disposal of the wastewater sludge continues to be one of the most difficult and expensive problems in the field of wastewater engineering (Tchobanoglous and Burton, 1991). The sewage sludge produced in South Africa is used for a number of activities, including the application on golf courses and use by municipalities for lawn cultivation, while some is collected by farmers for agricultural use. The disposal and beneficial use of sewage sludge in South Africa is summarized in Figure 2.1. The beneficial uses of sewage sludge under South African conditions include agricultural application for crop cultivation, soil reclamation in areas where mining activities take place and application in forestry.

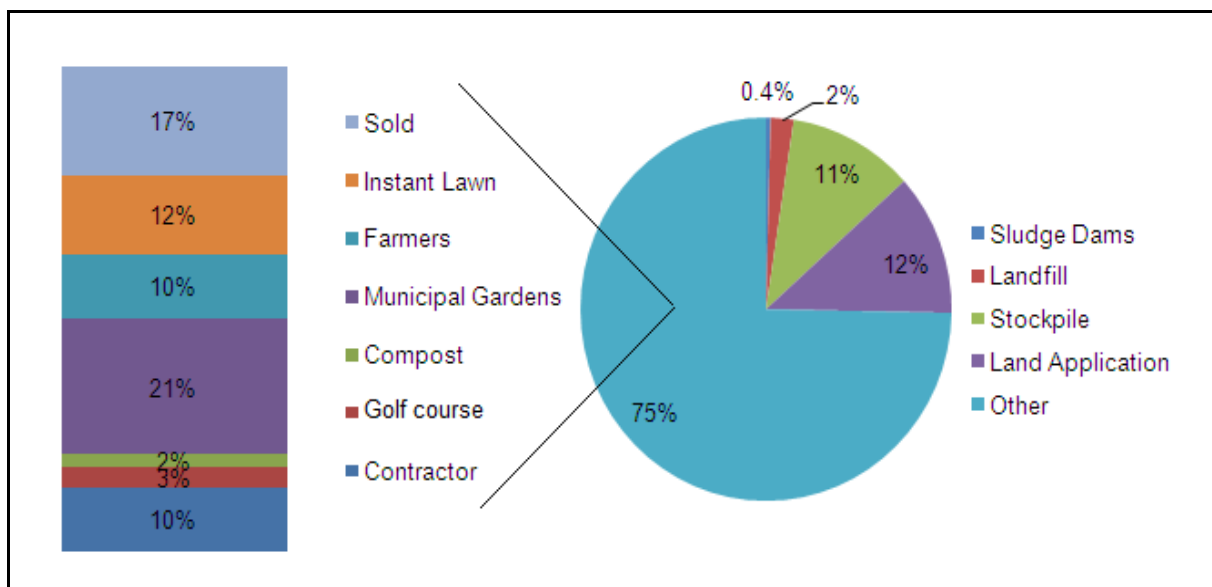


Figure 2.1 Sludge disposal in South Africa (du Preez *et al.*, 1999)

The application of sewage sludge to agricultural soils could provide an economical way to dispose off the increasing amounts of sludge generated in the major metropolitan areas of South Africa (Korentajer, 1991), especially considering that an estimated 11% of sludge produced in S.A. is accumulated at WWTPs (Figure 2.1). The long-term benefits of the application of sewage sludge to land are frequently limited by potentially toxic elements, such as heavy metals and human pathogens (Korentajer, 1991). Concentrations of these substances, originating from different sources can vary between WWTPs. Furthermore, the agricultural recycling of sewage sludge has to comply with the "Guide: Permissible Utilisation and Disposal of Sewage Sludge" (WRC, 1997) and the "Addendum to the guideline on Permissible Utilisation and Disposal of Sewage Sludge" (WRC, 2002).

The current legislation that regulates or controls the deep-row entrenchment of sludge is the National Water Act (Act 36 of 1998), enforced by the Department of Water Affairs (DWA), as well as the National Environmental Management: Waste Act 2008 (Act 59 of 2008). According to the studies by Herselman and Snyman (2006), Herselman and Snyman (2006b), Herselman and Snyman (2009), Herselman and Moodley (2009) and Herselman *et al.* (2009), which also appear in the literature review of Still and Salisbury (2008), other legislation which governs the disposal of sludge on land are;

- The National Health Act (Act 61 of 2003) (HA);
- The Water Services Act (Act 108 of 1997) (WSA);
- The Conservation of Agricultural Resources Act (Act 43 of 1983) (CARA);
- The Fertilisers, Farm Feeds, Agricultural Remedies and Stock Remedies Act (Act 36 of 1947) and
- The National Environmental Management Act (Act 107 of 1998) (NEMA).

2.4 NO₃ and P Movement from VIP and WWTW Sludge in Soils

The loss of N and P from soil by various biological processes and physical mechanisms is a common phenomenon in agricultural activities. These losses can result in a significant pollution of the aerial environment by ammonia volatilisation and the denitrification and contamination of surface and ground water supplies through the leaching of nitrate and surface run-off of both

nitrate and phosphate (Smith, 1996). It was found that the application of sewage sludge to soil decreased the run-off intensity and reduced soil erosion. This led to a decrease in the total P exported through surface run-off (van den Bossche *et al.*, 1999). Very little research has been done concerning P losses after sewage sludge applications to soil. However, nitrate leaching has been investigated more thoroughly by many researchers. Increased losses of nitrate by leaching, following the application of sewage sludge to soil have been frequently reported (Chang *et al.*, 1988; Wadman and Neeteson, 1992; Lotter and Pitman, 1997). Research has indicated that the addition of sludge stimulates microbial activity and the subsequent release of NH_4^+ -N. Nitrate production from the sludge does not immediately take place, it is slowly released over time. Nitrates from sewage sludge only become available after some time, through mineralisation. N can cause undesirable changes in soil properties, such as a decrease in pH, due to nitrification. N is leached mainly as NO_3^- , but in sandy soils, NH_4^+ can be leached as well. Unlike heavy metals and toxic organics, NO_3^- is not adsorbed on the soil constituents and is therefore very mobile in the soil. This is a particularly serious problem in areas of shallow groundwater tables (Korentajer, 1991). Leaching of N is common where soil NO_3^- levels are high and where the downward movement of water in the soil is strong.

2.5 Modelling and Simulation of Water and Nutrient Fluxes

The contamination of ground water from the deep trench application of WWTW and VIP sludge is of great concern. The HYDRUS-2D (Simunek *et al.*, 1999) modelling software have been used to simulate water and nutrient dynamics in wastewater applications to land and its impact on the surrounding subsurface environment. Studies have been carried out on wastewater application methods to land, such as landfilling, drains and septic tanks. Beach and McCray (2003) applied HYDRUS-2D to simulate the influence of the soil clogging of wastewater soil absorption systems on flow regimes. McCray *et al.* (2005) presented a critical review of model-input parameters to simulate the transport of on-site wastewater pollutants. Most studies reported in the literature, however, have focused on evaluating the performance of on-site systems or specific processes that are associated with on-site systems (e.g. nitrification and denitrification), and little has been reported on modelling the cumulative impact of on-site systems on ground water quality. The need to quantitatively predict potential cumulative effects of on-site systems on

groundwater quality has been indicated in the review by McCray *et al.* (2005). They commented that understanding the cumulative effects of on-site systems is critical for determining the adverse effects on the nearby drinking water supply wells. The impact of clustered septic tank systems on ground water quality in New Zealand has previously been investigated in two field studies performed at a site near Christchurch, in 1977 (Sinton, 1982) and in 1986 (Closeet *et al.*, 1989). Elevated NO_3 levels and locally high faecal coliform levels in ground water were found in both surveys. The 1977 survey (Sinton, 1982) also found a clear trend of increasing NO_3 concentrations in the down-gradient ground water, as the number of up-gradient septic tank systems increased. These studies can be extended to the deep trench application of WWTW and VIP sludge, to quantify the cumulative effect on groundwater and nearby streams. A conceptual model to simulate fluxes of water, nitrate and phosphorus in the trenches to soil, ground water and surface water is shown in Figure 2.2.

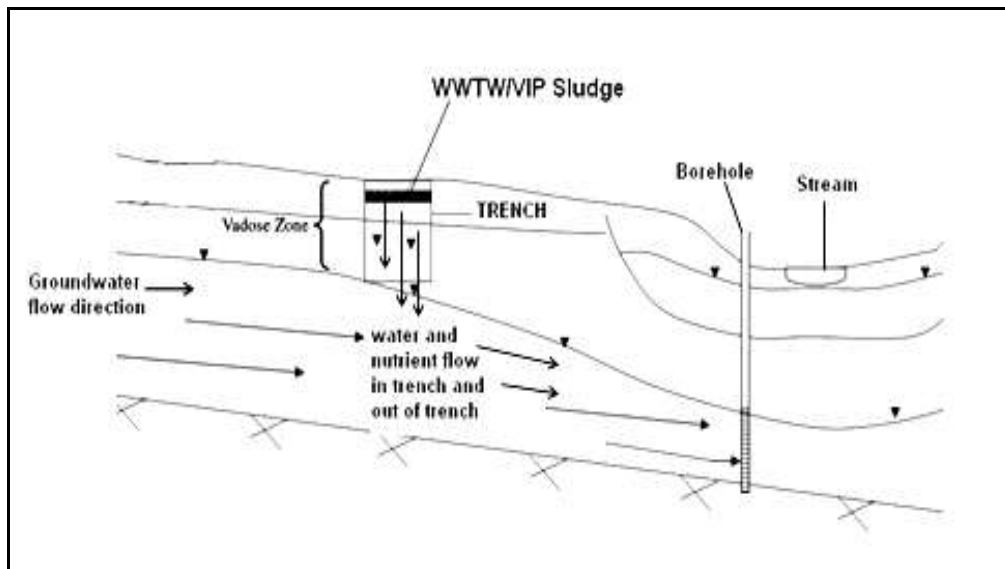


Figure 2.2 Conceptual model for water, NO_3 and P transport in trench to groundwater and stream

2.6 HYDRUS-2D

The HYDRUS-2D program is a finite element model for simulating movement of water, heat, and multiple solutes in variably saturated media. The program numerically solves the Richards' equation for saturated-unsaturated water flow and the Fickian-based advection-dispersion equations for heat and solute transport. HYDRUS-2D solves the Richards equation numerically (Equation 2.1) for variably saturated flow of water through soil. The van Genuchten equations (Equations 2.2 and 2.5) define the hydraulic characteristics of the soils. The resulting equations are solved iteratively. The governing flow equation considers two-dimensional isothermal Darcy flow of water in variably saturated porous medium. These conditions are given by a modified Richard's equation:

$$\frac{\partial \theta}{\partial t} = \frac{\partial}{\partial x_i} \left[K \left(K_{ij}^A \frac{\partial h}{\partial x_i} + K_{iz}^a \right) \right] - S \quad 2.1$$

where θ = volumetric water content [m^3/m^3]

h = soil water pressure head [m]

S = sink term for root water uptake [1/d]

$x_i (i=1, 2)$ = special coordinates [m]

t = time [d]

K_{ij}^A = components of a dimensionless anisotropy tensor K^A [-]

K = unsaturated hydraulic conductivity function [m/d]

where $K(h, x, z) = K_s(x, z) K_r(h, x, z)$

K_r = relative hydraulic conductivity [m/d]

K_s = saturated hydraulic conductivity [m/d]

The properties of the unsaturated soil, $\theta(h)$ and $K(h)$ in equation 2.1 are generally non-linear but not always functions of the pressure head. This knowledge of the soil hydraulic characteristic is essential to model water movement in the vadose zone. Therefore, HYDRUS-2D permits the use of three different analytical forms of the hydraulic relationship. These are:

- Brooks & Corey, 1964;
- Van Genuchten, 1980;
- Vogel & Cislerova, 1988.

During the simulations in this study, the van Genuchten characteristic equations were applied. The van Genuchten model uses a statistical pore size distribution model of Mualem (1976) to obtain the equation for the unsaturated hydraulic conductivity function in terms of soil retention parameters. The equations of the van Genuchten characteristics are given by:

$$\theta(h) = \theta_r + \frac{\theta_s - \theta_r}{\left[1 + |\alpha h|^n\right]^m} \quad h < 0 \quad 2.2$$

$$\theta(h) = \theta_s \quad h \geq 0 \quad 2.3$$

$$K(h) = K_s S_e^l \left[1 - (1 - S_e^{1/m})^m\right]^2 \quad 2.4$$

$$m = 1 - 1/n \quad n > 1 \quad 2.5$$

θ_r = residual water content [m^3/m^3]

θ_s = saturated water content [m^3/m^3]

α = inverse of the air-entry value [$1/\text{m}$]

n = pore size distribution index [-]

K_s = saturated hydraulic conductivity [m^3/m^3]

l = pore connectivity parameter [-]

S_e = effective water content $(\theta - \theta_r / \theta_s - \theta_r)$

These seven independent parameters describe the soil hydraulic properties. Where K_s , θ_r and θ_s can be determined by field measurements, the parameters α , n and l are merely empirical coefficients based on air entry pressure (α), pore size distribution (l) and Poiseuille's law defining the shape of the hydraulic functions.

There are two forms of HYDRUS-2D available. The first option includes the HYDRUS-2D executable code and a graphics-based user interface. A mesh generator is available for relatively simple rectangle domain geometry in this version. Users can either create the input files describing the domain geometry and associated finite element mesh by themselves or use the internal mesh generator to make a simple rectangular structured transport domain. The second option consists of the first version and a CAD program MESHGEN2D for designing more general domain geometry, and its discretization into an unstructured finite element mesh for a variety of problems involving variably-saturated subsurface flow and transport. The second version was used in this study. The finite element model is a numerical technique derived from variational method for finding approximate solutions to boundary value problems. It is numerically stable, meaning that errors in the input and intermediate calculations do not accumulate and cause the resulting output to be meaningless.

HYDRUS-2D is derived from the variably flow codes SWMS-2D of Simunek *et al.* (1992) and CHAIN-2D of Simunek and van Genuchten (1994). A complete HYDRUS-2D package consists of seven main modules: HYDRUS2D, PROJECT MANAGER, MESHGEN2D, H2D_BERC (boundary), H2D_CALC (HYDRUS2), H2D_CLCI (HYDRUS2) and H2D_GRAF (Graphics). HYDRUS-2D is the main program which controls execution of the program and determines which other modules need to be run for a particular simulation. HYDRUS2D contains a project manager and both the pre-processing and post-processing units. MESHGEN2D is a mesh generator for unstructured finite element grids. This program, based on Delaunay triangulation, is seamlessly integrated in the HYDRUS-2D environment. MESHGEN2D is used to define virtually any two-dimensional geometric transport domain and subsequently to design a finite element discretization for that domain. BOUNDARY module helps user to specify boundary and initial conditions for both water flow and solute transport, and define the spatial distribution of other parameters characterizing the flow domain (e.g., spatial distribution of soil materials, hydraulic scaling factors, root-water uptake parameters, and possible hydraulic anisotropy) and/or observation nodes. Three types of boundary conditions are possible with Richards' equation-based models: Dirichlet is prescribed head, Cauchy is prescribed flux, and Neumann is a prescribed hydraulic gradient. All the three types can be used in HYDRUS-2D. Nine options are available in HYDRUS-2D to specify boundary condition (BC): no flux, constant pressure,

constant flux, variable pressure, variable flux, free drainage, seepage face, and atmospheric. Free drainage BC is a Neumann-type, in which a unit vertical hydraulic gradient is imposed at the boundary. The atmospheric BC is a Cauchy type BC, in which the precipitation, potential evaporation, and potential transpiration rates must be specified. In the landfill cover simulations, free drainage BC is recommended for the bottom BC, seepage face BC is selected when drainage layer is installed above lysimeter bottom pan. Atmospheric boundary condition is for the surface condition, although one may wish to specify the infiltration rate as a constant or variable flux BC when testing landfill cover performance for an individual precipitation event. HYDRUS-2D cannot simulate erosion. HYDRUS2 (H2D_CALC, H2D_CLCI) implements the primary data analysis and calculations for HYDRUS-2D.

A Galerkin type linear finite element method was used to solve the governing equations. An implicit (backwards) finite difference scheme is used to achieve integration in time for both saturated and unsaturated conditions. The resulting equations are solved in an iterative fashion, by linearization and subsequent Gaussian elimination for banded matrices, a conjugate gradient method for symmetric matrices, or the ORTHOMIN method for asymmetric matrices. Additional measures were taken to improve solution efficiency in transient problems, including automatic time step adjustment and checking if the Courant and Peclet numbers do not exceed preset levels. The mass-conservative method proposed by Celia *et al.* (1990) was used to evaluate the water content term. Upstream weighting is included as an option for solving the transport equation to minimize numerical oscillations.

The ability of HYDRUS-2D to converge to a stable solution depends upon the discretization and temporal iteration schemes. The finite element mesh was recommended by Simunek *et al.* (1996) to be constructed with close nodal spacing where the hydraulic gradient is expected to be large, such as the soil surface for atmospheric BCs, and near internal source/sinks like tile drains. A closely spaced mesh is particularly needed for coarse-textured soil with high n -values and small α values. This principle is also true for layer interfaces where hydraulic properties change sharply and further applies to the time iteration criteria for minimum time steps. The unsaturated soil hydraulic properties are defined by a set of closed-form equations resembling the 1980 van Genuchten equations.

GRAPHICS manages the geographical, hydrogeologic and physical inputs required to run HYDRUS-2D and present results of a simulation by means of contour maps, isolines, spectral maps, and velocity vectors, and /or by animation using both contour and spectral maps. Output graphics include 2D contours (isolines or colour spectra) in areal or cross-sectional view for heads, water contents, velocities, and concentrations. Areas of interest can be magnified, and vertical scale can be enlarged for cross-sectional views. The mesh can be displayed with boundaries, and numbering of triangles, edges and points. Observation points can be added anywhere in the grid. Viewing of grid and/or spatially distributed results (pressure head, water content, velocity, or concentration) is facilitated using high resolution colour or grey scales.

HYDRUS-2D can handle flow regions delineated by irregular boundaries. The flow region itself may be composed of non-uniform soils with an arbitrary degree of local anisotropy. Flow and transport can occur in the vertical plane, the horizontal plane, or in a three dimensional region exhibiting radial symmetry about the vertical axis. HYDRUS-2D also implements a scaling procedure to approximate hydraulic variability in a given soil profile by means of a set of linear scaling transformations which relate the individual soil hydraulic characteristics to those of a reference soil. A small catalogue of soil hydraulic properties is included in the program.

Kirkley *et al.*, (2007) used HYDRUS-2D to model potential vadose-zone transport of nitrogen from onsite wastewater systems (OWS) at a development scale. The numerical model HYDRUS-2D was used, with input based on site-specific data and several transport parameters estimated from statistical distribution, to simulate nitrate concentrations reaching ground water. The model predictions were highly sensitive to mass-loading of nitrogen from OWS and the denitrification rate coefficient. Results of the modelling simulations show that best-estimate model input parameter values lead to complete removal of nitrogen from the soil. The best estimates for model parameters that could not be estimated from site-specific data (nitrification and denitrification rate coefficients) were assigned the 50 percentile cumulative frequency values based on work by McCray *et al.* (2005). They concluded that these values are reasonable when considering the cumulative impacts from OWS at larger scales.

Vogeler *et al.*, (2006) modelled nitrate and bromide leaching from sewage sludge using a deterministic model for assessing the risk of groundwater contamination by nitrate from land-based sludge disposal. A controlled large-lysimeter experiment was set up to monitor movement of nitrate through soil. Four large lysimeters of 900 mm length were packed with fine sandy loam (a Dystric Fluventric Eutrochrept), on top of which 200 mm of municipal sewage sludge was applied. One of the lysimeters was planted with pasture (*Lolium perenne* and *Festuca arundacea*), one with a willow tree (*Salix sp.*), another with a poplar tree (*Populus sp.*), and one was left bare. Bromide was used as a conservative tracer. Movement of bromide and nitrate was analysed in the effluent from the base of the lysimeters. They concluded that agreement between measured and simulated nitrate leaching was reasonable considering the simplified model and needs to be further tested before it can be used for developing sustainable sewage sludge disposal practices that provide adequate nitrogen for crop growth, and minimise leaching of high concentrations of nitrogen into the groundwater.

Kostyanovsky *et al.*, (2011) studied leaching potential and forms of phosphorus in deep row applied biosolids underlying hybrid poplar. The effects of DRI of anaerobically digested and lime-stabilized biosolids at four rates (213, 426 Mg ha⁻¹ for AD and 328, 656 Mg ha⁻¹ for LS) and a single rate of conventional P fertilizer on leaching of PO₄-P were investigated in a hybrid poplar plantation in a coastal plain heavy mineral mine reclamation site. The effects of biosolids aging on the transformations and losses of P applied with the biosolids were also studied. Zero tension lysimeters were installed at the site to collect leachate. Samples were collected at least monthly for 30 months between July 2006 and December 2008. The result indicated that P leaching potential from the biosolids decreased with aging.

HYDRUS model has also been successfully applied to simulate water flow and solute transport in several agricultural fields (Pang *et al.*, 2000; Ventrella *et al.*, 2000; Hassan *et al.*, 2004). They reported that HYDRUS provided a good description of water flow and solute transport dynamics in soils. Hassan *et al.* (2005; 2008) used HYDRUS-2D and 3D, respectively to simulate water flow behaviour and NO₃ transport where highly treated effluent was applied to soil via subsurface irrigation system. Their result was that the HYDRUS model was adequate to simulate effluent flow and NO₃ transport through soil domains under different environmental and

application conditions. In addition, Mailhol *et al.* (2001) studied the impact of fertilization practices on N leaching under irrigation through field experiments and numerical modelling (HYDRUS-2D). They found that in spite of a substantial water application depth, the amount of N leaching is not considerably high: 22 kg N/ha which represents 11% of nitrogen application, was obtained through field measurements and simulations using a modelling approach suited to 2D water and solute transfer: HYDRUS-2D. The measured soil nitrogen profile both under ridge and under furrow confirmed previous research work which underlined the utility of 2D water and solute transfer modelling rather than a 1D approach to simulate the nitrogen distribution and to estimate leaching risks according to the fertilisation technique analysed in this study. The changes in soil conditions over subsequent irrigations (mainly from first to second watering) affect the predictive character of the mechanistic model. Indeed, it is highly recommended to calibrate the model parameters for each irrigation events (especially for the first and second irrigation simulations). The knowledge of the temporal variability process of the soil hydraulic parameters would improve model predictions.

2.7 Electrical Resistivity Tomography

The purpose of the electrical survey is to determine the resistivity distribution of the subsurface by making measurements on the surface (Loke, 2000). This method provides insight to the subsurface structure without affecting or even destroying it.

2.7.1 ERT in hydrology

The most common application of ERT in hydrology is the exploration of the thickness and depth of an aquifer. In addition, ERT also provides the possibility to determine aquifer parameters such as transmissivity (Sri Niwas & Singhal, 1985) or hydraulic conductivity (Kemna *et al.*, 2002). A further possibility is to monitor a tracer experiment with ERT to improve the understanding of water and solute movement in the groundwater body or in the unsaturated zone (White, 1988; Kemna *et al.*, 2002).

The approach for determination of aquifer parameter with ERT is that current in analogy to water flows the way of lowest resistivity. Due to the high density of ions inside a matrix pore, it can be assumed that electric conductivity is stronger influenced by porosity and water conductivity than by the surrounding matrix material. Therefore, Sri Niwas & Singhal (1985), conclude that measured resistivity mainly reflects hydrologic conditions.

2.7.2 Basics of Electrical Resistivity Tomography

During an ERT measurement, current is injected into the conductive underground with two electrodes A and B as can be seen in Figure 4-1. The current flows in a semicircle from the positive potential at electrode A to the negative potential at electrode B. The result is a three dimensional potential field that depends on the different resistivities occurring in the subsurface. The electric resistivity is a characteristic physical material parameter. Its value is not only defined by the composition of the rock, but also primarily by the contained water and the proportion of dissolved substances, as well as the porosity and permeability of the rock. The effect of porosity and water content on the electrical resistivity is expressed by Archie's law:

$$\frac{\sigma_w}{\sigma_f} = F - \varepsilon^* p_e^{-m} \tag{2.1}$$

where, σ_w = conductivity of the water [-],

σ_f = conductivity of the formation as a whole [-],

F = „formation factor“, related to the volume and tortuosity of the pore space,

ε = empirical constant, typically 1 for unconsolidated sediments,

m = empirical constant, typically 2 for unconsolidated sediments,

p_e = effective porosity, the fraction of interconnected pore space.

The conductivity of many geological even crystalline rocks formations is well represented by this simple function of porosity. The originating potential field is detected by two additional electrodes M and N. The basis of the measurement is Ohm's law:

$$R = \frac{\Delta V}{I}$$

2.2

where I is the current induced through the current electrodes A and B and V is the voltage measured between electrodes M and N. In other words, V is the difference between the equipotential line at electrode M to the equipotential line at electrode N and R is resistivity. To account for the different electrode arrays a correction factor has to be included. Hence, for a homogenous half space the specific resistivity can be calculated.

2.7.3 Electrode array

Current follows circular pathways through the subsurface. The radius of the cycles depends on the distance between the injecting electrodes. The radius becomes bigger with increasing distance between electrodes and therefore reaches greater depth. Current is influenced to a growing extent by the resistivity of deeper material. The variation of the electrode positions was necessary to detect different subsurface structures and associate them to a certain depth. This principle is illustrated in Figure 2.3.

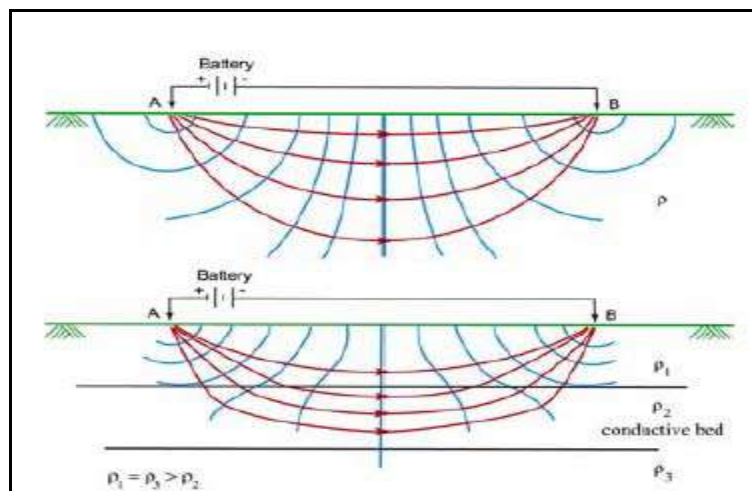


Figure 2.3 Schematic diagram of the distribution of current flow and equipotential lines for different cases of layered conductive and resistive beds (after Damiata, 2001).

The choice of array depends on the interest of the researcher concerning the outcome of a particular measurement. In this study, following arrays were applied:

- Schlumberger vertical electrical sounding (VES);
- Wenner switch and
- Dipole-Dipole switch.

These three methods are described briefly as follows.

1-D resistivity surveys and inversion

With the Schlumberger (VES), the centre point of the electrode array remains fixed, while the spacing between the electrodes is increased during the measurement to obtain more information about deeper sections of the subsurface. Due to this arrangement, only vertical changes in resistivity can be measured. Therefore a subsurface consisting of horizontal layers is the basic assumption used to interpret the measurements. However, in nature lateral changes of resistivity are commonly found (Loke, 2000). Such a lateral inhomogeneity might lead to the interpretation of a change with depth in the subsurface resistivity. Thus, the measured data needs to be interpreted very carefully. However, this method provides good penetration depth and is suitable to detect horizontal structures such as groundwater table and bedrock.

2-D resistivity surveys and inversion

The limitation of the 1-D resistivity survey is that it does not take lateral changes into account. This can be overcome by a two-dimensional measurement. The Wenner and Dipole-Dipole array are common used 2-D electrode arrays. To give an idea of a typical 2-D setup Figure 4-2 shows a Wenner array survey.

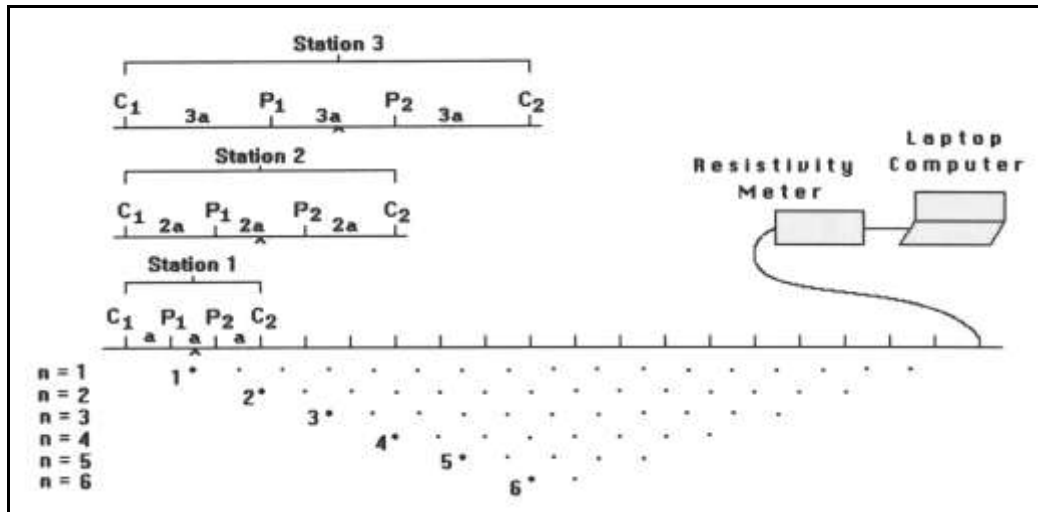


Figure 2.4 Sequence of measurements used to build up a pseudosection (Loke, 2000).

2.7.4 Tomography interpretation

The analysis of the measured resistivity collected was performed by a commercial inversion-software-program. In this study, the software RES2dinv was used. The use of inversion-software program is necessary to calculate out of a subsurface picture with “pseudo” depth and “pseudo” resistivities a “true” image of the subsurface. A top down approach is used with the assumption that the upper layer consists of only one resistivity a “true” depth is calculated. A model of the subsurface is generated which shows which resistivity response fits best to the measured resistivities. The quality of the fit is represented by the root mean squared (RMS). However, even good fits do not guaranty an accurate picture of the subsurface structure. Essential for the correct interpretation is to keep in mind how the image of the subsurface is created. Errors develop for example due to the 3-dimensional nature of resistivity data, which are transformed to point data and again interpolated to two dimensional images. As well the assumption that resistivity does not change perpendicular to the measurements profile has to be considered. Otherwise, neighbouring structures can be found on the 2-D picture of the profile while in reality they are located next to it. Due to the small resolution of ERT and averaging, a small subject with different resistivities will influence resistivity value for a much bigger region. Meyer de Stadelhofen (1994) therefore remarks that only several measurements and knowledge about the geological situation enables a clear interpretation of the measurements.

2.8 Stable Isotopes in Hydrology

Oxygen has three stable isotopes, ^{16}O , ^{17}O , and ^{18}O ; hydrogen has two stable isotopes, ^1H and ^2H (deuterium), and one radioactive isotope, ^3H (tritium), which is discussed separately. Oxygen and hydrogen are found in many forms in the earth's hydrosphere, biosphere, and geosphere. Oxygen is the most abundant element in the earth's crust. Hydrogen is also common in the biosphere and is a constituent of many minerals found in the geosphere. Most importantly, oxygen and hydrogen combine to form water, thus making their isotopic composition a powerful tracer of the hydrosphere. There are nine isotopic configurations for water, which are distinguished by their mass numbers as well as their characteristics. However, because of the low abundance of the heavier isotopes, almost all water molecules are of three isotopic combinations.

Table 2.1 Characteristics of three types of water molecules (excerpted from Hoefs, 1997)

	$^1\text{H}_2^{18}\text{O}$	$^2\text{H}_2^{18}\text{O}$	$^1\text{H}_2^{18}\text{O}$
Density @ 20°C	.997	1.1051	1.1106
Boiling point	100.0	101.42	100.14
Vapor pressure @ 100°C	760	721.60	?
Temperature density max	3.98	11.24	4.30

Models of oxygen/hydrogen isotopic fractionation have been developed and refined over the last century. Models of isotopic variability take into account vapor pressure, humidity, temperature, altitude, rainout and moisture content, evaporation and solute concentration, and combinations thereof. Because of their close relationship and the abundance and importance of water on the planet, O and H and their isotopic fractionation characteristics are usually considered together. As a result of fractionation, waters develop unique isotopic compositions that can be indicative of their source or the processes that formed them. Isotopic composition differs for sea water, polar ice, atmospheric water vapor, and meteoric water.

Oxygen and hydrogen isotopic ratios are measured using gas source isotope ratio mass spectrometry (IRMS). Oxygen and hydrogen compositions are reported as delta values. Delta values (δ) are commonly used in light stable isotope geochemistry to express isotopic

composition in terms of per mil (‰) deviation from a standard. Stable isotope ratios of deuterium/hydrogen ($^2\text{H}/^1\text{H}$) and $^{18}\text{O}/^{16}\text{O}$ of water are conventionally expressed as per mil (‰) deviation from SMOW (Standard Mean Ocean Water) or VSMOW (Vienna SMOW). In carbonates, the isotopic composition of oxygen is sometimes compared instead to PDB, a standard based on the Peedee Formation, a carbonate rock found in South Carolina.

2.8.1 Fractionation during Precipitation

Equilibrium fractionation describes isotopic exchange reactions that occur between two different phases of a compound at a rate that maintains equilibrium, as with the transformation of water vapor to liquid precipitation. For water in a closed system, equilibrium fractionation can be expressed as:



where v is the water vapor phase, l is the liquid phase, and the rate of exchange is constant ($k_1 = k_2$). Although the rate remains constant, it varies for different isotopic compositions. Thus, with ^{18}O :



and again $k_1 = k_2$.

Similarly, with ^{16}O :



and $k_1^1 = k_2^2$.

However, $k_1^{18} \neq k_1^{16}$; rather, $k_1^{18} < k_1^{16}$ such that $^{18}\text{O}/^{16}\text{O}_{(v)} < ^{18}\text{O}/^{16}\text{O}_{(l)}$; thus, ^{18}O becomes enriched in the liquid and ^{16}O becomes enriched in water vapor. The process is in equilibrium in both instances, but the rate of these exchanges is different, so that enrichment of one of the isotopes results.

2.8.3 Temperature effect

The fundamental control on the isotopic composition of precipitation is temperature. With increasing temperature, precipitation becomes enriched in the heavier isotopes, ^{18}O and ^2H , in a linear relationship. Temperature affects fractionation at a rate of approximately 0.5‰ for every $^\circ\text{C}$ for oxygen. Similar effects are shown with increasing elevation and increased distance from the equator (both of which correspond to lower temperature). Because precipitation becomes progressively enriched in light oxygen as it moves toward the cold polar regions, polar ice constitutes a reservoir of ^{16}O enriched water as compared to sea water.

2.8.4 Precipitation and equilibrium fractionation

The δD and $\delta^{18}\text{O}$ values for precipitation worldwide behave predictably, falling along the global meteoric water line (GMWL) as defined by Craig (1961b), who expresses the relationship between ^{18}O and ^2H in meteoric waters as follows:

$$\delta^2\text{H} = 8 \delta^{18}\text{O} + 10\text{‰} \quad 2.6$$

This relationship for ^{18}O and ^2H isotopes is primarily a reflection of differences in their equilibrium fractionation factors. The slope of the GMWL expresses this ratio, which is eight times greater for oxygen than hydrogen. The validity of the model is shown in Rozanski's (1993) compilation of average annual values for these isotopes (as plotted against the GMWL) for precipitation monitored at stations throughout the IAEA (International Atomic Energy Agency) global network (Figure 2.4).

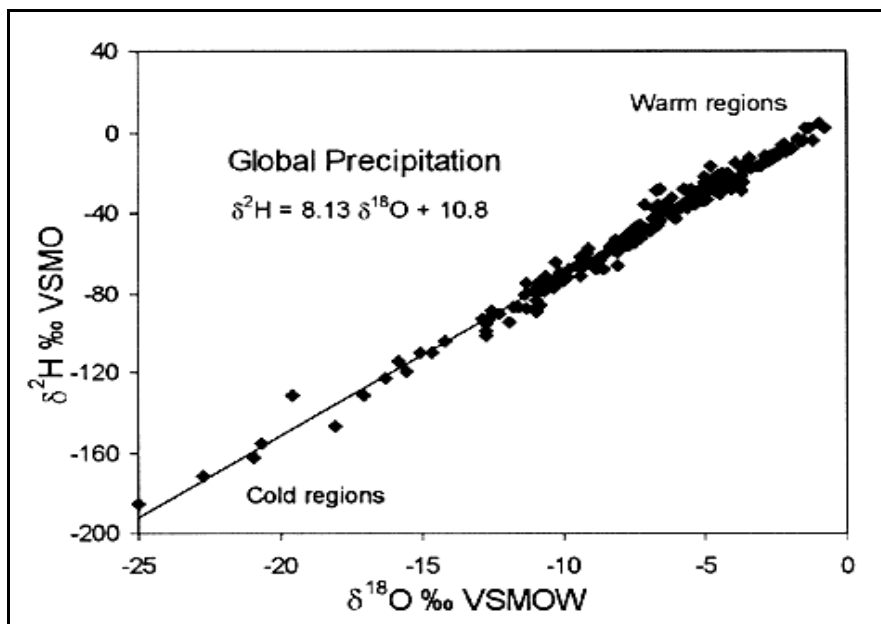


Figure 2.5 Clark and Fritz 1997, as compiled in Rozanski et al. 1993, modified by permission of American Geophysical Union

Local meteoric water lines in arid environments will exhibit the same slope, but plot higher in relation to $\delta^2\text{H}$ because of increased evaporation. Likewise, LMWLs of humid environments maintain the slope of 8, but the line shifts toward increased $\delta^{18}\text{O}$ because the phase change tends toward liquid precipitation.

2.8.5 Rainout effect

In precipitation, the initial liquid phase of rain is enriched in ^{18}O and ^2H as compared to the later precipitation. Consequently, in rain events, the precipitation gets lighter as the rain continues, a phenomenon known as "rainout effect" or "amount effect." Similarly, the center of a large land mass or continent has precipitation that is depleted in ^{18}O and ^2H , a phenomenon known as the "continental effect." Isotopically enriched rain forms and falls from a diminishing vapor mass, and the residual vapor becomes isotopically depleted with respect to earlier rains from the same cloud. Rainout consequently evolves to colder, isotopically-depleted precipitation: cold climates plot at the depleted end of the GMWL and warm environments plot at the upper end.

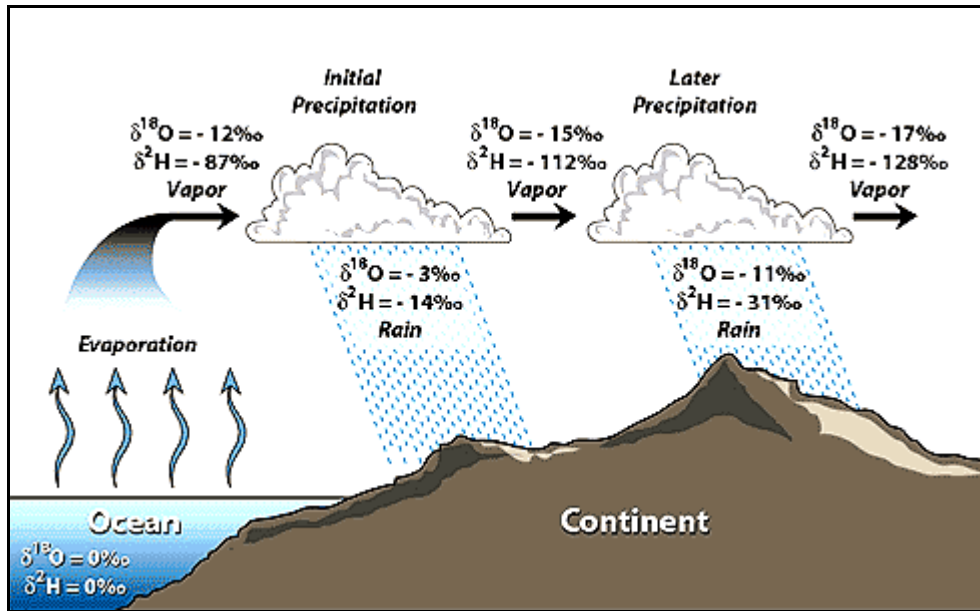


Figure 2.6 Rainout effect on $\delta^2\text{H}$ and $\delta^{18}\text{O}$ values (based on Hoefs 1997 and Coplen et al. 2000).

This progressive depletion of ^{18}O and ^2H is typically described using a Rayleigh distillation. The Rayleigh equation applies not only to the temperature-isotope evolution during rainout, but the progressive partitioning of heavy isotopes into a water reservoir as it diminishes in size:

$$R = R_0 f^{(\alpha-1)} \quad 2.7$$

where R_0 is the initial isotope ratio, R is the ratio after the process occurs, f is the residual component, and α is the equilibrium fractionation factor.

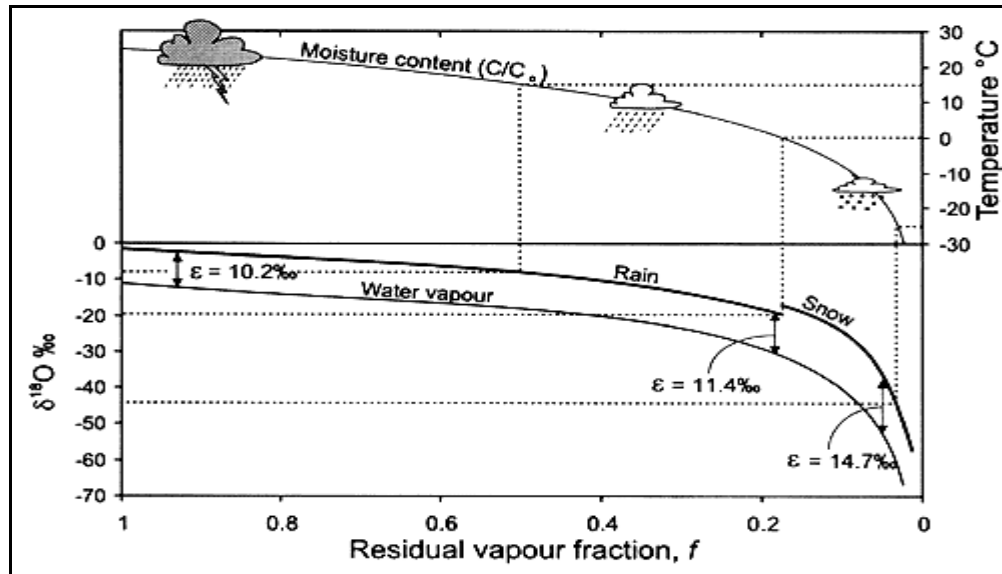


Figure 2.7 Change in the ^{18}O content of rainfall according to a Rayleigh distillation, starting with $\delta^{18}\text{O}_{\text{vapor}} = -11\text{‰}$, temp. = 25°C , and final temp. of -30°C . Note that at 0°C , fractionation between snow and water vapor replaces rain-vapor fractionation. The fraction remaining has been calculated from the decreases in moisture carrying capacity of air at lower temperatures, starting at 25°C . Dashed lines link $\delta^{18}\text{O}$ of precipitation with temperature of condensation (Clark and Fritz 1997)

2.8.6 Fractionation during evaporation

Kinetic fractionation is similarly related to mass differences between the nuclei of isotopes, but is associated with incomplete and unidirectional processes such as evaporation and diffusion. In general, the lighter isotope will react faster and will become concentrated in products. For water, the higher the mass number, the lower the vapor pressure. Thus, ^{16}O and ^1H preferentially enter the vapor phase, whereas ^{18}O and ^2H preferentially concentrate in the liquid phase. Consequently, in evaporation, water vapor is enriched in ^{16}O and ^1H , whereas the remaining liquid water is enriched in ^{18}O and ^2H . More specifically, H_2^{18}O is enriched in liquid water by 1% relative to its concentration in water vapor at the same temperature. Factors such as humidity, salinity, and temperature affect kinetic fractionation of water during evaporation. The effect of humidity on isotopic enrichment in evaporating water can be expressed as follows:

$$10^3 \ln a^{18}\text{O}_{l-v} = 14.2 (1-h)\text{‰} \quad 2.8$$

$$10^3 \ln a^2\text{H}_{l-v} = 12.5 (1-h)\text{‰} \quad 2.9$$

where h is relative humidity. The lower the relative humidity, the faster the evaporation rate and the greater the kinetic fractionation. Humidity affects oxygen and hydrogen differently such that the slope of the evaporation line will vary due to changes in relative humidity. At very low relative humidities ($< 25\%$) the slope of the evaporation line will be close to 4; for moderate relative humidities (25% to 75%) the slope will be between 4 and 5; only for relative humidities above 95% does the slope approach 8, the slope of the meteoric water line (Clark and Fritz 1997) (See Figure 2.7).

Likewise, relative humidity affects the isotopic composition of the water vapor. This is primarily reflected in the d value, or deuterium excess, of the meteoric water line. If the vapor source region for precipitation is arid (low humidity), d values will be high, upwards of 20. In contrast, d values for humid regions will be low, approaching 0.

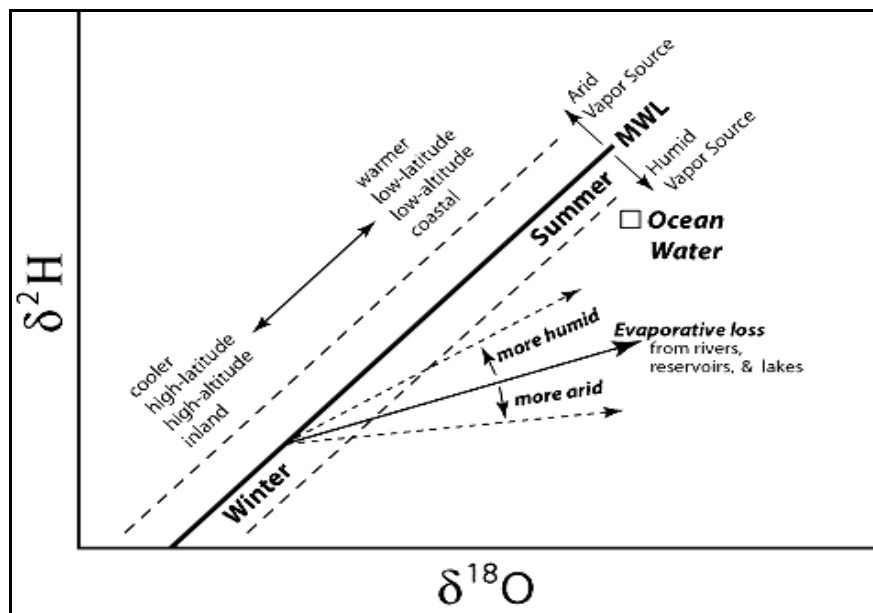


Figure 2.8 Summary diagram of how hydrologic processes affect oxygen and hydrogen isotopic composition of water

2.8.7 Hydrological applications

$\delta^{18}\text{O}$ and $\delta^2\text{H}$ can be used to trace the hydrological cycle from evaporation in the oceans to local precipitation and groundwater. Because $\delta^{18}\text{O}$ and $\delta^2\text{H}$ values have a strong positive correlation with temperature, their measurements in ice cores are valuable indicators of climate variability. Values can be used to date snow and determine average snow accumulation rates. Water isotopes can be used to determine open water evaporation from rivers, reservoirs, and lakes. Variations in the $\delta^{18}\text{O}$ and $\delta^2\text{H}$ values of precipitation can be used to differentiate relatively "old" (uniform) water and the more variable "new" water to determine their respective contributions to a stream during periods of storm runoff. Two-component hydrographs are used in this analysis to distinguish "event" and "pre-event" isotopic composition of streamflow. Successful hydrograph separation requires that:

- the isotopic component of the event is significantly different from the pre-event;
- the event component maintains a constant isotopic content;
- vadose water contributions to runoff are negligible, or vadose water and groundwater are isotopically equivalent;
- surface storage contributes only minimally to the runoff event. (Sklash and Farvolden 1979; Genereux and Hooper 1998).

With SiO_2 , $\delta^{18}\text{O}$ has been used to show multiple contributions to a streamflow: runoff, soil water, and groundwater (Hinton et al 1994). Similarly, DeWalle et al. (1988) have used a three-component model to separate storm streamflow into groundwater, soil water and channel precipitation, using a calculation of the rate of channel precipitation as the product of the throughfall rate and the surface area of the stream.

Isotopic composition studies can be used to trace water use, uptake, and transport by plants. Evaporative processes cause significant isotopic enrichment in a plant's xylem-sap and leaves at a magnitude dependent on leaf transpiration rate, humidity gradient, and the isotopic composition of atmospheric water.

3. METHODOLOGY

The SAPPI burial trial site (Figure 3.1) is located at the Shafton Karkloof Falls, about 10 km from Howick, in the Kwazulu-Natal province (29°24' S and 30°12' E). It is owned by SAPPI and used as a forest plantation. WWTW sludge accumulating from wastewater treatment works from Umgeni in Howick, was transported to the site. Sludge burial commenced in December 2009. The site lies in gently undulating terrain at 1260 m above sea level. The site is well-suited to *E. dunnii* and highly representative of commercial eucalypt stands in the KwaZulu-Natal Midlands, in terms of site index, climate, soil properties and historical land use. The mean annual rainfall is around 950 mm, the long-term mean monthly minima for the coldest month (June) and the warmest month (January) are 3.7°C and 14.8° C respectively, while corresponding maxima are 19.0° C and 25° C. The sites suitable for forestry in the Midlands of KZN are dominated by highly-weathered soils derived from sedimentary rocks (shale, sandstone and mudstones), with igneous (dolerite) intrusions. The soil at the trial site is derived from a mixture of dolerite and shale. It has a humus-rich, clayey A horizon (0 to 0.3 m depth) overlying a yellow-brown clayey B2 horizon, which grades into weathered shale at a depth of about 1.2 m.

At the Umlazi E Ponds site also in Figure 3.1, until 1999 operated a set of three oxidation ponds. In 1999, however, the works decommissioned after it was damaged in heavy flooding. The Umlazi E Ponds site is still owned by the eThekweni Municipality. It is, however, located in close proximity to a portion of Umlazi Township (E section). Umlazi is situated 20 km south of Durban and is also situated close to the Metro Industrial Development Belt, which stretches from Ezimbokodweni (Mbongitwini) in the south to Phoenix in the north. The Umlazi River in the north and the Ezimbokodweni River in the south, border Umlazi. Slopes are not very gentle, the severe fragmentation and very steep topography is associated with a multitude of tributaries to major rivers. Climatic conditions at Umlazi are typical of the Natal Subtropical East Coast Region. Here the summers are warm and humid, whereas winters are cool and dry. The average annual rainfall ranges between 900 mm and 1100 mm. These make the area humid. The Umlazi topography consists of valleys and slopes due to the rivers and tributaries found in Umlazi. The Umlazi River determines the incisive valleys in the north and the Ezimbokodweni River in the south, while the Isipingo and Mfongosi Rivers and their tributaries determine the internal

topographic structure. Most of the slopes seem to be gentle, but the tributaries tend to provide severe fragmentation and very steep topography.

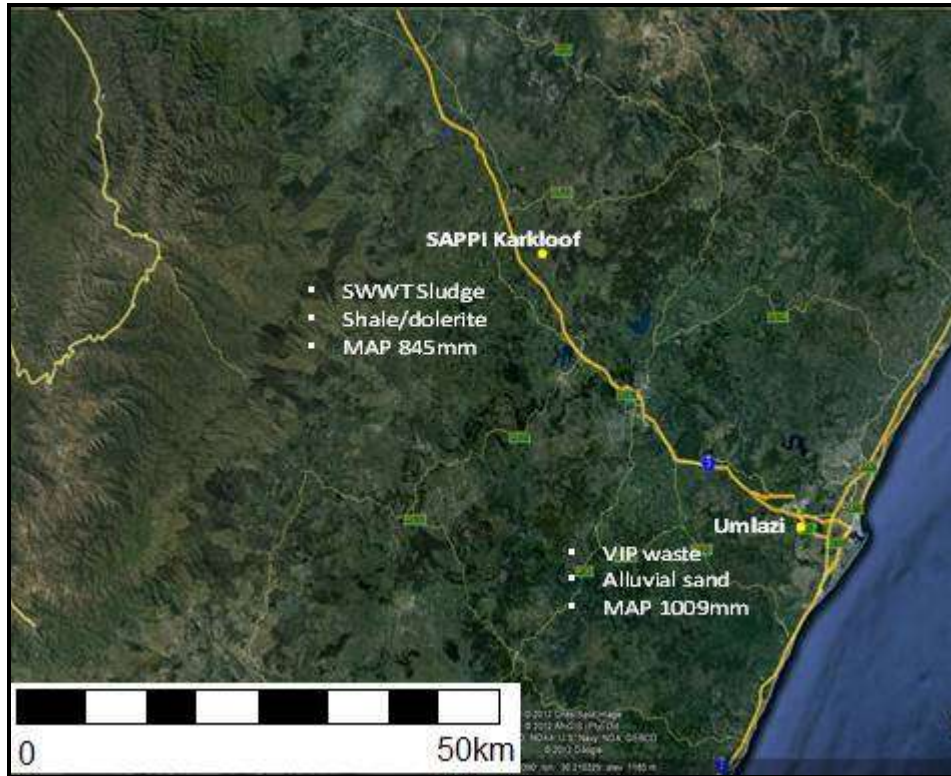


Figure 3.1 Location of SAPPI WWTW and Umlazi VIP pit latrine sludge burial sites (yellow dots), (Google earth map, accessed: 2012)

3.1 WWTW Sludge Trenching and Instrumentation

3.1.1 Trench layout and instrumentation at the SAPPI site

The trench layout at the SAPPI WWTW sludge burial site is shown in Figure 3.4. The trial consists of four treatments of WWTW sludge, assuming 1 % N in wet sludge:

- Treatment 1 (T1): 250 mm (sludge thickness) in trench, 5400 kg N/ha;
- Treatment 2 (T2): 500 mm (sludge thickness) in trench, 10800 kg N/ha;
- Treatment 3 (T3): 750 mm (sludge thickness) in trench, 16200 kg N/ha;
- Treatment 4 (T4): control, no sludge application and

- T5-Undisturbed locations.

Each of these were replicated to cover an area of 20 m x 20 m, which will allow for 6 rows of 20 m within each replicate and a tree spacing of 3 m between, and 2 m within, the rows. The trenches were dug to a depth of 1.2 m and a width of 1.0 m, using a backhoe. The trenches were backfilled, to allow for the required amount of sludge to be filled to 30 cm below the surface. They were then covered and all the soils replaced, creating a heaped overburden, which was anticipated to sink as dewatering of the sludge occurs. The trees were then planted into the overburden. Time domain reflectometry (TDR) probes to monitor the moisture contents within the profile, wetting front detectors (WFD), boreholes, piezometers to collect water samples from various locations to analyze nutrients and rain gauge to measure the amount of rainfall were installed at the site for monitoring purposes.. Figure 3.2 shows the location and installation setups and Figure 3.3 below shows the schematics of the instrumentation at the SAPPI site. All these are data required for input into model.

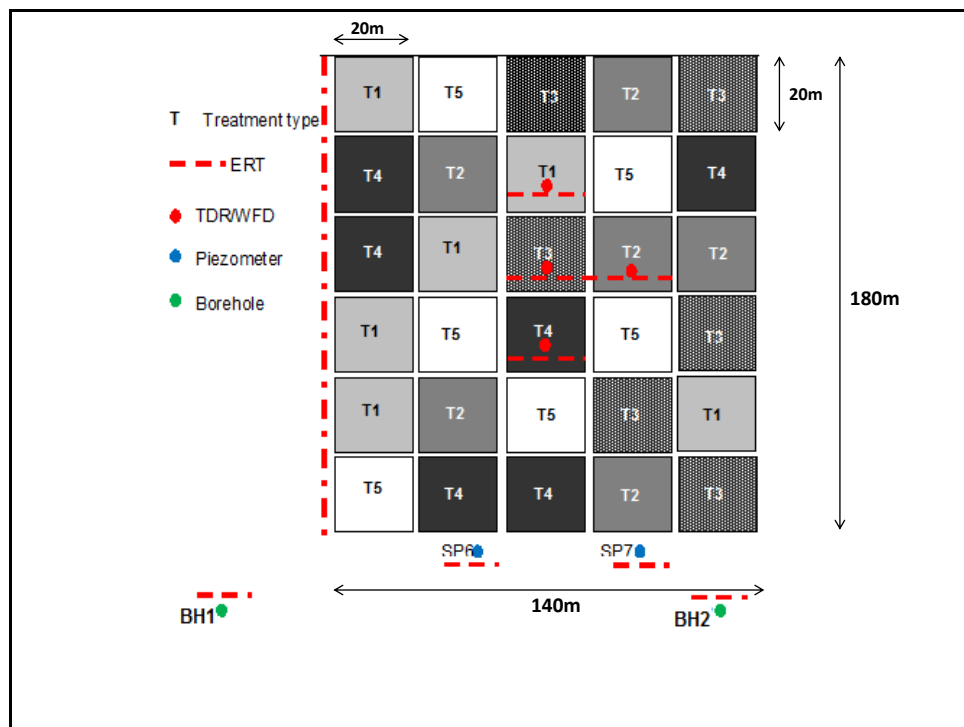


Figure 3.2 Experimental layout at SAPPI, Karkloof site

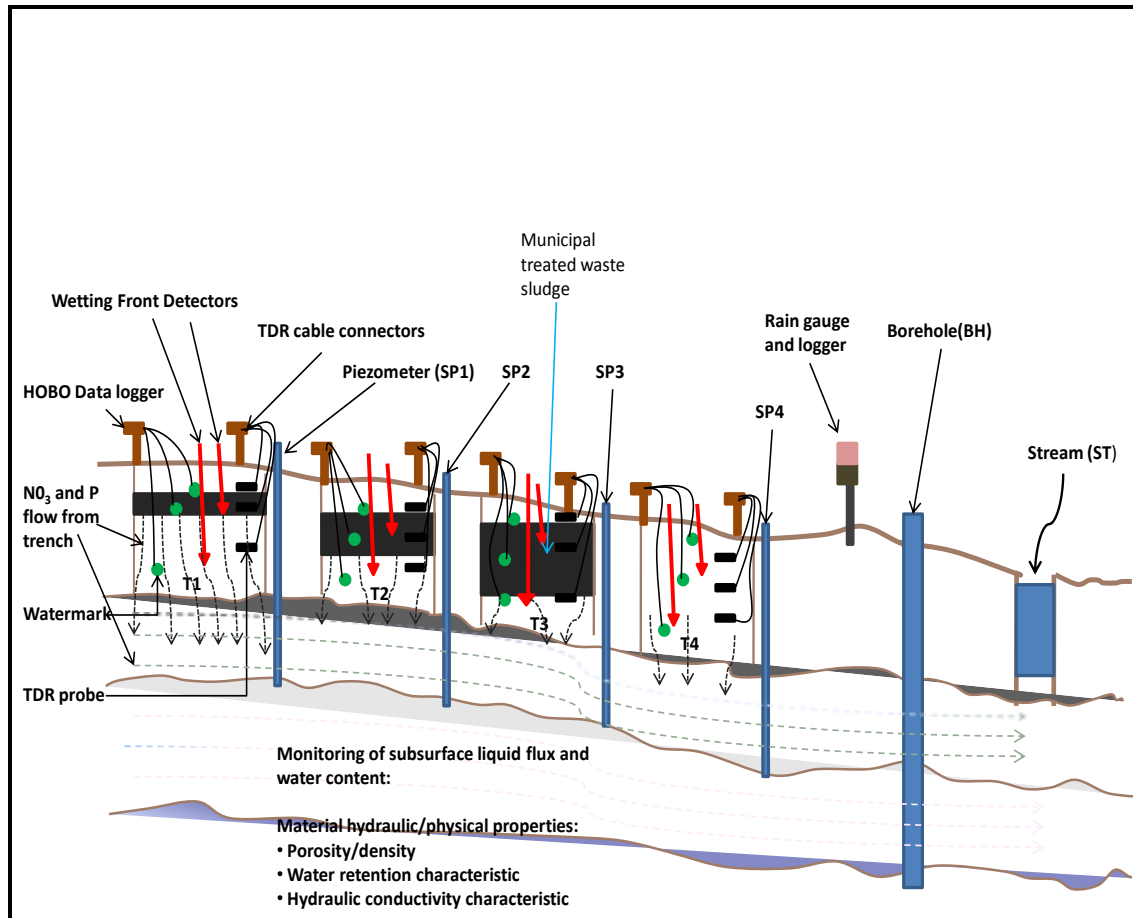


Figure 3.3 Schematics of instrumentation at the SAPPI Karkloof site

All the TDR instrumentation at the SAPPI trial site was set to read volumetric water contents and electrical conductivity (EC) at predetermined depths. Direct TDR measurements were used with no calibration. Relative comparisons and changes were deemed to be more important than absolute values. The water holding capacity of the soil was improved with decomposition was moisture contents within treatments with sludge T1, T2 and T3 were higher than T4. The depths considered were 0.15 m, 0.5 m and 1.2 m. The dielectric constant of soil primarily depends on the amount of water present in the soil, therefore the volumetric water content can be inferred from the reflected measurements. Soil bulk electrical conductivity is determined from the attenuation of the applied pulse. The power supply to the TDR100 instrument is a portable 12 v battery. TDR soil water content measurements are based on the travel time measurements of electromagnetic (EM) waves in the TDR probes installed in the soil (Topp *et al.*, 1980). The relative dielectric permittivity (ϵ_r) of the soil, which is strongly related to the volumetric water

content θ , determines the velocity (m/s) of the EM waves:

$$v = C_{\text{light}} / \sqrt{\epsilon_r} \quad 3.1$$

With: $c_{\text{light}} = \text{speed of light} = 3 \times 10^8 \text{ (m/s)}$

The decrease in amplitude of reflected EM waves can be used to calculate the electrical conductivity of the medium (Dalton and Van Genuchten, 1986). For the SAPPI WWTW sludge trenching site, a roaming approach was used to obtain real-time data; the power source and TDR100 were moved from location to location to perform the survey. During the loading of the trenches with the four different treatment applications, TDR probes were installed in at least one of the trenches of the four selected treatments for instrumentation. This enabled the use of the Campbell Scientific TDR100 system to measure the water contents in the materials which may become saline. The system measures volumetric water contents and electrical conductivity of the material simultaneously. Three TDR probes (P) were installed in one trench of the four treatments, at depths of 0.15 m, 0.5 m and 1.2 m (Figures 3.4 to 3.7):

- P1 – the topsoil covering the sludge (0.15 m);
- P2 – within the sludge material (0.5 m) and
- P3 – below the sludge (1.2 m).

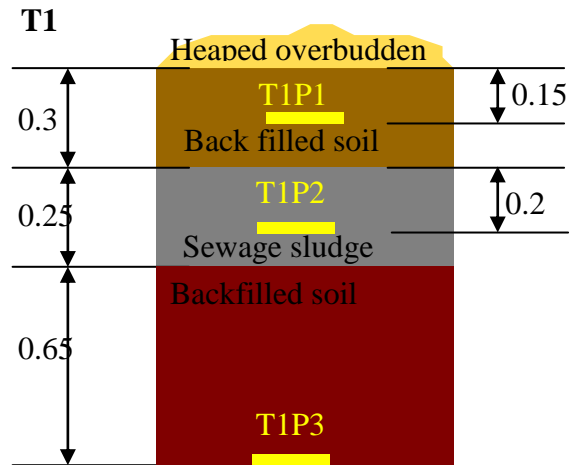


Figure 3.4 Schematic layout of TDR probes in T1 (Dimensions in m)

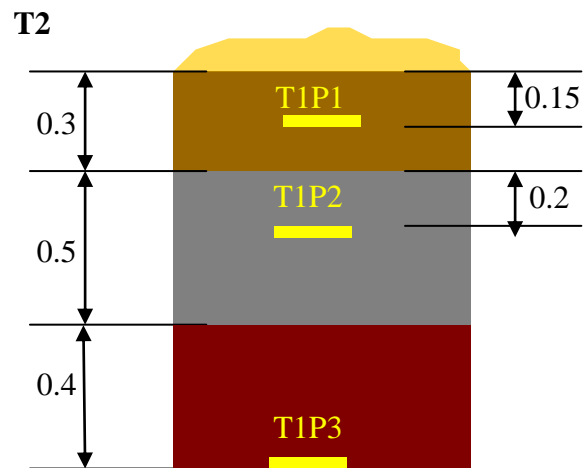


Figure 3.5 Schematic layout of TDR probes in T2 (Dimensions in m)

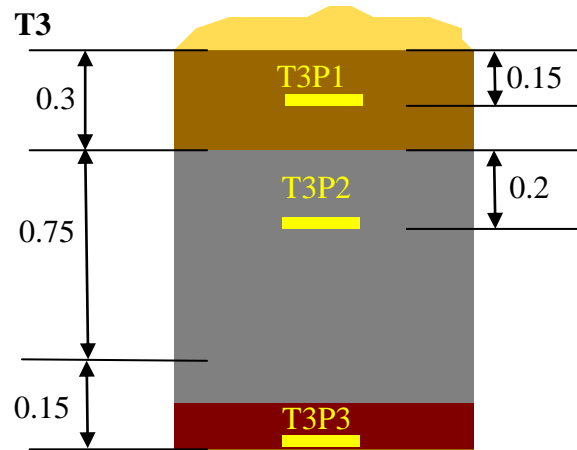


Figure 3.6 Schematic layout of TDR probes in T3 (Dimensions in m)

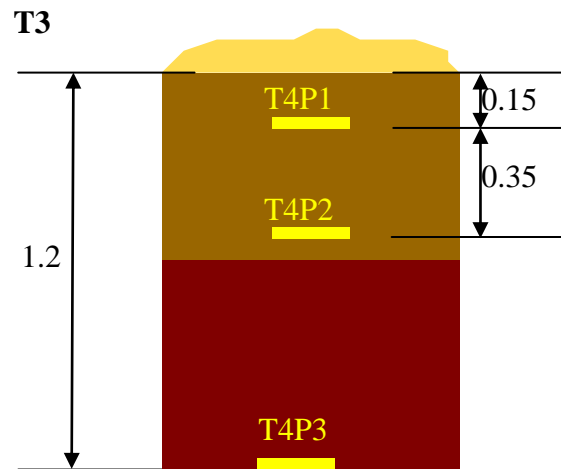


Figure 3.7 Schematic layout of TDR probes in T4 (Dimensions in m)

Full Stops were used to detect wetting front at predetermined depths to collect water samples after rain events for nutrient analysis. They comprise a specially shaped funnel, a filter and a float mechanism. The funnel is buried in the soil within the root zone of the plants or crop. When rain falls or the soil is irrigated, water moves downwards through the root zone. The water gets focused inside the funnel and the soil at the base becomes so wet that water seeps out of it, passes through a filter, and is collected in a reservoir (Stirzaker 2003). This water activates a float mechanism, which, in turn, operates an indicator flag above the soil surface. There are no wires, no electronics and no batteries. The red funnel part is buried in the soil, with the black tube protruding above the soil surface (Figure 3.10). When a wetting front reaches the detector, an indicator pops up. Detectors are usually placed in pairs, one shallow and the other deep

(Figure 3.8). Water collected in the funnel is extracted via a tube, using a syringe. In each of the four treatments, two WFD were installed in a trench at a depth 0.5 m, lying within the trenched WWTW sludge material, and 1.2 m, which is beneath the sludge.



Figure 3.8 Wetting Front Detector installation in trench at SAPPI

The piezometer provides a means to sample the hydraulic head at a point in the saturated zone and to measure the pressure head at a point. The elevation of water in the piezometer provides a measure of the hydraulic head $h(P)$. The borehole and piezometers also enable the sampling of water at different times for water quality analysis. At the SAPPI WWTW sludge burial site, two boreholes were constructed, up-gradient (BH1) (4 m) and down-gradient (BH2) (15 m), between the experimental plot and the nearby stream. Five piezometers were installed at the bottom left corner of each treatment and two between the stream and the experimental plot, denoted as SP1, SP2, SP3, SP4, SP5, SP6 and SP7. The average depth of the installed piezometers ranges from 2.5 to 3 m.

3.1.2 Trench layout and instrumentation at the Umlazi site

The Umlazi E ponds site has approximately 800 m³ of pit latrine sludge buried in 20 trenches. Ground water monitoring equipment and boreholes were installed, and ground water samples were taken on a monthly basis. About 250 trees (Eucalyptus and wattles) were planted. Core samples of buried sludge were collected and analyzed for NO₃ and P concentrations. The trench layout at the Umlazi VIP sludge burial site is shown in Figure 3.9 and Figure 3.10.

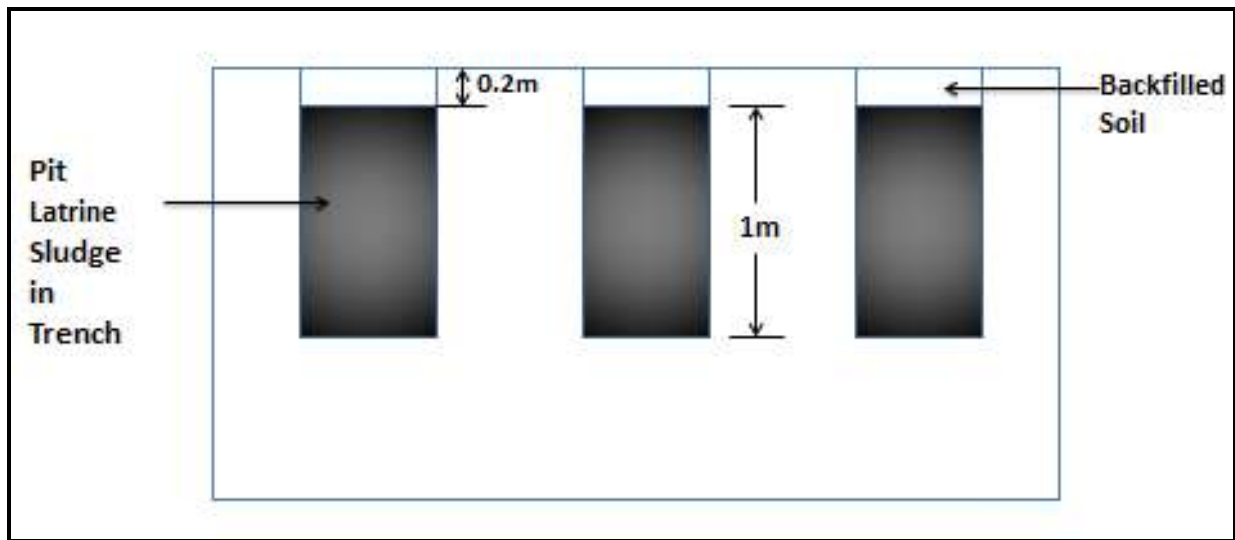


Figure 3.9 Trench layout at the Umlazi sludge burial site



Figure 3.10 Umlazi VIP sludge trenching in progress

The following instrumentation was installed at the Umlazi VIP sludge trenching site:

- Watermark sensors (soil water tension automatic recording at various depths (Umlazi_WM_01, Umlazi_WM_02);
- Wetting front detectors (WFD) (UEP3- 200mm, UEP3-300mm, UEP3- 500mm, UEP3-800mm) and
- Piezometers (near surface water levels and sampling) (UEP1, UEP2, UEP3, UEP4 and UEP5) (Figure 3.11).



Figure 3.11 Location of piezometer/Wetting Front Detector (WFD) at the Umlazi sites

In addition, five monitoring deep sampling boreholes (15 - 20 m) were established between the trenching site and the river, BH1, BH2, BH3, BH4 and BH5 (Figure 3.12).



Figure 3.12 Location of boreholes at Umlazi



Figure 3.13 Installation of wetting front monitors (left) and monitoring of piezometers (right)

Samples from the five background monitoring boreholes were taken every 1-2 months. The depth to the water table at each well was recorded and twice the volume of the standing water within the well was purged, prior to water sampling to ensure that the sample was representative of the ground-water around the well, rather than of the water standing in the well, with the use of a water bailer.

A reliable ground water sampling procedure is very important in order to ensure that all groundwater quality data collected are representative of the aquifer layer. The collection of groundwater samples from the boreholes followed four main steps namely; field sampling equipment preparation, measuring of water level in boreholes, purging the boreholes and collecting and delivering the water samples to the laboratory for analysis. The measurements of water level in each of the five boreholes were the first exercise performed. This was an important exercise because it provided an estimate of the volume of water that should be purged and can be used in calculating groundwater flow directions and seasonal changes of the aquifer layer (Weaver *et al*, 2007). A dip meter was used in measuring the water level in each of the five boreholes. The dip meter was made up of a twin core cable and an ohm meter. The end of each cable is bared to avoid contacts. At the top end of the cable, an ohm meter is connected when the other end of the cable is immersed in the water, causing a deflection on the ohm meter. The length of the cable from the cap of the borehole to the end that made contact with the water in the borehole was then measured using a measuring tape. This gives the static depth to water level in the borehole. The standing/stagnant volume of water in the borehole can then be calculated. This is calculated using the equation given below;

$$V = \frac{\Pi \times d^2 \times h}{4000} \quad 3.1$$

Where;

V = Volume of standing/stagnant water in litres

d = Diameter of borehole in millimeters

h = Height of water column in meters

The height of water column is calculated as; Borehole depth – static depth to water level.

Purging of boreholes is an important exercise required to be carried out before groundwater sample can be collected. This was done in order to remove any stagnant water in the borehole casings and ensured that ground water samples collected originated from the aquifer layer. In practice, borehole purging generally involves pumping out sufficient amount of water from a borehole until field parameters such as pH, electrical conductivity, dissolved oxygen, temperature and turbidity becomes stabilized. pH, temperature and electrical conductivity were the three field parameter considered during the purging of the five boreholes at the Umlazi sludge burial site. The readings of the field parameters during the purging exercise are taken and logged at different time interval and are recorded. It is necessary that water sample from boreholes be collected within six hours after purging of boreholes have been done (Weaver *et al*, 2007). Samples from boreholes at the Umlazi sludge burial site were collected immediately after purging. The valve on the pump was lowered after purging before samples were taken so that water will flow slowly without aeration. Sample bottles were properly labeled and used to collect water samples. Samples are then placed in the cooler box containing ice blocks and then transported to laboratory where specific analysis were carried out.

Samples were analysed for nitrate, phosphorus, pH and electrical conductivity. The Hach Model DR/2010 Spectrophotometer was used to analyse the nitrate and phosphorus concentration in the water samples from the piezometers and WFD's, as well as the borehole samples of 20 July 2011. Unfortunately, the WaterMarks and wetting front detectors were destroyed in the early stages of the study. Due to an inundation of leaked water from a local main and the fact that the wetting front detectors required burial simultaneously with the sludge disposal, these instruments were not replaced. Water samples were collected from the piezometers on one occasion and thereafter were found dry. The stream was also sampled during the monitoring period. Rainfall, temperature, relative humidity and solar radiation measurements were obtained from the nearest weather station (Data for station [0240808A2]-Durban South AWS -29.9650 30.9460) from the South Africa Weather Services for computation of time variable conditions for modelling.

3.2 Geophysical Electrical Resistivity Tomography (ERT) Characterisation

The purpose of the electrical survey is to determine the resistivity distribution of the subsurface, by making measurements on the surface (Loke, 2000). This method provides insight into the subsurface structure, without affecting or even destroying it. In addition, ERT also allows for the possibility of determining aquifer parameters, such as transmissivity (Srinivas and Singhal, 1985) or hydraulic conductivity (Kemna *et al.*, 2002). A further possibility is to monitor a tracer experiment with ERT, to improve the understanding of water and solute movement in the ground water body or in the unsaturated zone (White, 1988; Battle-Aguilar *et al.*, 2004; Kemna *et al.*, 2002). The ERT survey is one of the geophysical techniques which has also proved able to identify soils, geological and hydrogeological features. This technique was used in the SAPPI WWTW and Umlazi VIP sludge trenching research sites. The ERT technique is a 2D electrical imaging system which reveals in-homogeneities in a porous medium, from which soils and geological features can be deduced. It is carried out by the use of a number of electrodes connected to a multi-core cable (Griffiths and Barker, 1996).

The ABEM Lund Imaging System together with a Terrameter SAS 1000 was used on site for data acquisition. The Lund system consists of a basic charging unit, Electrode Selector ES10-64; four Lund spread cables, a suitable quantity of cable joints and cable jumpers, a supply of electrodes (ABEM, 2005), as shown in Figure 3.14. The quantity of cables joints and cable jumpers depending on survey type, depth and length of profile under investigation.



Figure 3.14 Terrameter SAS 1000 instrument and Probe

GPS readings were also taken every 10 m along this transect, using the Trimble differential GPS to allow for the topographical rectification of the ERT data.

ERT surveys were conducted in eight transects at the SAPPI trenching site using the Wenner Long and Wenner Short protocols with an electrode spacing of 0.5 m or 1 m. This spacing enables the resistivity modelling of near-surface profiles since the depth of the trenches are 1.2m. The deep surveys included a long transect along the entire length of the site (Transect A-B), as well as transects adjacent to each of the two boreholes (BH1 and BH2). Shallower surveys were conducted at the two piezometers on the lower slope (SP6 and SP7) and along the short transect intersecting the trenches for each of the four trenched treatments (T1, T2/T3 combined and T4). The transects surveyed are shown in Figure 3.15. The topsoil at the site was generally moist and offered good contact with the electrodes. Occasionally, water was poured over the soil, to improve electrode contact with the soil. Due to a cable malfunction, some electrode positions had to be excluded, when measuring at several stations during the survey. Later in the trial, ERT surveys were concluded on the lower end of the trial area to confirm the across-slope connectivity of groundwater sources. Umlazi ERT transects surveyed with the same method as SAPPI are presented alongside the results in the next chapter.

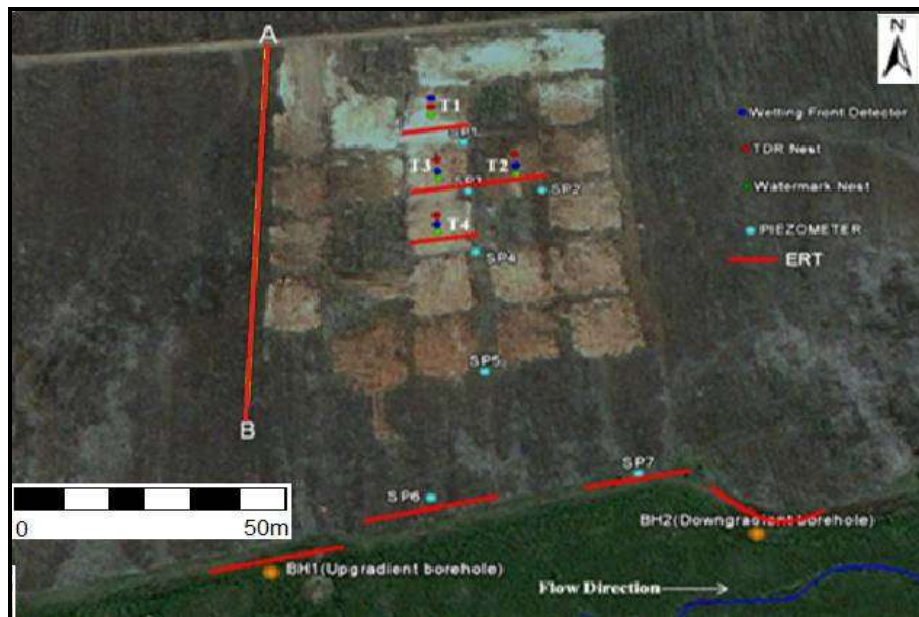


Figure 3.15 Map of ERT transects, boreholes, piezometers and soil water sensing nests at the SAPPI Shafton sludge burial site (Google Earth image 23-Dec-2010)

3.3 Soil Hydraulic Characterization

An accurate knowledge of hydraulic properties for unsaturated soils is critical in addressing problems in a variety of disciplines, such as hydrology, ecology, environmental sciences, soil science and agriculture. The characterization of soils and the vadose zone includes the estimation of the soil water retention and unsaturated hydraulic conductivity relations over a wide range of volumetric water content values. Although occasionally only specific data points are needed, parametric models for both hydraulic properties are preferred. The demand for these expressions is driven by their use in numerical models for simulating fluid flow and mass transport.

3.3.1 SAPPI site

At the SAPPI WWTW sludge trenching sites, hydraulic properties were estimated for soils in the trenches of all the treatments. The measured parameters include bulk density and soil particle size distribution (percent fraction of sand, silt and clay), which were used to predict the van Genuchten parameters (α , n , L), using the Rosetta program based on USDA textural class. The saturated hydraulic conductivity was also measured in the field. These data were used as input for the Hydrus-2D model, to analyze the movement of water, nitrate and phosphorus in the soil. Four undisturbed samples were collected by hammering a 5-cm diameter steel coring rings by at depths 0-30 cm, 30-60 cm, 60-90 cm, and 90-150 cm, in order to determine the soil hydraulic characteristics for the soil profile. These depths were where chosen because soil survey at site indicates uniformity of profiles within these ranges. Another set of undisturbed soil samples and sludge collected and were collected and taken to the laboratory, where the standard Hydrometer method (Gee and Baunder, 1986) was used to determine the particle size distribution. This was to determine the quantity of each of the main sand, silt and clay percent fractions in samples of the soil. The four undisturbed soil samples from each treatment (T1, T2, T3 and T4) at depth intervals of 0-30, 30-60, 60-90, and 90-150, were used to determine the soil water retention curve at 2, 5, 10, 20, 50, 100, 200, 500, 1000, 1500 kPa, using the controlled outflow cell and pressure plate extractor. Results are shown in Appendix B. The most sensitive parameter to model water flow is the saturated hydraulic conductivity (K_s). To determine this parameter, two commonly-used methods were used, the soil infiltration rates (cm/h) were determined under

saturated conditions at depths of 0-30 cm, 30-60 cm, 60-90 cm and 90-150 cm, using the double ring method (*in situ*) for T3 and T4 and the Guelph permeameter test for T1 and T2.



Figure 3.16 Double ring infiltrometer (left) and Guelph permeameter test at SAPPI

3.3.2 Umlazi site

The characterisation of the material in the disposal zone was also carried out at the Umlazi VIP trenching site, to quantify the fluxes associated with water ingress, uptake and distribution, as well as contaminant movement. This data was also used as input for the Hydrus-2D model to analyse the movement of water and dissolved compounds in the soil. The characterizations of material included:

- Particle size distribution;
- Hydraulic conductivity and
- Water retention.

Representative examples are given of the outcomes of the experiments in this section and the rest of the results are shown in the Appendix B. In this section, a short overview is given of the set-up of the activities to collect the soil hydraulic parameters for the site in Umlazi, including field measurements and laboratory work. In Figure 3.17 below, the Umlazi measurement site is shown, with a sketch of the measurements and sampling points. The blue lines in the picture show the trenches. The general objective of the distribution of the measurement points (yellow

dots), is to have 5 points for surface measurements covering the area (No. 1 to 5), 5 points on top of the filled trenches (No. 6 to 10) and 2 locations for measurements at different depths (No. 11 and 12). The depths that are assessed are 10, 20, 40, 60, 80, 100 and 150 cm. GPS coordinates were taken at every location, but the accuracy is not sufficient to pinpoint the locations on site. In-situ measurements were made at five surface points in the survey area (yellow dots 1-5), five points on top of the filled trenches (yellow dots 6-10) and two locations for measurements at different depths (yellow dots 11-12).

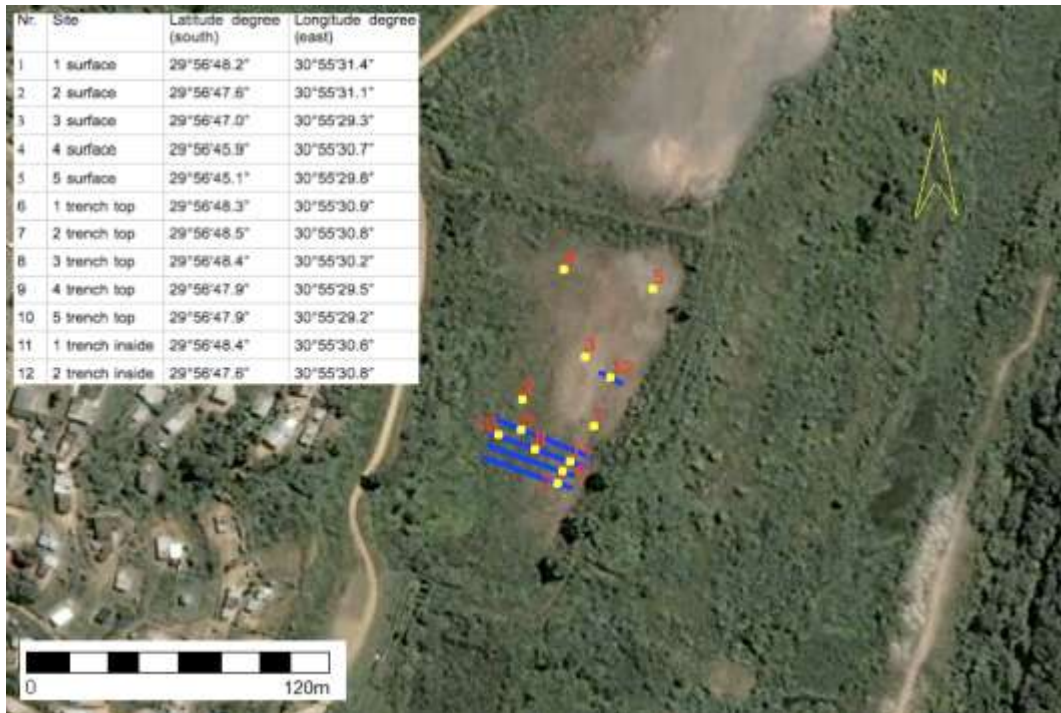


Figure 3.17 Sketch of the site at Umlazi, with indication of trenches and measurement spots

At every location, a standard procedure was followed (Lorentz, 2001): tension infiltrometer measurements were done in duplicate, followed by a double ring infiltrometer measurement in duplicate on the same spot. Thereafter, the rings were removed and undisturbed soil samples were taken of the material beneath the measurement location. In addition, at each duplicate location, one disturbed sample was taken of the soil condition before the measurement and one undisturbed sample after the tension infiltrometer measurement. These two samples were to give the initial and final water content needed for the unsaturated hydraulic conductivity analysis. The

undisturbed sample was also be used to determine the water retention characteristic in the laboratory. A particle size distribution experiment was done with part of the disturbed sample. The hydraulic conductivity data was collected and analysed, initially using the Ankeny method (Ankeny *et al.*, 1991). The particle size distribution analysis was also done for all the samples. Table 3.1 shows the locations and the types of measurements performed at the Umlazi site.

Table 3.1 Locations of Soil Characteristic Measurements at the Umlazi site

No.	Site	Depths (cm)	Particle Size	K _{sat}	K _{unsat}	Water Retention
1	1 surface	0	•	•	•	
2	2 surface	0		•	•	
3	3 surface	0		•	•	
4	4 surface	0		•	•	
5	5 surface	0		•	•	
6	1 trench top	0	•	•	•	
7	2 trench top	0		•	•	
8	3 trench top	0	•	•	•	
9	4 trench top	0	•	•	•	
10	5 trench top	0	•	•	•	
11	Trench 1	0				
		10		•	•	
		20	•			
		40				
		60	•			
		150		•	•	
12	Trench 2	0				
		10		•	•	
		20		•	•	•
		40		•	•	•
		60		•	•	
		80		•	•	•
		100		•	•	

3.4 HYDRUS Application

3.4.1 SAPPI

Simulation of water and solute movement was performed at two scales at the SAPPI site. At the local scale the water balance of the trenches was simulated using the HYDRUS-2D model and at the hillslope scale, the mass loading from the near surface was estimated using Darcy's law for saturated flow. Local scale observations at each trench type comprised soil water content and capillary pressure dynamics; collection of infiltrated water and subsequent analysis for nitrates and phosphorus, as well as observations of accumulation of water and solutes at the soil/bedrock interface through piezometer and boreholes. The water content dynamic record was used to inform the water balance simulations, while the nitrate and phosphorus concentrations of water collected within the profiles was used to inform the simulation of nutrient fluxes.

The material characteristics, the soil water and solute dynamics time series were analysed to develop parameters for simulation and calibration of the soil water and solutes. The soil hydraulic characteristics measurements were used to predict the van Genuchten parameters (α , n , L), using the Rosetta program which is used for estimating the hydraulic properties of soil. These predictions were modified during the Hydrus-2D modelling to accurately predict the variability of observed water content and nitrate and phosphorus concentrations in the soil. From these simulations the soil water fluxes of evaporation, transpiration, drainage and the solute migration fluxes were quantified for each site. A historic time series of meteorological data could be used to simulate beyond the monitoring period in order to assess the impact of wet and dry periods as well as extreme events.

The depths of soil layers in the trenches of each treatment were 0-30, 30-60, 60-90, 90-150 cm; but with variation inside the trenches of each treatment with the introduction of sewage sludge of different depths. The boundary conditions used for each cross-section were atmospheric boundary condition at the surface, free drainage boundary condition at the bottom and no-flux boundary condition at the right and left sides (Figure 5.1). To run the simulation in HYDRUS 2-D, observation points were placed at points 0.15 m, 0.5 m and 1.2 m within the trench (Figure

5.2) in order to compare the simulation and the observation at that point. These were the same positions where TDR probes have been placed for volumetric water content reading in a trench in each treatment. Wetting front detectors located at 0.5 m and 1.2 m also collected samples for nitrate and phosphorus analysis. The initial condition of nitrate and phosphorus transport at the beginning of the simulation (1 January 2010) for each cross-section were assigned using measured nitrate (357 mg/l) and phosphorus (23 mg/l) concentrations from samples collected from wetting front detectors installed in the sludge. The constructed finite element mesh with the selected boundary and initial conditions were used to simulate water flow, nitrate and phosphorus transport. In addition to precipitation, the potential evaporation and the potential transpiration were required for model application. Daily potential evapotranspiration rates were calculated with the ACRU model (Smithers *et al.*, 2002), to derive the time variable boundary condition (see Appendix E), using data from the nearby weather station near the SAPPI site. A crop factor was applied by choosing the vegetation “Forested e.g. wattle trees” in the ACRU model to account for crop factor.

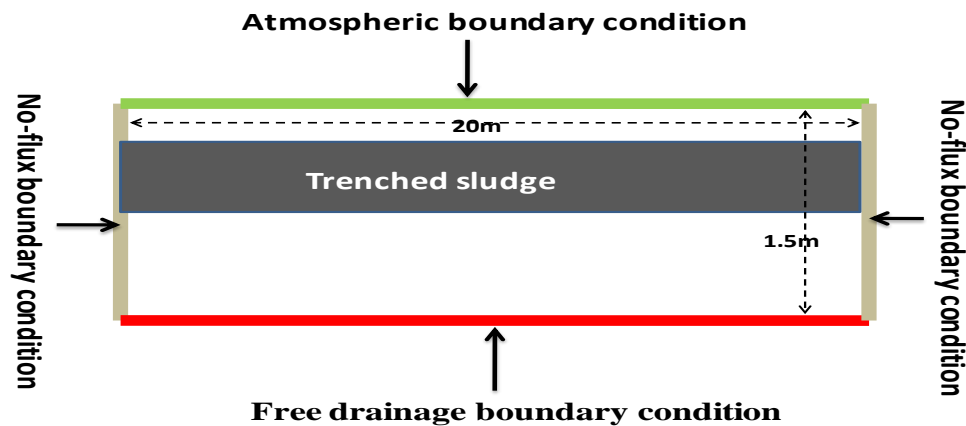


Figure 3.18 Conceptual model and boundary conditions for SAPPI

3.4.2 Umlazi

At the Umlazi VIP sludge trenching site a two-dimensional finite element grid was generated for a subsurface cross-section between the trench site and the stream, using the HYDRUS-2D

model. ERT profiles were applied to define the spatial dimensions of the outer boundary, as well as the distribution of different soil materials and the geological layout of the subsurface. Schematic cross sections of the subsurface, showing the trenches, stream and boundary condition, are shown in Figure 3.19. Crucial for the model application is the setting of reasonable boundary conditions. Three groups of input variables were used to model soil water and nutrient fluxes:

- Initial conditions for topography, hydrologic characteristics of the soil materials, distribution of hydraulic head and location and concentration of solutes;
- Boundary conditions describing the rules that govern the movement of water into and out of the perimeter of the modelled area and
- Time-dependent conditions, including changing rainfall and vegetation water-use rates are model characteristics that influence the time-step selection and the iterative process used to evaluate groundwater and solute movement over the duration of the model run time.

Daily potential evaporation and transpiration rates were estimated, based on temperature and humidity data from the nearby weather station, using the ACRU model, to derive the time variable boundary conditions used in the simulation. Initial concentrations of solutes (nitrate and phosphorus), were set at zero in the whole domain and only the sludge application area was set at a uniform value of 581 mg/l nitrate and 225 gm/l phosphorus, based on measurements of the leachates collected in WFD's installed in the trenches, with the HACH spectrophotometer instrument. The minimum permissible soil potential at the surface, input as a constant value to restrict soil water evaporation when the soil surface becomes dry, was set at 15000 cm. Every triangle (or element) in the finite element space was formed by three nodes. On the boundary, these nodes were set with specific water flux and solute transport conditions. The light green boundary indicates an atmospheric boundary condition which allows precipitation as in-flux and actual evapotranspiration as out-flux (Figure 3.19). The dark green boundary at the stream is a seepage face that allows water to leave the profile, when positive water pressures develop at this boundary. Because these boundary conditions assume unhindered outflow, it could not be assigned to the entire vertical side, or the profile would have drained completely. In reality, water backs up on the fractured crystalline bedrock. To imitate this process, a constant flux boundary

condition was applied that enabled outflow at the bottom. Because crystalline bedrock has small porosity (between 0-10 %, according to Ward and Robinson, 2000) and small coefficients of hydraulic conductivity (between 0-8.64 cm/day) the applied fluxes were set at 0.9 cm/d. In order to observe the simulated pressure heads, water content and nutrient concentrations, three observation points were positioned in the grid at selected positions in the profile.

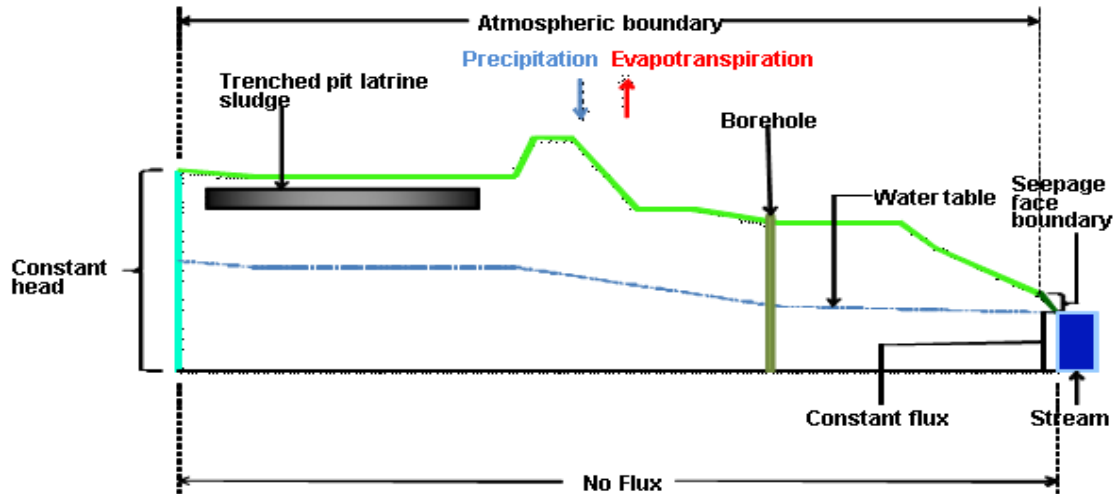


Figure 3.19 Conceptual model and boundary conditions for Umlazi

3.5 Monitoring and Analysis

Piezometers were monitored at regular intervals for the collection of water samples for analysis. It was observed that piezometers SP1 to SP5 were not able to collect any water samples during the monitoring period. This may possibly be due to the location of these piezometers on rocks at a depth of 2.2 m, resulting in the quick lateral flow of water after a rainfall event. Piezometers SP6 and SP7, which were located outside the treatment area, collected samples during the rainy season. Groundwater depths in the boreholes (BH1 and BH2) were monitored and water samples collected for analysis. Samples were collected from the installed WFD when available, especially during the wet season. The stream was also sampled at regular intervals during the monitoring period. The volumetric water content within the trench of each treatment was measured by roaming method by means of PCTDR software on a laptop at least once a month during the dry season, and once a week during the wet season. Rainfall, temperature, relative humidity and solar

radiation measurements for the SAPPI site were downloaded from the weather station located at the SAPPI airstrip located 800 m from the site for computation of time variable conditions for modelling . The water samples were analysed for the following:

- **^2H and ^{18}O Isotopes** - The stable isotope ratios of hydrogen and oxygen in natural waters (^2H and ^{18}O) were measured for water samples collected from boreholes, stream and piezometers at SAPPI, using the spectroscopic instrument, LGR DLT-100 at the School of Agricultural Earth and Environmental Sciences (Figure 3.20).

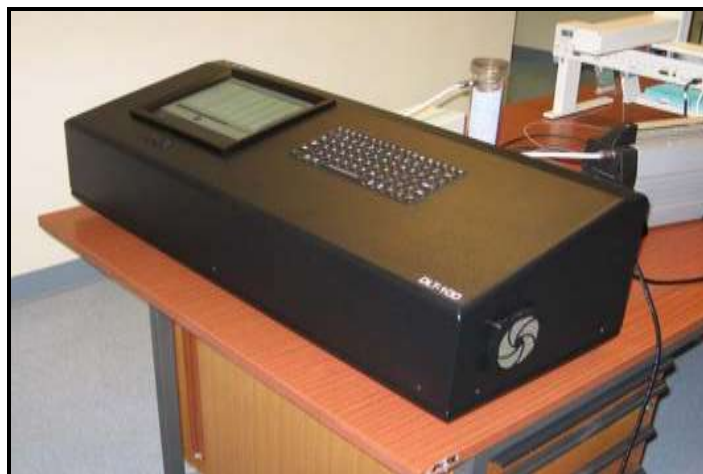


Figure 3.20 Spectroscopic instrument LGR DLT-100.

The standard for hydrogen and oxygen stable isotopes is VSMOW (Vienna Standard Mean Ocean Water) is maintained, distributed, and calibrated with great care by the authorities of the Section of Isotope Hydrology, International Atomic Energy Agency (IAEA) in Vienna. Lippmann *et al.* (1999). The hydrogen and oxygen isotope of water varies in time and space because fractionation of isotopes occurs in the natural environment. Isotope fractionation is accompanied by a variety of processes, such as phase change, transportation, diffusion, reduction, oxidation, chemical reaction and biological metamorphism. Environmental isotopes now routinely contribute to such investigations, complementing geochemistry and physical hydrogeology. Meteoric processes, for instance, modify the stable isotopic composition of water, and so the recharge waters in a particular environment will have a characteristic isotopic signature. This signature then serves as a natural tracer for the provenance of groundwater.

Assessing the abundance of isotopes in water, solutes and solids, tells us about ground water quality, geochemical evolution, recharge processes, rock-water interaction, the origin of salinity and contaminant processes, but in this case only stable isotopes of water were used;

- **Nitrate (NO₃) and Phosphorus (P)** - The Hach Model DR/2010 spectrophotometer was used to analyze the nitrate and phosphorus concentration in the water samples collected from the SAPPI and the Umlazi sites, which were transported to the laboratory. The HACH instrument was calibrated to convert measured nitrate of nitrogen (NO₃-N) to nitrate (NO₃) and orthophosphate to phosphorus (P) as follow.

For Nitrate test, 25 ml sample and 25 ml blank (deionized water) are prepared by adding Nitra Ver 5 Nitrate reagent in each of them. The blank is used to Zero calibrate the instrument. For phosphorus test, 25 ml sample is prepared by adding only phos Ver 3 phosphorus reagent and 25 ml of blank containing only deionized water. Entering for both tests the concentration values in mg/l of nitrate and phosphorus for prepared samples are measured and digitally displayed. To make a standard solution of 100 mg/l P required:

- 1 litre volumetric flask
- 0.439 g of KH₂PO₄

0.439 g of KH₂PO₄ was measured on a three decimal scale and poured into the 1 litre volumetric flask. The flask was then filled to the mark with distilled water and shaken.

For the calibration of the HACH spectrometer standard concentrations of P were made starting from 0.1 mg/l up to 0.8 mg/l in 0.1 mg/l increments. The results are shown in Table in Appendix B and the Figure 3.21 shows the calibration curve. To make a standard solution of 100 mg/l NO₃⁻ required:

- 1 litre volumetric flask
- 0.163 g of KNO₃

0.163 g of KNO₃ was measured on a three decimal scale and poured into the 1 litre volumetric flask. The flask was then filled to the mark with distilled water and shaken.

For the calibration of the HACH spectrophotometer standard concentrations of NO₃ were made of 2 mg/l, 5 mg/l, 10 mg/l, 20 mg/l, and 30 mg/l. The results are shown in Table in Appendix B and the Figure 3.21 shows the calibration curve.

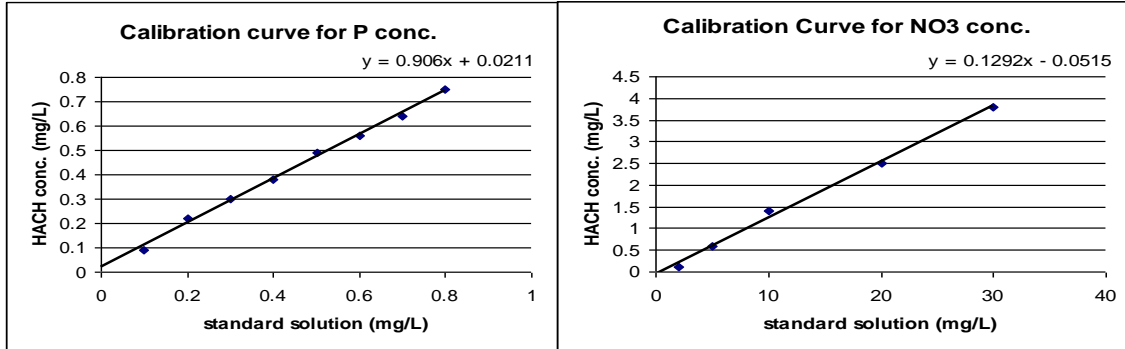


Figure 3.21 Calibration curve for P (left) and NO₃ (right)

- **Electrical Conductivity (EC)** - Electrical conductivity is an important indicator for water quality assessment. Electrical conductivity (EC) estimates the amount of total dissolved salts (TDS), the total amount of dissolved ions, in the water. The HANNA instrument was used in measuring EC for water samples collected from piezometers, boreholes and stream. There are a number of sources of pollutants, which may be signal by increased EC, e.g. wastewater from sewage treatment plants (point source pollutants).
- **pH** –The measurement of pH is carried out to determine the acid balance of the water on a scale of 1 (strongly acidic) to 14 (strongly alkaline). Ideally, pH was measured in the field at the time of sampling, using the Crison portable Instrument. As portable pH meters are more accurate than indicator papers and relatively inexpensive, this is the recommended method of measuring pH. The operation of such a portable device needs to follow its specific manual, which usually also includes instructions for field calibration.
- **Oxidation Reduction Potential (ORP)** - Measurement of ORP is carried out to characterize the oxidation-reduction state of the water on a scale from approximately-300 mV (strongly reducing) up to +500 mV (strongly oxidizing). ORP was measured in the field at the time of sampling with the Crison instrument. Although the measurement of ORP is straightforward, interpretation is limited, due to interference from other factors. Therefore, the main application of this parameter is in recording significant changes in the redox potential.

4. RESULTS AND DISCUSSIONS

The monitoring and observation of ground water at the WWTW sludge trenching site at SAPPI and VIP sludge trenching site at Umlazi, were carried out during the period of January 2010 to September 2011. The results obtained from these observations are discussed in this chapter. They include the volumetric water content, nitrate and phosphorus concentrations in sampled groundwater, EC, pH, ORP, climatic conditions and the stable isotopes (^2H and ^{18}O) of sampled groundwater. During the observation period, the climatic conditions from January to April 2010 were wet, from May to September 2010 was a dry period, from October 2010 to April 2011 was another wet period and from May to September 2011 was a dry period, for both sites.

4.1 Electrical Resistivity Tomography (ERT) Survey

4.1.1 ERT at SAPPI site

Transect A-B, completed early in the trial (December 2009), reveals a top layer of 1-2 m, with low resistivity values ranging from 300 to 800 Ωm , suggesting a relatively moist soil (Figure 4.1). The layer below this has high resistivity values of up to 3000 Ωm , which vary laterally, suggesting weathered and fractured igneous or metamorphic bed-rock. The geology of the site from drilling report indicated a layer of shale followed by delorite. Below 10 m, the resistivity drops, suggesting the presence of a fractured aquifer or possibly delorite or a change in geology.

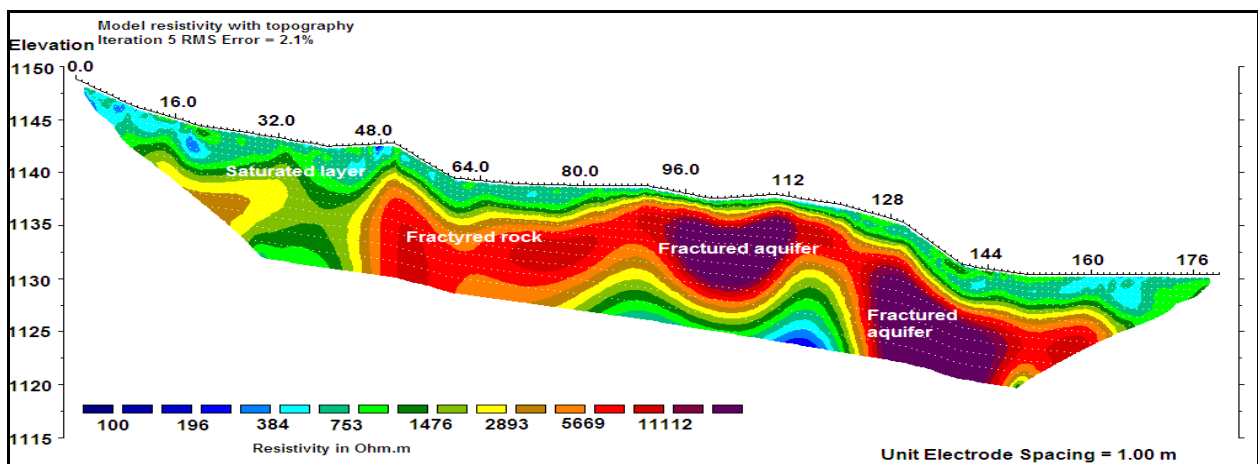


Figure 4.1 Transect A-B SAPPI Karkloof inverse resistivity model with topography

The study of a 60 m transect 5 m north of borehole BH1, indicated an igneous or metamorphic bed-rock on the eastern side (resistivity values $> 5000 \Omega.m$), with lower resistivity values on the western side ($<1000 \Omega.m$), suggesting relatively shallow, fractured and weathered bed-rock containing water (Figure 4.2). The drilling report indicated that borehole BH1 had 4 m of shale and loam, then 26 m of dolerite, showing more evidence of weathering than the transect near BH2. Observed groundwater depths in BH1 varied between 2 to 3.5 m, suggesting a shallow supply from the weathered shale, overlying the fractured dolerite in the west.

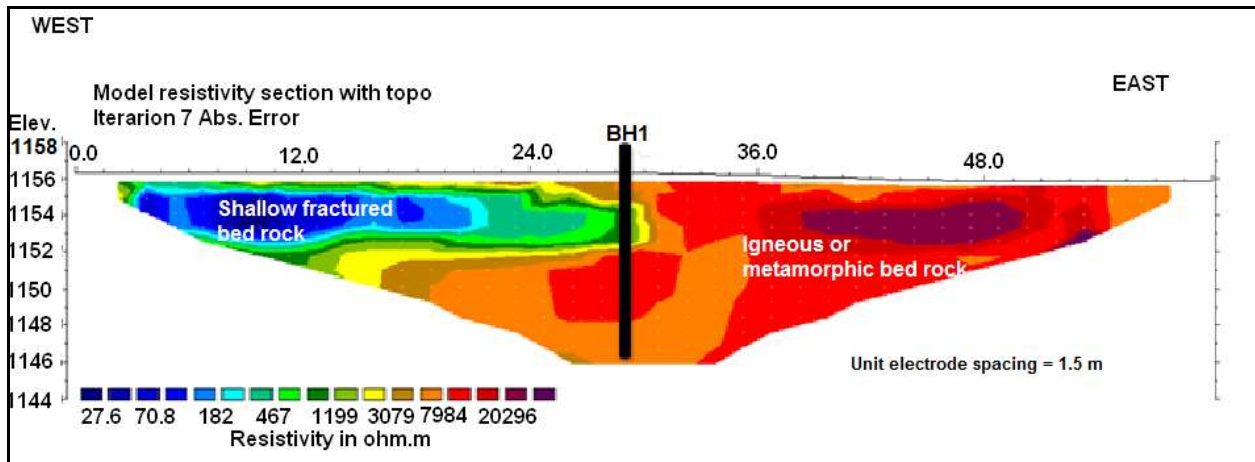


Figure 4.2 Resistivity for transect near Borehole BH1 (12-18 July 2011)

Near borehole BH2, the survey of a 60m transect, shown in Figure 4.3, indicated a layer of topsoil of 1 m in thickness (resistivity values ranging from $1000 \Omega.m$ to $5000 \Omega.m$) above a layer of igneous or metamorphic bed-rock (resistivity values $> 5000 \Omega.m$). At a depth of 10 m, resistivity decreased, suggesting the presence of an aquifer located in weathered bedrock or possibly a deposit of dolerite with correlation against boreholes (Figure 4.3). The drilling report indicated borehole BH2 had two meters of loam and 28 meters of dolerite. The average water depth in borehole BH2 was measured at 10 m, confirming a source in the fractured dolerite.

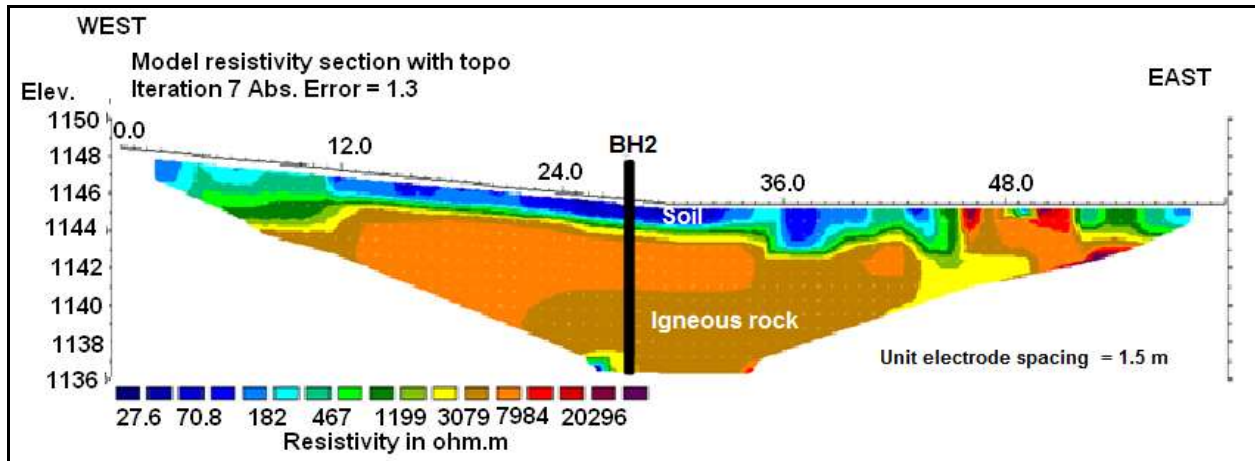


Figure 4.3 Resistivity for transect near Borehole BH2 (12-18 July 2011)

The first of the shallower surveys in June 2011 comprised a 40 m transect, surveyed on the northern side of the road at the downslope edge of the trial, near piezometer SP6 (Figure 4.4). This indicated a top layer of approximately 1 m to 2 m of topsoil, with resistivity values ranging from 1900 Ω .m to 5000 Ω .m above a layer 4 m in depth with lower resistivity (<300 Ω .m), indicating a water source in weathered material. Depths of water during the summer period at SP6 ranged between 1.3 and 2.8 m below the surface, confirming this as a zone of near-surface preferential flow.

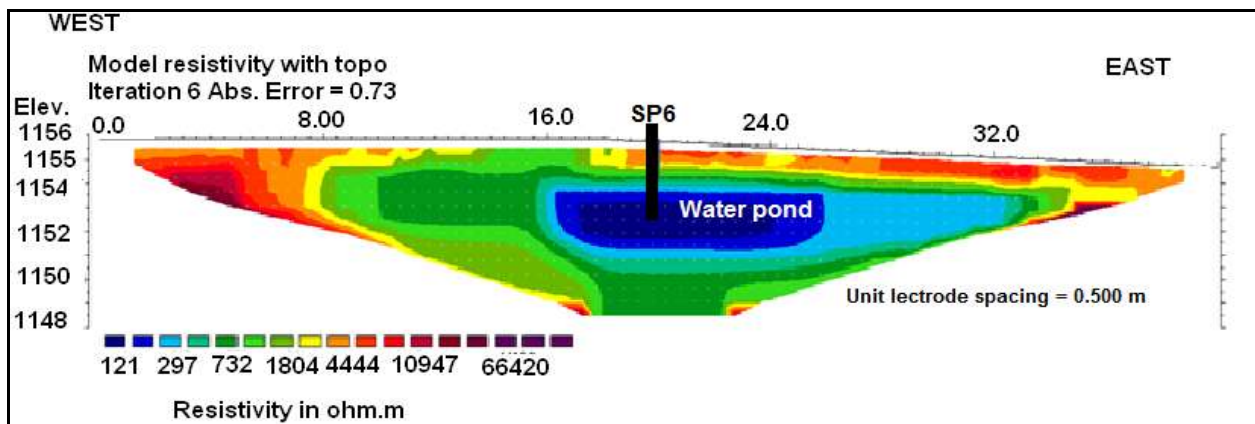


Figure 4.4 Resistivity for transect near piezometer SP6 (12-18 July 2011)

A transect on the northern side of the road, 5 m south of piezometer SP7, was also surveyed in June 2011 (Figure 4.5). The top 4 m showed resistivity values ranging between 2000 Ω .m and 5000 Ω .m, corresponding to soil with high clay content with a deeper layer showing high

resistivity values ($> 5000 \Omega.m$), suggesting igneous or metamorphic bed-rock, confirmed by evidence of outcrop at 4 m north of transect. Variations in resistivity in the near surface in this transect, also suggests the existence of a preferential pathway, which could conduct near-surface lateral flows rapidly during high rainfall events. Water levels observed during the summer at this location, varied between 2.3 and 2.8 m.

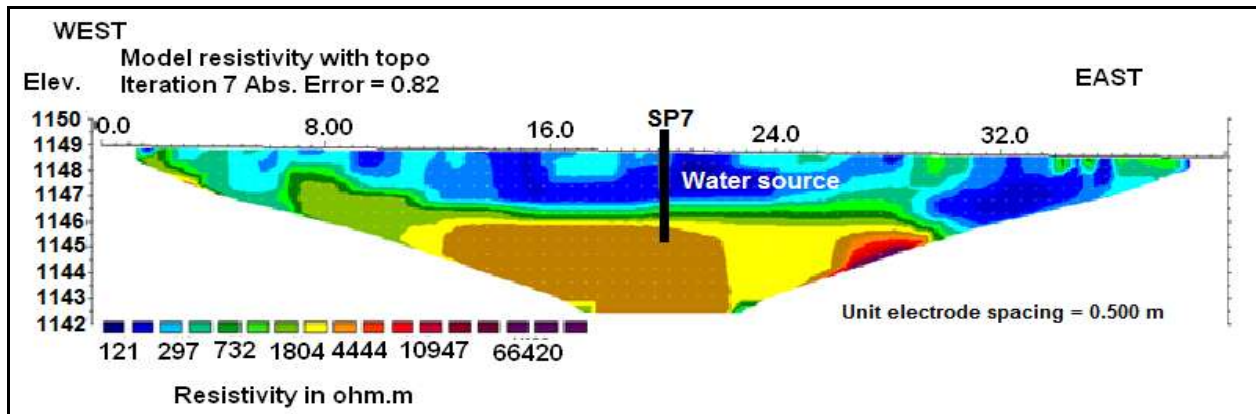


Figure 4.5 Resistivity for transect near piezometer SP7 (12-18 July 2011)

Surveys within the trial area were conducted, to assess the water distribution within and between the trenches. A 20 m transect surveyed in the Treatment 1 (T1) plot revealed high resistivity values ($>2500 \Omega.m$) in the trenches, contrasting with the more conductive layer of unsaturated soil ($<1000 \Omega.m$) adjacent to it (Figure 4.6). This could be attributed to the different bulk densities and water-holding capacities of the sludge and the native soil.

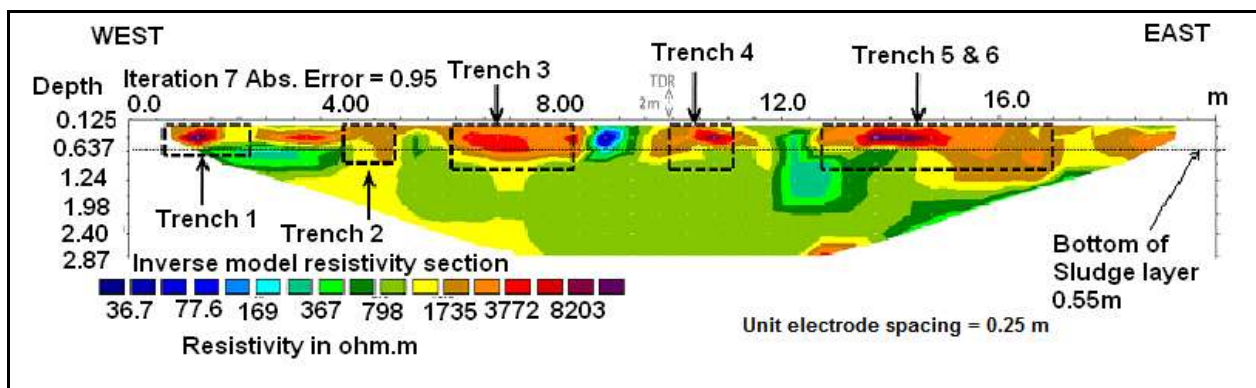


Figure 4.6 Resistivity for transect of T1 plot (12-18 July 2011)

A 55 m section transecting adjacent T2 and T3, a plot (and including the 10 m buffer between the plots) was surveyed. On the surface, the trenches had high resistivity values ($>2500 \Omega.m$), in contrast with the more conductive layer of the unsaturated soil between the trenches ($<1000 \Omega.m$) (Figure 4.7). However, the bottom of the trenches (1.2 m) was not as clearly defined in this survey as in the other treatment plots that were surveyed. This could have been caused by the presence of water in a layer between 0.7 m and 2 m. Between the treatments, below 2 m, the soil had a high resistivity of $<3000 \Omega.m$, suggesting dry conditions from the surface to a lower bed-rock. The data indicate that, although the trenches are dry at the time of this winter survey, sufficient moisture has been supplied to adjacent areas, possibly due to ingress through the trenched material in the summer.

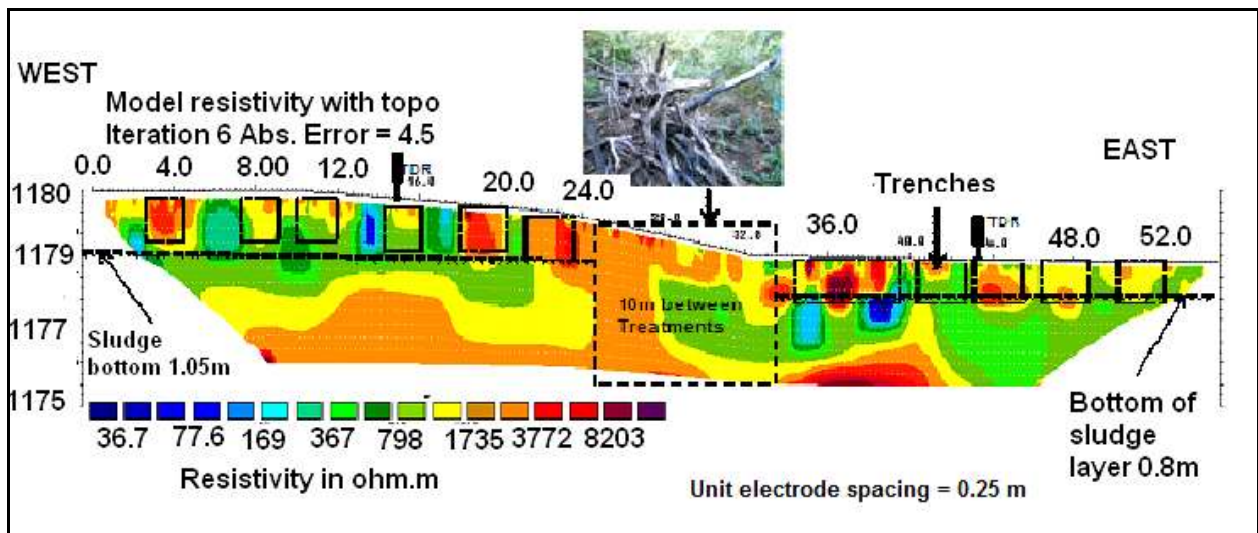


Figure 4.7 Resistivity for transect across T2 and T3 treatments (12-18 July 2011)

An ERT survey was conducted on a 20 m transect in the Treatment 4 (T4 plot). High resistivity values in the trenches ($>2500 \Omega.m$) contrasted with the more conductive layer of unsaturated soil ($<1000 \Omega.m$) between the trenches (Figure 4.8). Lower resistivity at a depth of 0.7 m to 1.7 m may have been caused by a hole 3 m north of the section that had been dug for soil sampling. Saturated hydraulic conductivity measurements were conducted in this hole leaving water in it prior to prior to ERT survey. This might have accounted for the lower resistivity recorded in that section.

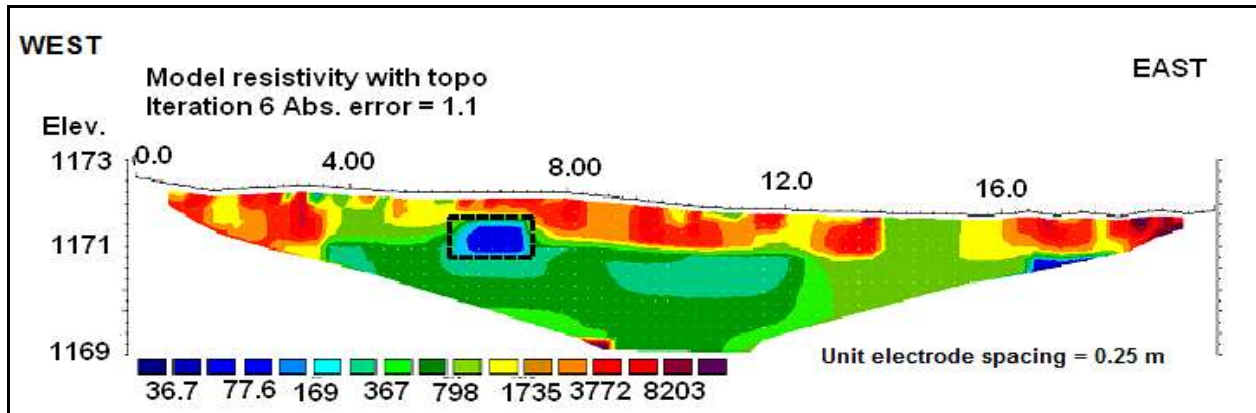


Figure 4.8 Resistivity for transect of T4 plot (12-18 July 2011)

This transects were selected to evaluate the changes in the entrenchment zone and also groundwater from directions outside the experimental area.

4.1.2 ERT at Umlazi site

Geophysical Electrical Resistivity Tomography (ERT) of the Umlazi burial site, across its long axis (transect 1), and of the ground between the burial site and the river (transect 2), was conducted in September 2008 before the trenching of the waste (Figure 4.9). A Wenner Long protocol, with 2m electrode spacing was used for transect 1 and both Wenner Long and Short with electrode spacing of 1.5 m was used for the transect 2 measurement, all without topographical corrections due to flat nature of terrain.

The first was 120 m long on the long axis of the deposition area, as shown in Figure 4.9, and the second, between the disposal site and the river, was 60 m long. The survey indicated a perched water table at about 2 m below surface, probably fed by the local hill-slope, with a shallow high resistivity zone at the northern end (Transect 1) (Figure 4.10). Electrical conductivity was found to be relatively low, indicating that salinity or EC could be used as a tracer after the application of the sludge, considering the porous nature of the soil.



Figure 4.9 Map of ERT transect at the Umlazi sludge burial site

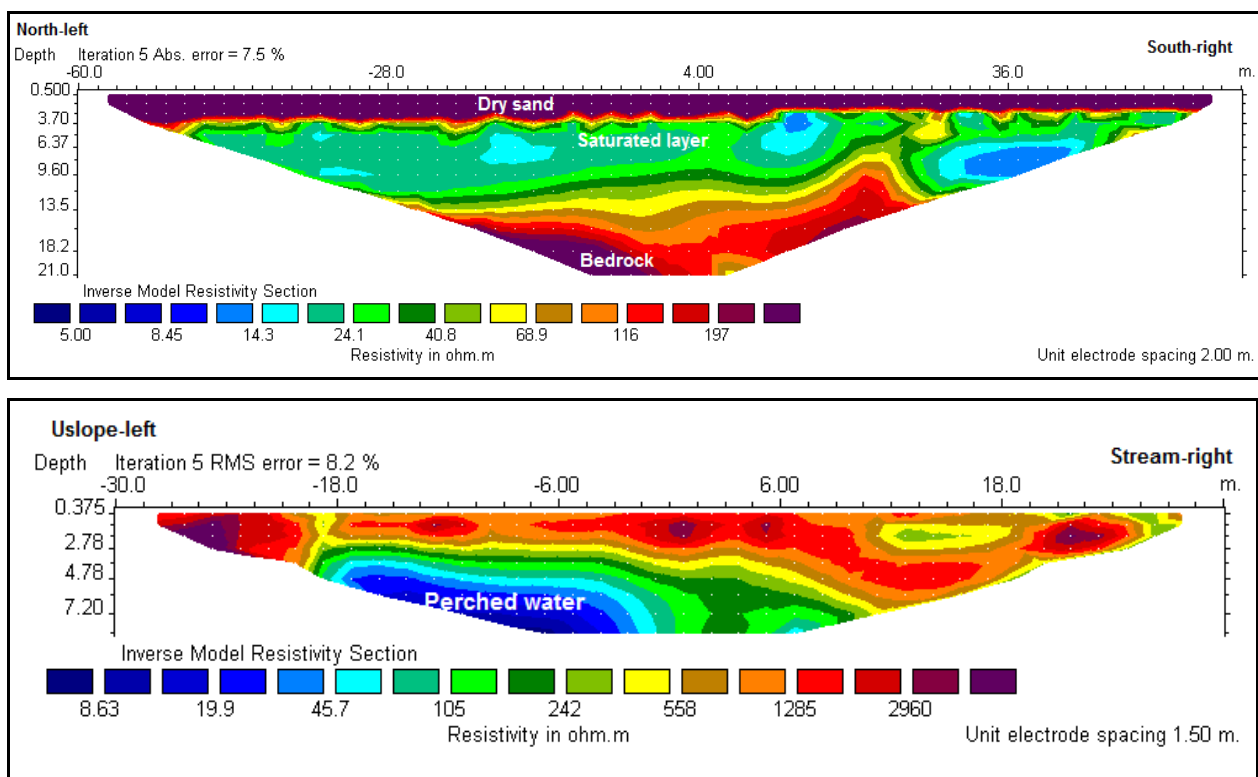


Figure 4.10 ERT Transects 1 (top) and Transect 2 (bottom) before trenching in 2008

Additional Geophysical Electrical Resistivity Tomography (ERT) survey was conducted on the embankment (Transect 1), one later in August, 2009 on the same (approximate) transect as the initial survey. The electrical resistivity distribution indicated a resistive layer of dry sand above a conductive saturated layer (aquifer) and a resistive bed-rock (Figure 4.11) as before the waste burial. However, the saturated layer was less conductive before entrenchment. The presence of the sludge entrenched above the saturated layer may have contributed to the change in resistivity distribution. The difference in the shapes of the layers was the result of the noise effect caused by the presence of wires, covering the planted trees after entrenchment.

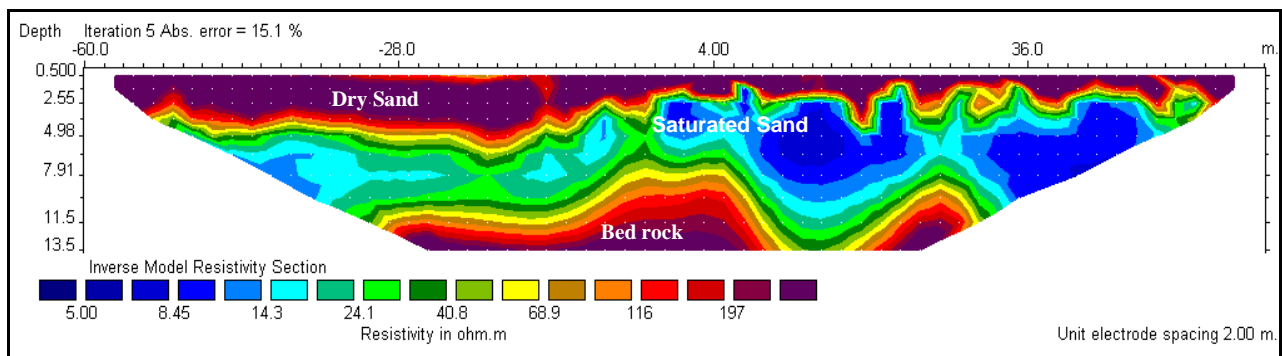


Figure 4.11 Transect 1 inverse model resistivity a year later in August 2009

Another ERT survey was conducted in July, 2011 on four new transects, as shown in Figure 4.12. The survey indicated a resistive 2 m layer of dry sand ($>2500 \Omega.m$) lying above a conductive saturated layer (aquifer) ($<300 \Omega.m$).



Figure 4.12 Transects Umlaz1-4 used for the ERT study in July 2011

Transect Umlaz1 showed lateral variations of resistivity in the top 2 m layer, which may have resulted from the presence of the trees and root activity (Figure 4.13). Transect Umlaz2 indicated a relatively moist sandy soil ($1500 \Omega.m$) in the top meter (Figure 4.13). In Transect Umlaz3, the material in the trenches appeared to have only marginally lower resistivity than the topsoil at the same depth, which may have been caused by the presence of the trees or the sludge within the trenches; high reeds at this location were also indicative of the presence of water close to the surface or a sill/dyke. Umlaz4 indicated a resistive layer of dry sand and rock ($>2500 \Omega.m$) over a depth of 3 m and at about 5 m it shows very low conductivity, suggesting the presence of water at the south side of this transect (Figure 4.13). This coincides with the water levels recorded in the boreholes in this area.

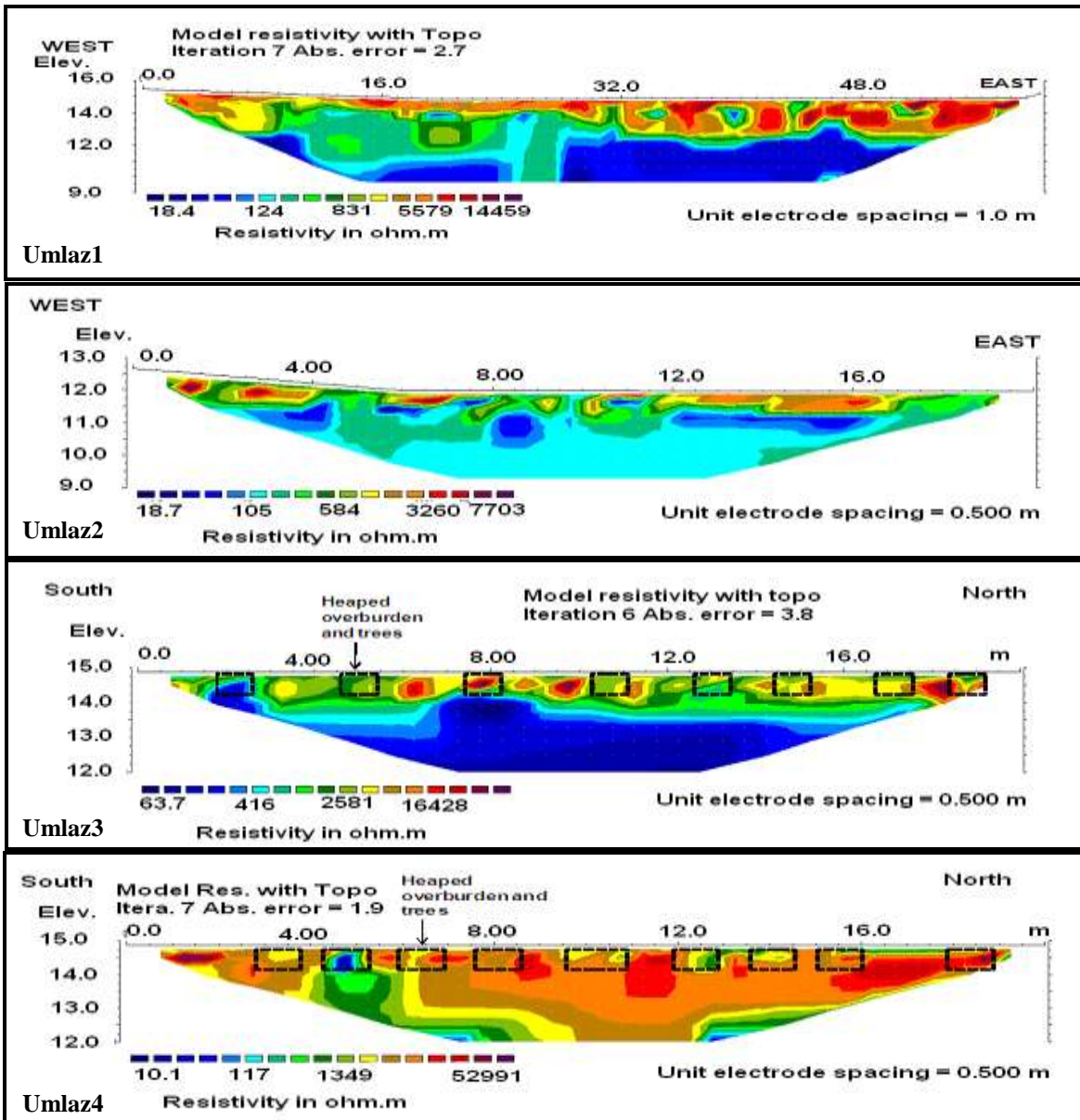


Figure 4.13 ERT inverse resistivity section Umlazi 1 to 4 from top to bottom (July, 2011)

4.2 Soil Water Analysis for SAPP1 Site

4.2.1 Volumetric water contents at SAPP1 site

All profiles where data were collected from TDRs¹, were wet during the late summer of 2010 (water content >0.30) and became dry during the winter (<0.20) (Figures 4.14-4.17). Measurements from probes located within the sludge (0.5 m depth) displayed the highest amplitude in wetting and drying, indicating the relatively high capacity of the sludge to store and release water. For the T3 trench (highest sludge loading), water content at this depth remained high throughout the dry season. There was a steep fall in water content within sludge in all treatments indicating a rapid drainage of water from the sludge at the time.

None of the profiles responded to the extreme event of March 2010 (140 mm), reflecting the dampening effect of the trees and possibly runoff effect. The levels of drying and subsequent wetting in the profiles (except T3 for the first season), reflect the wetting and drying dynamics in the trench without sludge T4 (Figure 4.17), indicating that the sludge, apart from an initial slow release of moisture, behaves similarly to the disturbed parent soil filled into the trench at T4.

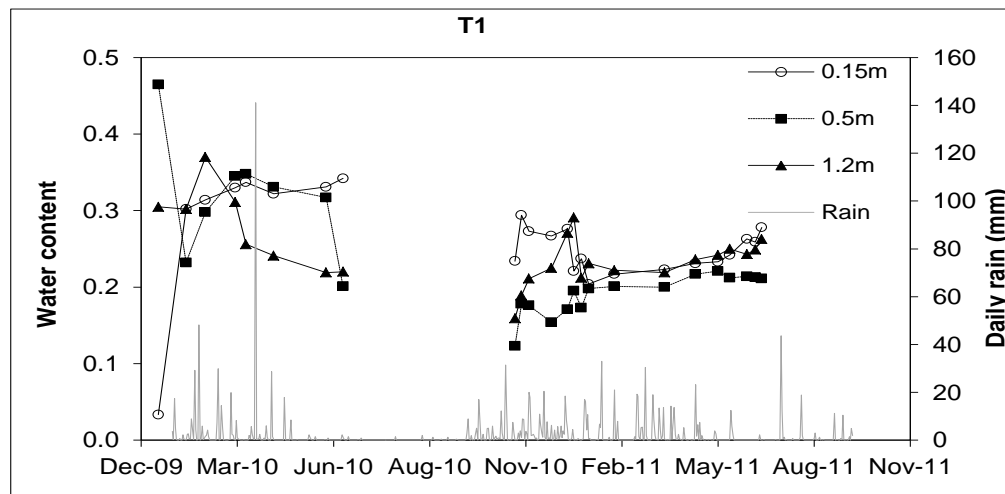


Figure 4.14 Water content and rainfall dynamics in T1 at the SAPP1 site

¹ The missing data for Treatments 1 and 4 occurred due to TDR cable damage at the site which was later repaired.

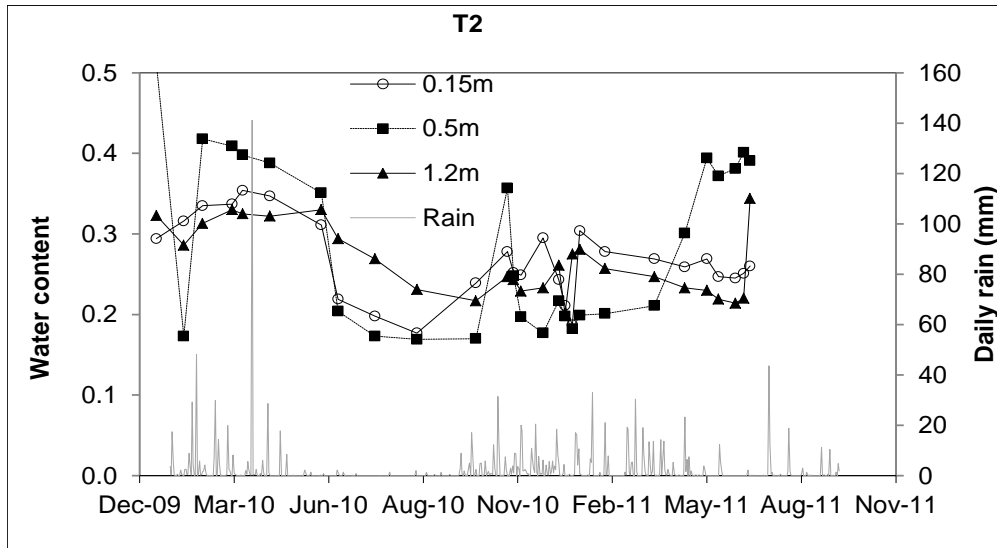


Figure 4.15 Water content and rainfall dynamics in T2 at the SAPPI site

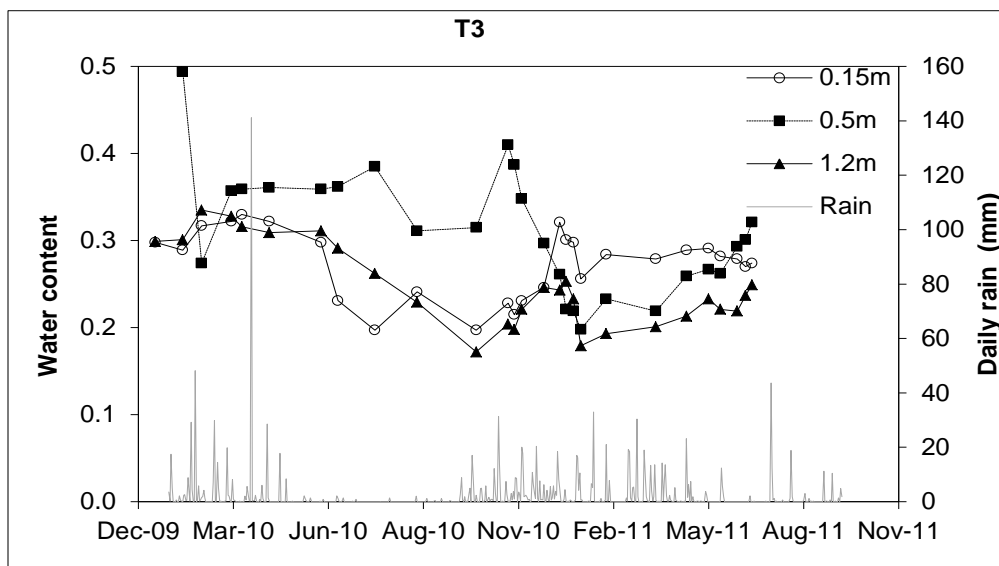


Figure 4.16 Water content and rainfall dynamics in T3 at the SAPPI site

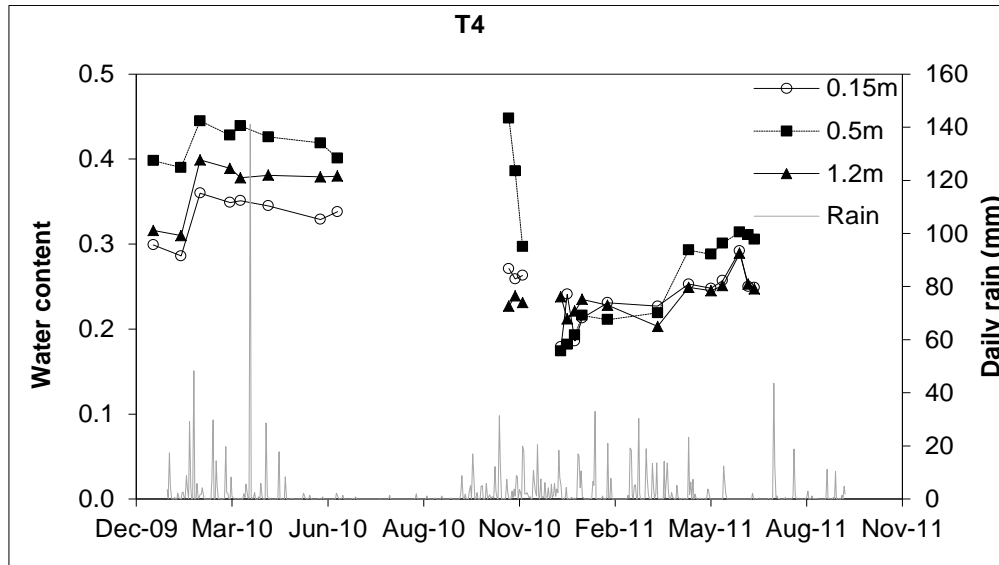


Figure 4.17 Water content and rainfall dynamics in T4 at the SAPPI site

4.2.2 Water sample analysis from WFD at the SAPPI site

Samples collected from wetting front detectors were analyzed for nitrate, phosphorus, pH and Oxidation-Reduction Potential (ORP). Data for pH and ORP are presented in Appendix A. Nitrate concentrations in all three sludge treatments at both depths (0.15 m and 1.2 m), as shown in Figures 4.19 to 4.21, decreased gradually after initial installation and then increased, with the onset of rain in October 2010, peaking in December 2010. After the initial flushing of available nitrate by rain, concentrations built up in the profile again over a period of three months. For the T3 trench (highest sludge loading), the deep concentrations did not begin this increase in October 2010, but continued decreasing until December 2010. However, the concentrations at 1.2 m in T3 site (Figure 4.18), were the highest throughout the early period of observation. In general, the observed concentrations were high (100-500 mg/l), even for an agricultural soil environment and continued monitoring is advised. WFD's installed in T4 were not able to capture and store leachates after rainfall events for nutrient analysis during the short monitoring period. This could be as a result of rapid redistribution of water at this location coupled with the disturbance of soil and lack of sludge in the trench.

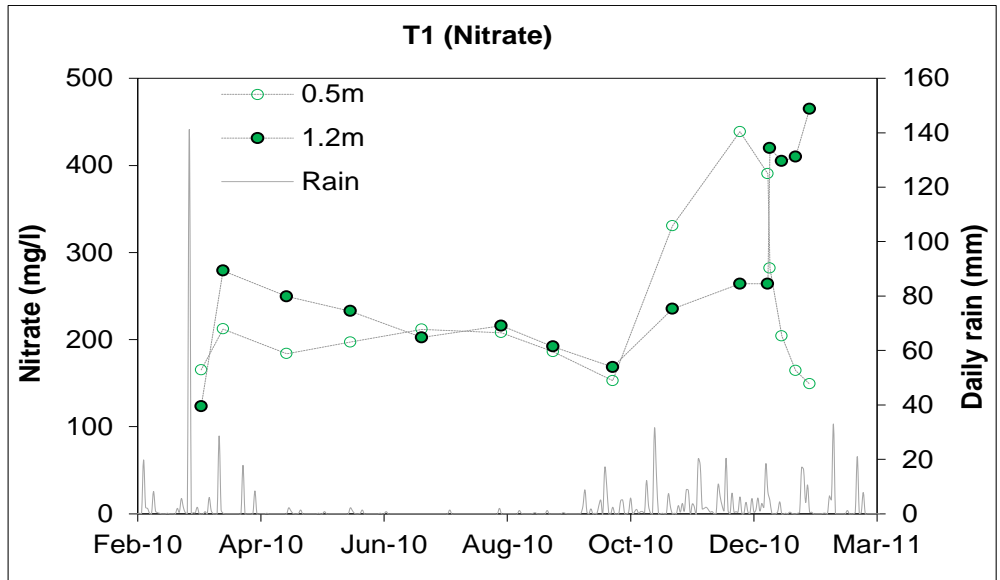


Figure 4.18 Observed nitrate concentrations in T1 at the SAPPI site

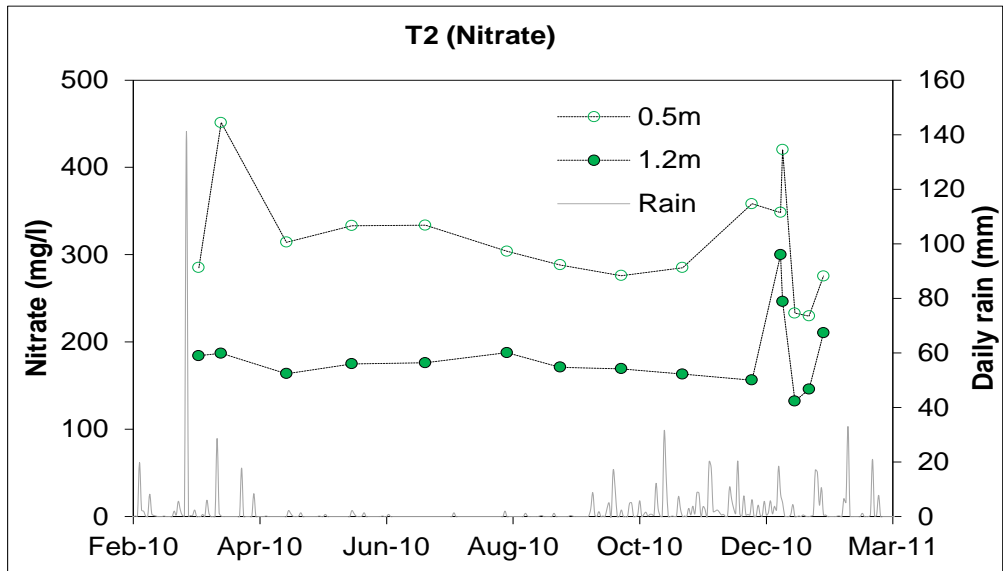


Figure 4.19 Observed nitrate concentrations in T2 the SAPPI site

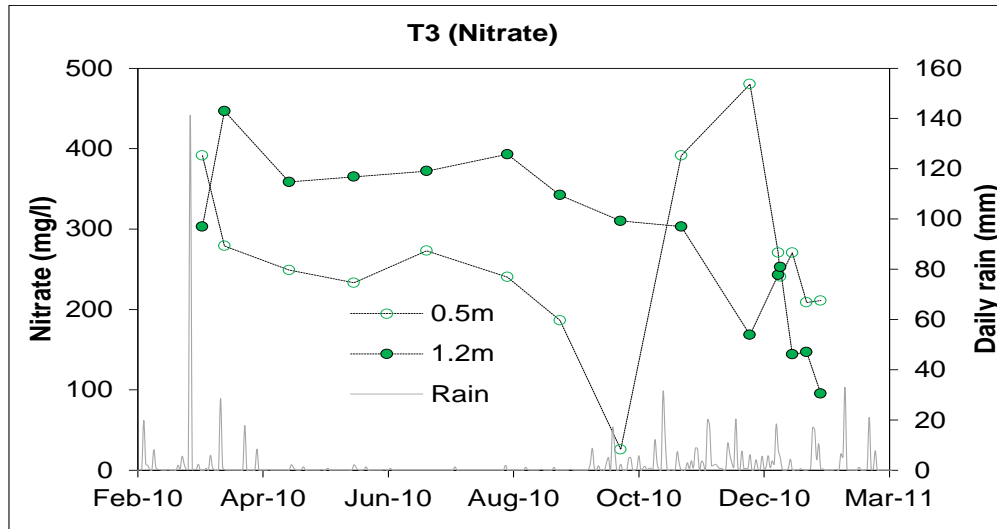


Figure 4.20 Observed nitrate concentrations in T3 the SAPPI site

The phosphorus concentrations in the middle of the T1 treatment sludge layer were consistently high (20 mg/l), which appeared to be an anomaly, as concentrations at all other sites and depths were generally below 3 mg/l, with the exception the 0.5 m level in T3, where phosphorus levels reached a peak of approximately 18 mg/l in October 2010. These results reflect the spatially varied source of phosphorus in the sludge and also the temporal variations in phosphorus movement, as shown in Figures 4.22 to 4.24. The high P concentration in T1 relative to the others could also be as a result of observed high clay content at treatment T1 compared to the others, resulting in little or no mobility of phosphorus.

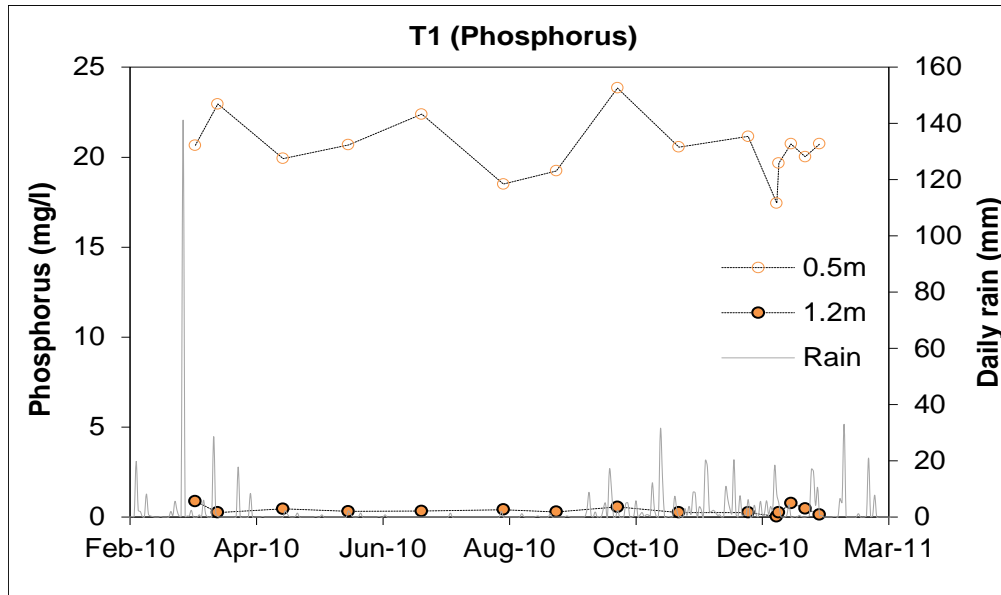


Figure 4.21 Observed phosphorus concentrations in T1 at the SAPPI site

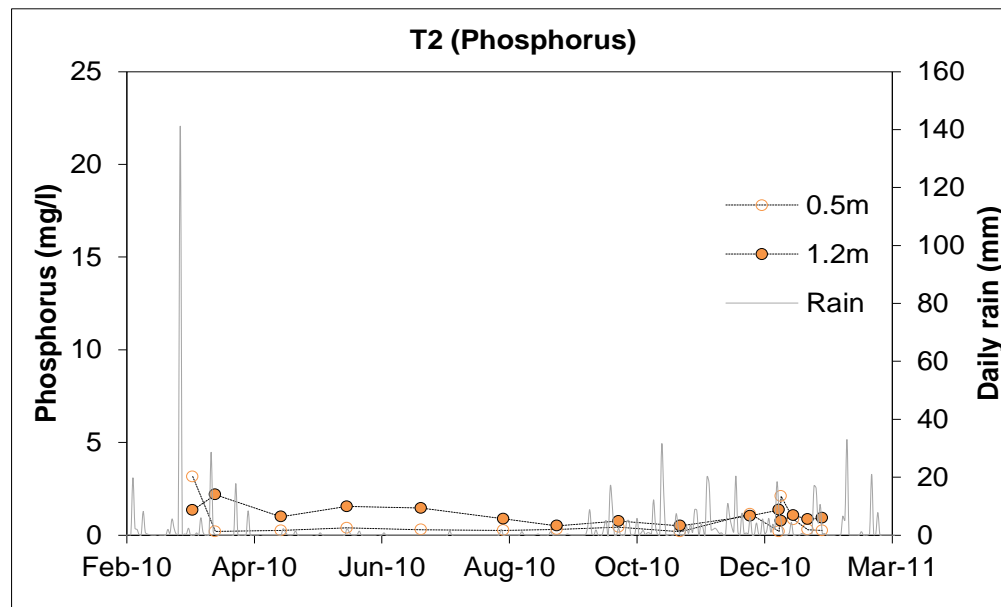


Figure 4.22 Observed phosphorus concentrations in T2 the SAPPI site

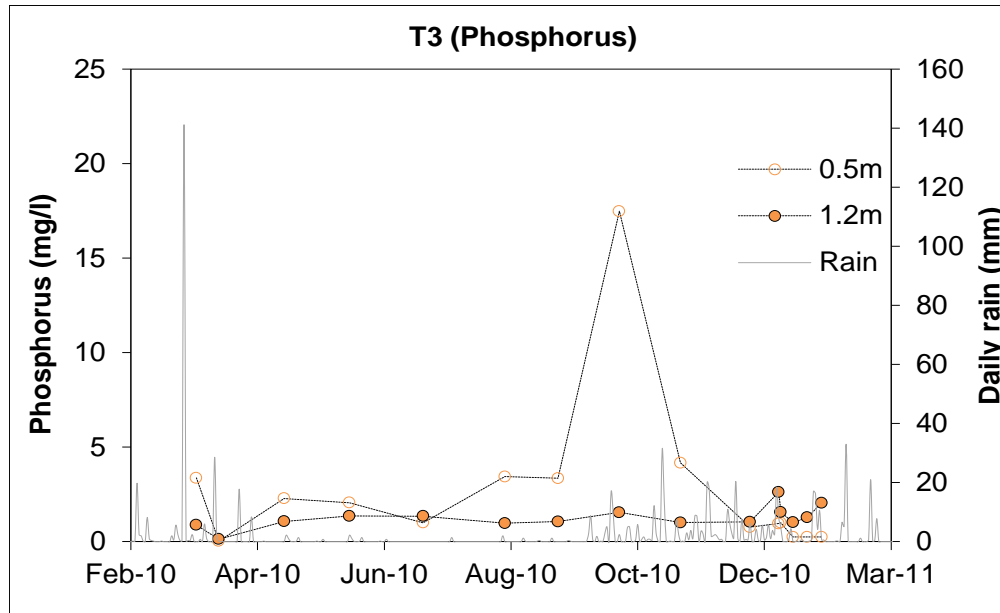


Figure 4.23 Observed phosphorus concentrations in T3 at the SAPPI site

4.2.3 Water sample analysis from piezometers, boreholes and stream at the SAPPI site

The borehole water levels, as shown in Figure 4.24, reflected the intersection of two different sources, as suggested by geophysics. The upslope borehole, BH1, has phreatic water at an average of 2.1 m below the surface throughout the observation period, while the downslope borehole, BH2, with a lower ground surface elevation, has an average phreatic surface at 11.3 m below ground. The isotopic values also indicate that the sources of water to these boreholes are different.

Nitrate concentrations in the boreholes, as shown in Figure 4.26, increased with the onset of the wet season in October 2010, peaked in April 2011 and then subsided. These concentrations were not nearly as high as those found in the infiltrating water and may reflect natural seasonal variations in nitrate concentrations. The values were well below the drinking water standard (45mg/l as NO₃) and the range of concentrations in the boreholes was similar to that in the stream.

Nitrate concentrations in piezometers SP6 and SP7 (Figure 4.26) varied widely: concentrations in the shallower piezometer, SP6, ranged from 10 to 200 mg/l, while concentrations in the deeper piezometer, SP7, ranged from 100 to 700 mg/l. These variations reflected an accumulation along the preferential flow paths during the wet season, rather than a direct response to rainfall events. Piezometer SP6, which is located in a subsurface waterway, had a deeper flow regime than that of SP7 and also continued for much longer than in SP7. Concentrations in SP6 were similar to those intercepted by the wetting front detectors in the trench profiles, suggesting a connection between the infiltrated water and the accumulated subsurface, free water discharge at the soil/bedrock interface. This mechanism of the interception of buried waste by rapid, near surface lateral flow is often overlooked and requires monitoring and an assessment of the total load from these pathways.

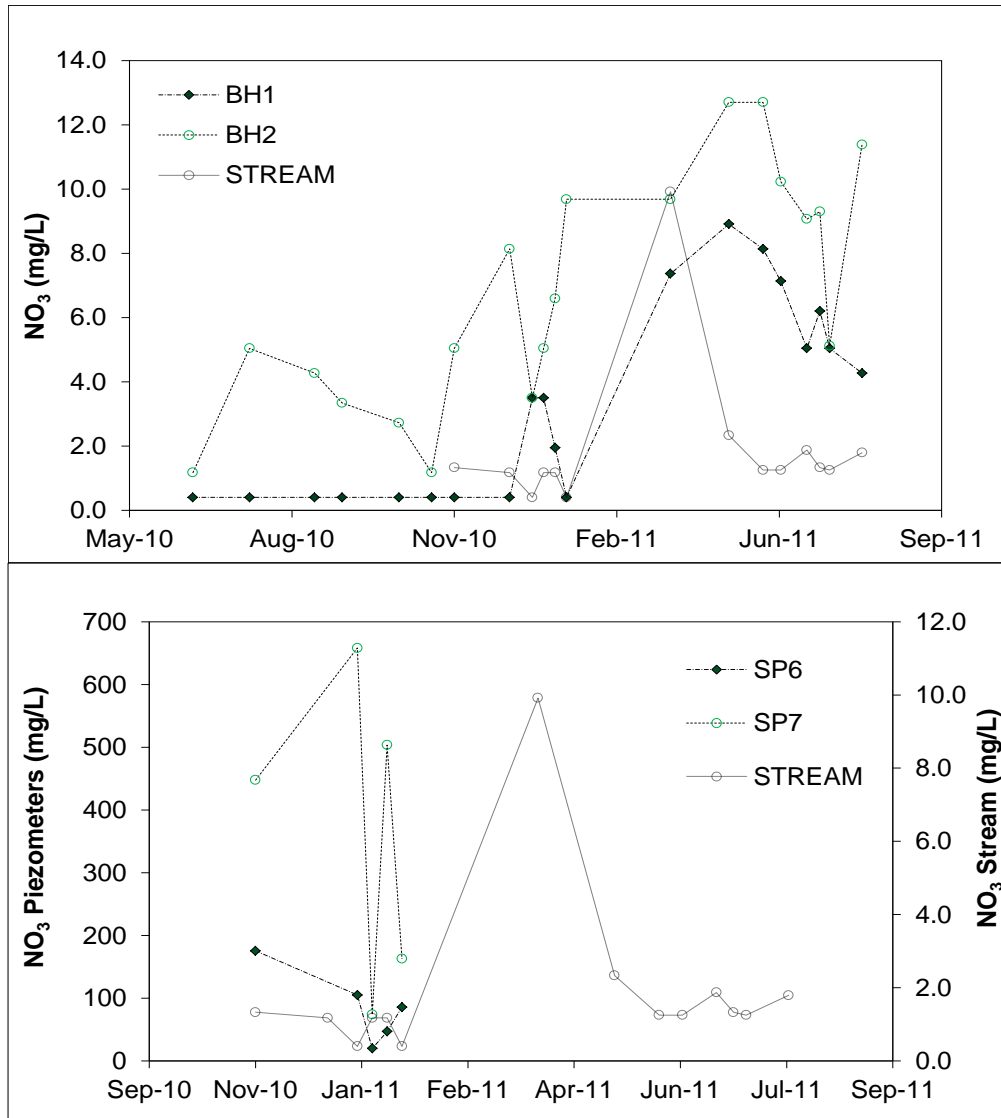


Figure 4.26 Observed nitrate concentration in boreholes and stream at the SAPPI site

Phosphorus (P) concentrations in the boreholes and stream (Figure 4.27) varied throughout the monitoring period, but generally there was a drop (June-July 2011) and an increase from May 2011 onwards. The range of P concentrations in the boreholes was equal to that in the stream and was assumed to be similar to natural subsurface contributions upstream of the trial site.

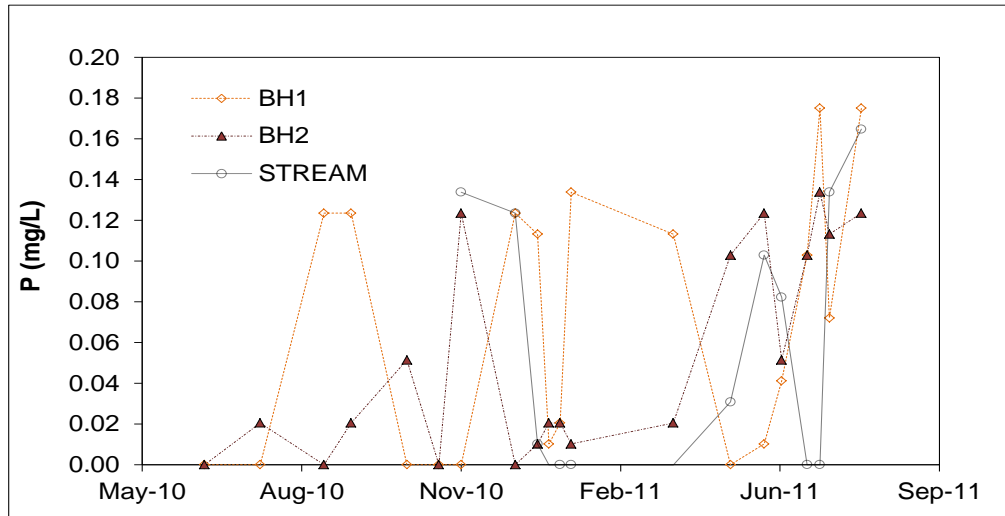


Figure 4.27 Observed phosphorus concentrations in boreholes and stream at SAPPI site

Phosphorus concentrations ranged widely (0.1-23 mg/l) in piezometers SP6 and SP7 (Figure 4.28), but were similar to infiltrated water detected in the wetting front detectors. The phosphorus concentrations exhibited similar responses to the nitrate concentrations in these piezometers, with SP7 having higher phosphorus concentrations than SP6 during the later part of the wet season.

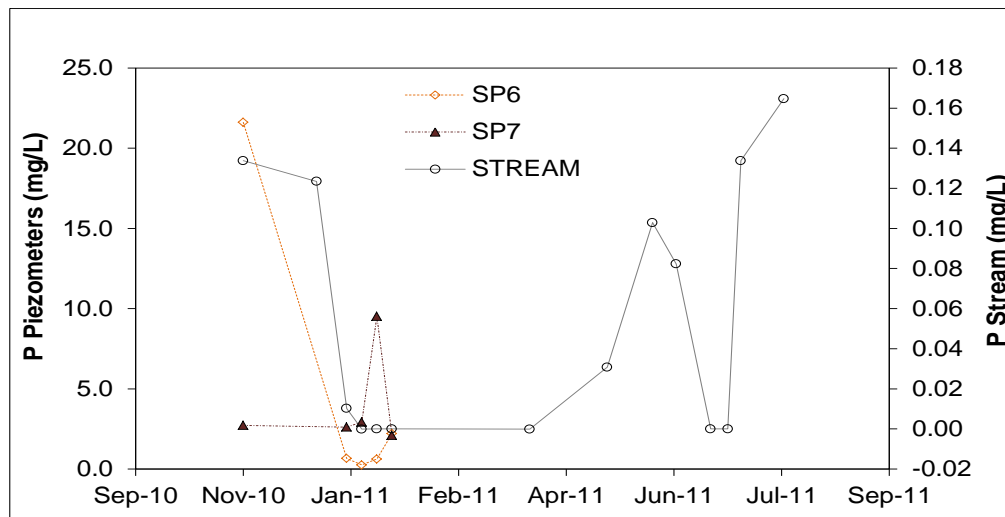


Figure 4.28 Observed phosphorus concentrations in piezometers and stream at SAPPI site

4.2.4 Stable isotopes of water samples for the SAPPI site

Hydrogen and oxygen isotopes of water vary in time and space due to their fractionation in the natural environment. Isotope fractionation is accompanied by a number of processes, including phase change, transportation, diffusion, reduction, oxidation, chemical reaction and biological metamorphism. Data from samples drawn from the boreholes, piezometers and the stream (ST), (Figure 4.29) clustered to the left of the global meteoric water line (GMWL). The range indicated that they were predominantly of meteoric origin.

The borehole isotopes clustered in two intersecting zones, with isotopes from BH1 being generally more depleted than those of BH2, indicating different sources and pathways of the ground water in these two boreholes (Figure 4.30 and 4.31). The piezometer and stream water isotope values also clustered in the region of BH1, indicating a probable connection of these shallower sources with the stream (Figure 4.29). This highlights the importance of the near surface lateral flows in contributing solutes to the stream.

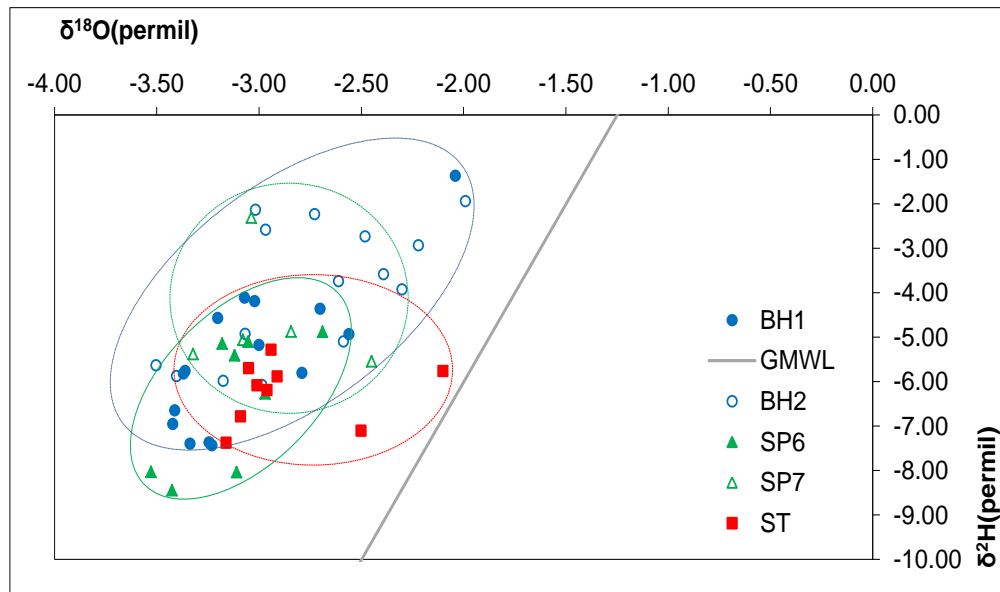


Figure 4.29 Stable isotope responses in the boreholes, piezometers and stream at the SAPPI site

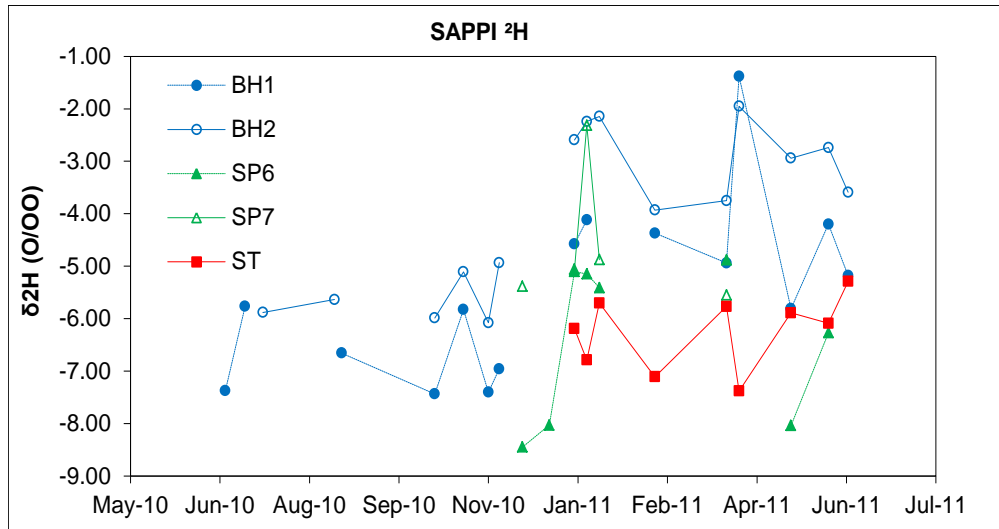


Figure 4.30 Stable isotope of ^2H responses in the boreholes, piezometers and stream at the SAPPI site

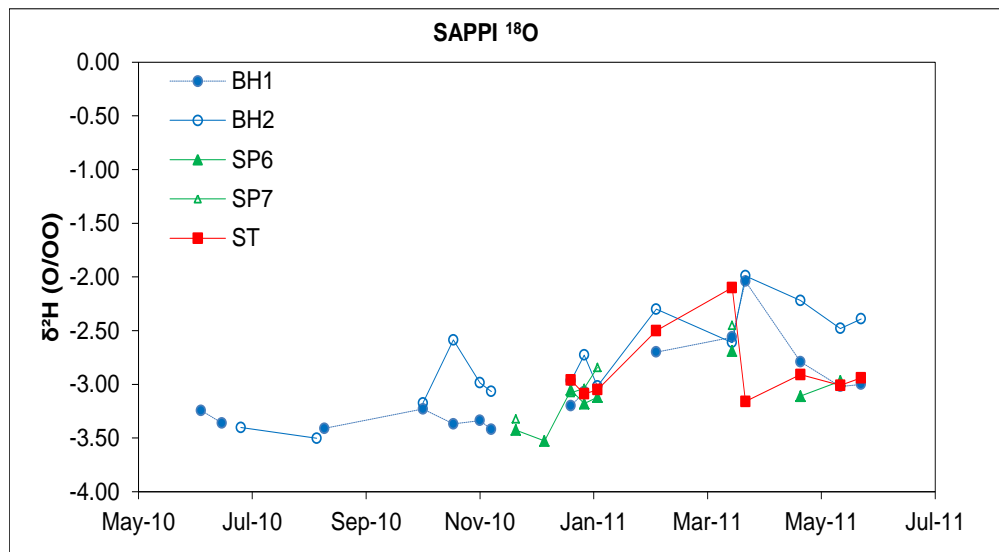


Figure 4.31 Stable isotope of ^{18}O responses in the boreholes, piezometers and stream at SAPPI site

4.2.5 Soil properties at the SAPPI WWTW sludge trenching site

The results of particle size distribution by the standard Hydrometer method (Gee and Baunder, 1986) for SAPPI are shown in Tables 4.1 to 4.5. Water retention characteristics of materials from the various depths in each treatment and which were fitted with van Genuchten curves,

were derived for the soil samples collected from the SAPPI site. Figure 4.32 shows a water retention curve, with a fitted van Genuchten curve, at a depth of 0-30 cm and the rest of the results are shown in Appendix B.

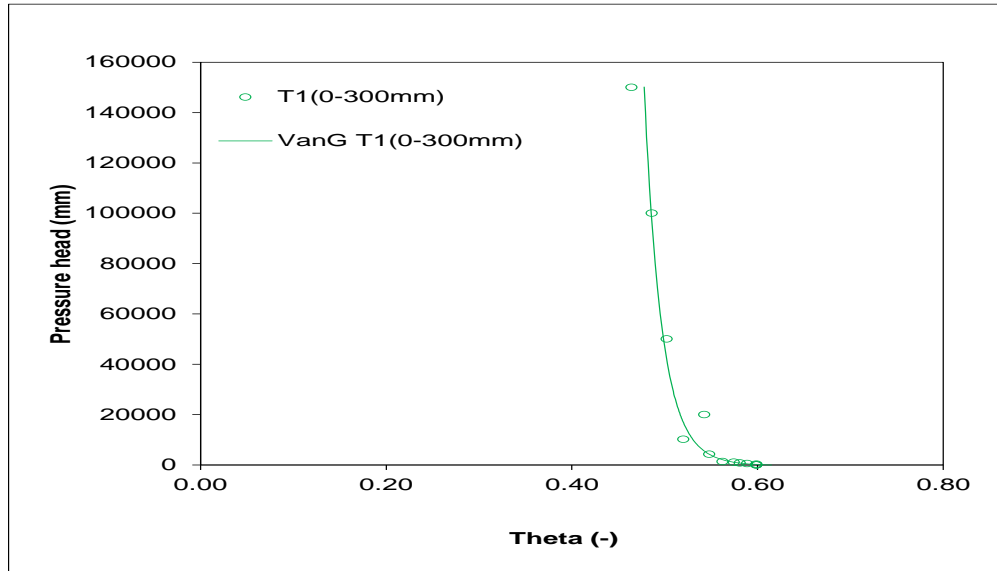


Figure 4.32 van Genuchten Fitted Soil Water Retention curves in treatments at the SAPPI site

Table 4.1 Physical properties of soil in Treatment 1

Profile	Depth (cm)	Sand %	Silt %	Clay %	Texture class	Bulk density (g/cm ³)
T1	0-30	63.6	19.0	17.4	Sandy loam	1.063
	30-60	51.9	19.2	29.0	Sandy clay loam	0.931
	60-90	84.0	7.6	8.4	Loamy sand	1.047
	90-150	70.1	14.6	14.8	Sandy loam	1.069

Table 4.2 Physical properties of soil in Treatment 2

Profile	Depth (cm)	Sand %	Silt %	Clay %	Texture class	Bulk density (g/cm ³)
T2	0-30	66.5	10.4	23.0	Sandy clay loam	1.324
	30-60	73.6	12.1	14.3	Sandy loam	1.159
	60-90	78.4	5.2	16.5	Sandy loam	1.388
	90-150	51.6	21.6	26.8	Sandy clay loam	1.488

Table 4.3 Physical properties of soil in Treatment 3

Profile	Depth (cm)	Sand %	Silt %	Clay %	Texture class	Bulk density (g/cm ³)
T3	0-30	56.9	15.7	26.8	Sandy clay loam	1.060
	30-60	77.3	8.0	14.7	Sandy loam	0.999
	60-90	79.0	7.3	13.7	Sandy loam	0.751
	90-150	54.9	19.8	26.1	Sandy clay loam	1.396

Table 4.4 Physical properties of soil in Treatment 4

Profile	Depth (cm)	Sand %	Silt %	Clay %	Texture class	Bulk density (g/cm ³)
T4	0-30	82.9	10.4	6.7	Loamy sand	1.152
	30-60	57.7	20.2	23.1	Sandy clay loam	1.018
	60-90	67.9	18.5	14.5	Sandy loam	1.197
	90-150	65.7	19.1	15.3	Sandy loam	1.164

Table 4.5 Physical properties of sewage sludge

Profile	Sand %	Silt %	Clay %	Texture class	Bulk density (g/cm ³)
Sewage sludge	12.7	32.6	54.6	Silty clay loam	1.210

4.3 Soil Water and Properties for the Umlazi VIP Trenching Site

The surface topography of two transects were surveyed on 29 June 2011, in order to determine the water table gradients (Figure 4.33). The first transect ran from the trench site to the stream and the second along the borehole line from BH2 to BH5. The water table lay at a depth of approximately 2 m below the entrenchment site and was typically 5 m below the surface at the boreholes between the site and the river. The flow from along the hill slope was channelled downward to the river, as indicated by the expected pathway of water and nutrients in Figure 4.35. Throughout the monitoring period, December 2008 to June 2011, the depth varied between 3 m and 6 m below surface, being lowest in the dry season of 2010 (Figure 4.34).

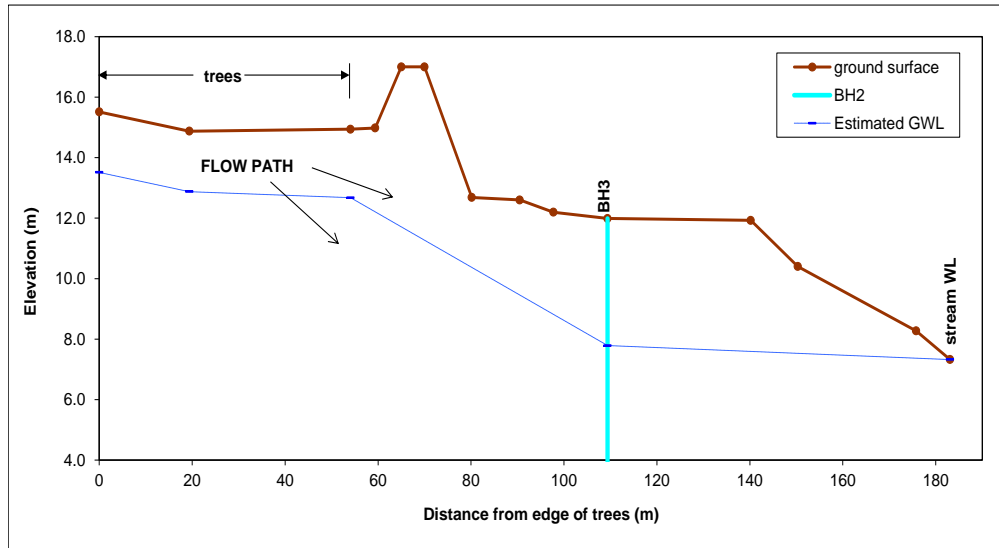


Figure 4.33 Surface topography, expected flow path and groundwater levels at 01 July 2009 at the Umlazi site (Umlaz1 and Umlaz2 transect together)

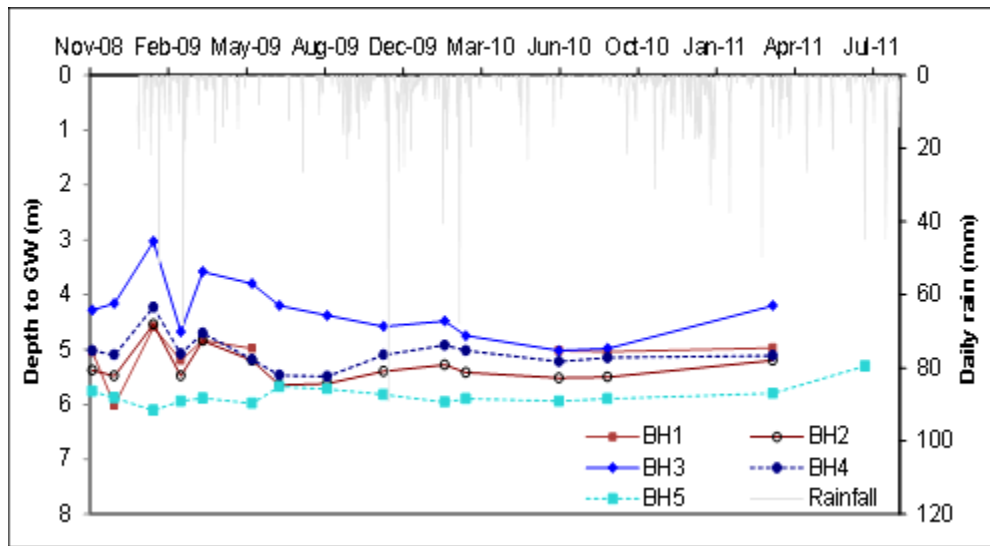


Figure 4.34 Time series of borehole water levels at the Umlazi site

The nitrate concentration in water samples collected from the piezometers and wetting front detectors before they were destroyed, ranged from approximately 50 mg/l to as high as 600 mg/l (Figure 4.35). This can be attributed to their proximity to the entrenched sludge. Nitrate fluctuations in the boreholes (Figure 4.36), remained within acceptable ranges (less than 44mg/l measured as Nitrate, EPA drinking water standard) throughout the period of the study, exhibiting only two outliers. The first outlier (30mg/l) was measured in borehole BH5 on 25 February 2009

and was associated with an elevation of NO_3 concentrations in the remaining boreholes, but these were all below 5mg/l on that day. These increases in concentration could be due to a series of dry days during the wet season, resulting in concentrated recharge from the unsaturated soils. The second outlier (36mg/l) occurred in BH3 on 28 February 2010. None of the other boreholes reflected this increase and thus this value in BH3 (Figure 4.36) should be ignored. Besides similar periods of slightly elevated concentrations, no seasonal pattern could be discerned in the nitrate record.

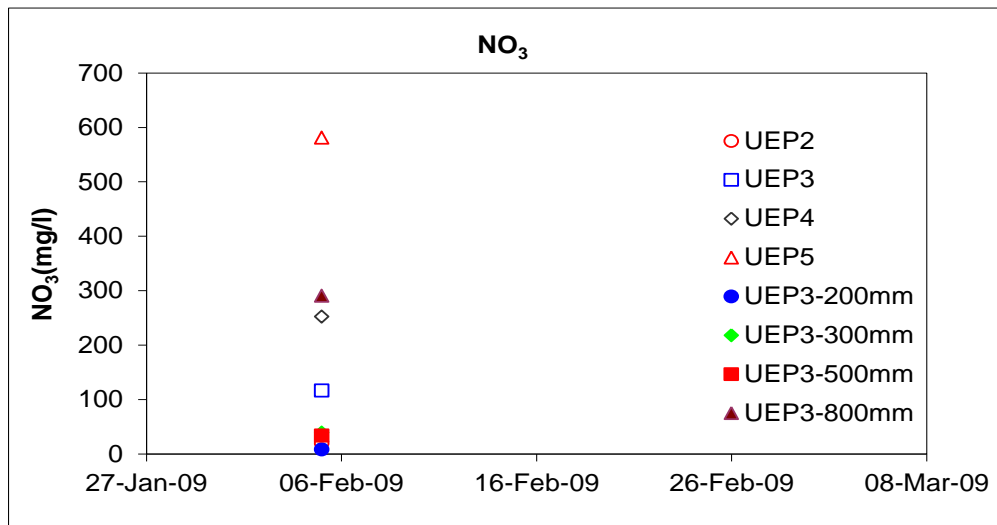


Figure 4.35 Nitrate concentration in piezometers and WFD before they were destroyed at the Umlazi site

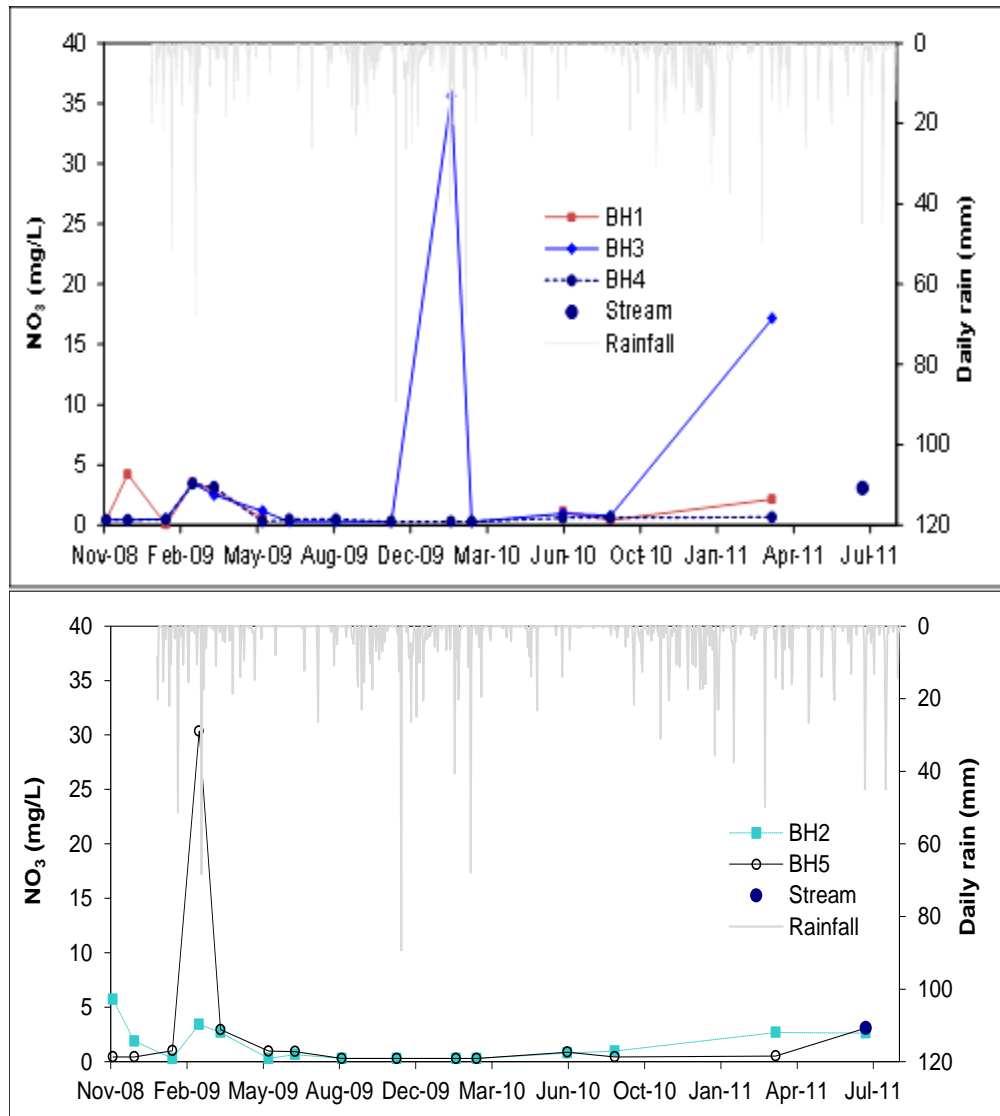


Figure 4.36 Nitrate concentration in boreholes and the stream at the Umlazi site

Water samples collected from the piezometers and wetting front detectors before they were destroyed, were also analysed for phosphorus concentration. Water samples from the wetting front detector at a depth of 800 mm (UEP3-800 mm) analysed at the beginning of monitoring, indicated the highest phosphorus concentration of 225mg/l. This wetting front detector was located at the bottom of the trenched VIP sludge and hence accumulated the highest concentration of leachates generated from the sludge (Figure 4.37). The other wetting front detectors and piezometers indicated phosphorus concentrations ranging between 0.26 and 9.26 mg/l at the initial stages of monitoring (Figure 4.37). The water quality in the boreholes (Figure 4.38) frequently exceeded the eutrophic critical value for orthophosphate, P of 0.05 mg/l,

recommended by the EPA and also occurred above the South African Water Quality Guideline for eutrophication (0.025-0.25 mg/l) during the monitoring period. The phosphorus concentration in the stream was 0.17 mg/l (19 July 2011) and consistent elevated P concentrations in the stream was evidenced by the fact that algae and water hyacinth covered most of the waterway. These were all considerably higher than the recommended eutrophication threshold value, 0.05 mg/l, although, in a highly-impacted catchment. The Department of Water Affairs (DWA) in South Africa has recommended a treatment works effluent orthophosphate concentration of 0.5 mg/l, to reduce eutrophication. Borehole phosphorus concentrations were also higher during the dry periods, apparently due to lower dilution, and declined during the rainy period, as infiltrated precipitation caused dilution.

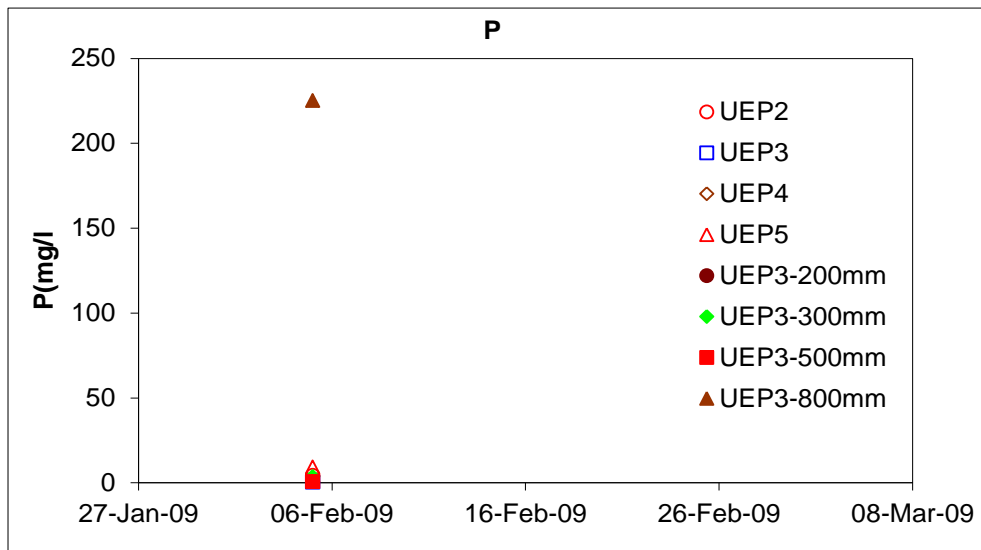


Figure 4.37 Dissolved phosphorus concentration in piezometers and wetting front detectors at the Umlazi site

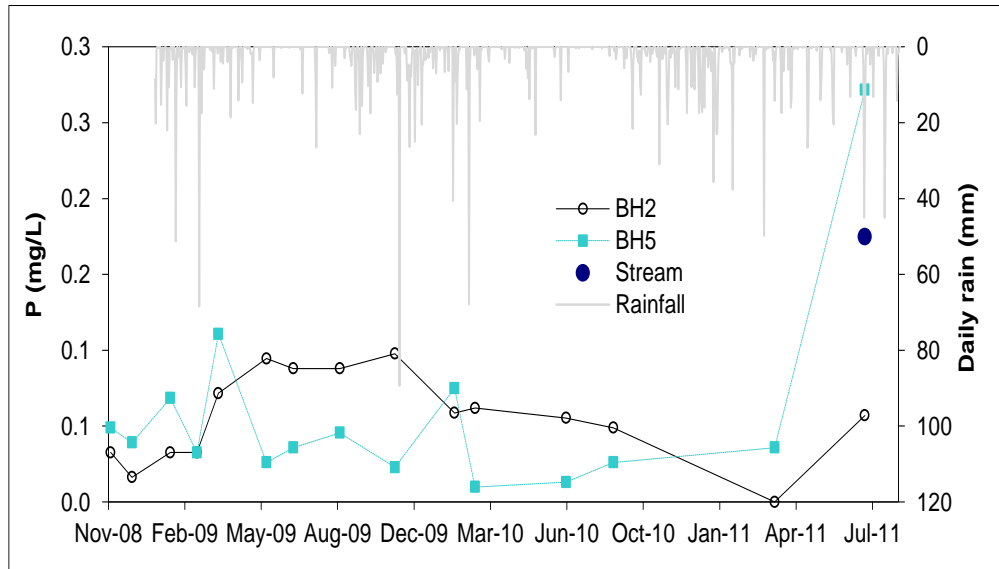


Figure 4.38 Phosphorus concentration in boreholes 2 and 5 and stream at the Umlazi site

Elevated phosphorus levels in the buried sludge indicated the leaching of phosphorus from the sludge, either by adsorption to and transport with colloids, or as organic phosphorus. Nevertheless, these mechanisms do not appear to extend beyond the trenched area, as the orthophosphate concentrations in groundwater are considerably lower than those measured in the trenched zone. This is possibly a result of the high phosphorus binding capacity of the materials in the unsaturated zone and the groundwater aquifer between the trench site and the groundwater monitoring location. The entrenchment of sludge cannot be assumed to be related to the level of phosphorus recorded in stream water, as refuse and other waste material were observed to be dumped into the stream by nearby residents. The phosphorus concentrations in the ground water peaked during the dry season of 2009, but only once did they exceed 0.5 mg/l, (BH3 0.58 mg/l on 27 May 2009). However, the dry seasonal P concentration frequently exceeds the concentration for eutrophication (recommended 0.25 mg/l by South African water quality guideline of 2009) in all boreholes during the wet season. The elevated P concentration may be as a result of lack of dilution from percolating rainfall, however, these data do not indicate an increasing trend, such as may result from consistent elevated loading from the trenched area.

The pH is a measure of the acidity of groundwater: the lower the pH, the more acidic the water. At the typical temperature of groundwater (16.5 -21°C), a pH of 7 is considered neutral. Therefore, a pH less than 7 is acidic and a pH greater than 7 means the water is alkaline. The pH

state of surface water is especially important, since aquatic organisms are able to tolerate only a very narrow pH range. A pH value higher than 8, or lower than 6 for stream water can threaten the survival of aquatic organisms and compromise the diversity of the ecosystem in the stream. High pH levels can occur when algae and aquatic vegetation use CO₂ for photosynthesis. Low pH can also be caused by the respiration of aquatic vegetation, or from bacterial decay of organic matter in the water, producing high levels of CO₂. Low pH in the water can also cause toxic chemicals to become mobile. Measured pH in boreholes ranged from 6.3 to 7.5 and can therefore be said to have been within acceptable levels. pH levels appear to drop slightly on occasions, possibly in response to recharge rain events (Figure 4.39).

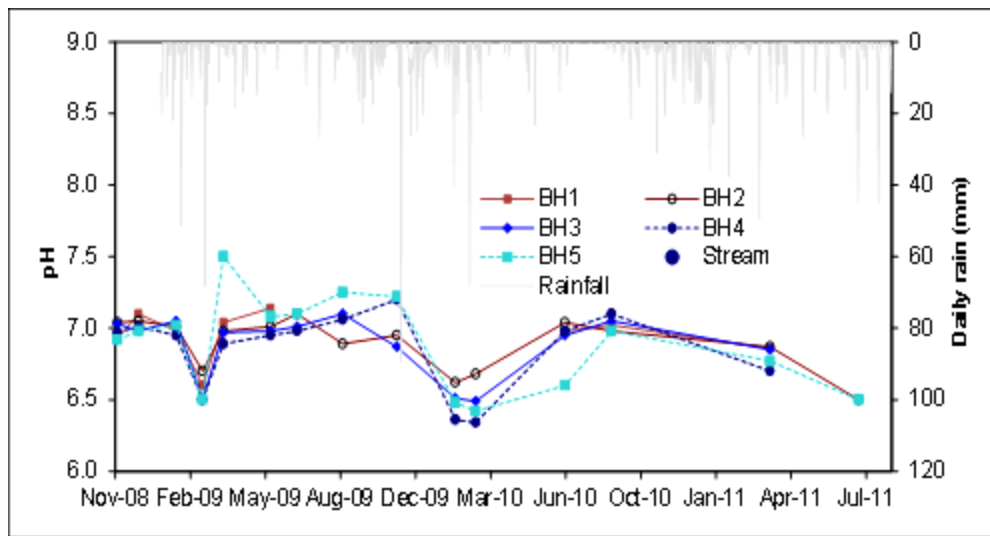


Figure 4.39 pH of borehole water samples and stream at the Umlazi site

Electrical conductivity (EC) values shown in Figure 4.40 reflect the concentration of total ions and range between 40 and 95 mS/m. On only two occasions (2 December 2008: 95mS/m in BH1 and 31 August 2009: 85 mS/m in BH2) does the EC exceed a value recommended for drinking and irrigation, 75 mS/m (EPS standard converted from 500 mg/l). EC variations did not correlate with nitrate or phosphorus variations and generally fluctuated around the EC of the stream, measured in July 2011.

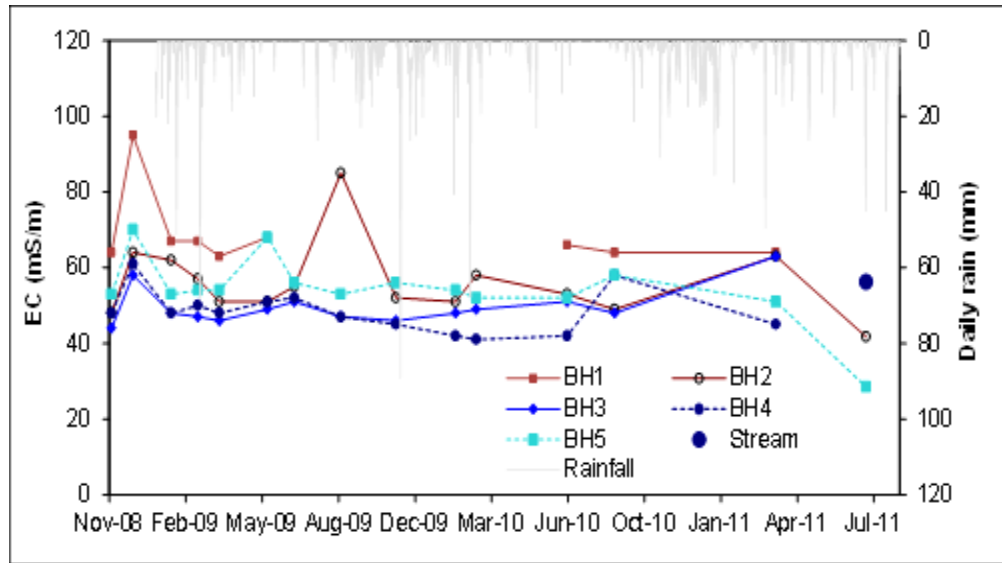


Figure 4.40 EC of borehole water samples and stream at the Umlazi site

Soil samples were collected from the prepared pits in April 2008 and analysed for particle size distributions. Soils from all sampling points and depths fell under the USDA classification of sands with textures similar to one another, indicating high infiltration rates and low water-holding capacities. The soils were found to be acidic, indicating that the pH of the sludge was critical with respect to the microbial population and trees grown on the site (Table 4.6).

Table 4.6 Analysis of soil samples collected from pits in April 2008

Sample name	Particle size analysis				pH	EC mS/m
	Sand %	Silt %	Clay %	Texture class		
Southeast (1.3m)	93.2	2.9	3.8	Sand	5.1	0.079
Southwest (2m)	94.3	2.6	3.1	Sand	5.9	0.061
Northeast (1.2m)	97.1	0.7	2.1	Sand	5.3	0.033
Northwest (2m)	97.2	0.7	2.1	Sand	5.0	0.06

The hydraulic properties of the soil were characterised, in order to understand the influx, uptake and distribution of water in the entrenchment zone, which could impact on the movement of pollutants out of the trenches. This was done by estimating the retention of water in the soil and

the hydraulic conductivity in saturated and unsaturated soils, on the basis of a wide range of measurements.

All of the soil samples tested fell into the sand category, with clay percentages varying between 1 and 7 %, except for the Surface 5 position, which was classified as a sandy loam with a clay content of 20 % (Table 4.7).

Table 4.7 Summary of particle size fractions at the Umlazi site

Site	Depth (mm)	Sand (%)	Silt (%)	Clay (%)
Surface position 1	0	91	5	4
Surface position 3	0	85	8	7
Surface position 4	0	94	3	3
Surface position 5	0	82	18	20
Trench top position 1	0	96	2	2
Trench1 inside	200	94	4	2
Trench1 inside	600	97	2	1

The hydraulic characteristics for the water retention and hydraulic conductivity are shown in Figure 4.42 and the rest, in Appendix C. For clarity and completeness, the saturated hydraulic conductivity is shown on the plot at a tension value of 1 mm. It is worth noting that many of the characteristics showed an order of magnitude difference between the saturated hydraulic conductivity of the ponded double ring infiltrometer test and the unsaturated hydraulic conductivity at a small tension of 5 mm.

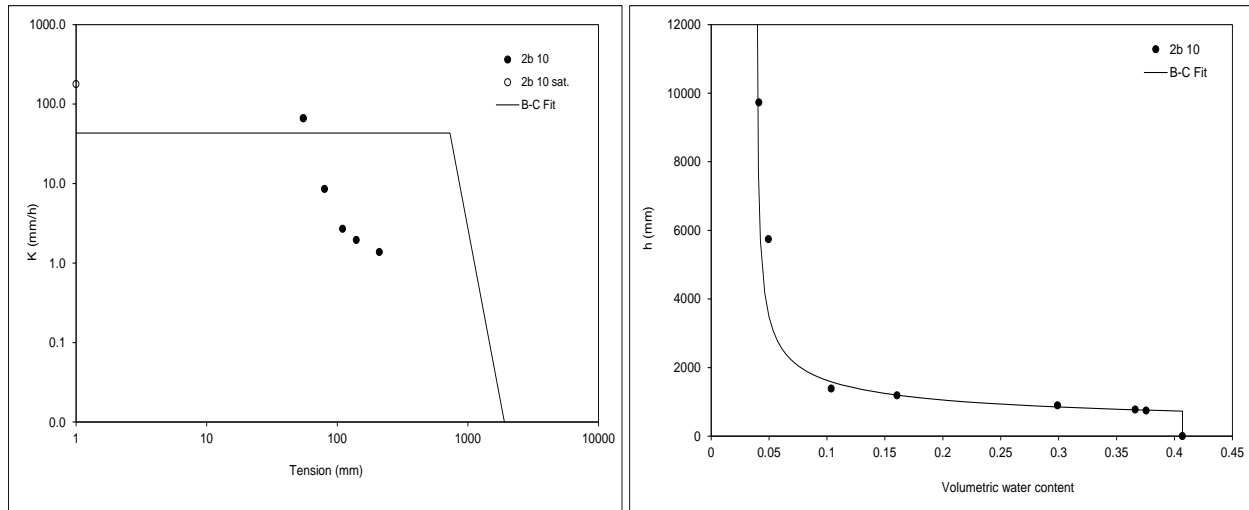


Figure 4.41 Hydraulic conductivity and retention characteristics at Trench 2 100mm at the Umlazi site

The K_{sat} determinations on the undisturbed surface and those at 100 mm below the surface in the trenches, were generally lower than the deeper K_{sat} values determined in the trenches. The 10 measurements performed on undisturbed surface material were generally lower than those completed on the surface of the disturbed trench fill (Table 4.8).

Table 4.8 Summary of the saturated hydraulic conductivities at surface and trenched sites (the number in brackets represents the site number shown in Figure 4.44)

SURFACE				SUBSURFACE			
Surface		Surface on trench		Trench 1 (11)		Trench 2 (12)	
Position	Ksat (mm/h)	Position	Ksat (mm/h)	Depth (mm)	Ksat (mm/h)	Depth (mm)	Ksat (mm/h)
1a (1)	89	1a (6)	404	100	30	100	123
1b (1)	98	1c (6)	385	100	21	100	178
2a (2)	96	2a (7)	713	200	327	200	382
2b (2)	36	2b (7)	936	400	312	200	366
3a (3)	82	3a (8)	827	400	369	400	346
3b (3)	150	3b (8)	885	600	866	400	172
4a (4)	183	4a (9)	1020	600	822	600	553
4b (4)	132	4b (9)	531	800	1226	600	312
5a (5)	571	5a (10)	249	800	930	800	366
5b (5)	375	5b (10)	251	1000	888	800	290
				1000	911	1000	596
				1500	1699	1000	229
				1500	3109		

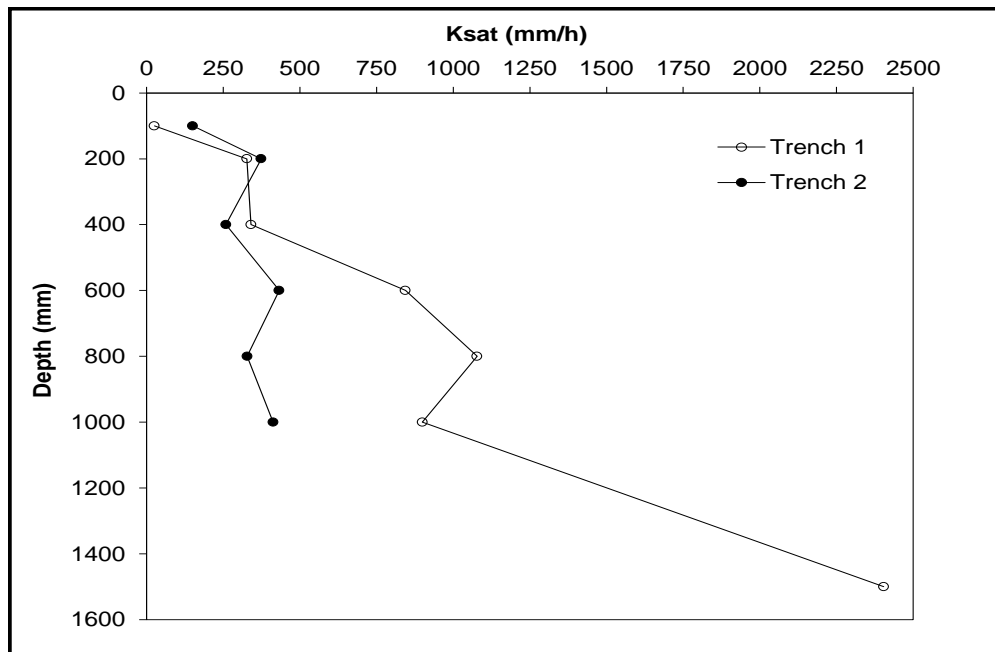


Figure 4.42 Saturated hydraulic conductivity variation in trenched with depth Umlazi

5. MODELLING

A model may be defined as a simplified version of a real-world system (e.g. ground water system) that approximately simulates the relevant excitation-response relations of the real-world system. Models may be used throughout all phases of the site investigation and remediation processes (USEPA, 2009). Selecting the appropriate conceptual model for a given problem is one of the most important steps in the modeling process. In modeling the flow of water and nutrient in the unsaturated zone at the WWTW sludge trenching site at SAPPI, the model HYDRUS-2D was selected.

The HYDRUS-2D model requires values for K_s , α , n , bulk density, and dispersivity. The measured parameters include bulk density and soil textural class i.e. fraction of sand, silt and clay which were used to predict the van Genuchten parameters (α , n , L) using the Rosetta program. Hydraulic conductivity was also measured in the field. This data was used as input for the Hydrus-2D model to analyze the movement of water, nitrate and phosphorus in the soil. For the simulations measured values of K_s were used except for the sludge where K_s value derived from particle size distribution optimized from RETC was used in the model.

After the field surveys, material characterisation and monitoring of subsurface water and solutes, soil hydraulic modelling was conducted to simulate the fluxes of water and nutrients at the SAPPI and Umlazi sites. The software package HYDRUS 2D/3D (Simunek et al., 2006) designed for the simulation of water, heat and solute fluxes in variably saturated porous media in both 2- and 3-dimensions was used. This software was chosen because:

- It has the ability to model unsaturated flow and nutrient transport in soils;
- It comes with graphical user interface of the input of the model results;
- It can model the fluxes of water and nutrients from the time history of observations and
- It also allows for prediction of long term behaviour in natural systems, based on short term calibrated observations.

5.1 SAPPI Karkloof WWTW Sludge Trenching Site

The Hydraulic parameters optimised from the RETC input data from particle size distribution measurements and water retention together with measured K_s values are presented in Table 1.5 and 5.2. However, the measured saturated hydraulic conductivity values were used in modelling.

Table 5.1 Hydraulic parameters for sewage sludge

Profile	θ_r $\text{mm}^3.\text{mm}^{-3}$	θ_s $\text{mm}^3.\text{mm}^{-3}$	α mm^{-1}	n (-)	K_s $\text{mm}.\text{day}^{-1}$	l (-)
Sewage sludge	0.099	0.497	0.0017	1.269	229.0	0.5

Table 5.2 Van Genuchten parameters for hydraulic characteristics in Treatments 1-4

Profile	Depth (mm)	θ_r $\text{mm}^3.\text{mm}^{-3}$	θ_s $\text{mm}^3.\text{mm}^{-3}$	α mm^{-1}	n(-)	K_s $\text{mm}.\text{day}^{-1}$ (predicted)	K_s $\text{mm}.\text{day}^{-1}$ (measured)	l (-)
T1	0-300	0.001	0.615	0.004	1.366	243.90	2.69	0.5
	Sludge: 300-550	0.001	0.615	0.004	1.366	229.00		0.5
	550-600	0.000	0.644	0.000	1.314	93.70	4.21	0.5
	600-900	0.000	0.600	0.000	1.837	360.60	7.38	0.5
	900-1500	0.000	0.592	0.000	1.399	346.40	1.09	0.5
T2	0-300	0.000	0.501	0.002	1.427	168.10	5.02	0.5
	Sludge: 300-800	0.099	0.497	0.002	1.268	229.00		0.5
	800-900	0.000	0.459	0.000	1.602	360.60	7.09	0.5
	900-1500	0.000	0.421	0.000	1.369	100.70	1.31	0.5
T3	0-300	0.000	0.589	0.000	1.388	119.00	2400.3	0.5
	Sludge: 300-1050	0.099	0.497	0.002	1.269	229.00		0.5
	1050-1500	0.000	0.479	0.001	1.345	115.30	5111.8	0.5
T4	0-300	0.000	0.557	0.002	1.631	1201.10	2978.3	0.5
	300-600	0.000	0.582	0.000	1.430	146.00	1943.4	0.5
	600-900	0.000	0.464	0.000	1.462	323.30	4415.4	0.5
	900-1500	0.000	0.562	0.006	1.436	294.80	3002.4	0.5

These parameters were also used by *Hassan et al.*, 2010 to study solute transport dynamics where highly treated effluent is applied to soil at varying rates and dosing frequencies. In the study, a series of soil columns were used to simulate a subsurface drip irrigation system dosed with recirculating media filter effluent at varying application rates (518, 1,036, and 2,071 cm³/d) and dosing frequencies (6, 12, and 24 doses/d). The two-dimensional code in HYDRUS-3D was used to simulate solute transport (Cl, NO₃ and PO₄⁻³) in this system. Results show that most of the Cl was lost from the system in seepage (91 % to 98 %), whereas seepage (65 %) and denitrification (31 %) were the primary mechanisms for reducing NO₃ concentrations in the soil. Most of the PO₄⁻³ remained in the soil (between 94 % and 98 %), with seepage loss accounting for a relatively small percentage of the PO₄⁻³ added (from 90.01 % to 4 % at the 518 and 2,071 cm³/d application rates, respectively). Agreement between the measured and simulated Cl, NO₃, and PO₄⁻³ concentrations indicated that HYDRUS adequately simulated transport of these solutes through the soil under a range of environmental and effluent application conditions. The simulated PO₄⁻³ concentrations in the soil leachate tended to be slightly higher than measured concentrations and may indicate underestimation of P immobilization based on P sorption isotherms. Adsorption and desorption are among the most important chemical processes in soils affecting PO₄⁻³ transport and contamination in ground and surface water ecosystems (Johnson and Cole, 1980). Langmuir PO₄⁻³ adsorption isotherm coefficient for soil textural class was adapted from the study by Hassan et al. (2010), and used in this study for Phosphorus transport.

Specific physical and chemical parameters are needed when simulating the transport of nitrates and phosphorus through soils. These parameters (nitrate transport) were adapted from a study by Hassan *et al.*, 2008. in modelling effluent distribution and nitrate transport through an On-Site wastewater system. Nitrate (NO₃) migration was simulated at 55 and 120 cm depths within and downslope of the SDIS using a two-dimensional code in HYDRUS-3D. The solute transport parameters adapted for simulations at SAPPI are shown in Table 5.3.

Results from the simulation at SAPPI show that the NO₃ concentrations were 0.248 and 0.176 mmol NL⁻¹, whereas simulated values were 0.237 and 0.152 mmol NL⁻¹ at 55 and 120 cm depths, respectively. Observed unsaturated conditions decreased the potential for NO₃ to migrate in more concentrated plumes away from the SDIS. The agreement (high R² values ≈0.97)

between the measured and simulated NO₃ concentrations indicates that HYDRUS adequately simulates NO₃ through soil domains.

Table 5.3 Solute transport and reaction parameters for Treatments T1-T4 at SAPPI

Profile	Depth (mm)	Soil texture class	NO ₃				P
			SinkL1' (day ⁻¹)	LongD (mm)	TrsnsD (mm)	D (mm ² d ⁻¹)	K _d (mg ⁻¹ mL ³)
T1	0-300	Sandy loam	0.005364	200	40	84	30
	Sludge:300-550	Silty clay loam	0.005364	150	30	84	34
	550-600	Sandy clay loam	0.005364	50	10	84	30
	550-900	Loamy sand	0.005364	100	20	84	34
	900-1500	Sandy loam	0.005364	200	40	84	30
T2	0-300	Sandy clay loam	0.005364	50	10	84	30
	Sludge:300-800	Silty clay loam	0.005364	150	30	84	34
	800-900	Sandy loam	0.005364	200	40	84	30
	900-1500	Sandy clay loam	0.005364	50	10	84	30
T3	0-300	Sandy clay loam	0.005364	50	10	84	30
	Sludge:300-1050	Silty clay loam	0.005364	150	30	84	34
	1050-1500	Sandy clay loam	0.005364	50	10	84	30
T4	0-300	Loamy sand	0.005364	100	20	84	34
	300-600	Sandy clay loam	0.005364	50	10	84	30
	600-900	Sandy loam	0.005364	200	40	84	30
	900-1500	Sandy loam	0.005364	200	40	84	30

SinkL1': first-order degradation rate constant for dissolved phase in the decay chain reaction (1/day);

LongD: longitudinal dispersivity (mm);

TransD: transverse dispersivity (mm);

D: molecular diffusion coefficient in free water (mm²/day);

K_d: Langmuir PO₄⁻³ - P adsorption isotherm coefficient (3/mg mL³).

Observation points were positioned to correspond to measurement locations so that comparisons of simulations with measured values can be used to assess model performance and thereby have confidence on model predictions. Volumetric water content readings from TDR were used as observed data. The different patterns of water content distributions between the treatments are thought to be mainly due to the amount of sewage sludge in the trench (Figure 5.1). Soil physical properties in the four treatments did not show significant variation. The results as seen in Figures 5.2 to 5.13 showed that simulated and observed water contents follow a similar trend. The

correlation coefficient between observed and simulated water contents in all treatments (T) at the 3 depths (P1=0.15m, P2=0.5m and P3=1.2m) varies from 0.0642 to 0.785 with the exception of T3P2 with a value of -0.793. Root mean square error (RMSE) between simulated and observed values was also estimated to examine the predictability of the model. RMSE values varied from 0.019 to 0.059. While the direct correlations are generally poor the responses of the simulation and observations are similar and the absolute magnitudes of the simulated and observed water contents are mostly close with certain periods showing differences (maximum difference is 0.20). Moreover, the similarities are true for the range of depths simulated in each profile. Hence simulated fluxes can be accepted.

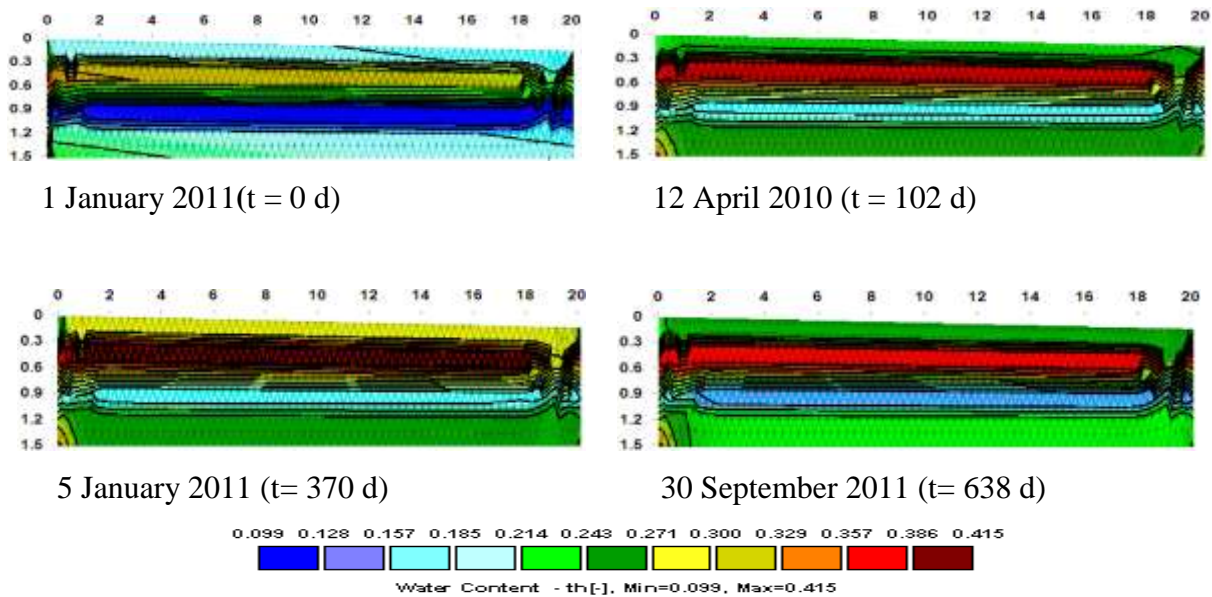


Figure 5.1 Simulated water content in Treatment 1 for 4 characteristic times during the period from 1 January 2010 to 30 September 2011 at the SAPPI site (dimensions in m)

Water contents simulated by HYDRUS-2D compared to the water content from field data collected from each treatment at SAPPI (by TDR) for the top 120 cm of the soil profile over the season (Figure 5.4 to 5.15) indicated that the model over-estimated the measured water contents over most of the season at all treatments, potentially due to under-estimation in the amount of free drainage occurring at the sites and an over-estimation of the soil porosity. From December January 2010 to September 2011, the model under-estimated the measured water contents at

some sites at certain periods; potentially the result of an over-estimation in the amount of free drainage (default free drainage parameter in HYDRUS was used) or ET. The difference in the observed and simulation may be due to the undisturbed samples taken, while the profile was highly disturbed during trenching of sludge.

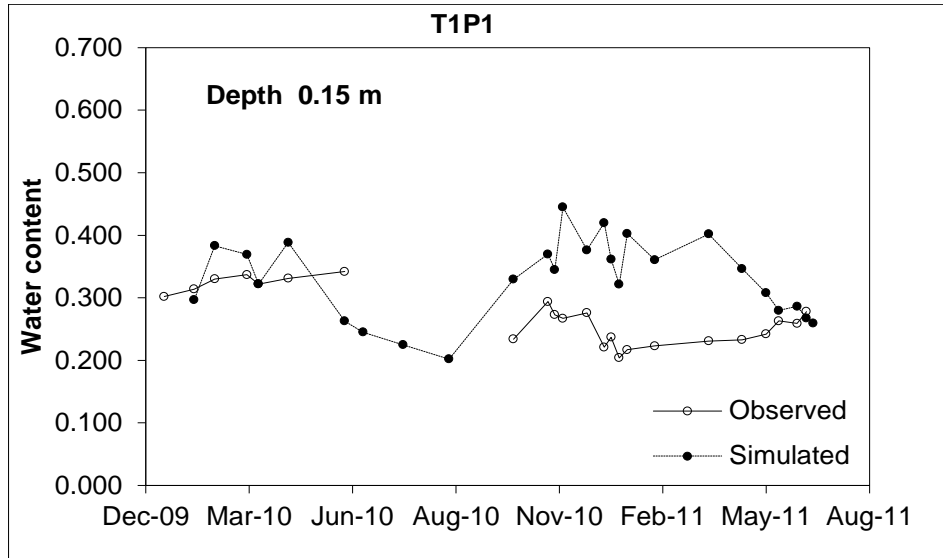


Figure 5.2 Observed and simulated water contents in treatment 1 (T1) at SAPPI

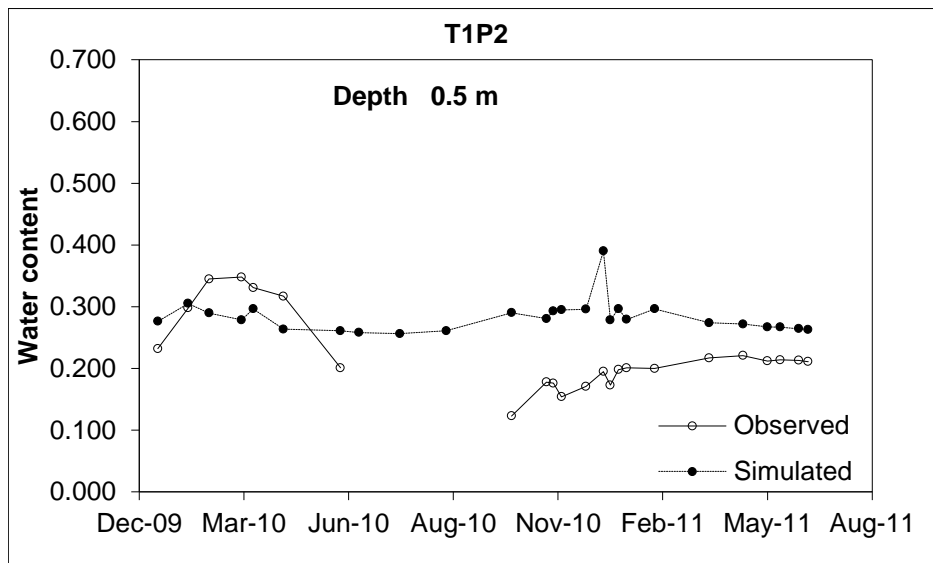


Figure 5.3 Observed and simulated water contents in treatment 1 (T1) at SAPPI

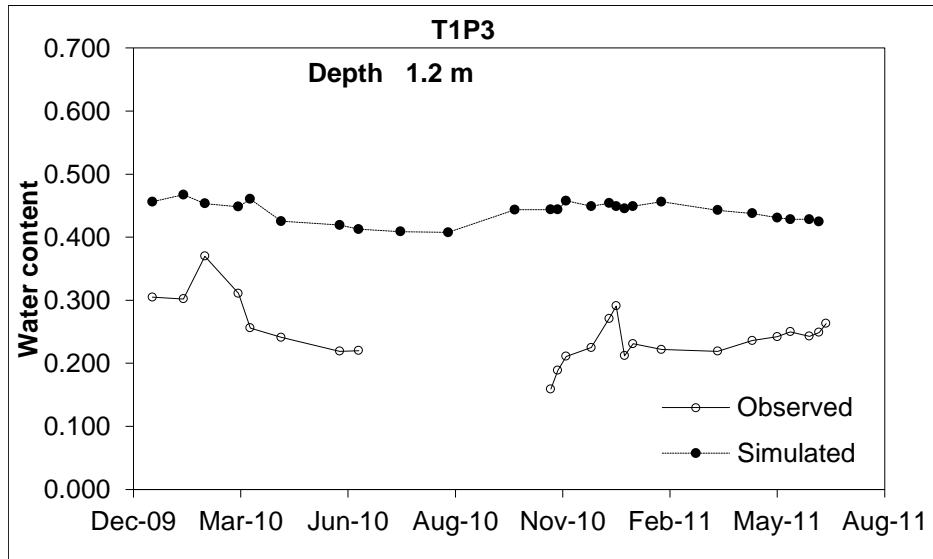


Figure 5.4 Observed and simulated water contents in treatment 1 (T1) at SAPPI

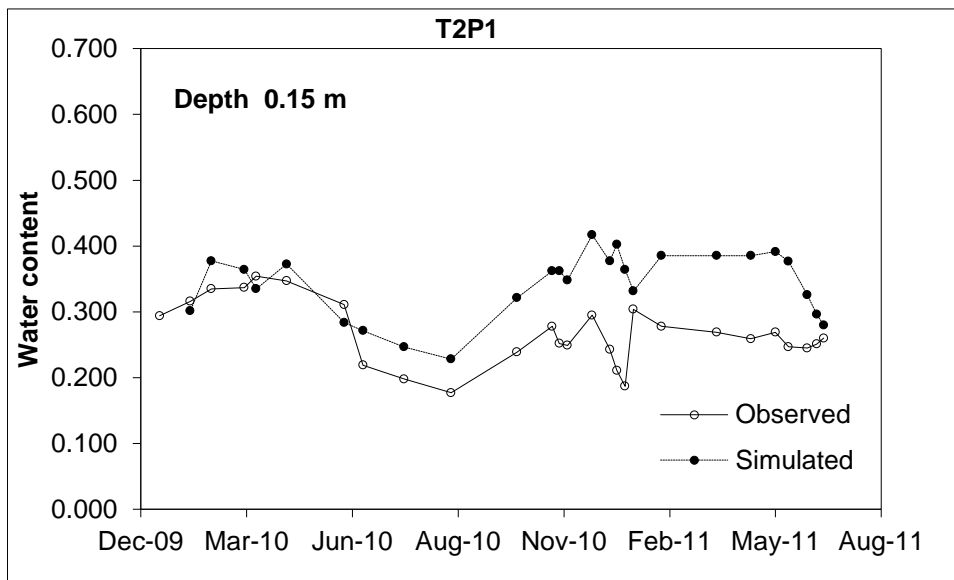


Figure 5.5 Observed and simulated water contents in treatment 2 (T2) at SAPPI

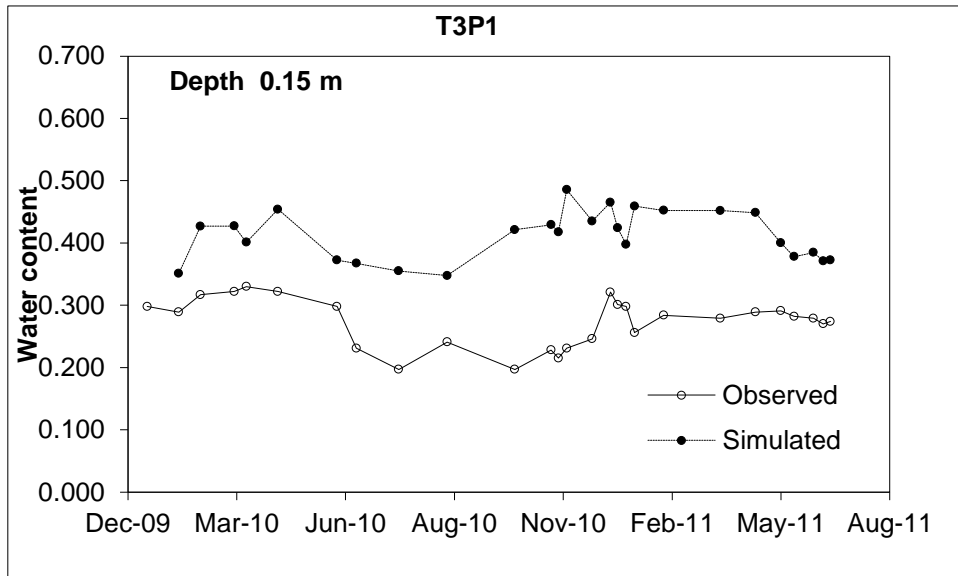


Figure 5.8 Observed and simulated water contents in treatment 3 (T3) at SAPPI

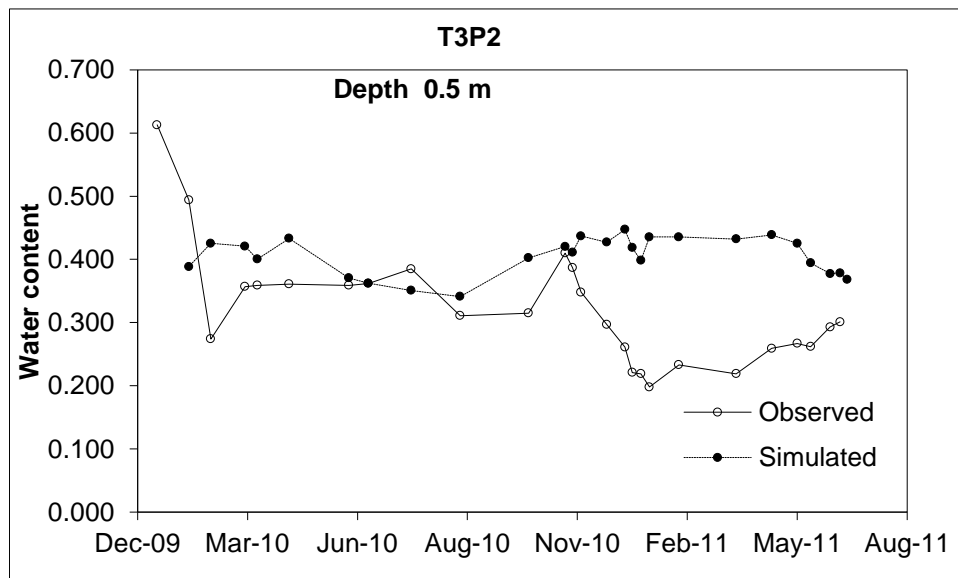


Figure 5.9 Observed and simulated water contents in treatment 3 (T3) at SAPPI

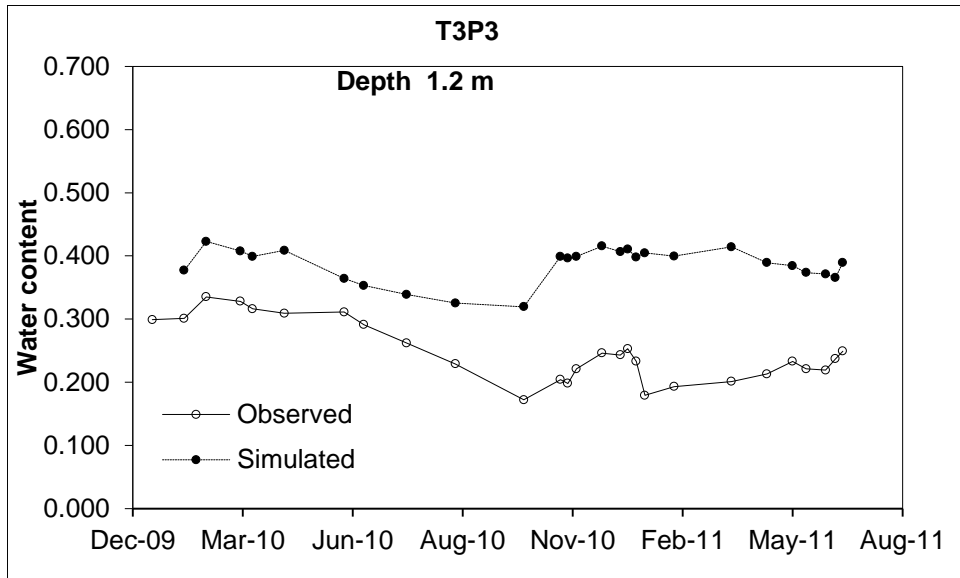


Figure 5.10 Observed and simulated water contents in treatment 3 (T3) at SAPPI

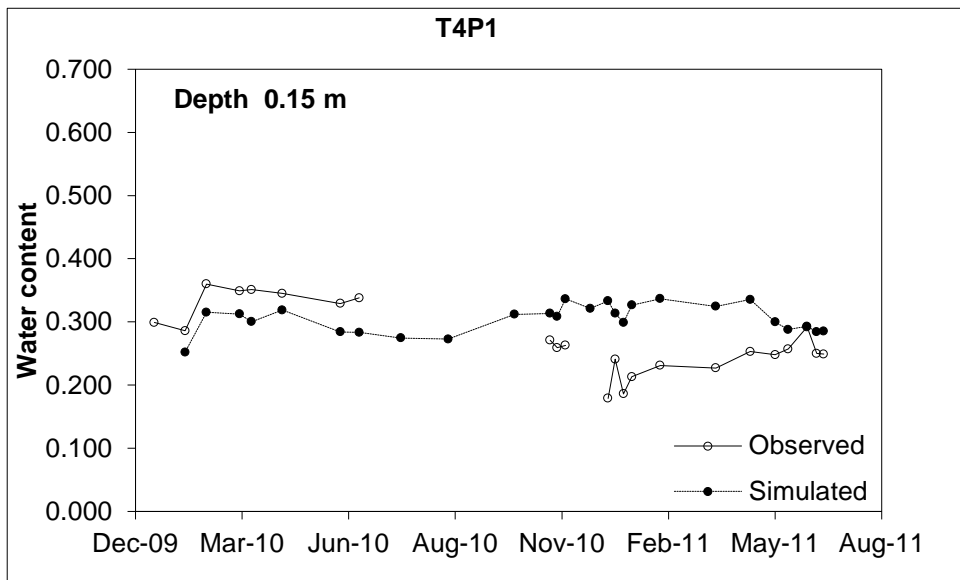


Figure 5.11 Observed and simulated water contents in treatment 4 (T4) at SAPPI

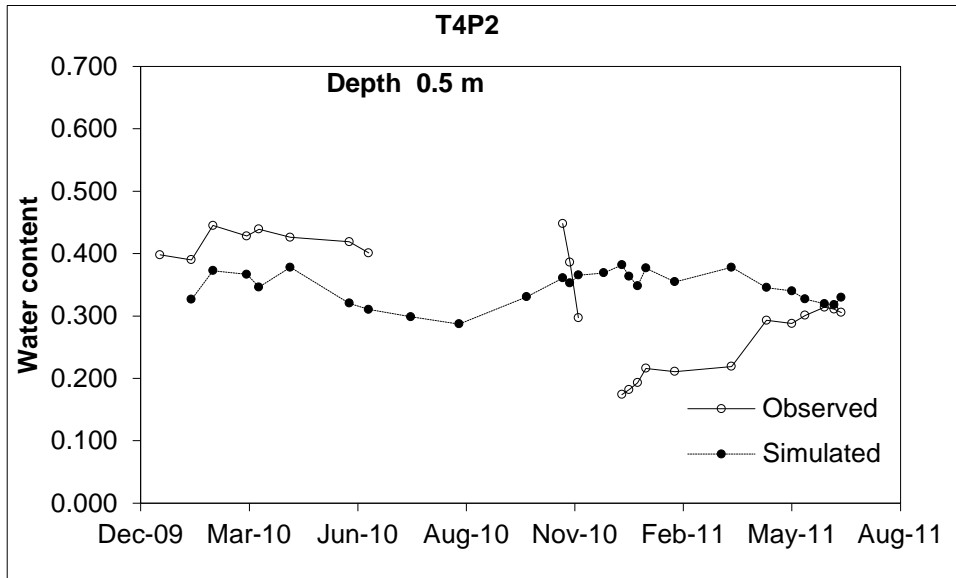


Figure 5.12 Observed and simulated water contents in treatment 4 (T4) at SAPPI

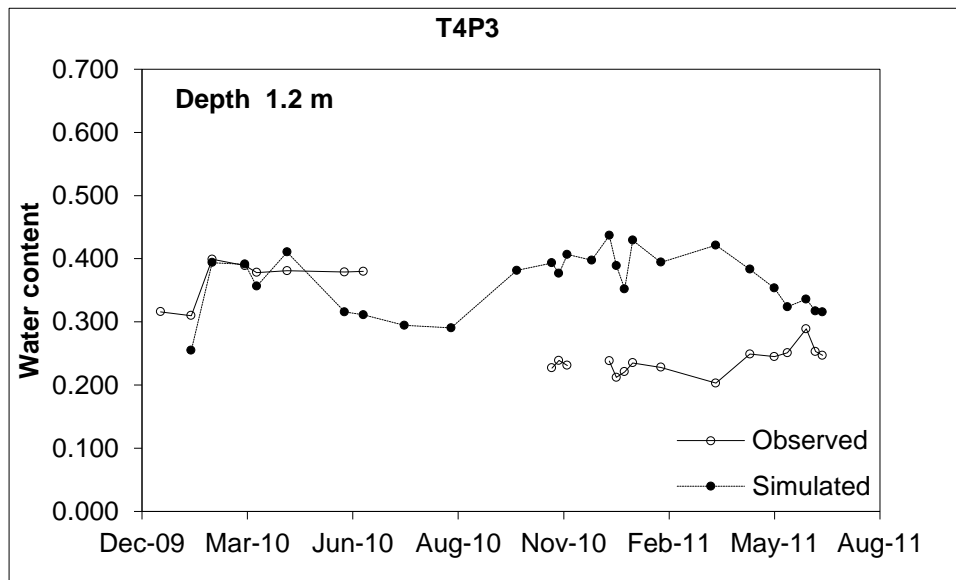


Figure 5.13 Observed and simulated water contents in treatment 2 (T2) at SAPPI

Using dispersivity values adapted from Reneau *et al.* (2005), observed and simulated nitrate concentrations were compared for treatments T1, T2 and T3. To examine the predictability of the model, the simulation was carried out to predict the nitrate distribution, using a simulation period of 638 days (number of days from the start of experiment to the last day of data collection). Simulated and observed values of nitrate indicated some differences in treatments at certain depths (Figures 5.12 to 5.20). The correlation coefficient between simulated and observed nitrate

concentration varied from -0.602 to 0.959. The RMSE between simulated and observed varied from 3.84 to 74.19. These differences might have occurred through biological or chemical changes following collection, which affected the observed data. The collected samples were kept in cold storage until analysis, but further precautions may have been necessary. For example, the samples could have been treated with mercuric chloride (HgCl_2) to inhibit bacteria, which are applicable for nitrogen and phosphorus forms. In addition, the parameter selection such as dispersivity values and hydraulic properties may require accurate measurements. Simulated nitrate transport in Treatments 3 (T3) for six characteristic times at the SAPPI site is shown in Figure 5.18.

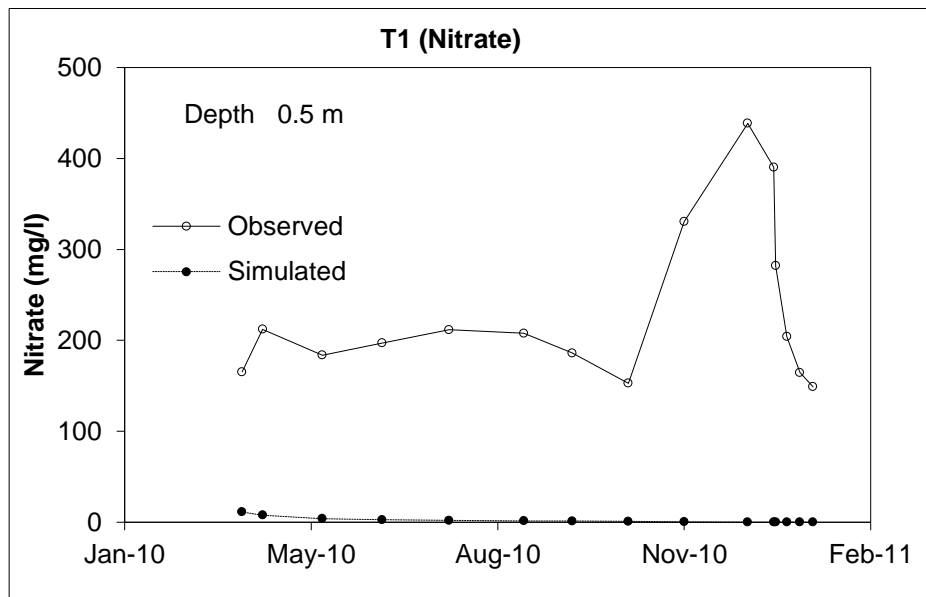


Figure 5.14 Observed and simulated nitrate in treatment 1 (T1) at a depth of 0.5 m at the SAPPI site

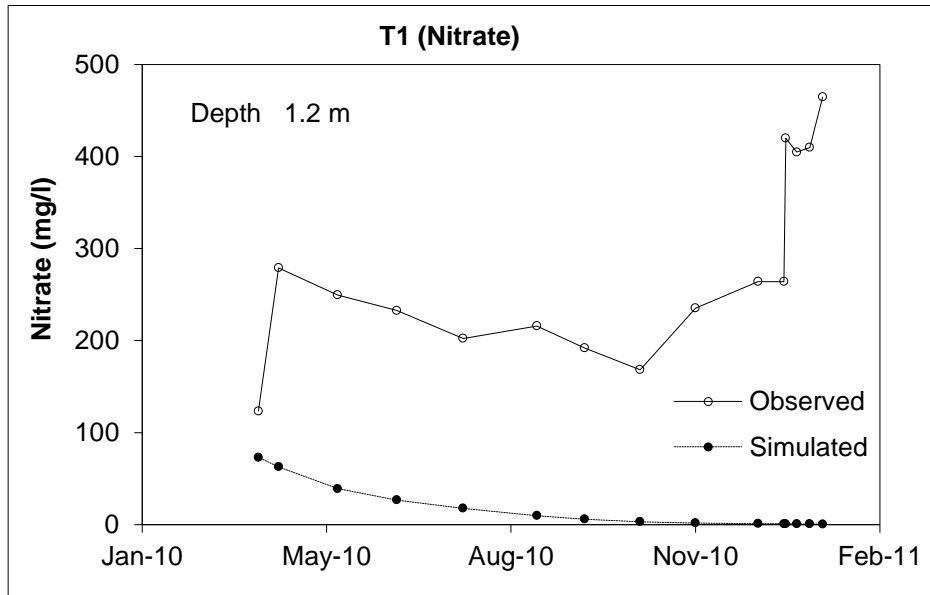


Figure 5.15 Observed and simulated nitrate in treatment 1 (T1) at a depth of 1.2 m at the SAPPI site

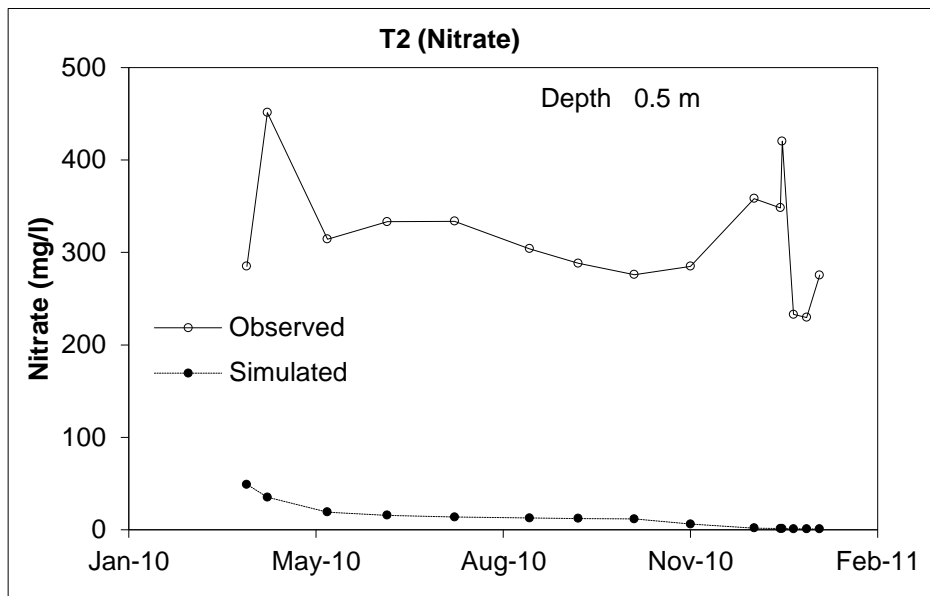


Figure 5.16 Observed and simulated nitrate in treatment 2 (T2) at a depth of 0.5 m at the SAPPI site

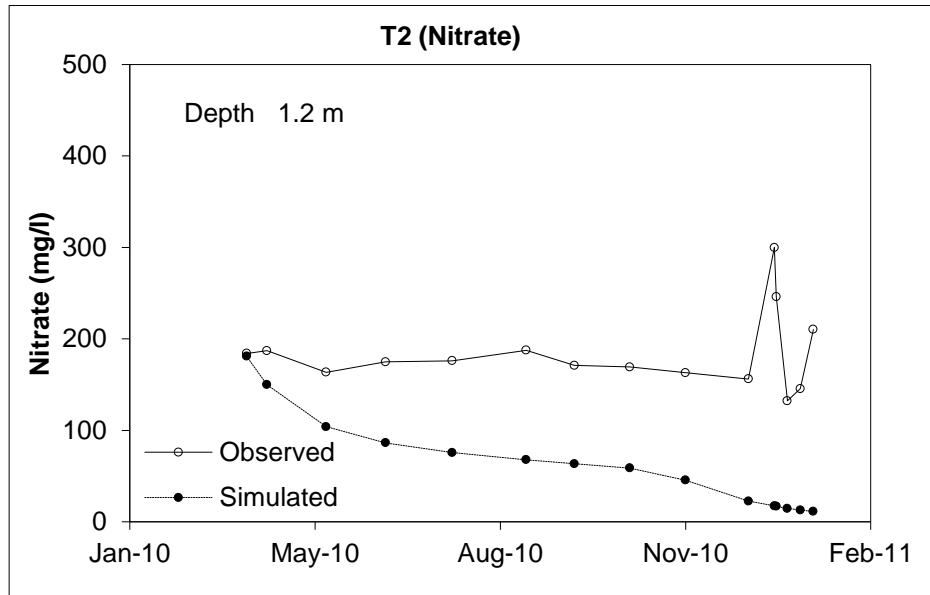
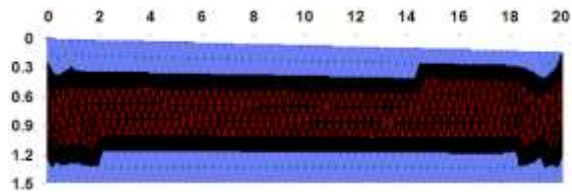
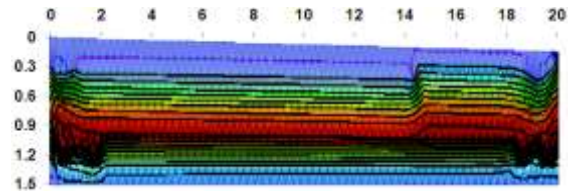


Figure 5.17 Observed and simulated nitrate in treatment 2 (T2) at a depth of 1.2 m at the SAPPI site

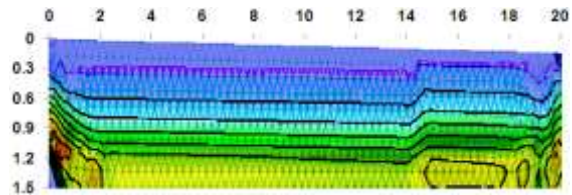
HYDRUS 2-D simulations, compared to the field data from wetting front detectors indicated an under-estimation of nitrate concentrations in the profile in most of the treatments at SAPPI. Clearly, the degradation rates used in the model should be reduced. The simulations, thus provide evidence that nitrate degradation values derived from a study on the use of effluent in irrigation (Hassan et al., cannot be transferred to this case where the soil water nitrate was derived from seepage from the waste sludge.



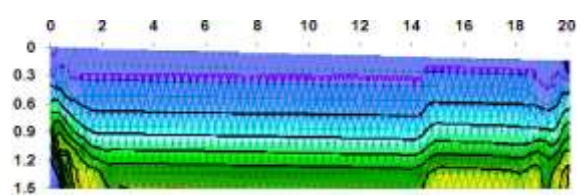
1 January 2010 (t = 0 d)



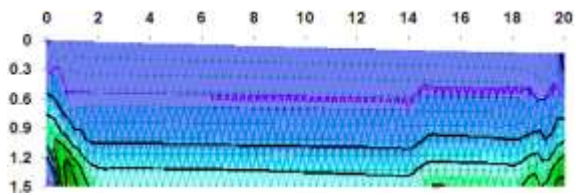
7 February 2010 (t= 38 d)



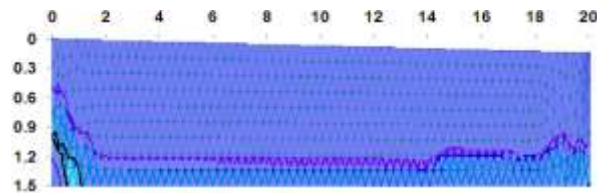
12 April 2010 (t = 102 d)



18 August 2010 (t = 230 d)



5 January 2011 (t = 370 d)



30 September 2011 (t = 638 d)

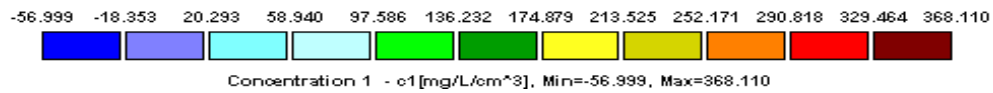


Figure 5.18 Simulated nitrate transport in Treatments 3 (T3) for six characteristic times
At the SAPPI site (Dimensions in m)

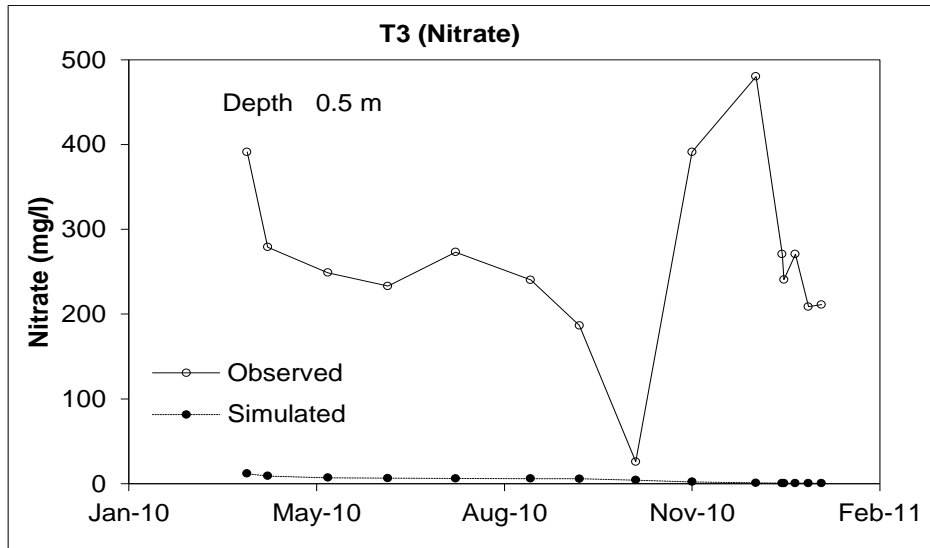


Figure 5.19 Observed and simulated nitrate in treatment 3 (T3) at a depth of 0.5 m at the SAPPI site

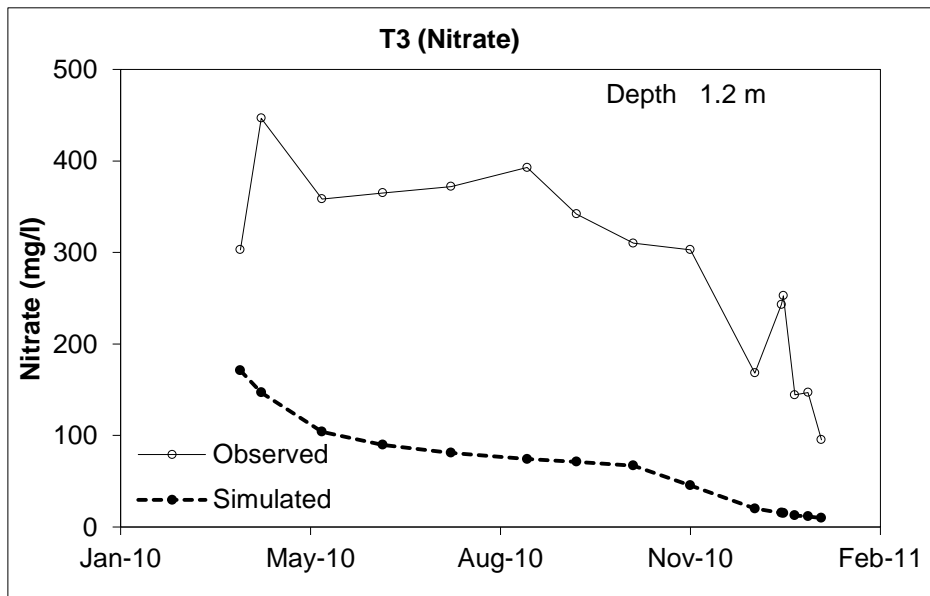


Figure 5.20 Observed and simulated nitrate in Treatment 3 (T3) at a depth of 1.2 m at the SAPPI site

Phosphorus (P) in solutions is attached soil particles and is strongly absorbed by the soil, forming stable bonds with the soil. The soil absorbs P molecules in the soil solution. Phosphorus then interacts with soil particles in its exchangeable form. Although phosphate is strongly absorbed by soil particles, many recent studies have shown that phosphate can easily be found in subsurface

fresh water (Enright and Madramootoo, 2003; Simard, 2005). As the concentration of phosphate increases in the soil solution, the phosphate is adsorbed to the soil, while the concentration of phosphate in the solution is depleted, the phosphate adsorbed in the soil dissolves back into solution. The prediction of phosphorus transport in soil can be improved with the correct application of computer modelling for simulating P distribution under laboratory and field conditions. Ben-Gal and Dudley (2003) concluded in their experiment that the Langmuir isotherm, provided with the HYDRUS-2D model, is inadequate for describing P sorption. It assumes instantaneous equilibrium between the solid and solution interfaces. The comparison of simulated and observed P (Figures 5.21 to 5.26) in all treatments, shows that there was no significant variation in concentration over the monitoring period, except in a few cases, where the model over-estimated the P concentrations at certain depths. This could be due to an inappropriate adsorption coefficient (too low) used in the model for these soils.

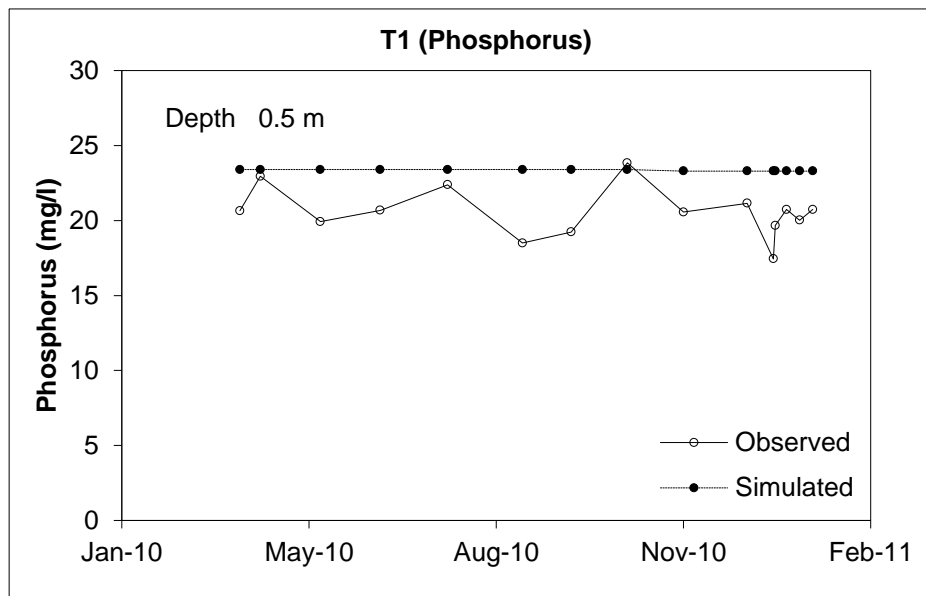


Figure 5.21 Observed and simulated phosphorus in Treatment 1 (T1) at a depth of 0.5 m at the SAPPI site

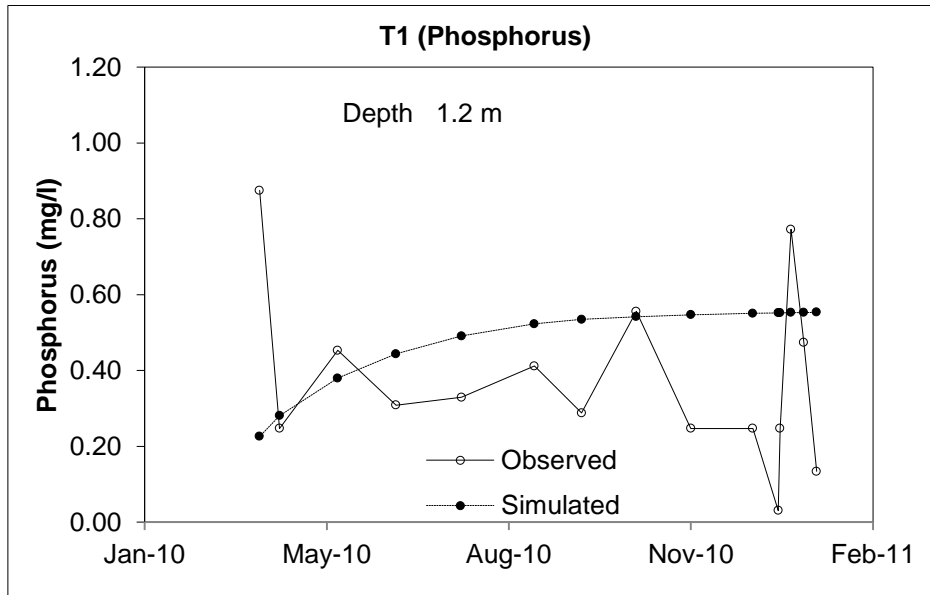


Figure 5.22 Observed and simulated phosphorus in Treatment 1 (T1) at a depth of 1.2 m at the SAPPI site

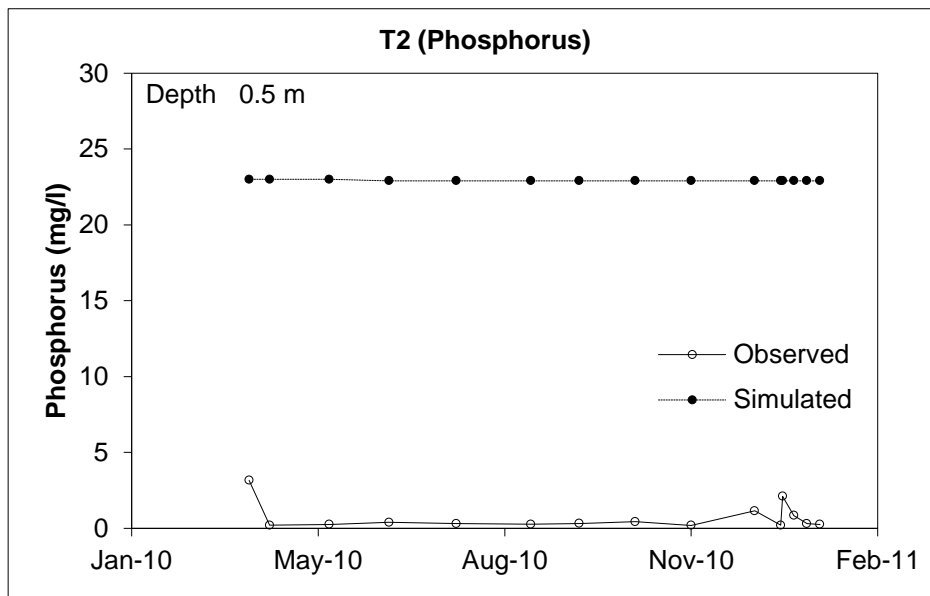


Figure 5.23 Observed and simulated phosphorus in Treatment 2 (T2) at a depth of 0.5 m at the SAPPI site

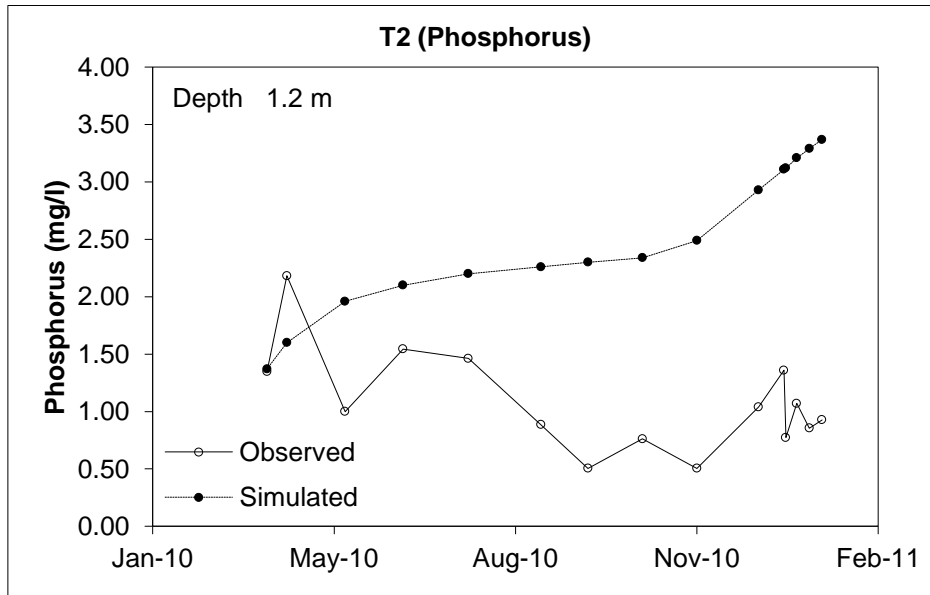


Figure 5.24 Observed and simulated phosphorus in Treatment 2 (T2) at a depth of 1.2 m at the SAPPI site

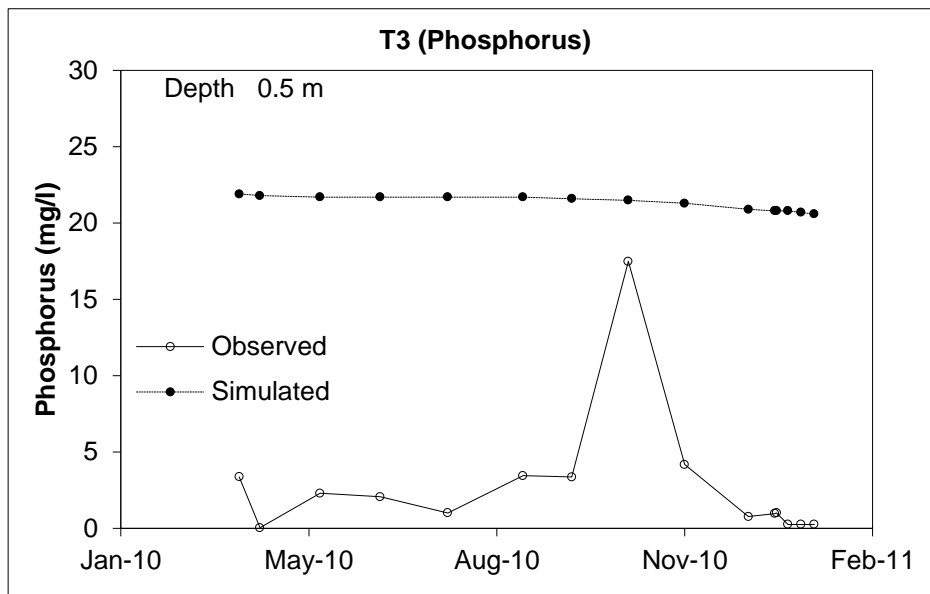


Figure 5.25 Observed and simulated phosphorus in Treatment 3 (T3) at a depth of 0.5 m at the SAPPI site

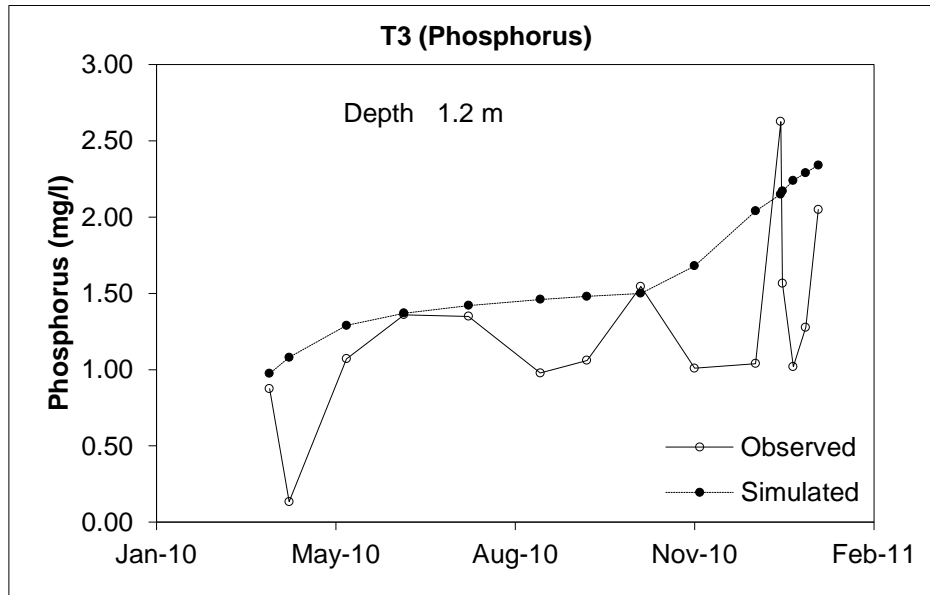


Figure 5.26 Observed and simulated phosphorus in Treatment 3 (T3) at a depth of 1.2 m at the SAPPI site

The results indicated that there was good correlation between observed and simulated NO_3 and P concentrations in some of the treatments and depths, while some show significant differences. Treatment 3 (T3) at the depth of 1.2 m showed the highest R^2 value of 0.5746 between observed and simulated nitrate concentrations, and R^2 value 0.3405 for phosphorus concentration, and also in T2 at the depth of 1.2 m with R^2 value of 0.3405 for phosphorus concentrations. T1 at the depth of 0.5 m also indicated moderately less R^2 value of 0.1057 and R^2 value of 0.2015 and 0.1545 for nitrate and phosphorus concentrations respectively at T1 at the depths of 0.5 m and 1.2 m. The rest of the treatments and depths indicated very low R^2 values from 0.0023 to 0.0953 for nitrate and phosphorus concentrations. The higher R^2 values indicated a good correlation and the smaller R^2 values an indication of significant differences between observed and simulated concentrations (Table 5.4). While the direct correlations are generally poor the responses of the simulation and observations are similar. Moreover, these similarities are true for the range of depths simulated in each profile. Hence simulated nutrient fluxes can be accepted. The differences between model and experiments may be as a result of the application of default free drainage boundary condition in HYDRUS, without sufficient time for the reaction between the soil and solute. Overall, the simulated P concentration in the treatments tended to be slightly higher than observed concentrations. These differences may also occur as a result of the increase

in error with depth, due to preferential flow paths and/or the choice of incorrect adsorption isotherms. Hillslope scale observations included the accumulated lateral flow observed in piezometers at the downslope edge of the trial area. Borehole levels and concentrations were also used to interpret the likely pathways and contribution of nutrients to the fractured rock aquifer from the buried sludge. Nutrient concentrations measured in the stream were used as a baseline in assessing fractured rock groundwater impact.

These observations were used collectively to derive a sketch of the likely flow paths and storage elements in the trial site (Figure 5.27). Water infiltrating into the profile was subject to evapotranspiration. During periods of high rainfall, subsurface water accumulated on the soil/bed-rock interface, resulting in lateral flows down-gradient. These responses were rapid in most parts of the hill-slope, but extended periods of perched water were observed at the lower end of the trial site. While some seepage water may have percolated into the fractured bedrock, no evidence of this was found in the borehole monitoring.

Table 5.4 Correlation between observed and simulated NO₃ and P concentrations at SAPPI

Treatment	Depth(m)	R ²	
		NO ₃	P
T1	0.5	0.1057	0.0953
	1.2	0.2015	0.1545
T2	0.5	0.0501	0.0967
	1.2	0.021	0.3405
T3	0.5	0.0023	0.0847
	1.2	0.5746	0.3405

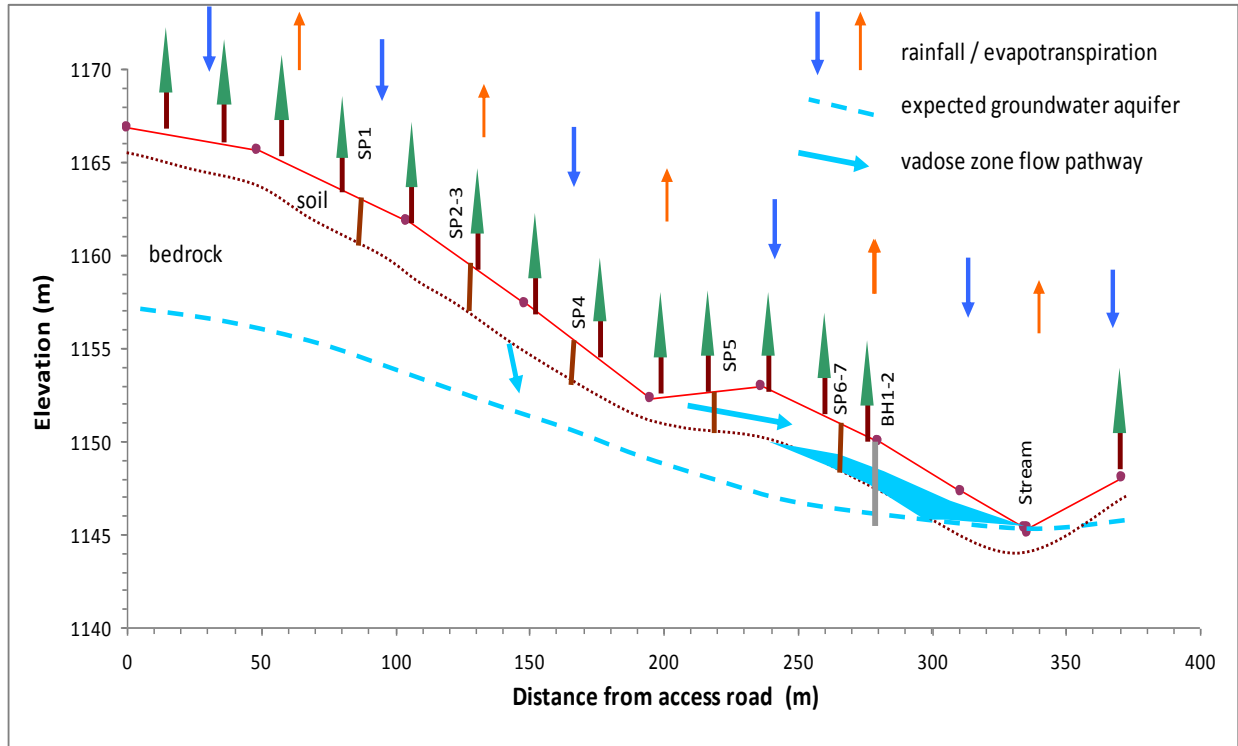


Figure 5.27 SAPPI trial site schematic flow path, showing rainfall input, evapotranspiration, subsurface pathways and accumulation, boreholes (BH-) and piezometers (SP-)

From an estimate of the likely load discharging from the near-surface, lateral flow source has been estimated. The geophysics sections of the SP6 and SP7 piezometer locations were used, together with observed depths in the piezometers, to calculate a cross-sectional area, A_i , of down slope discharge, as shown in Figure 5.28, for the prevailing depth of flow. The hydraulic gradient, $\Delta H/\Delta L$, of this near-surface discharge was taken as the surface slope, surveyed along the western edge of the trial (Figure 5.29) and the hydraulic conductivity of the material, K_{sat} , was measured using, the Guelph permeameter. The discharge, Q_i , for each time interval, Δt_i , between sampling events, was then calculated, using Darcy's law as:

$$Q_i = A_i \cdot K_{sat} \cdot \Delta H / \Delta L \quad 5.6$$

The mass load, M , of NO_3 and P was determined for each sampling interval, i , by multiplying the respective concentration, C_i with the discharge, Q_i and the time interval. These were summed, to derive the cumulative mass load during the sampling period as:

$$M = \sum_{i=1}^n Q_i C_i \Delta t_i$$

5.7

The mass loading in the stream was also estimated for the monitored period, as a comparison of the mass contributed from the trial hillslope. The catchment area of the stream (Figure 5.39) was multiplied by the average monthly runoff factor and measured rainfall for the monitored months, to determine an average discharge in the stream. This was multiplied by the measured concentrations of NO₃ or P and the time interval, to yield a mass load. These loads were cumulated and are shown in Figure 5.30.

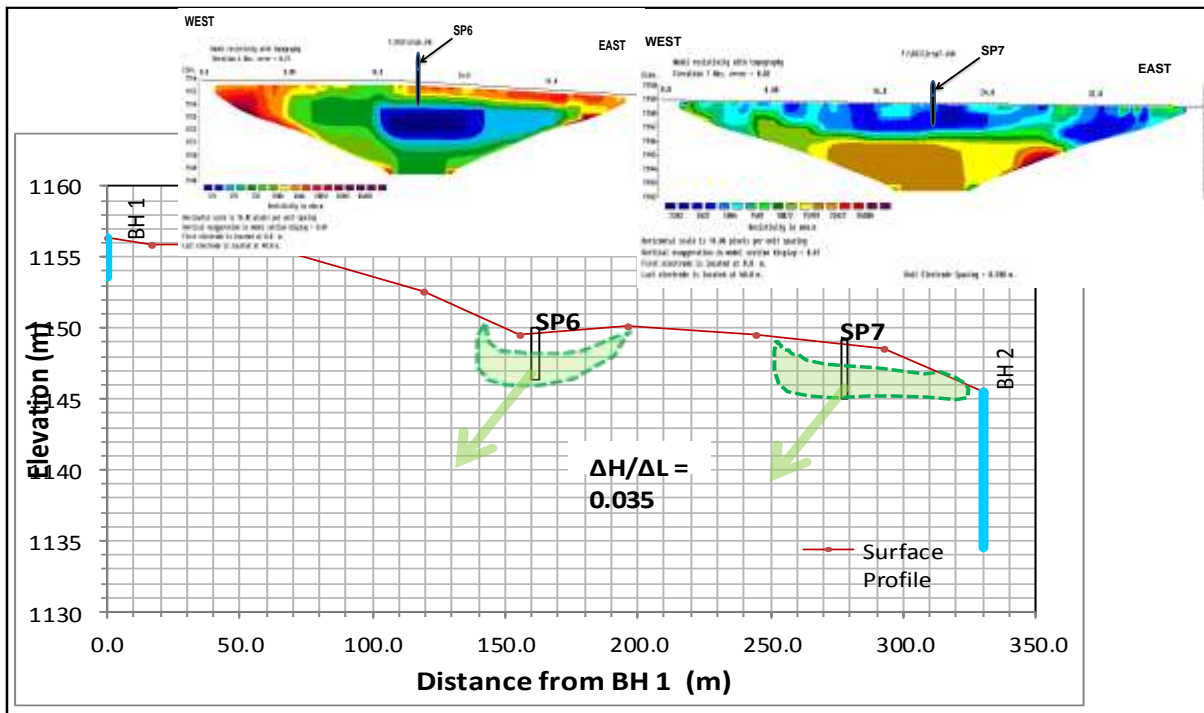


Figure 5.28 Illustration of the near surface preferential flowpath cross-sectional areas at piezometers SP6 and SP7 at the SAPPI site. The green arrows show the downslope flowpath direction.

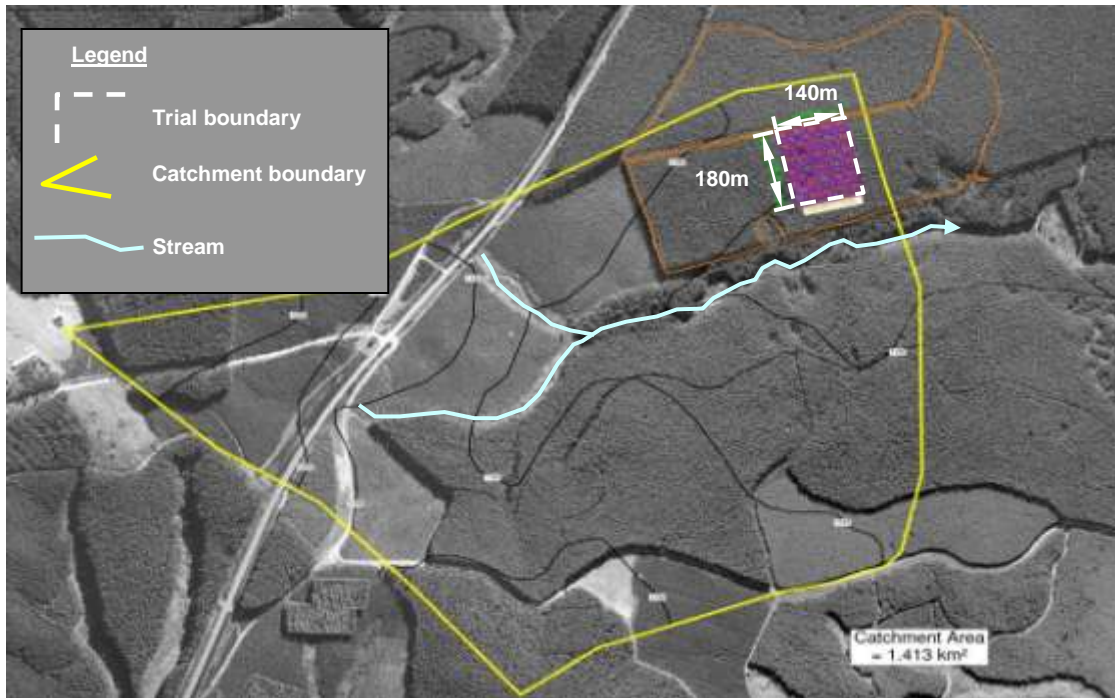


Figure 5.29 The catchment area of the stream on the southern edge of the trial at SAPPI

The mass loading of NO_3 from the hillslope, as shown in Figure 5.30, exceeded that in the stream in the wet season of 2010/2011. The mass loading of P from the hillslope was similar to that in the stream for the monitored period. It is not possible to determine whether the mass loads in the stream were derived as a direct consequence of the discharge from the trial hillslope, since the stream sampling did not include upstream (background) sampling. However, the potential loading from the hillslope is high, with a potential load of 400 kg NO_3 and 4 kg P estimated to discharge from the trial site from December 2010 to February 2011. It was estimated that the potential discharge from the trial site will be about 11 kg/ha/year and 0.11 kg/ha/year for NO_3 and P respectively. There is a buffer zone of open grassland between the trial site and the stream and this could possibly take up a significant portion of the nutrient load from the trial (Fertilized grassland can take up between 100 and 500 kg/ha/year, Whitehead 2000).

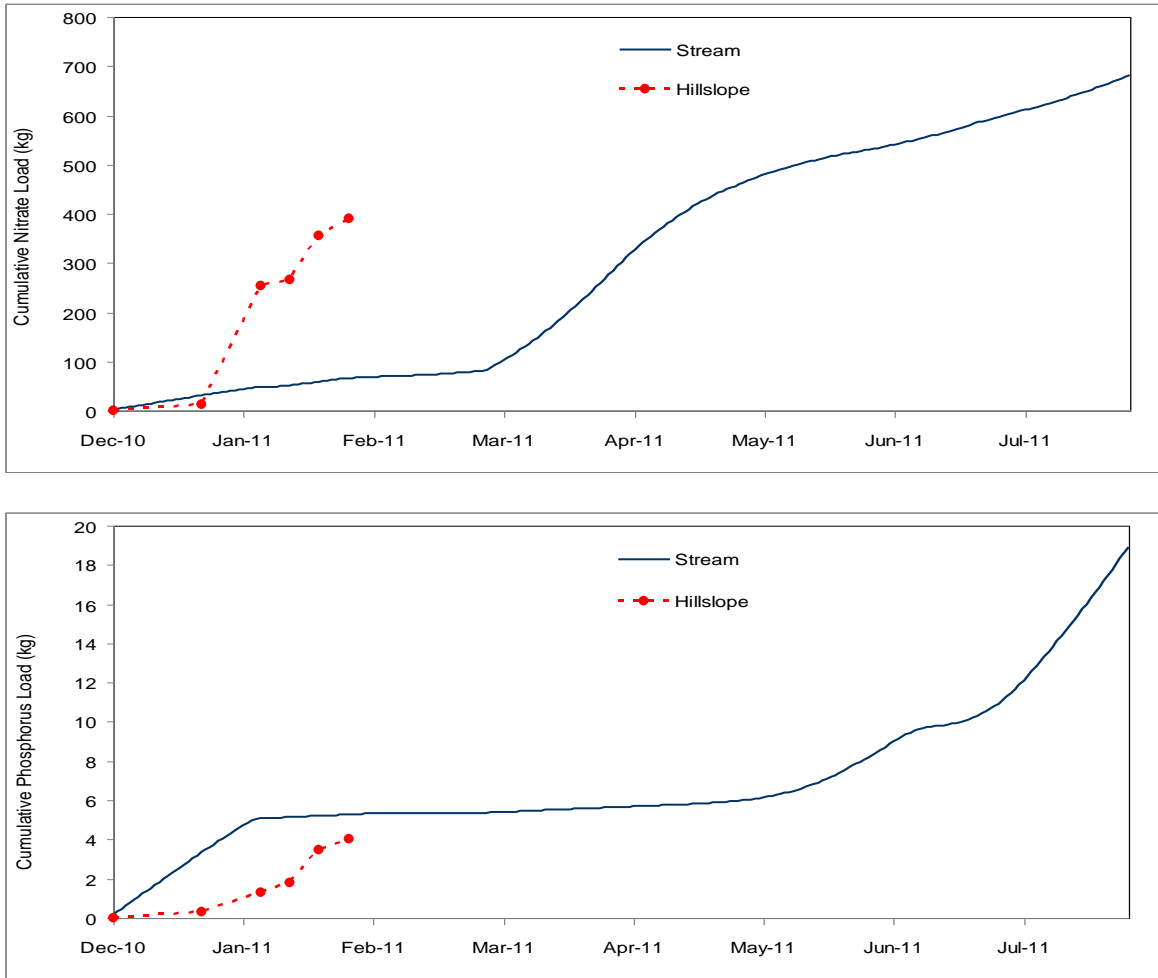


Figure 5.30 Cumulative loads of NO_3 (above) and P (below) from the near surface source and in the stream at the SAPPI site

5.2 Umlazi VIP pit latrine sludge trenching site

Saturated water content, residual water content, water retention parameters and saturated hydraulic conductivity, values in the cross-section, were assigned based on clay, silt and sand percentages derived from subsurface sampling (Table 5.5). The measured data were not used, as it resulted in model instability. Hydraulic properties for WWTW sludge was applied, for the VIP pit latrine sludge, since this analysis was not performed.

Table 5.5 Fitted hydraulic characteristics (van Genuchten and Mualem) of different soil layers and VIP sludge used in the initial simulation.

Material	Class	θ_r cm ³ /cm ³	θ_s cm ³ /cm ³	α (cm ⁻¹)	n (-)	K_s cmday ⁻¹	l (-)
1	Loamy sand	0.057	0.41	0.124	2.28	350.2	0.5
2	VIP sludge	0.0999	0.4972	0.01	1.2685	22.1	0.5
3	Clay loam	0.095	0.41	0.019	1.31	6.24	0.5

θ_r = residual volumetric water content (cm³/cm³),
 θ_s = volumetric water content at saturation (cm³/cm³),
 K_s = Hydraulic conductivity at saturation (cmday⁻¹),
 α = approximation for the inverse of the air entry pressure (cm⁻¹),
 n = pore size distribution index and
 l = pore connectivity parameter.

Water flow and solute transport were modelled within the flow domain comprising the 180 m between the sludge burial site and the nearby stream and the soil profile depth of 14 m. Three materials or layers, pit latrine sludge, loamy sand and clay loam, were distinguish, as shown in Figure 5.32.

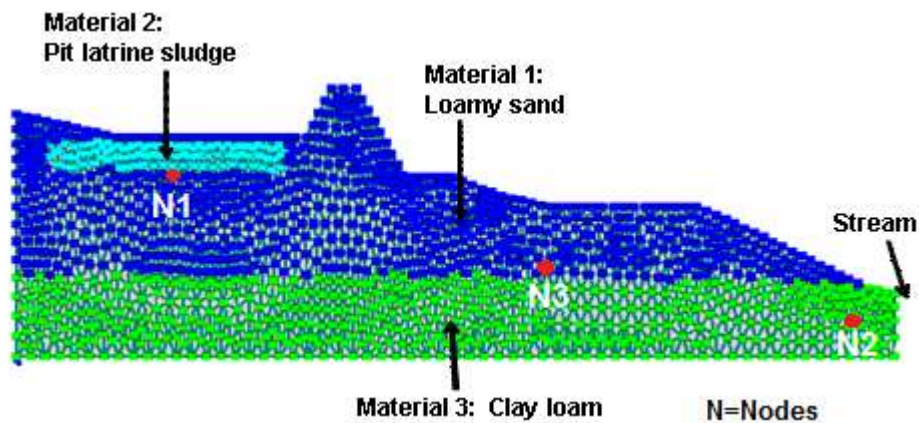


Figure 5.31 Material distributions in profile at Umlazi site

Specific physical and chemical parameters (phosphorus adsorption isotherms, denitrification rate constant and dispersion coefficient) were used to simulate the movement of nitrate and phosphorus through the soil profile. Concentrations of nitrate, which was about 581 mg/l and phosphorus 225 mg/l, measured (using HACH instrument) from samples from installed WFD in trench prior to the simulation (1 January 2009), were assumed to be constant across the pit latrine

sludge in the trench and were used as the initial condition for solute transport. The solute transport parameters applied at the Umlazi site are the same parameters adapted from Hassan *et al.*, 2010 which were previously explained are presented in Table 5.5. The analysis considered the Umlazi soil profile to 14 m below the surface. Root water uptake was not simulated initially, since the tree water uptake was considered low over the first year of simulation. This also comprised a worst case scenario for the migration of nutrients towards the stream. Longitudinal dispersivity and transverse dispersivity values, adapted from Hassan *et al.*, 2010, were also selected for the simulation. These parameters determine the rate of spreading (and thus dilution) of the nutrient solute plume, in the direction of flow (longitudinal), as well as orthogonal to the flow path (transverse), as it moves in the subsurface.

Table 5.6 Solute transport and reaction parameters for materials outside trench (adapted from Hassan *et al.*, 2010).

Material	Bulk density	NO ₃				P
		SinkL1' (d ⁻¹)	L (cm)	T (cm)	D (cm ² d ⁻¹)	K _d (mL ³ mg ⁻¹)
1	1.6	0.005364	20	4	0.84	30
2	1.21	0.005364	10	2	0.84	34
3	1.27	0.005364	10	2	0.84	34

SinkL1': first-order degradation rate constant for dissolved phase in the decay chain reaction (day⁻¹);

L: longitudinal dispersivity (cm);

T: transverse dispersivity (cm);

D: molecular diffusion coefficient in free water (cm²day⁻¹) and

K_d: Langmuir PO₄⁻³ – P adsorption isotherm coefficient (.ml³. mg⁻¹).

The simulation results can be taken as illustrative of the likely solute plume migration and dispersion. Wetting and drying, due to rainfall and soil water evaporation results in the formation of wet and dry zones in the near the surface of the soil profile. The sludge pack dewarped from the top down. Varying soil conditions impact the transport of rainfall and, by association, the leaching of soluble component out of the trench; this effect was expected to be immediate and pronounced in sandy soils characterised by high hydraulic conductivities at the Umlazi site. Hence the buried pit latrine waste was specified as initially containing dissolved nutrients of concentrations measured in the first few months and therefore being subject to rain water leaching and soil water evaporation, without further generation of nutrients from the buried

waste. This was justified by the rapid depletion observed in other studies (Kostyanovsky *et al.*, 2011) as discussed in the literature review. Simulation for the Umlazi site was performed from 01/01/2009 to 30/09/2011.

The progress of the nitrate plume is clearly illustrated in the simulated profiles shown in Figure 5.32. Although the simulation was started only in January 2009, the nitrate plume has migrated outside of the burial site by the winter of 2009 (20 July 2009 in Figure 5.32). The dispersion of the original concentrations is also evident, as dilution due to mixing, adsorption and chemical modification, occur in the migration pathway. By 17 May 2010, the simulation reveals plume concentrations to be similar to background sources.

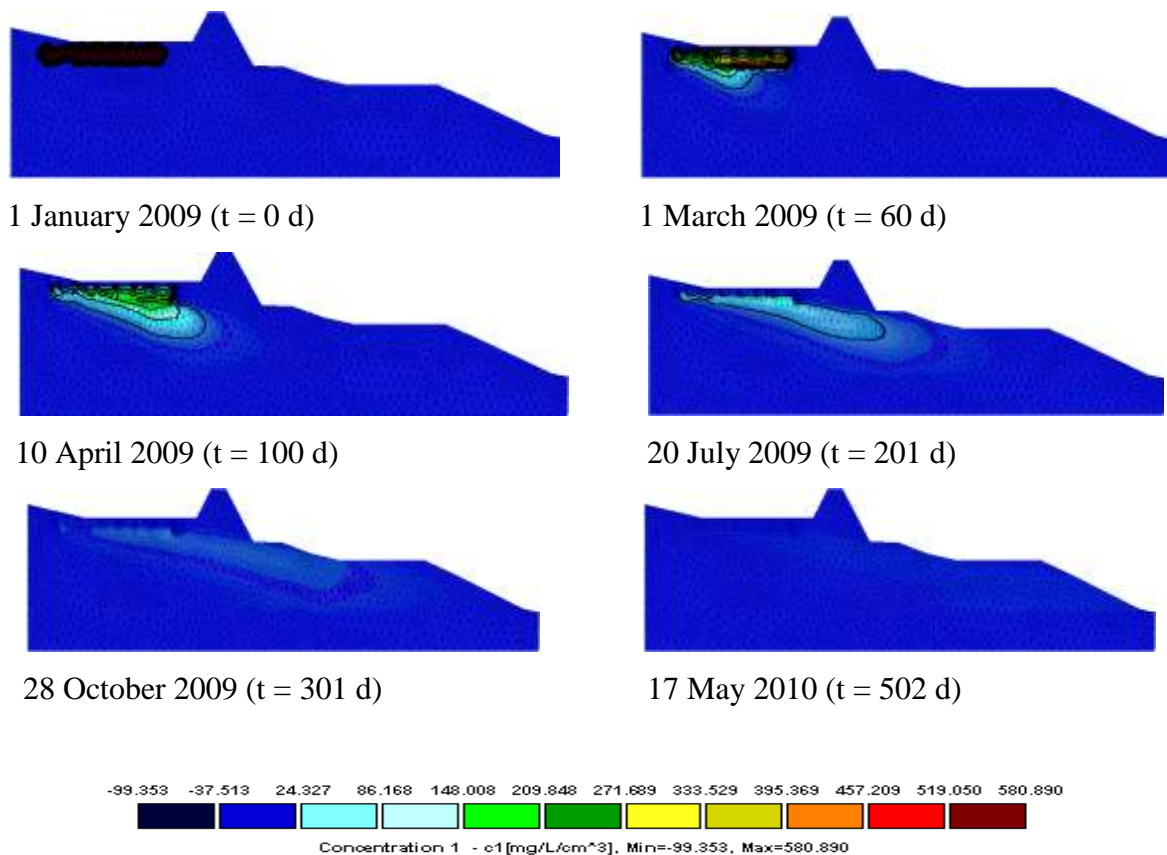


Figure 5.32 Simulated NO₃ concentration distributions in the flow domain for eight characteristic times during the period from 1 January 2009 to 30 September 2011 at the Umlazi site

The arrival of the plume and the dispersion and dilution process is also evident in the time history of nitrate concentrations at the observation node points. At observation Node 1, below the waste trenches, the nitrate concentration peaks within the first 100 days at 100 mg/l. However, by the time the peak of the plume reaches the borehole observation site (Node 3, 110 m from trenches), 200 days later, the maximum concentration has been reduced to 7 mg/l. Nitrate concentrations peak at the near-stream observation node (Node 2) a further 200 days later and peak nitrate concentrations are below 1mg/l. Comparing the simulated nitrate concentrations at the boreholes with the observed series (Figure 5.33) reveals similar concentrations between simulated and observed time series, so the dilution, dispersion and change processes appear to have been simulated accurately. The simulated peak concentrations seem to have a delayed response, compared to the measured data. This could be due to the simulations starting in January 2009, while the wastes were buried in late 2008. Nevertheless, the simulations confirm that the nitrate plume from the trenched site does not elevate nitrate concentrations in the ground water above natural levels.

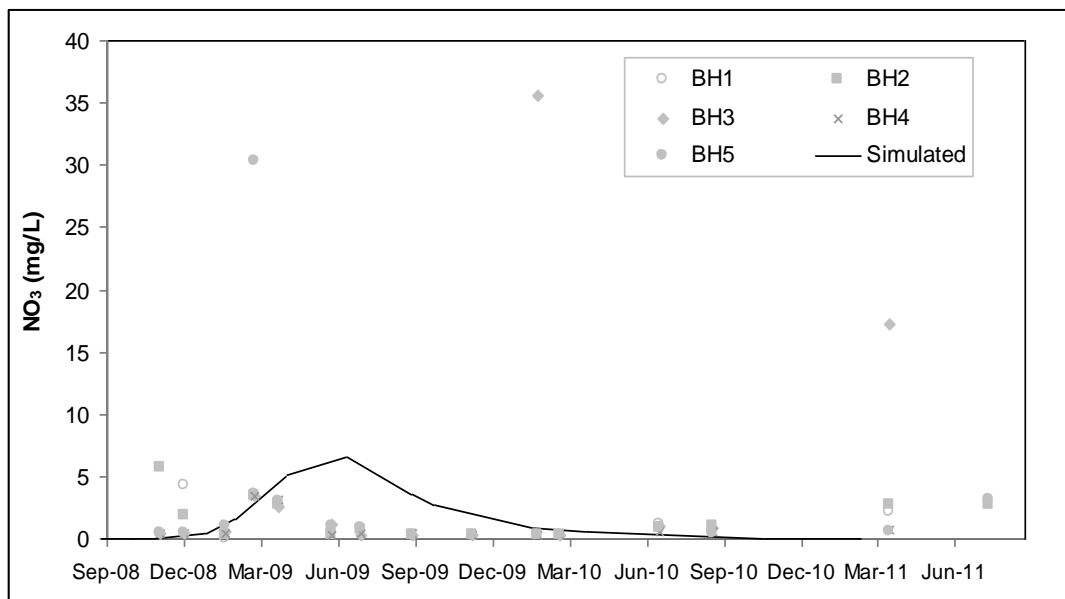


Figure 5.33 Observed (all boreholes) and simulated (node 3) NO₃ concentration at Umlazi

Observations of the phosphorus plume are shown in Figure 5.38. Due to the strong adsorption of P to the soils, concentrations of the dissolved phase continue throughout the simulation period. However, simulated concentrations are systematically reduced along the flow pathway and are

well below those observed at the borehole sites (Figure 5.39). In general, background P was greater than simulated P from buried sludge.

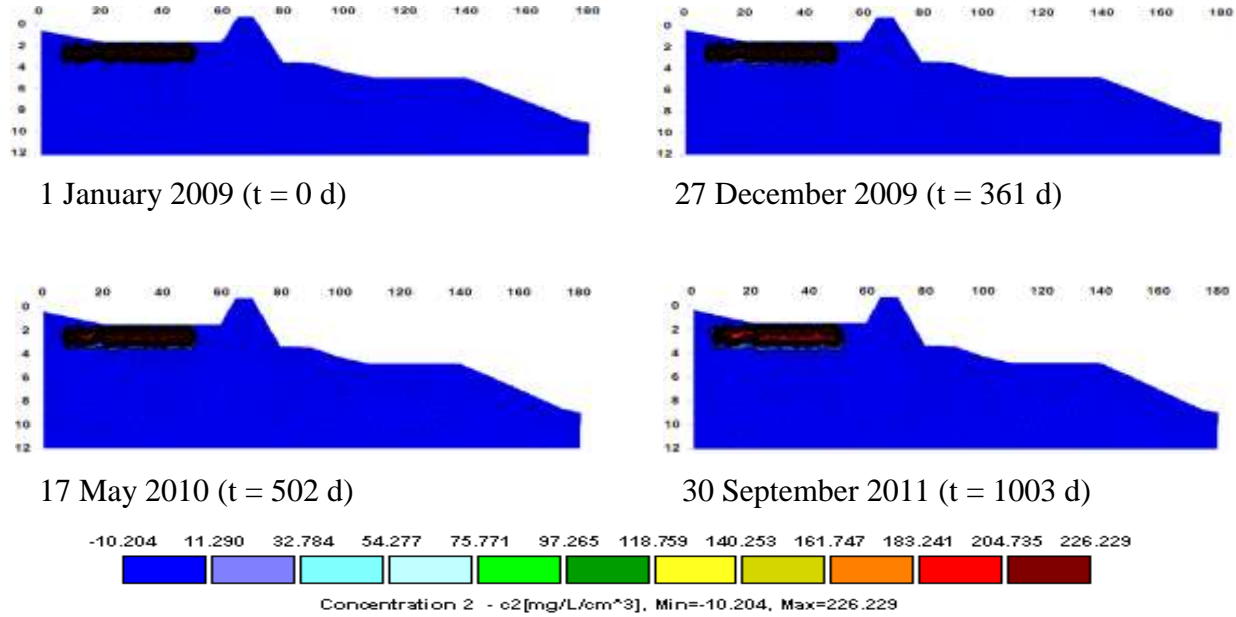


Figure 5.34 Simulated phosphorus concentration distributions in the flow domain for four characteristic times during the period from 1 January 2009 to 20 September 2011 at Umlazi. (y-axis represents depth of profile and x-axis represents distance to stream in m)

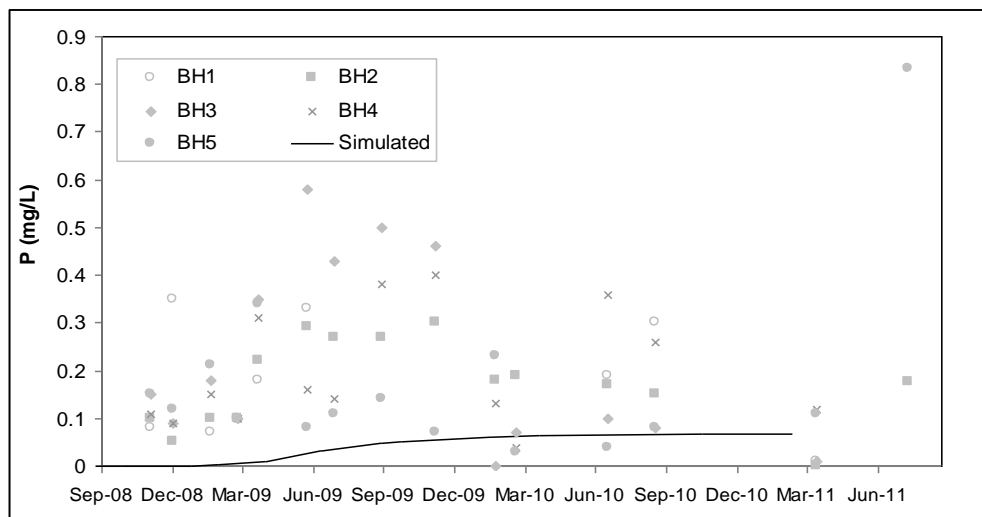


Figure 5.35 Observed (all boreholes) and simulated phosphorus concentration at the Umlazi site

6. CONCLUSIONS

6.1 SAPPI

The movement of water and solute (nitrate and phosphorus), within and below entrenched WWTW sludge has been characterised. High concentrations of nutrients were evident in the water infiltrating into and through the sludge at all treatments. High concentrations of nutrients were evident in perched lateral flow and in preferential flow pathways at the downslope perimeter of the trial. The potential for a mass loading of nutrients in this flux and pathway during the wet season (December 2010 to April 2011) and for extreme events, has been estimated at the SAPPI site to be approximately 400 kg NO₃ and 4 kg P. It was estimated that the potential discharge from the trial site will be about 11 kg/ha/year and 0.11 kg/ha/year for NO₃ and P respectively. The calculations based on rainfall from literature estimated leaching values of 4.43 kg/ha/year and 1.68 kg/ha/year for NO₃ and P respectively (FAO, 2003). The nitrate discharge estimated for SAPPI is considered on the high range, even though the contributing area (sludge trenching area 180 m x 140 m) is small. The P is below the estimated discharge, suggesting utilisation by the planted trees. Also there effects of a vertical seepage of nutrients into the deep aquifer in fractured rock was not observed in the deep borehole, but the potential for seasonal fluctuations and future increases has not been determined.

The use of modelling to simulate the processes and interactions of nutrients and water fluxes within the vadose zone, require accurate field measurements to quantify the processes and validate the simulation results. Continuation of this project is quite possible, with several different aspects requiring further investigation such as, measurements of dispersivity of nutrients in the soil, accurate hydraulic and solute transport parameter determination. It has been identified that additional work would be required to simulate plant water and nutrient uptake, for understanding the total water and nutrient fluxes. With the potential for the use of a soil-water and nitrate movement model being demonstrated, further research into the calibration and validation of the model has, a potential to improve the model performance. A continued monitoring of the deep groundwater through the two boreholes and the near-surface lateral flows

through the piezometers is recommended for at least one further season. This should be conducted in conjunction with upstream (background) and downstream sampling in the stream.

6.2 Umlazi

Although the monitoring at the Umlazi site was hampered by drainage and instrumentation problems, sufficient observations have been made to conclude that:

- No excessive loading of nitrate or phosphorus has moved beyond the burial site;
- Simulations indicated a response distance time of 100 days between burial and observation of a nitrate plume at the borehole. However, the peak plume concentrations do not exceed a background seasonal variations of nitrate;
- Occasional elevated concentrations of nitrate and phosphorus were observed in the borehole record, but the long-term mass loading from the buried waste site seems unlikely to exacerbate eutrophic conditions and
- The modelling of phosphorus and nitrogen are further enhanced by the inclusion of relevant parameters and processes and the extended observations.

It is recommended that the monitoring of the available borehole sites is continued and that periodic gravimetric sampling of the profiles within and between the trenches continues, in order to track the level of nutrients at the source.

6.3 Comparison of Sites

The differences between the SAPPI and Umlazi experiments included differences in waste type, as well as the subsurface properties. The Umlazi site was on a flat, alluvial, sandy deposit, with a shallow water table (5 m). The waste type comprised VIP pit latrine contents. The SAPPI site was located on shales, overlying a dolerite sill on a relatively steep slope, with opportunities for near-surface, preferential flow, which could intersect the waste trenches and carry nutrients downslope. It is apparent that NO_3 and P concentrations generated within the trenches in the early phase of the experiment are similar at both sites and waste types (Table 6.1). The VIP pit latrine waste may yield higher P concentrations than the sewage sludge, but observations from

piezometers, downslope of the deposits at both locations, were similar. Off-site concentrations observed in boreholes are similar at both sites and do not appear to be affected by effluent from the trenched waste, at least over the monitored period. Water in the receiving streams does not appear to have been affected in excess of their seasonal concentration variations. However, the rapid and highly concentrated mass loading from the near-surface at the SAPPI site requires further observation.

Table 6.1 Comparison of the nutrient concentrations between the SAPPI and Umlazi site.

Location	SAPPI WWTW Sludge in Shale/Dolorite Hillslope						UMLAZI Pit Latrine Waste in Alluvium					
	NO ₃			P			NO ₃			P		
	Min	Max	Median	Min	Max	Median	Min	Max	Median	Min	Max	Median
In trench	26	480	234	0.03	23.9	1	8	290	36	0.6	225.3	3.5
In piezometer	20	658	134	0.3	21.6	2.4	20	581	184	0.3	9.3	2.5
In borehole	0.4	13	5	0	0.17	0.03	0.04	35.6	0.6	0	0.83	0.15
In stream	0.4	10	1.3	0	0.16	0.02			3.1			0.17

Based upon the limited sampling data during the period following the WWTW and VIP sludge application, the entrenchment of VIP sludge in very sandy soils containing little organic matter and low clay contents has not revealed any significant risks to groundwater through nutrient leaching. Nitrogen loss is most likely, typically occurring initially as ammonium N. Nitrate leaching probably increased as nitrification progressed. The magnitude of this loss will depend on the capability of the Eucalyptus and wattle trees planted at the site to assimilate N. While the concentrations of P in leachate were more often higher than eutrophication standards, simulated P transport shows a decline. The potential loss of P via leaching through coarse-textured soils will likely be controlled by the content of P-binding capacity constituents, (i.e., Fe, Al) in the VIP sludge.

The pathway of nitrate and phosphorus at the Umlazi site suggests vertical flow in the unsaturated state below the trenches to the shallow groundwater body. Here nutrients are mixed

with groundwater discharge towards the stream. The slow rate of recharge limits the movement of nutrients towards the stream. However, the likely level of loading VIP sludge in trenches for sustainable groundwater protection, will depend on the pedology and hydrological characteristics of the catchment and therefore has to be thoroughly investigated first, before trenching of the VIP sludge. The limited data were inadequate to verify simulated local fluxes at the site. This was because of the destruction of installed equipment at an early stage of the study. It is recommended that monitoring is continued, both in the boreholes as well as in the piezometers established in the trenched area.

Although the monitoring period reported for WWTW sludge trenching at SAPPI has been limited, some clear indications of flow pathways and sources are evident. High concentrations of nutrients are evident in the water infiltrating into and through the sludge in all trench types. Continuous monitoring of the flux and pathway are required to assess the mass loading during the wet season and for extreme events. The effect of vertical seepage of nutrients, into the deep aquifer in fractured rock has not been observed in the deep borehole, although this needs to be continuously observed for seasonal fluctuations and future increases.

The potential for the use of the HYDRUS-2D to model soil-water, phosphorus and nitrate movement for the trial, was investigated. It was determined that it is a valid approach to determining water flow and nutrient fluxes. Results suggest that repeated intensive monitoring of nutrient movement in profile, following the deep trenching of VIP pit latrine and WWTW sludge, coupled with numerical modelling might aid in the understanding of the impact of nutrients on soils, subsurface environment and surface water.

Models can help to understand the processes and interactions of nutrients and water fluxes within the vadose zone. However, accurate field measurements are necessary to quantify the processes and validate the simulation results. Where the model results have not represented the observations accurately (simulation of nitrates at the SAPPI site), deductions can be drawn about the suitability of model parameters from different effluents.

Continuation of this project is quite possible, with several different paths requiring further investigation. It has been identified that additional work is required to simulate plant water and nutrient uptake, for understanding the total water and nutrient fluxes. With the demonstration the potential for the use of a soil-water and nitrate movement model, further research into the calibration and validation of the model has the potential to improve the model's performance. This experiment was successful at characterizing the water movement and solutes (nitrate and phosphorus) within and under the deep trench application of WWTW sludge. There is enormous potential for disposing of sludge in trenches that recover nutrients for trees and reducing the need to dedicated disposal sites.

7. RECOMMENDATIONS

Future work is required for additional data and evaluation to provide more insight to the processes occurring in the soil profile. Suggestions for further data gathering and study include:

- The installation and evaluation of pan lysimeter and suction lysimeter sample volume records over time, to determine trends that may provide insight to saturated vs. unsaturated conditions in the soil profile;
- Analysis of soil cores for cation exchange capacity and P adsorption isotherm for improved simulation;
- Collection and analysis of biosolids in the experimental plot on a yearly or twice yearly basis to determine decomposition rates at different depths in the trench;
- Installation of tensiometers at depths consistent with sample collection equipment to more definitively study soil moisture conditions in the soil profile;
- Sampling for pathogens should be done in conjunction with soil coring and piezometer water sampling. The results should be tested used to evaluate the simulation of pathogen transport and persistence of fecal bacteria in agricultural soils and subsurface drainage water;
- Three-dimensional modelling can help improve the system dynamics, along with the geophysical analysis in conjunction with soil sampling and
- Simulation with HYDRUS 3-D and other computer modelling software, to compare with HYDRUS model output, to evaluate various model performances against the relevant mechanisms of transport.

8. REFERENCES

ABEM. 2010. Instruction Manual, ABEM Instrument AB. ABEM printed Matter 93109, Hamngatan 27, S-17266 Sandbyberg, Sweden.

Ahmed, S., Khanbilvardi, R.M., Fillos, J. and Gleason, P.J., 1992. Two-dimensional leachate estimation through landfills. *J. Hydraul. Eng.*, 118:306-322.

Akesson, M, and Nilsson, P.1997. Seasonal changes of leachate production and quality from test cells. *Journal of Environmental Engineering*, 123:892–900.

Akthar, MS, Richards, BK, Medrano, PA, deGroot, M, and Steenhuis, TS. 2003: Dissolved Phosphorus Losses from Undisturbed Soil Cores: Related to Adsorption Strength, Flow Rate, or Soil Structure? *Soil Sci. Soc. of Am. J.* 67:458-470.

Alexander, M. 1999: Biodegradation and Bioremediation, 2. ed., Academic Press, San Diego, an unsaturated field soil. *Water Resour. Res.* 27:2533-2541.

Anderson, MP. 1984: Movement of Contaminants in Groundwater: Groundwater Transport-Advection and Dispersion: in Groundwater Contamination, Studies in Geophysics. National Academy Press, Washington D.C., pp. 429-437.

Anderson, MP. 1979: Using models to simulate the movement of contaminant through groundwater flow system. *Crit. Rev. Environ. Controls* 9(2):97-156.

Ankeny, J, Mushtaque, A, Kaspar, TC, and Horton, R. 1991. Simple field method for determining unsaturated hydraulic conductivity. *Soil Sci. Soc. Am. J.* 55:467-470.

Augenstein, D, and Pacey, J. 1991. Modeling landfill methane generation. *Proc. Sardinia 91*, Third International Landfill Symposium, Sardinia, Italy.

Badger, MR, and Price, GD. 1992. The Carbon dioxide Concentrating Mechanism in Cyanobacteria and Micro-algae. *Physiologia Plantarum* 84:606-615.

Barlaz, MA, Mike, MW, and Ham. 1990. GaS production parameters in sanitary landfill simulators. *Waste Management Res.* 5:27-39.

Battle-Aguilar, J, Coquet, Y, Tucholka, P, and Vachier, P. 2004. Axisymmetrical water infiltration in soil imaged by non-invasive electrical resistivity, Geophysical Research Abstracts, Vol. 6, 01343 (unpublished), <http://www.cosis.net/abstracts/EGU04/01343/EGU04-J-01343>.

Baumgartner, A, and Liebscher, HJ. 1996. Hydrology of Germany-quantitative Hydrology, 2nd Edition, Gebrüder Borntraeger, Berlin.

Beaven, RP, Dollar, L, Oni, OA, and Woodman, N. 2005. A Laboratory Scale Saturated and Unsaturated Tracer Test Through Waste. In: Gourc, JB. (Ed.), International Workshop, Hydro-physico-mechanics of Landfills. Grenoble, France.

Beaven, RP, and Hudson, AP. 2003. Description of a tracer test through waste and application of a dual porosity model. Ninth International Waste Management Symposium, Sardinia.

Bell, P. 1990. The Status of Eutrophication in the Great Barrier Reef Lagoon. Paper Presented at Conference on Environmental Management of Enclosed Coastal Seas, Kobe.

Ben-Gal, A, and Dudley, LM. 2003. Phosphorus availability under continuous point source irrigation. *Soil Sci. Soc. Am. J.* 67:1449-1456.

Bendz, D, Singh, VP, Rosqvist, H, and Bengtsson L. 1998. Kinematic wave model for water movement in municipal solid waste. *Water. Resour. Res.*, 34, 2963-2970.

Bendz, D, Singh, VP, Rosqvist, H, and Bengtsson L. 1997. The flow regimes in landfills-implication for modeling. *Proc. Sardinia 97, 6th international landfill symposium, Sardinia, Italy.*

Beltaos, S, and Day TJ. 1978: A field study of longitudinal dispersion, *Can, J. Civil Eng.* 5:572-585.

Bohn, HL, Mc'neal, BL, and O'conner, GA. 1985. Soil chemistry. A. Wiley-Interscience Publication. New York, NY.

Brooks, RH, and Corey, AT. 1964. Hydraulic properties of porous media, Hydrology. Paper. 3, Colo. State Univ., Fort Collins.

Celia, M.A, Bououtas, ET, and Zarba, RL. 1990. A general mass-conservative numerical solution for the unsaturated flow equation. *Water Resour. Res.* 26:1483-1496.

Chang, AC, Page, AL, Pratt, PF, and Warneke, JE. 1988. Leaching of nitrate from freely drained-irrigated fields treated with municipal sludges. In: *Planning Now for Irrigation and Drainage in the 21st Century.* Lincoln, Nebraska, USA.

Cheshire, MV, Bedrock, CN, Williams, BL, Christensen, BT, Thomsen, I, and Alpendre, P. 1999. Effect of climate and soil type on the immobilization of nitrogen by decomposing straw in northern and southern Europe. *Biol. Fertil. Soils.* 28: 306-312.

Christensen, TH, Kjeldsen, P, and Lindhardt, B. 1996. Gas-generating processes in landfills. In T.H. Christensen, R. Cossu and R. Stegman (Eds). *Landfilling of waste: Biogas.*, E & FN Spon, London, pp. 27-44.

Clark, I, and Fritz, P. 1997. *Environmental Isotopes in Hydrogeology*, Lewis Publishers, Boca Raton.

Colins, F, Vincent, F, Beaudoin, G, Bonin, H, Navarro, A, Legret, M, and Raimbault, G. 1991. Waste behavior modeling: description and result of a co-ordinated European research programme. *Pro. Sardinia 91, Third international Landfill Symposium, Sardinia, Italy*.

Constantini, A, Loch, RJ, Glanville, SF, and Orange, DN. 1995. Evaluation of the potential to dispose of sewage sludge. I. Soil hydraulic and overland flow properties of pinus plantations in Queensland. *Aust. J. Soil Res.*, 33, pp. 1041-1052

Cooke, CM, GoveL, Nicholson FA, Cook H, and Beck, AJ. 2001. Effect of drying and Composting biosolids on the movement of nitrate and phosphate through repacked soil columns under steady-state hydrological conditions. *Chemosphere*, 44, pp. 797-804.

Coplen, TB, Herczeg, AL, and Barnes, C. 2000. Isotope engineering: using stable isotopes of the water molecule to solve practical problems, in *Environmental Tracers in Subsurface Hydrology*, ed. by P.G. Cook and A.L. Herczeg, Kluwer Academic Publishers, Boston.

Cornway, GR, and Pretty, JN. 1991. *Unwelcome Harvest: Agriculture and Pollution*. Earthscan Publications Limited, London.

Craig, H. 1961a. Standard for reporting concentrations of deuterium and oxygen-18 in natural waters, *Science*, 133, 1833-1934.

Craig, H. 1961b. Isotopic variations in meteoric waters, *Science*, 133, 1702-1703.

Craig, H, and Gordon, LI. 1965. Deuterium and oxygen-18 variations in the ocean and the marine atmosphere, in *Stable Isotopes in Oceanographic Studies and Paleotemperatures*, Soletto, July 26-27, 1965, Consiglio Nazionale delle Ricerche, Laboratorio di Geologia Nucleare, Pisa, 1-22, 1965.

Dagan, G. 1982. Stochastic modelling of groundwater by unconditional and conditional probabilities. 2. The solute transport, *Water Resour. Res.* 18:835-848.

Dalton, FN, and Genuchten, MTh. 1986. The time-domain reflectometry method for measuring soil water content and salinity. *Geoderma*, 38:237-250.

Damiata, B. 2001. Assessment of the Skagafjörður archaeological settlement survey, Cotson Institute of Archaeology, ucla, ca, u.s.a.. <http://sass.ioa.ucla.edu/2001>.

De Walle, DR, Swistock, BR, and Sharpe, WE. 1988. Three component tracer model for stormflow on a small Appalachian forested catchment, *J. of Hydrology*, 104: 301-310.

Dematracopoulos, AC, Sehayek, L, and Erdogan, H. 1986. Modeling leachate production from municipal landfills. *J. Environ. Eng.*, 112-886.

Dominguez, J, Edwards, CA, and Subler, S. 1997. A Comparison of Vermicomposting and Composting. *Biocycle*. April 1997:57-59.

Du Preez, LA, Van Der Merwe, W, and Terblanche, JS. 1999. Biosolids management at 18 wastewater treatment plants in South Africa - Optimisation strategies. Proceedings of Specialised Conference on Disposal and Utilization of Sewage Sludge: Treatment Methods and Application Modalities. Athens, Greece.

Dunigan, EP, and Dick, RP. 1980. Nutrient and coliform losses in runoff from fertilizer and sewage sludge-treated soil. *J. Environ. Qual.*, 13, pp. 122-126.

Ekama, GA. 1992. Sludge Management for land disposal. *Water Sewage and Effluent* 12 (3): 19-27.

El-Fadel, M, Findikakis, AN, and Leckie, JO. 1997. Modeling leachate generation and transport in solidwaste landfills. *Environ. Technol.*, 18:669-686.

El-Fadel, M, Findikakis, AN. and Leckie, JO. 1996. Temperature effects in modeling solid waste biodegradation. *Environ. Techn.*, 17:925-935.

Enright, P, and Madramootoo, CA. 2003. Phosphorus losses in surface runoff and subsurface drainage waters on two agricultural fields in Quebec. *CSAE Annual Meeting Paper* 03-111, McGill University.

Environmental Management of Enclosed Coastal Seas (EMECS). 1990. Proceedings of the International Conference on the Environmental Management of Enclosed Coastal Seas. *EMECS*, Kobe.

Epstein, E, Taylor, JM, and Chaney, RL. 1976. Effects of sewage sludge and sludge compost applied to soil on some soil physical and chemical properties. *Journal of Environmental Quality* 5:422-426. 3.

FAO. 2003. Assessment of soil nutrient balance: Approaches and Methodologies.
www.fao.org/docrep/006/y5006e00

Fatoki, OS, Gogwana, P, and Ogunfowokan, AO. 2003. Pollution Assessment in the Keiskamma River and the Impoundment Downstream. *Water SA* 29(2):183-187.

Faure, G. 1986. Principles of Isotope Geology, 2nd ed., John Wiley and Sons, New York.

Gat, J.R. 1980. The isotopes of hydrogen and oxygen in precipitation, in Handbook of Environmental Isotope Geochemistry, Vol. 1A, edited by P. Fritz and J.C. Fontes, pp. 21-47, *Elsevier*, Amsterdam.

Fetter, CW. 2004: Applied Hydrogeology, Fourth Edition. Prentice Hall. ISBN 0-13-088239-9

Fischer, HB. 1973: Longitudinal dispersion and turbulent mixing in open channel flow. *Ann. Rev. Fluid Mech.* 5, 59-78.

Fox, R, Hohmann, G, Killpack, T, and Rjio, L. 1980. Topographic effects in resistivity and induced polarization surveys. *Geophysics*, 45:75-93.

Fried, JJ. 1975: Groundwater Pollution, Elsevier, Amsterdam, 330 pp. Gee, GW, and Baaunder, JW. 1979. Particle size analysis by hydrometer: a simplified method for textural analysis and sensitivity test of measured parameters. *Soil Sci Soc. Am. J.* 43:1004-1007.

Gelhar, LW, and Axness, CL. (1981): Stochastic Analysis of Macro-Dispersion in Three Dimensionally Heterogeneous Aquifer, Geophysical Research Centre, Hydrology Research Program, Rep. No. H8, New Mexico Inst. of Mining and Technology, Socorro, New Mexico, 140 pp. Golden, Colorado, p. 202.

Genereux, DP, and Hooper, RP. 1998. Oxygen and hydrogen isotopes in rainfall-runoff studies, in *Isotope Tracers in Catchment Hydrology*, ed. by C. Kendall and J.J. McDonnell, pp. 319-346, *Elsevier*, Amsterdam.

Geotomo Software, 2004: RES2DINV ver. 3.54 - Rapid 2-D Resistivity & IP inversion using the least-squares method, www.geoelectrical.com.

Gonfiantini, R. 1986. Environmental isotopes in lake studies, in *Handbook of Environmental Isotope Geochemistry*, vol. 2, edited by P. Fritz and J.-Ch. Fontes, pp. 113-168, *Elsevier*, Amsterdam.

Grathwohl, P. 1997: Diffusion in natural porous media-Contaminant transport, sorption/desorption and dissolution kinetics, Kluwer, Dordrecht.

Griffiths, DH, and Barker, RD. 1993. Two-dimensional resistivity imaging and modelling in areas of complex geology. *Journal of Applied Geophysics* 29:211-226.

Guha, S, Peters C, and Jaffé P. 1999: Multisubstrate biodegradation kinetics of naphthalene, phenanthrene, and pyrene mixtures. *Biotechnol Bioeng* 65:491-499.

Gunnerson, CG, and French, JA. 1996. Wastewater Management for Coastal Cities-The Ocean Disposal Option. *Springer* Verlag, Berlin.

Haldeman, WR, Chuang, Y, Rasmussen, TC, and Evans, DD. 1991: Laboratory analysis of fluid flow and solute transport through a fracture embedded in porous tuff, *Water Resour. Res.* 27(1), 53-65.

Hand, P. 1988. Earthworm Biotechnology (Vermicomposting). In: Greenshields, R. (ed). Resources and Applications of Biotechnology, The Macmillan Press Ltd, London. pp 49-58.

Hassan, G, Persaud, N, and Reneau, Jr. RB. 2004. Utility of HYDRUS-2D in modeling profile soil moisture and salinity dynamics under saline water irrigation of soybean. *Soil Sci.* 170:28–37.

Hassan, G, Reneau, Jr. RB, Hagedorn, C, and Saluta, M. 2005. Modeling water flow behaviour where highly treated effluent is applied to soil at varying rates and dosing frequencies. *Soil Sci.* 170:692–706.

Hassan, G, Reneau, B, and Hagedorn, C. 2008. On-site waste treatment and disposal by sequencing batch reactor-drip irrigation: Effluent distribution and solute transport. *Commun. Soil Sci. Plant Anal.* 39:1–17.

Hassan, G, Reneau, B, and Hagedorn, C. 2010. Solute Transport Dynamics Where Highly Treated Effluent Is Applied to Soil at Varying Rates and Dosing Frequencies. *Soil Science.* Vol 175 (6).

Herselman, J E. 2009a. Technical Support Document to the Development of the South African Sludge Guidelines: Volume 4: Requirements for the Beneficial Use of Sludge at High Loading Rates. Water Research Commission K5/1622/2/09, Pretoria, South Africa.

Herselman, JE. 2009b. Technical Support Document to the Development of the South African Sludge Guidelines: Volume 5: Requirements for Thermal Sludge Management Practices and for Commercial Products Containing Sludge. Water Research Commission K5/1622/3/09, Pretoria, South Africa.

Herselman, JE, Burger LW, and Moodley P. 2009. Guidelines for the Utilisation and Disposal of Wastewater Sludge: Volume 5 of 5: Requirements for Thermal Sludge Management Practices and for Commercial Products Containing Sludge. Water Research Commission TT351/09, Pretoria, South Africa.

Herselman, JE, and Moodley, P. 2009. Guidelines for the Utilisation and Disposal of Wastewater Sludge: Volume 4 of 5: Requirements for the Beneficial Use of Sludge at High Loading Rates. Water Research Commission TT 350/09, Pretoria, South Africa.

Herselman, JE, and Snyman, HG. 2009a. Guidelines for the Utilisation and Disposal of Wastewater Sludge: Volume 3 of 5: Requirements for the On-site and Off-site Disposal of Sludge. Water Research Commission TT 349/09, Pretoria, South Africa.

Herselman, JE, and Snyman, HG. 2009b. Technical Support Document to the Development of the South African Sludge Guidelines: Volume 3: Requirements for the On-site and Off-site Disposal of Sludge. Water Research Commission K5/1622/1/09, Pretoria, South Africa.

Hillel, D. 1988. Environmental Soil Physics. Academic Press, San Diego, CA, pp: 771.

Hinton, MJ, Schiff, SO, and English, MC. 1994. Examining the contribution of glacial till water to storm runoff using two and three-component hydrograph separations, *Water Resour. Res.*, 30, 983-993.

Hoefs, J. 1997. Stable Isotope Geochemistry, 4th ed., Springer-Verlag, Berlin.

Sklash, MG, and R.N. Farvolden, RN. 1979. The role of groundwater in storm runoff, *J. of Hydrology*. 43: 45-65.

Horan, NJ. 1990. *Biological Wastewater Treatment Systems: Theory and Operation*. John Wiley and Sons Ltd. Baffins Land, Chichester, West Sussex. 41pp.

Jamieson, RC, Gordon, RJ, Sharples, KE, Stratton, GW, and Madani, A. 2002. Movement and persistence of fecal bacteria in agricultural soils and subsurface drainage water: A review. *Can. Biosyst. Eng.* 44: 1.1–1.9.

Johnson, DW, and Cole, DW. 1980. Anion mobility in soils: Relevance to nutrient transport from forest ecosystems. *Environ. Int.* 3:79Y90.

Joshua, WD, Blasi, M, Osborne, GJ. 2001. Simplified functional model for estimating nitrogen mineralisation and leaching in biosolids-amended soil. *Aust. J. Exp. Agric.* 41, pp. 1207-1216.

Jimenez, B, Maya, C, Sanchez, E, Romero, A, Lira, L, and Barrios, JA. 2002. Comparison of the Quantity and Quality of the Microbiological Content of Sludge in Countries with Low and High Content of Pathogens. *Water Science and Technology* 46(10):17-24.

Jüttner, F, and Henatsch, JJ. 1986: Anoxic hypolimnion is a significant source of biogenic toluene. *Nature* 323: 797-798.

Kays, JS, Flamino, EJ, Felton, G, and Flamino, PD. 2000. Use of deep-row biosolids applications to grow forest trees: a case study. In C.L. Henry, R.B. Harrison, and R.K. Bastian (Eds.), *The Forest Alternative: Principles and Practice of Residuals Use*. (pp.105-110). Seattle, WA: University of Washington College of Forest Resources.

Kemna, A, Binley, A, and Slater, L. 2002. Imaging and characterisation of subsurface solute transport using electrical resistivity tomography (ERT) and equivalent transport models, *Journal of Hydrology* 267:125-146. Elsevier Science Publishers B.V, Amsterdam.

Kemna, A, Binley, A, and Slater, LD. 2004: Crosshole IP imaging for engineering and environmental applications, *Geophysics* 69:97-107.

Kirkley, K, Heatwole, JE, and McCray, E. 2007. Modeling potential vadose-zone transport of nitrogen from onsite wastewater systems at the development scale. *Journal of Contaminant Hydrology*. Volume 91, Issues 1–2, 1 April 2007, Pages 184–201.

Koenig, B. 2005: Operation manual for the 2-dimensional resistivity meter. ABEM Terrameter system, BEEH, University of Kwazulu Natal, Pietermaritzburg, Unpublished.

Kollert, R. 1969. Groundwater exploration by the electrical resistivity method. Geophysical memorandum ABEM printed matters (90019). Sweden.

Korentajer, L. 1991. A review of the agricultural use of sewage sludge: benefits and Potential hazards. *Water SA*, 17(3):189-196.

Korfiatis, GP, Demetracopoulus, AC, Bourodimos, EL, and Nawy, EG. 1984. Moisture transport in a waste column. *J. Environ. Eng.* 110:780-796.

Kostyanovsky, KI, Evanylo, GK, Lasley, KK, Shang, C, Sukkariyah, BF, and Daniels, W.L. 2011. Transformations of nitrogen and carbon in entrenched biosolids at a reclaimed mineral sands mining site. *J. Environ. Qual.* 40:67-75.

Kudo, A, and Miyahara, S. 1991. A Case History: Minimata Mercury Pollution in Japan-From Loss of Human-lives to Decontamination. *Water, Science and Technology* 23:283-290.

Lawes, JB, Gilbert, and Warington, R. 1882:.. On the amount and composition of the rain and drainage water collected at Rothamstead. Williams Clowes and Sons, Ltd., London.

Lee, DR, Cherry, JA, and Pickens, JF. (1980):. Groundwater transport of a salt tracer through a sandy lake-bed, *Limnol. Oceanogr.* 25:45-61.

Lee, JJ, Shin, SH, Lee, W, and Chung, H. 1991. Simulation of leachate quality using laboratory simulator. *Proc. Sardinia 91*, Third international landfill symposium, 865-875.

Lippmann, J, Groening, M, and Rozanski, K. 1999. 2nd interlaboratory comparison for deuterium and oxygen-18 analysis of water samples, Report prepared by Isotope Hydrology Laboratory, Agency's Laboratories Seibersdorf, International Atomic Energy Agency, Vienna, July 1999, 32 pp.

Loch, RJ, Constantini A, Barry GA, Best EK. 1995. Evaluation of the potential to dispose of sewage sludge. II. Potential for off-site movements of solids and solutes. *Aust. J. Soil Res.*, 33, pp. 1053-1062.

Loke, MH. 1999. Electrical imaging surveys for environmental and engineering studies - A practical guide to 2-D and 3-D surveys. Penang, Malaysia.

Loke, MH. 2000. Electrical imaging surveys for environmental and engineering studies - A practical guide to 2-D and 3-D surveys, <http://www.geoelectrical.com>.

Lorentz, S. 2001. Hydrological Systems Modelling Research Programme: Hydrological Processes. Phase I: Processes Definition and Database. Report to the Water Research Commission on the project: Hydrological Systems Modelling Research Programme: Processes Research. WRC Report 637/1/01.

Lotter, LH, and Pitman, AR. 1997. Aspects of Sewage Sludge Handling and Disposal. WRC Report 316/1/97.

Mailhol, JC, Ruelle, P, and Nemeth, I. 2001. Impact of fertilization practices on nitrogen leaching under irrigation. *Irrig. Sci.* 20:139-147.

Martin, EJ, and Johnson, JH. 1977. Hazardous Waste Management Engineering. Von Nostrand Reinhold Company, New York.

Marx, CJ, Alexander, WV, Johannes, WG, and Steinbach-Kanes, S. 2004. A Technical and Financial Review of Sewage Sludge Treatment Technologies. Water Research Commission Report No. 1240/1/04. Water Research Commission, Pretoria.

Matheron, C, and G. DeMarsily, G. 1980: Is transport in porous media always diffusive? *Water Resour. Res.* 16:901-917.

McCray, JE, Kirkland, SL, Siegrist, RL, and Thyne, GD. 2005. Model Parameters for Simulating Fate and Transport of On-Site Wastewater Nutrients. *Ground Water*, 43 4:628-639.

McCown, RL, Hammer GL, Hargreaves JNG, Holzworth DP, and Freebairn, DM. 1996. APSIM: a novel software system for model development, model testing, and simulations in agricultural system research. *Agric. Syst.*, 50, pp. 255-271.

McLaren, RG, Clucas, LM, Taylor, MD, Hendry T. 2003. Leaching of macronutrients and metals from undisturbed soils treated with metal-spiked sewage sludge 1. Leaching of macronutrients *Aust. J. Soil Res.*, 41, pp. 571-588.

Muse, JK, Mitchell, CC Jnr, and Mullins, GL. 1991. Land Application of Sludge. Community Resource Development Publications, Auburn University, Auburn.

Neretnieks, I, 2002: A stochastic multi-channel model for solute transport - analysis of tracer tests in fractured rock. *J. Contaminant Hydrol.* 55(3-4):175-211.

Nielsen, PH, and Christensen, TH. 1994: Variability of biological degradation of aromatic hydrocarbons in an aerobic aquifer determined by laboratory batch experiments. *J. Contam. Hydrol.* 15:05-320.

Odegaard, H, Paulsrud, B, and Karlsson, I. 2002. Wastewater Sludge as a Resource: Sludge Disposal Strategies and Corresponding Treatment Technologies aimed at Sustainable Handling of Wastewater Sludge. *Water, Science and Technology* 46(1):295-303.

Oni, OA, and Richards, DJ. 2004. Estimating moisture volume in a municipal solid waste landfill during refuse infill. *Proceedings of the 19th International conference on solid waste technology and management. Philadelphia*, pp:446-455.

Oni, OA. 2009. Studying pollutant solute transport in saturated msw using multi-tracer tests. *Aust. J. Basic Appl. Sci.* 2(4): 3727-3740.

Pang, L, Close, ME, Watt, JPC, and Vincent, KW. 2000. Simulation of picloram, atrazine, and simazine leaching through two New Zealand soils and into groundwater using HYDRUS-2D. *J. Contaminant Hydrol.*, 44: 19-46.

Parlange, JY, Steenhuis, TS, Glass, RJ, Richard, TL Pickering, NB, Waltman, WJ, Bailey, NO, Andreine, MS, and J.A. Throop, JA. 1988: The flow of pesticides through preferential paths in soils .N.Y. *Food Life Sci. Quart.* 8:20-23.

Pescod, MB. 1992. Wastewater Treatment and Use in Agriculture. Food and Agricultural Organisation (F.A.O.) Irrigation and Drainage Paper No. 47. Food and Agricultural Organisation of the United Nations, Rome.

Phillips, VR. 1988. Engineering Problems in Animal Waste by Earthworms. In: Edwards, C.A. and Neuhaser, EF. (eds). *Earthworms in Waste and in Environment Management*. SPB Academic Publishing, Hague. pp 111-118.

Pickens, JF, and Grisak, GE. 1981b: Modeling of scale-dependent dispersion in hydrogeologic systems, *Water Resour. Res.* 17:1701-1711.

Pyrak, LR, Myer, LR, and Cook, NGW. 1985: Determination of fracture void geometry and contact area at different effective stress, *Eos Trans. AGU Abstract*, 66(46), 903.

Reneau Jr, BB, Hassan, G, Hagedorn, C, and Saluta, M. 2005. On-site Waste Treatment and Disposal by Sequencing Batch Reactor: Drip Irrigation. Crop and Soil Environmental Sciences Dept., Virginia Polytechnic Institute and State University, Blacksburg, VA, P 72.

Richards, B, Schulte, B, and Heilig, A. 2004. Environmental Impacts of Applying Manure, Fertiliser and Sewage Biosolids on a Dairy Farm. *Journal of the American Water Resources Association* 4:1025-1042.

Riley, JP, Grasshoff, K, and Vipio, A. 1972. Nutrient Chemicals. In: Goldberg, E.D. (ed). A Guide to Marine Pollution. Gordon and Beach, New York. pp 81-110.

Ritsema, JC, Dekker, LW, Nieber, JL, and T.S.Steenhuis. 1998: Modelling and field evidence of finger formation and finger recurrence in a water repellent sandy soil. *Water Resour. Res.* 34(4):555-567.

Robain, H, Albouy, Y, Dabas, M, Descloitres, M, Camerlynck Ch, Mechler P, Tabbagh, A 1999: The location of infinite electrodes in pole–pole electrical surveys: consequences for 2D imaging, *Journal of Applied Geophysics* 41, 313-333.

Rosqvist, H, and Bendz, D. 1999. An experimental evaluation of the solute transport volume in biodegraded municipal solid waste. *Hydrol. Earth Syst. Sci.*, 3(3): 429-438.

Rosqvist, H, and Destouni, G. 2000. Solute transport through preferential pathways in municipal solidwaste. *J. Contam. Hydrol.*, 46 (1-2): 39-60.

Sabine, JR. 1978. The Nutritive Value of Earthworm Meal. In: Hartenstein, R. (ed). Utilisation of Soil Organisms in Sludge Management. Natural Technological Information Services, Springfield, Virginia. pp 122-130.

Salanitro, JP, Dorn, PB, Huesemann, MH, Moore, KO, Rhodes, IA, Jackson, LMR, Vipond, TE, Western, MM, and Wisniewski, HL. 1997: Crude Oil Hydrocarbon Bioremediation and Soil Ecotoxicity Assessment. *Environmental Sciences and Technology*, 31(6):1769-1776.

Schwarzenbach RP, Gschwend PM, Imboden, DM, 1992: *Environmental Organic Chemistry*. 255.

Seagren, EA, Rittmann, BE, and Valocchi. A.J., (1993): Quantitative evaluation of flushing and biodegradation for enhancing in situ dissolution of non aqueous-phase liquids. *J. Contam. Hydrol.*12:103-132.

Selker, JS, Steenhuis, TS, and Parlange, JY. 1996: An Engineering Approach to Fingering of Vadose Pollutant Transport. In: *Fingering Flow in Unsaturated Soil: From Nature to Model*, T.S. Steenhuis, C.J. Ritsema, and L.W. Dekker, Eds. Special Issue of *Geoderma* 70:197-206.

Sklash, MG, Farvolden, RN, and Fritz, P. 1976. A conceptual model of watershed response to rainfall, developed through the use of oxygen-18 as a natural tracer, *Can. J. Earth Sci.*, 13, 271-283.

Skibitzkie, HE, and Robinson GM. 1963: Dispersion in groundwater flowing through heterogeneous materials. *U.S. Geol. Survey. Prof. Pap.* 386-B, 5 pp.

Shephard, MA. 1996. Factors affecting nitrate leaching from sewage sludges applied to a sandy soil in arable agriculture. *Agric. Ecosyst. Environ.*, 58, pp. 171-185.

Sikora, LJ, Burge, WD, and Jones, JE. 1982. Monitoring of a municipal sludge Entrenchment site. *J. Environ. Qual.* 11(2):321-326.

Simunek, J, and van Genuchten MTh. 1994. The CHAIN_2D code for simulating two dimensional movement of water flow, heat, and multiple solutes in variably-saturated porous

media. Version 1.1, Research Report No 136, U.S. Salinity laboratory, USDA, ARS, Riverside, California.

Simunek, J, Sejna, M, and van Genuchten, MTh. 1999. The HYDRUS-2D software package for simulating two-dimensional movement of water, heat, and multiple solutes in variably saturated media. Version 2.0.

Simunek, J, van Genuchten, MTh, and Sejna, M. 2006. The HYDRUS Software Package for Simulating Two- and Three-Dimensional Movement of Water, Heat, and Multiple Solutes in Variably-Saturated Media, Technical Manual, Version 1.0, PC Progress, Prague, Czech Republic, pp. 241.

Singer, MJ, and Munns, DN. 1992. Soils: An Introduction. 2nd ed. Macmillan Publishing Company, New York.

Slichter, CS. 1905. Field measurement of the rate of underground water, *U.S. Geol. Surv. Water Supply Pap.* 140, pp. 9-85.

Smith, SR. 1996. Agricultural Recycling of Sewage Sludge and the Environment CAB International, Wallingford, UK, pp. 382.

Smithers. J, Schulze, R. 2002. ACRU Agrohydrological Modelling System User Manual. Version 3.00.

Sri Niwas and Singhal, DC, 1985. Aquifer transmissivity of porous media from resistivity data. *Journal of Hydrology* 82.

Still, DA. 2001. Guidelines for the Removal and Disposal of Faecal Waste from Pit Latrines and Septic Tanks. Report prepared for the Mvula Trust and the Department of Water Affairs and Forestry. South Africa.

Straub, WA, and Lynch, DR. 1982. Modeling of landfill leaching: Moisture low and inorganic strength. *J. Environ. Eng.* 108:231-250.

Taylor, G.I., (1921): Diffusion by continuous movements, *Math.Soc.Ser.2.20*, 196-212.

Taylor, G.I., (1953): The dispersion of matter in solvent flowing slowly through a tube, *Prac. R. Soc. London. Ser. A* 219, 189-203.

Tchobanoglous, G, and Burton, FL. 1991. Design of facilities for the treatment and disposal of sludge. In: *Wastewater Engineering. Treatment, Disposal and Reuse.3rd edn*, Metcalf and Eddy, Inc. McGraw-Hill, Inc., New York, pp. 765-926.

Tong, L, and Yang, C. 1990. Incorporation of topography into 2-D resistivity inversion. *Geophysics*, 55, 354-361.

Topp, GC, Davis, JL, and Annan, AP. 1980. Electromagnetic determination of soil water content: Measurements in coaxial transmission lines. *Water Resour. Res.* 16:574-582.

Trinidade, H, Coutinho, J, Jarvis, S, and Moreira, N. 2001. Nitrogen mineralisation in sandy loam soils under an intensive double-cropping forage system with dairy-cattle slurry applications. *Eur. J. Agron.* 15:281-293.

Uguccioni, M, and Zeiss, C, 1997. Comparison of two approaches to waste moisture movement through municipal solid waste. *J. Environ. Syst.* 25:41-63.

United States Environmental Protection Agency (U.S.E.P.A.). 1985. A Review of Techniques for Incineration of Sewage Sludge with Solid Wastes. United States Environmental Protection Agency Report No. 600/2-76-288. United States Environmental Protection Agency, Washington DC.

USEPA. 2009. Understanding the Use of Models in Predicting the Effectiveness of Proposed Remedial Actions at Superfund Sediment Sites. Sediment Assessment and Monitoring Sheet (SAMS) No. 2 OSWER Directive 9200.1-96FS.

van Den Bossche, H, Audic, JM, Huyard, A, Gascuel-Oudou, C, Trolard, F, and Bourrie, G. 1999. Phosphorus losses from sewage sludge disposed on field: Evidence from storm event simulations. In: *Proceedings of Specialised Conference on Disposal and Utilization of Sewage Sludge: Treatment Methods and Application Modalities*. Athens, Greece.

van Genuchten, MT. 1980. A closed-form equation for predicting the hydraulic conductivity of unsaturated soils, *Soil Sci. Soc. Am. J.*, 44:892-898.

Ventrella, D, Mohanty, BP, Simunek, J, Lasavio, N, and van Genuchten, MTh. 2000. Water and chloride transport in a fine-textured soil: Field experiment and modeling. *Soil Sci.*, 165:624-631.

Vincent, F, Beaudoin, G, and Colin, F. 1991. Waste behaviour modelling: a numerical model to describe the flow, transport and biodegradation processes. *Proc. Sardinia 91*, Third international Landfill Symposium, 847-855.

Vogel T, Cislerova M. 1988. On the reliability of unsaturated hydraulic conductivity calculated from the moisture retention curve. *Transport in Porous Media*. 3, 1-15.

Vogeler, I, Horn R, Wetzel, H, and Krummelbein, J. 2006. Tillage effects on soil strength and solute transport. *Soil and Tillage Research* 88: 193-204.

Wadman, WP, and Neeteson, JJ. 1992. Nitrate leaching losses from organic manures -The Dutch experience. *Aspects of Appl. Biol.* 30:557-560.

Wagenet RJ, Hutson JL. 1989. LEACHM: Leaching Estimation and Chemistry Model developed by Cornell University, Ithaca, NY.

Walker C, Lin, HS, and Fritton, DD. 2006. Is the tension beneath a tension infiltrometer what we think it is? *Vadose Zone Journal* 5: 860-866.

Walker, JM. 1974. Trench incorporation of sewage sludge. From: Proceedings of the National Conference on Municipal Sludge Management, Allegheny County, PA. Information Trans., Inc. Washington, D.C.

Walter, MT, Kim, JS, Steenhuis, TS, Parlange, JY, Heilig, A, Braddock, RD, Selker, JS, and Boll, J. 2000: Funneled flow mechanisms in a sloping layered soil: Laboratory investigation, 2000. *Wat. Resources Res.* 36(4):841-849.

Ward, RC, and Robinson. M.2000. Principles of Hydrology, McGraw-Hill Publishing Company (UK), ISBN 0077095002.

Water Research Commission. 1997. Permissible Utilisation and Disposal of Sewage Sludge. 1st ed. WRC, Pretoria. ISBN 1-86845-281-6.

Water Research Commission. 2002. Addendum 1 to Edition 1.1997 of Guide: Permissible Utilisation and Disposal of Sewage Sludge. Water Research Commission, Pretoria.

White, P.1988. Measurement of groundwater parameters using salt water injection and surface resistivity, *Ground Water* Vol. 26, No.2:179-186.

Weaver, MC, Cave, L, and Talma, A. 2007. Groundwater sampling: A comprehensive guide for sampling methods. Water Research Commission. Research Report No.TT 303/07, Pretoria. South Africa.

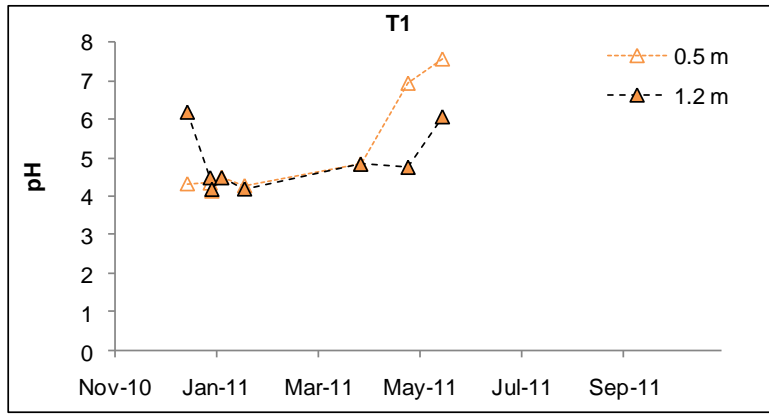
White, P. 1988. Measurement of groundwater parameters using salt water injection and surface resistivity, *Ground Water* Vol. 26, No.2: 179-186.

Whitehead, DC. 2000. Nutrient elements in grassland: soil-plant-atmosphere relationships. Cambridge University Press.

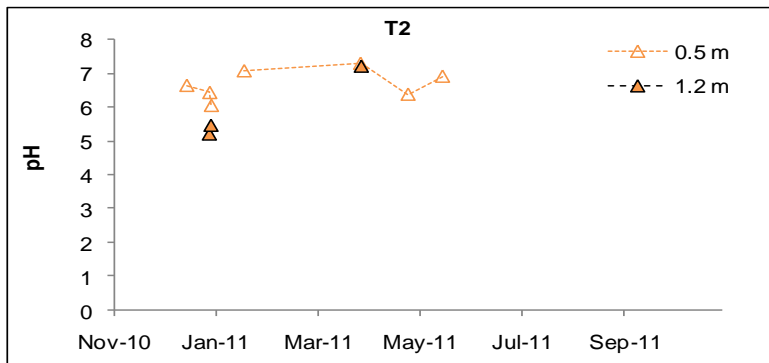
Zeiss, C., and Major, W. 1993. Moisture flow through municipal solid waste: pattern and characteristics. *J. Environ. Syst.* 22:211-231.

Zobell, CE. 1946. Marine Microbiology, Chronica Botanica Co, Waltham, Massachutes.

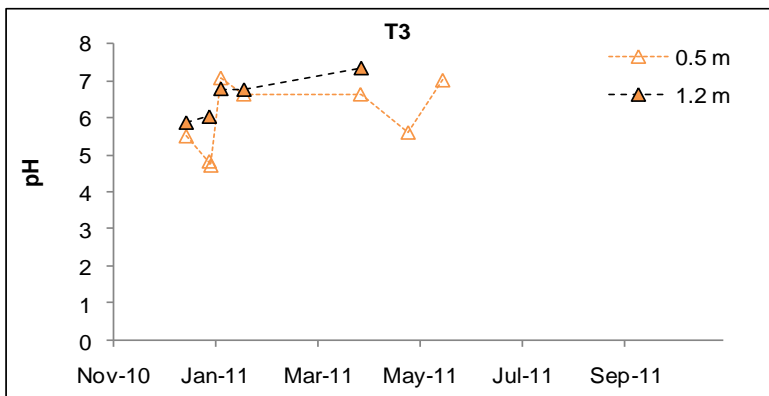
APPENDIX A



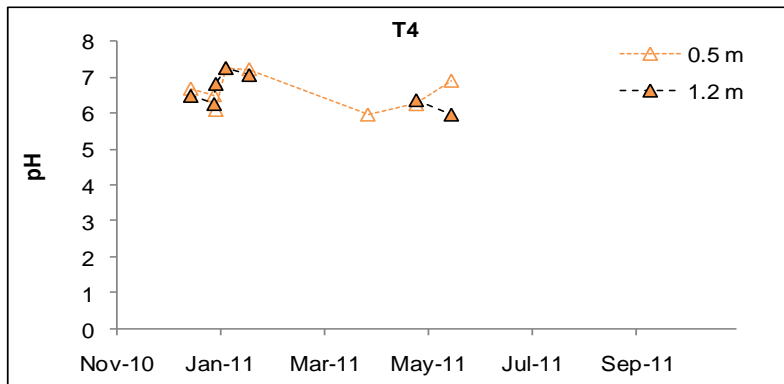
Observed pH in T1.



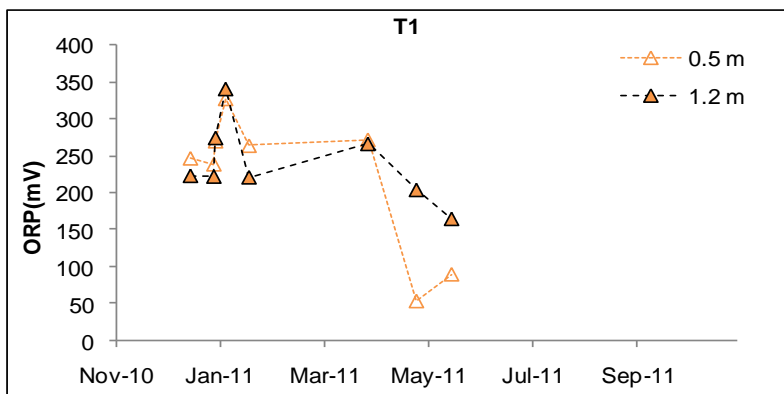
Observed pH in T2.



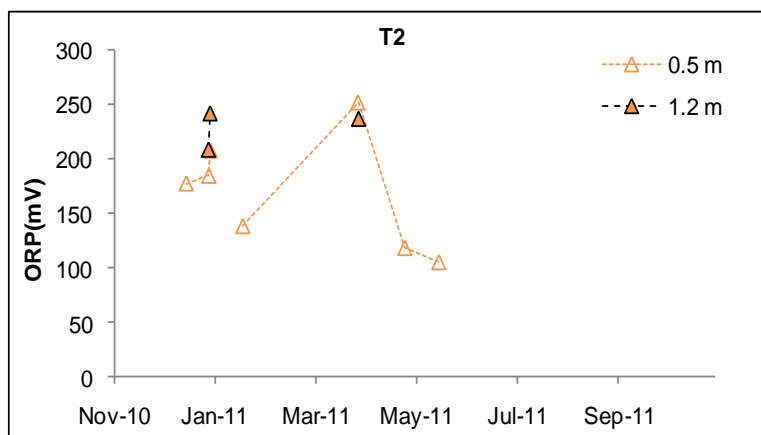
Observed pH in T3.



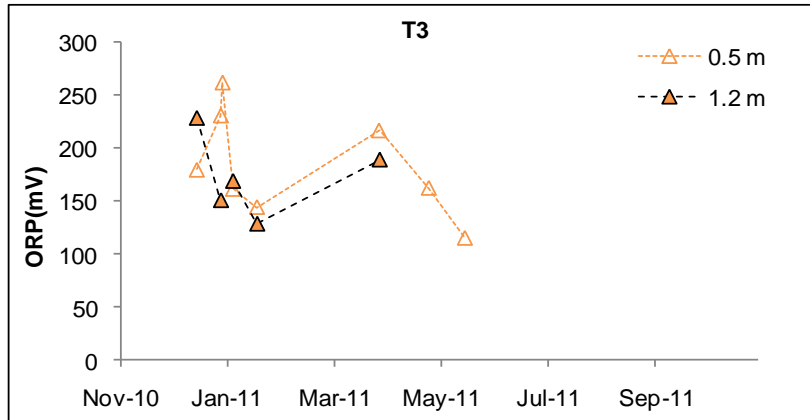
Observed pH in T4.



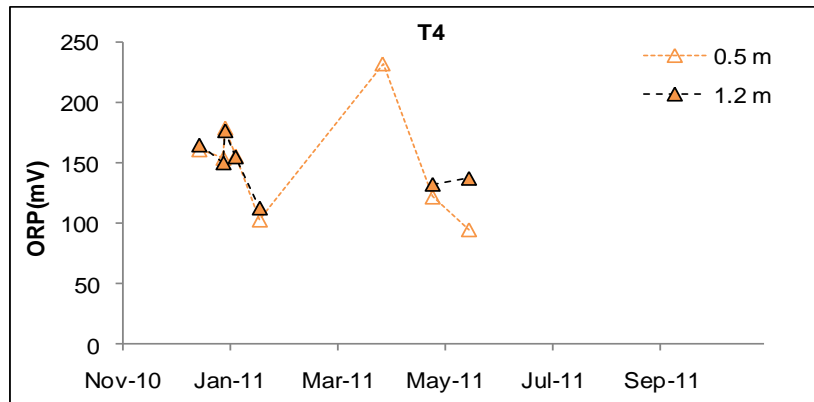
Observed ORP in T1.



Observed ORP in T2.



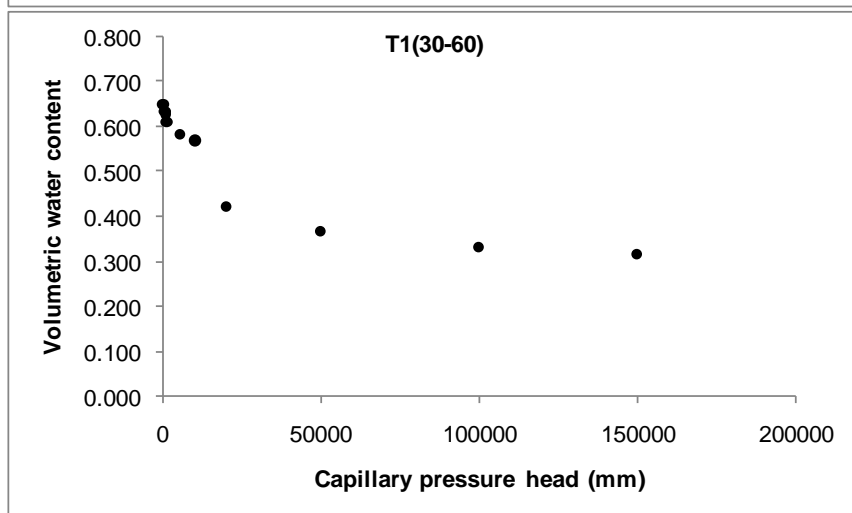
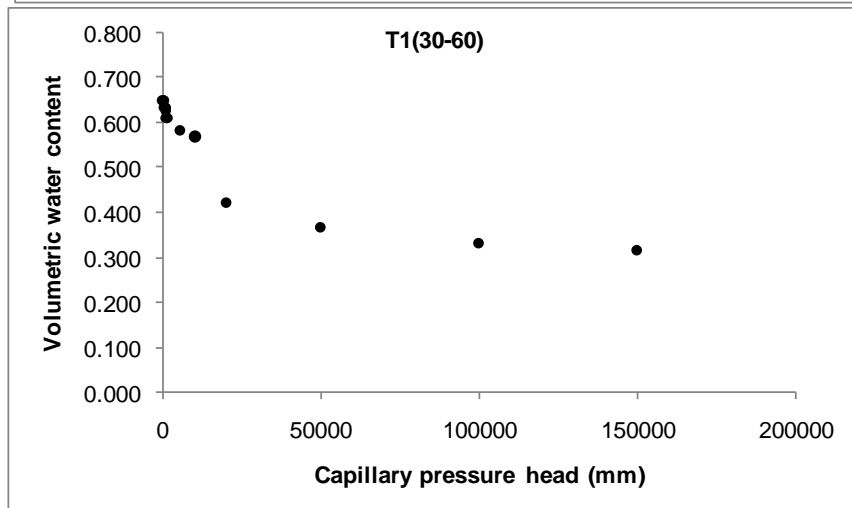
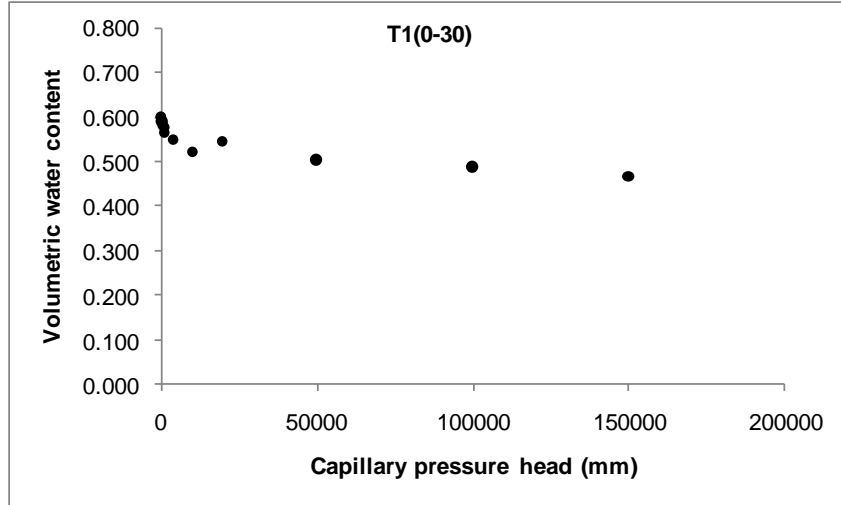
Observed ORP in T3.

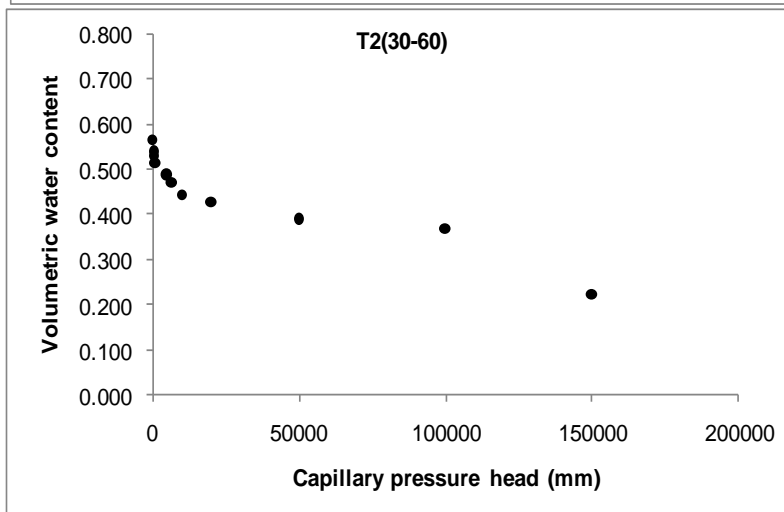
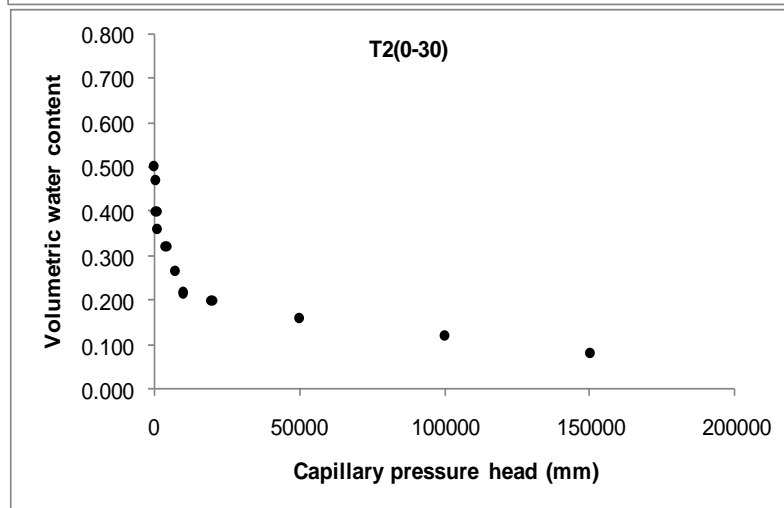
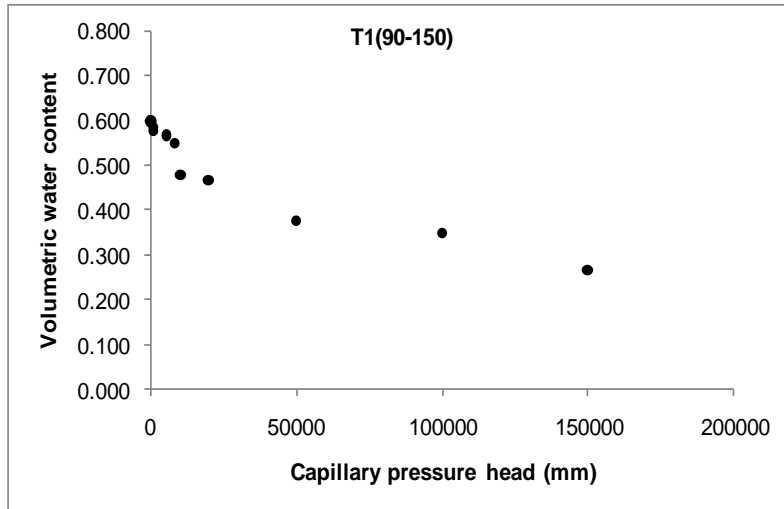


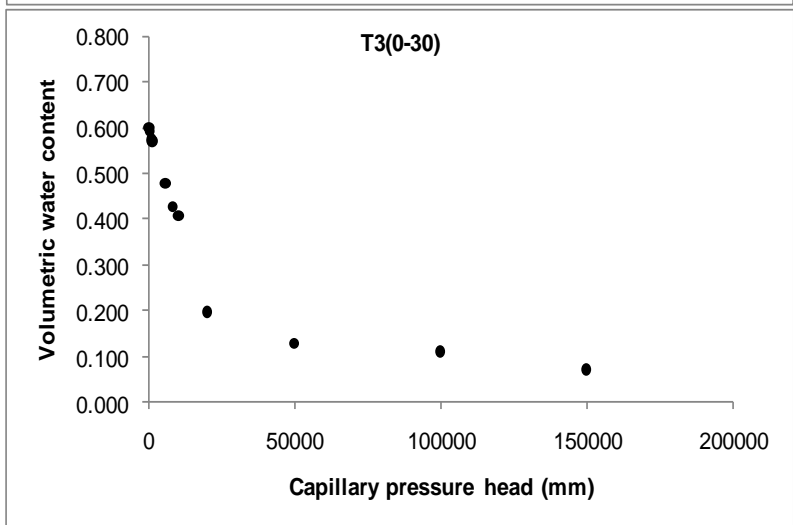
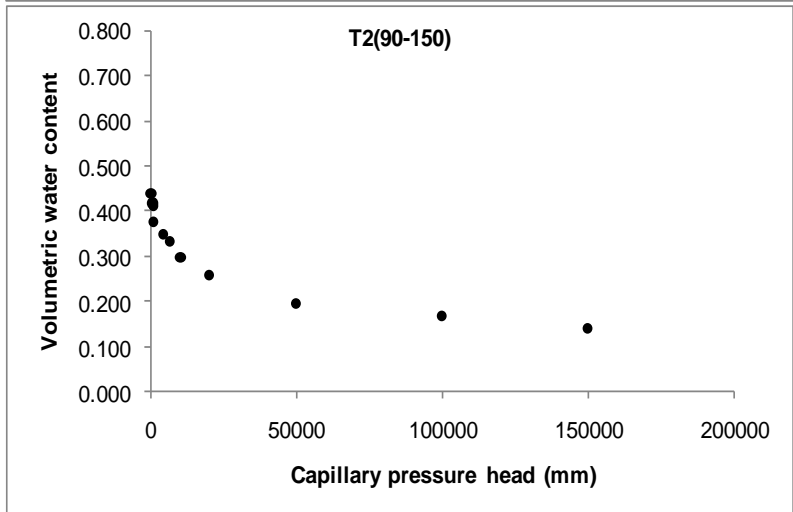
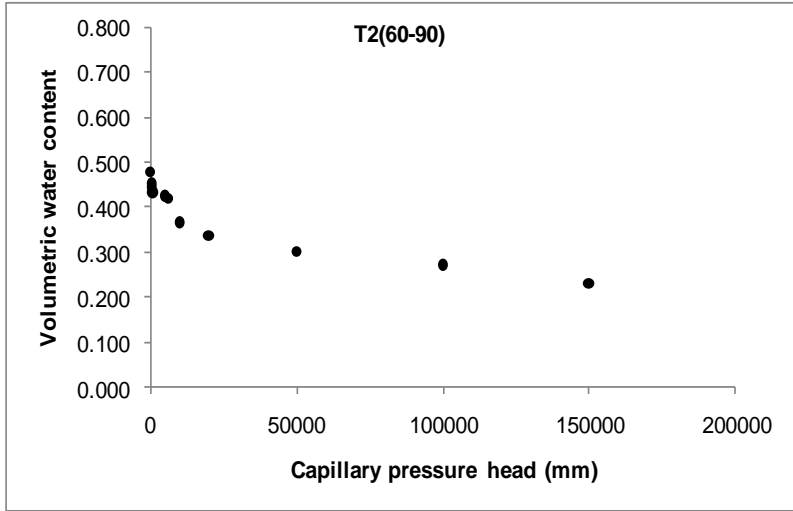
Observed ORP in T4.

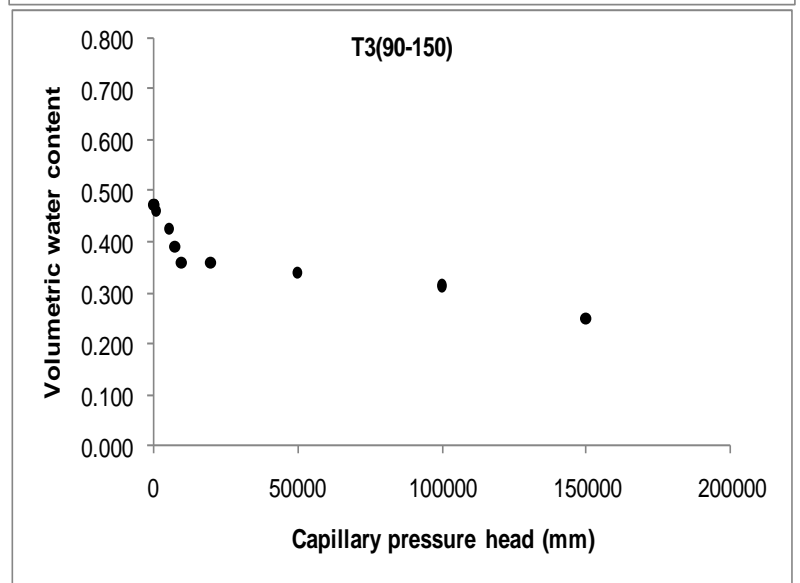
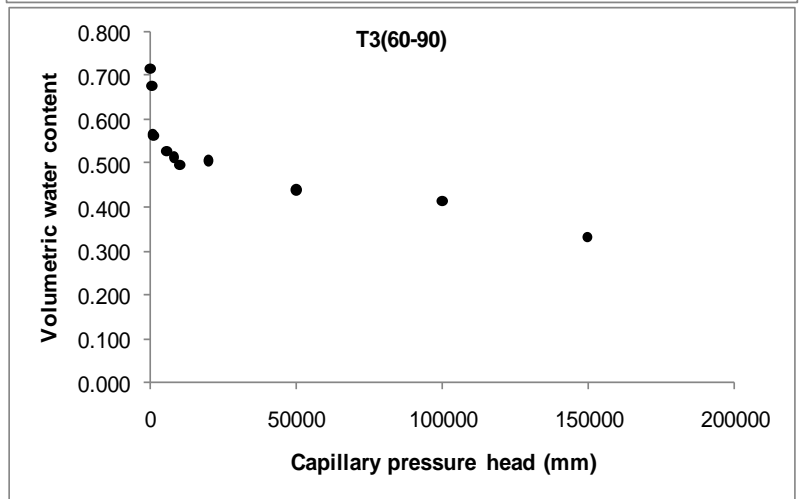
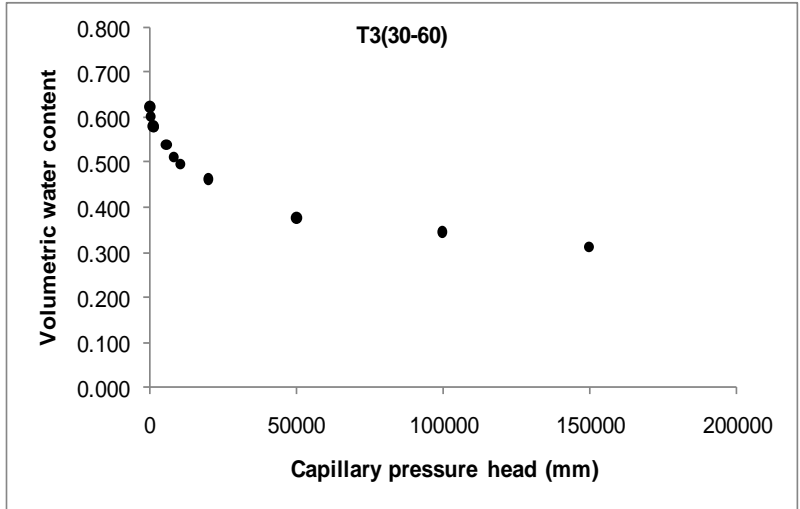
APPENDIX B

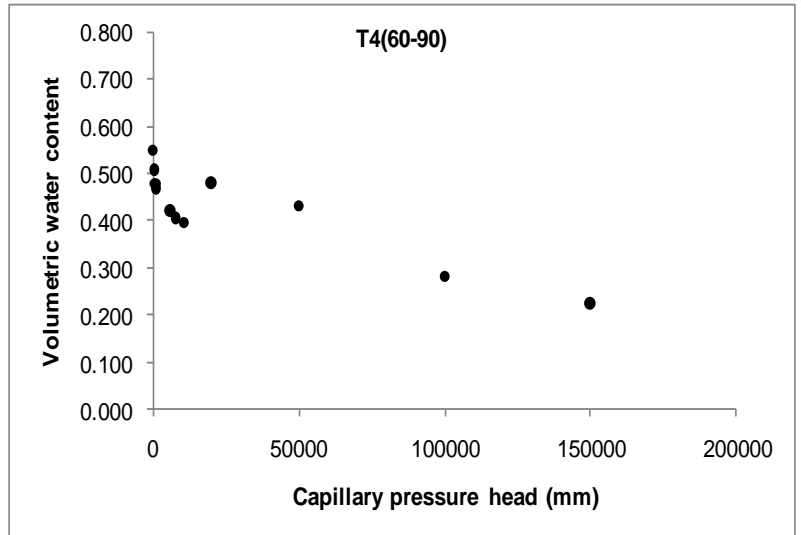
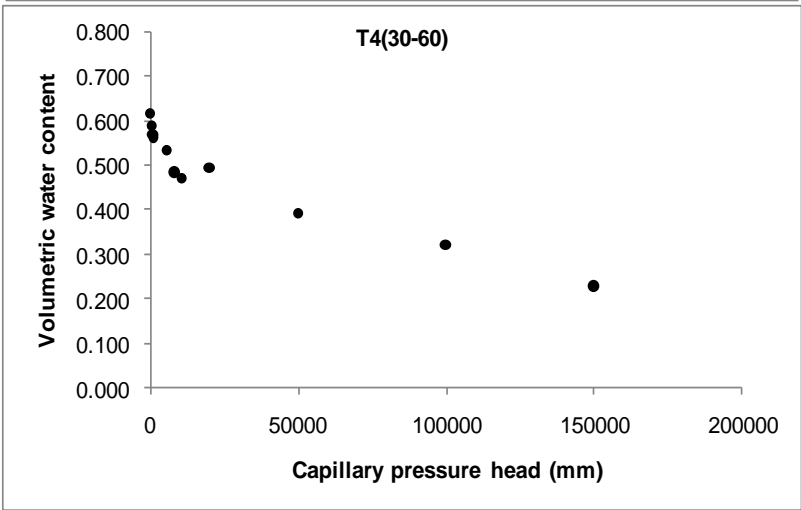
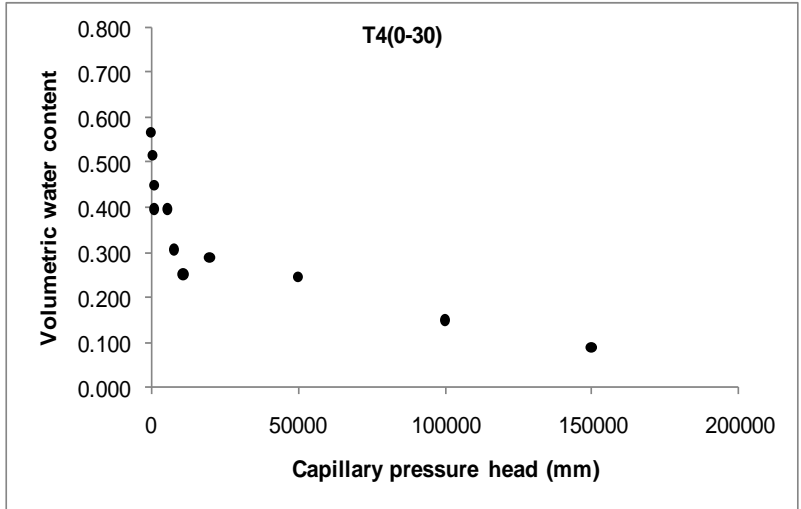
Measured water retention characteristics in treatments at SAPPI

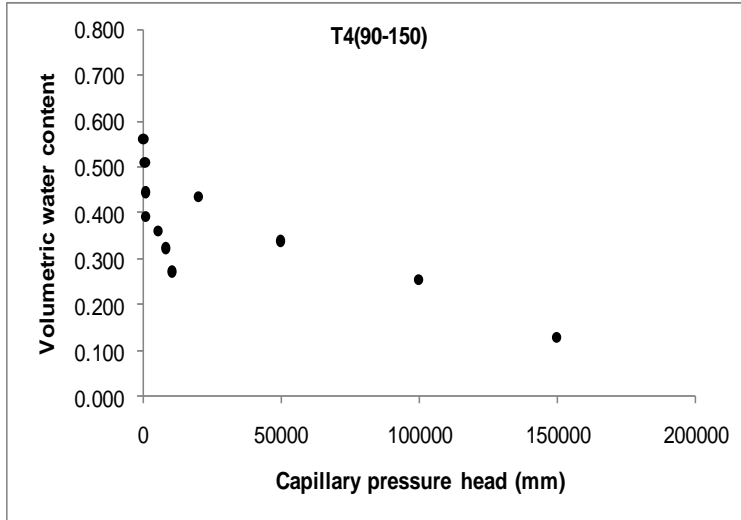




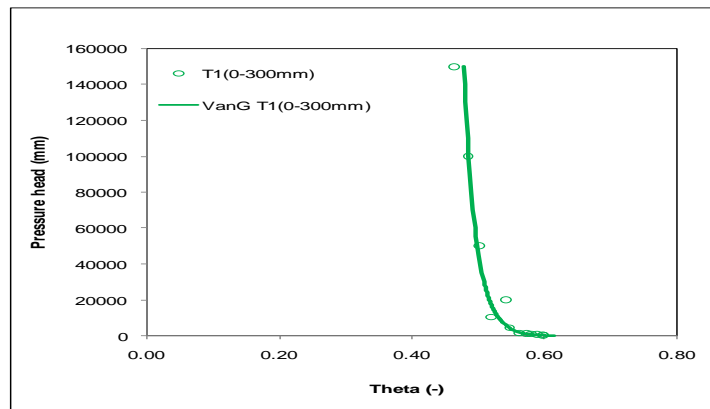




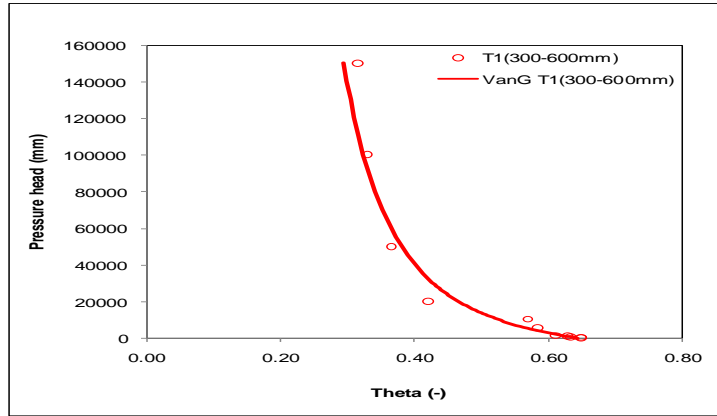




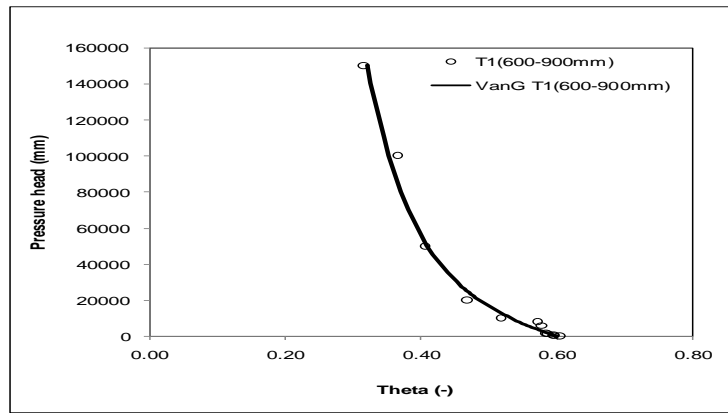
van Genuchten Fitted Soil Water Retention curves in treatments at SAPPI site



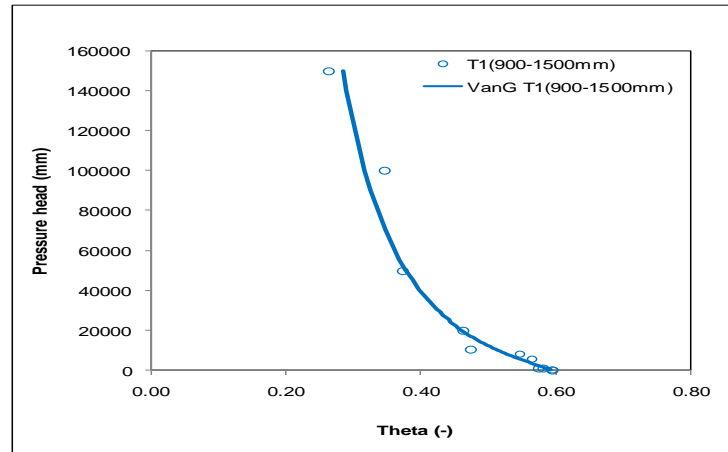
van Genuchten Fitted Soil Water Retention curve for T1 (0-30 cm)



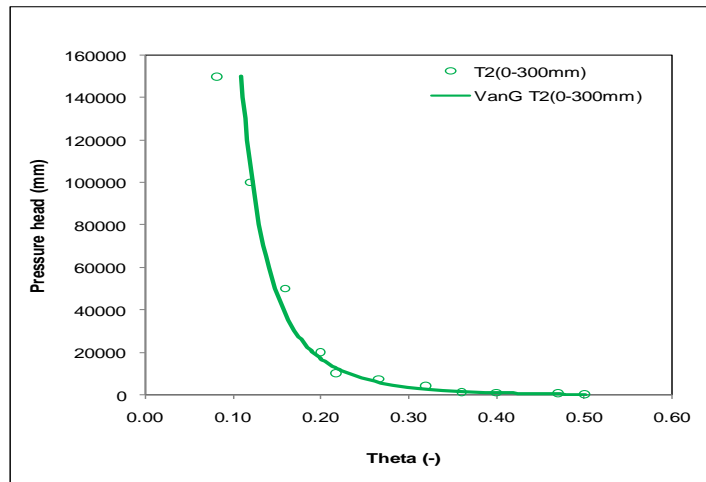
van Genuchten Fitted Soil Water Retention curve for T1 (30-60 cm)



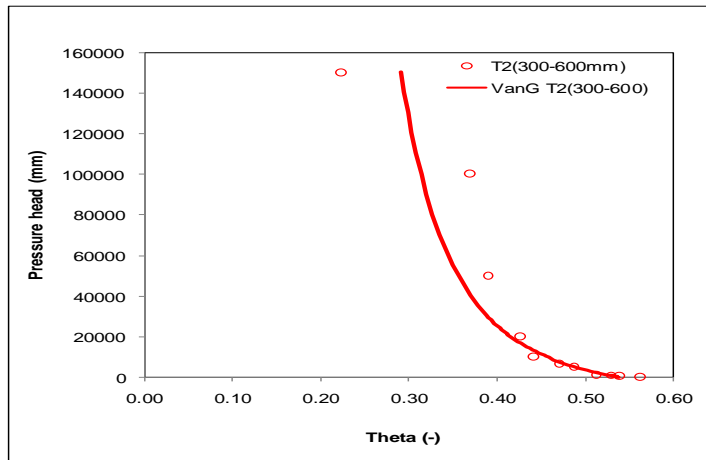
van Genuchten Fitted Soil Water Retention curve for T1 (60-90 cm)



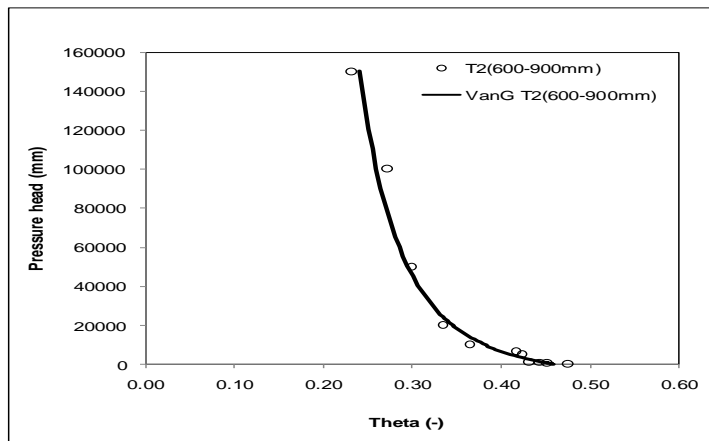
van Genuchten Fitted Soil Water Retention curve for T1 (90-150 cm)



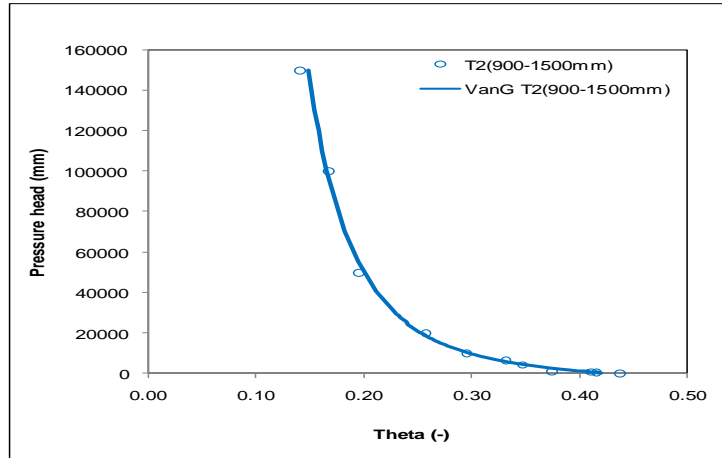
van Genuchten Fitted Soil Water Retention curve for T2 (0-30 cm)



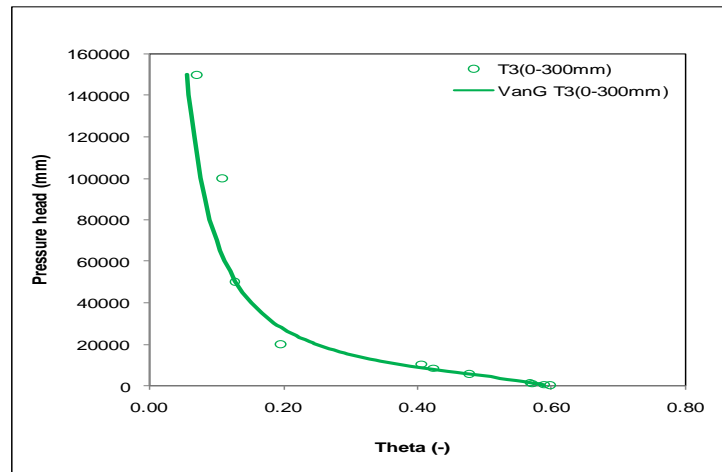
van Genuchten Fitted Soil Water Retention curve for T2 (30-60cm)



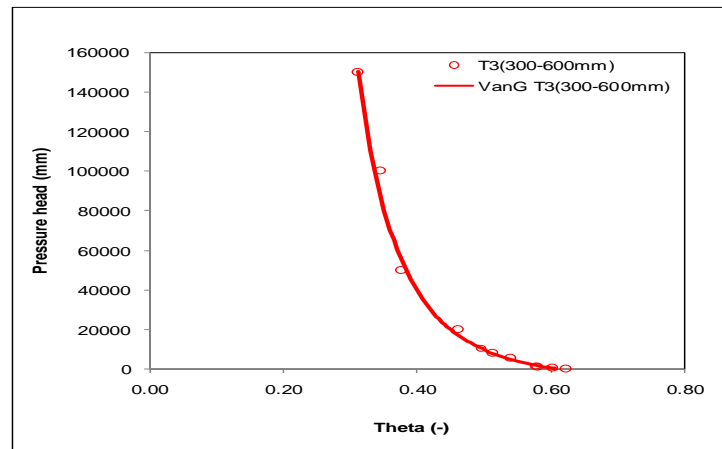
van Genuchten Fitted Soil Water Retention curve for T2 (60-90 cm)



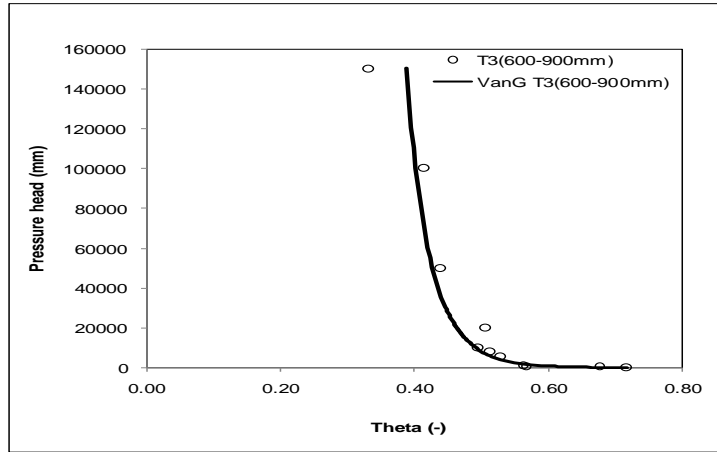
van Genuchten Fitted Soil Water Retention curve for T2 (90-150 cm)



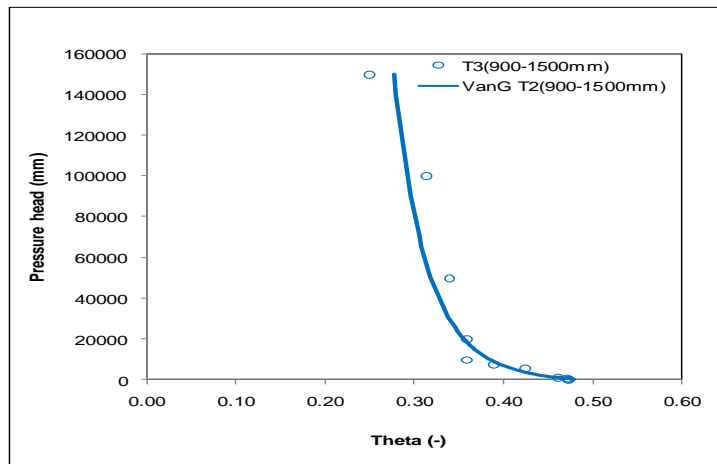
van Genuchten Fitted Soil Water Retention curve for T3 (0-30 cm)



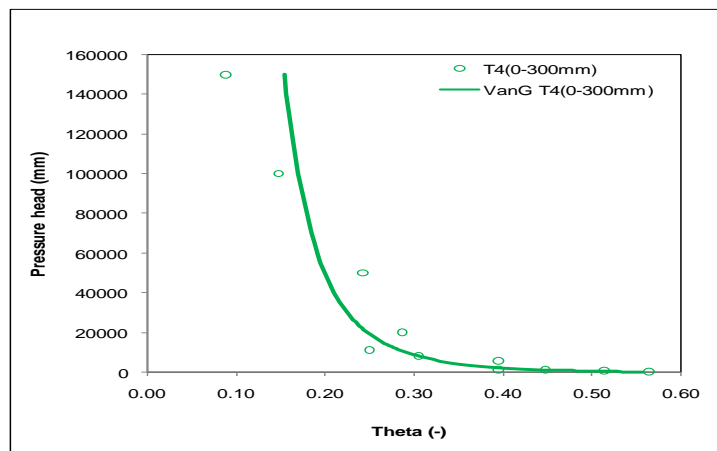
van Genuchten Fitted Soil Water Retention curve for T3 (30-60 cm)



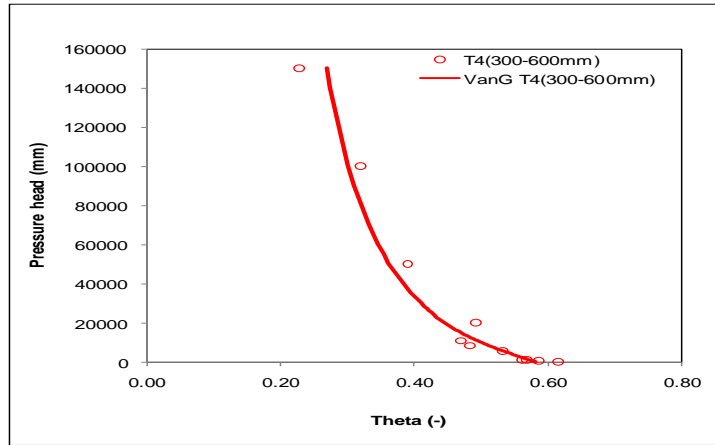
van Genuchten Fitted Soil Water Retention curve for T3 (60-90 cm)



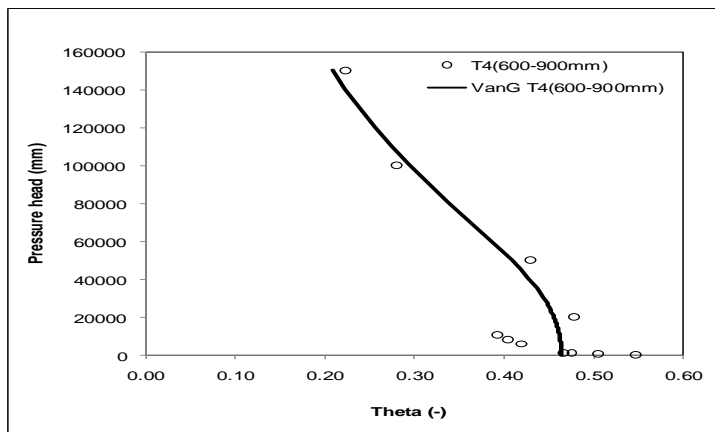
Soil-water retention curve for T3 (90-150cm)



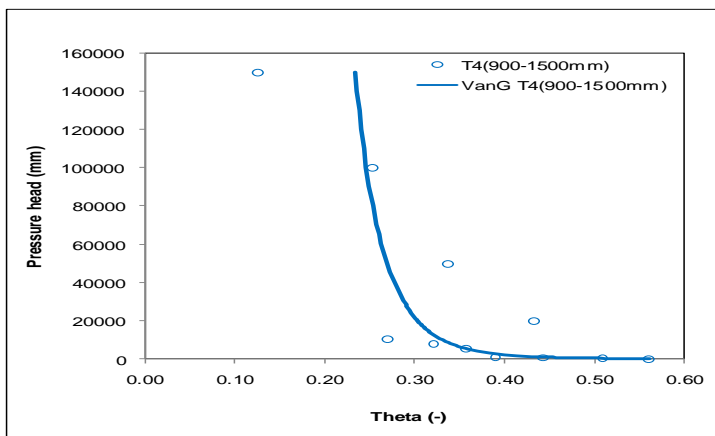
van Genuchten Fitted Soil Water Retention curve for T4 (0-30 cm)



van GenuchtenFitted Soil Water Retention curve for T4 (90-150 cm)

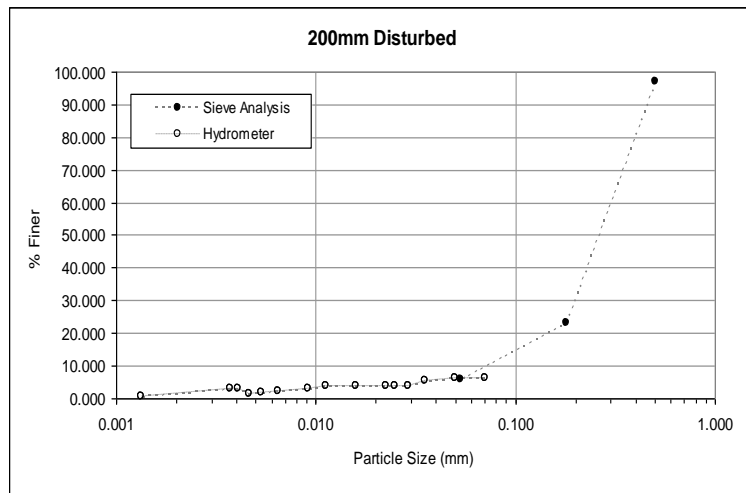
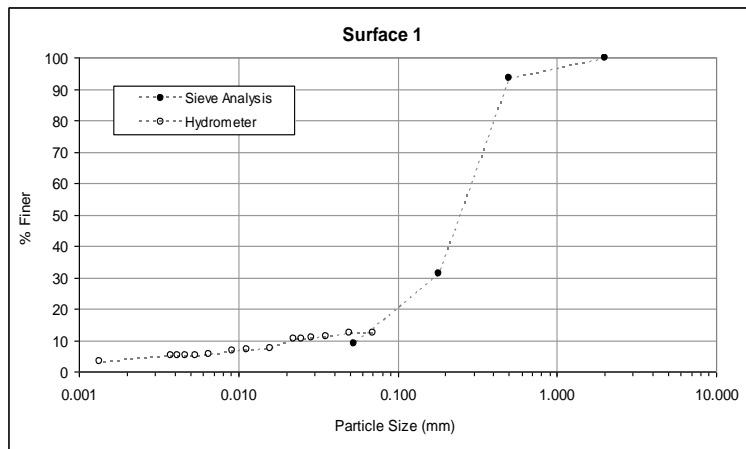
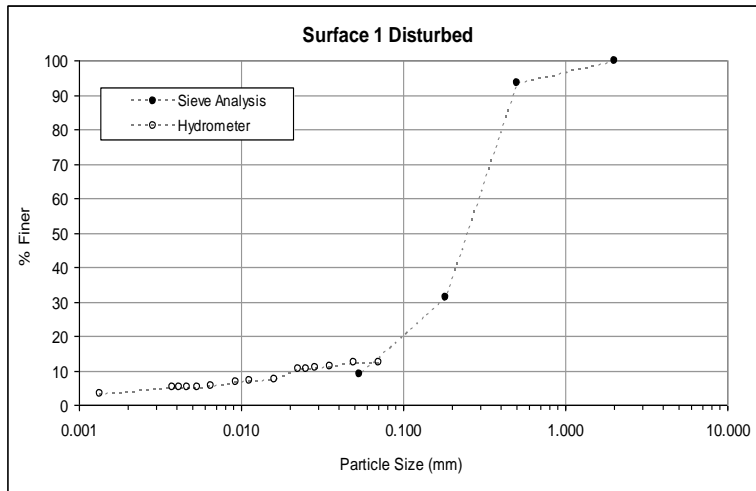


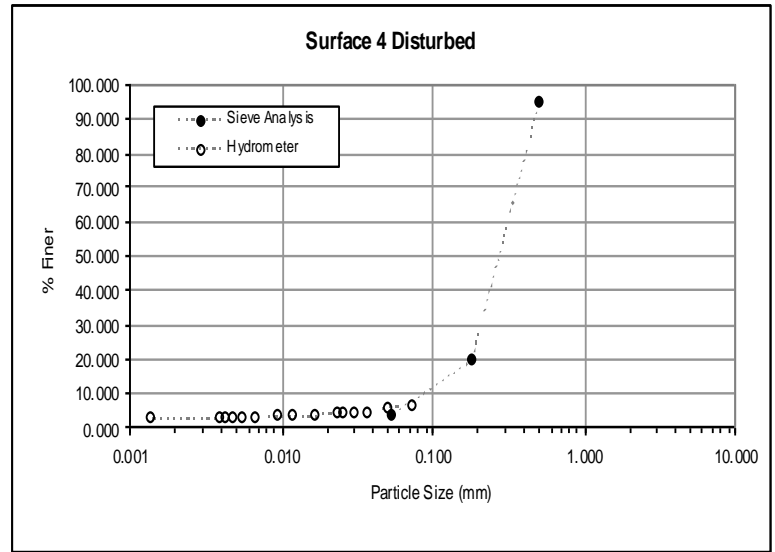
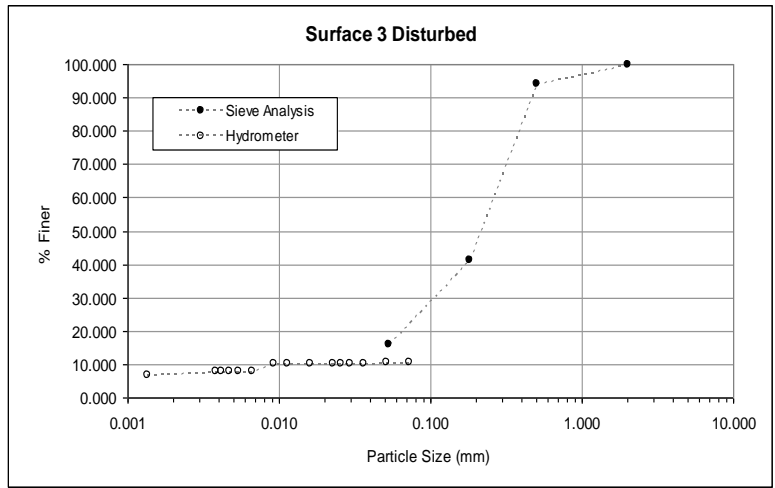
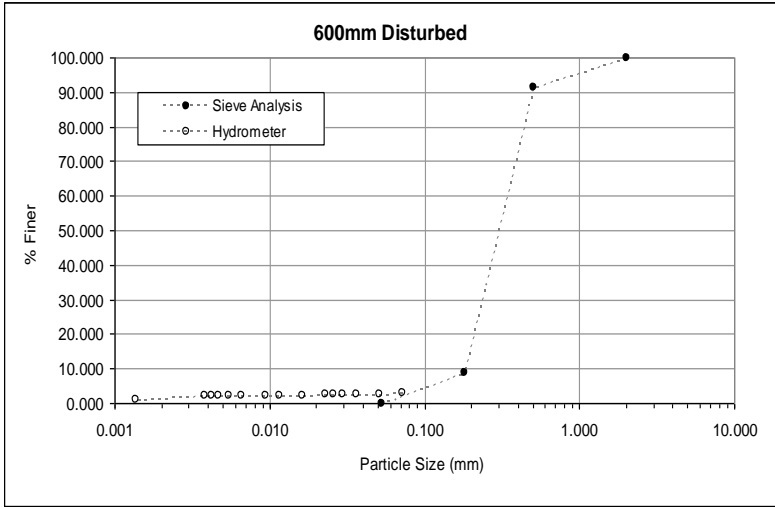
van GenuchtenFitted Soil Water Retention curve for T4 (60-90 cm)

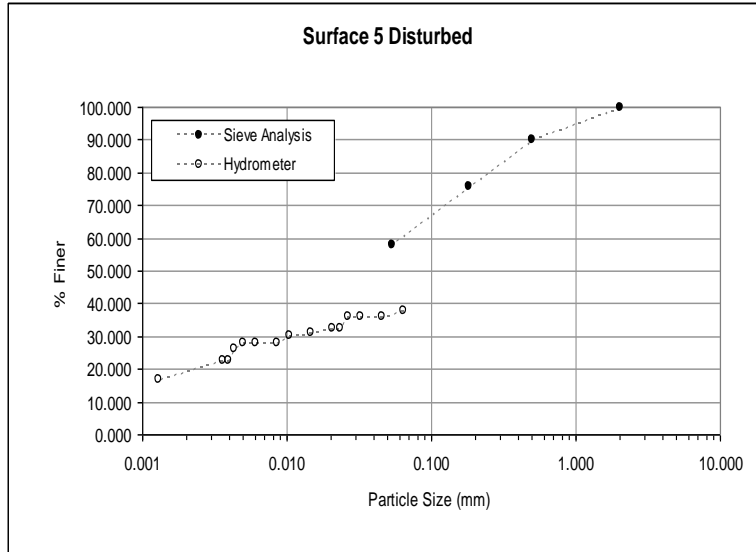


van GenuchtenFitted Soil Water Retention curve for T4 (90-150 cm)

Particle Size Distribution at the Umlazi site







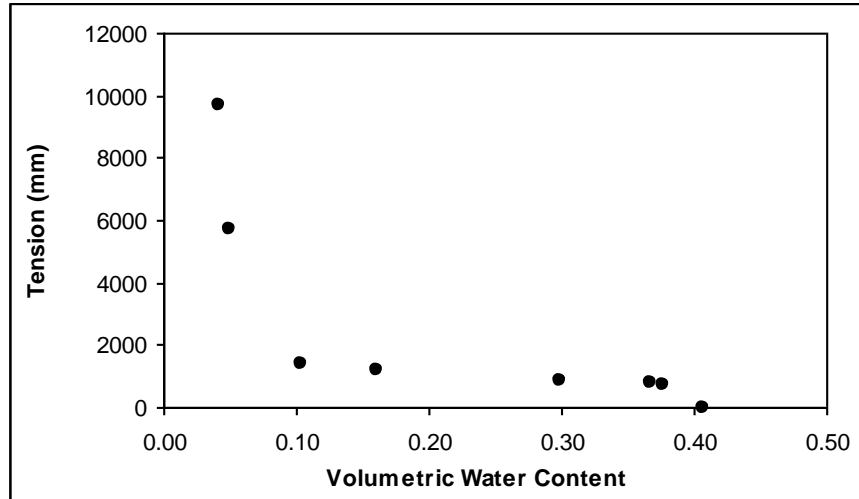
Calibration values for P and NO₃.

CALIBRATION VALUES FOR P AND NO ₃			
standard solution conc. P (mg/l)	HACH P conc. (mg/l)	standard solution conc. NO ₃ (mg/l)	HACH NO ₃ conc. (mg/l)
0.1	0.09	2	0.1
0.2	0.22	5	0.6
0.3	0.3	10	1.4
0.4	0.38	20	2.5
0.5	0.49	30	3.8
0.6	0.56		
0.7	0.64		
0.8	0.75		

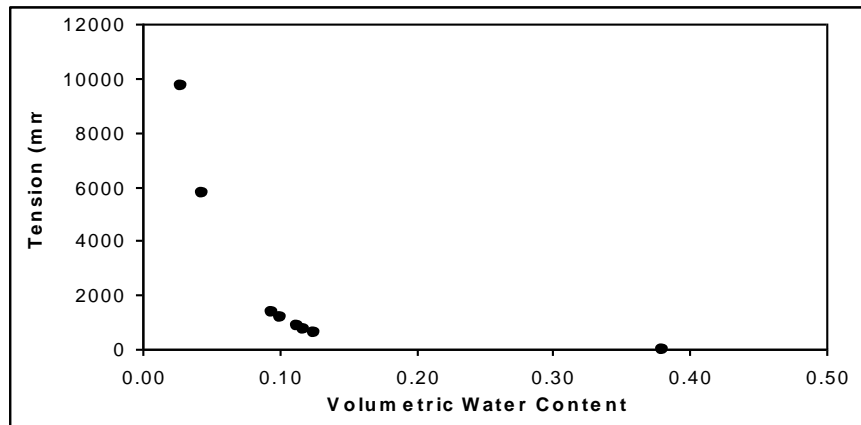
APPENDIX C

Water Retention Characteristics

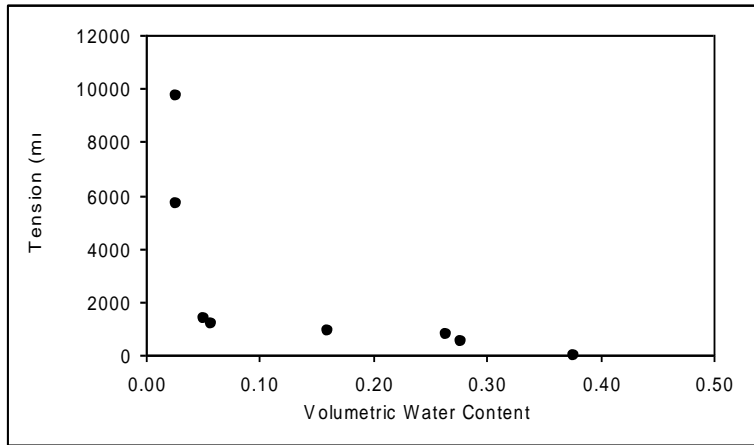
Trench 2 100mm



Trench 2 200mm

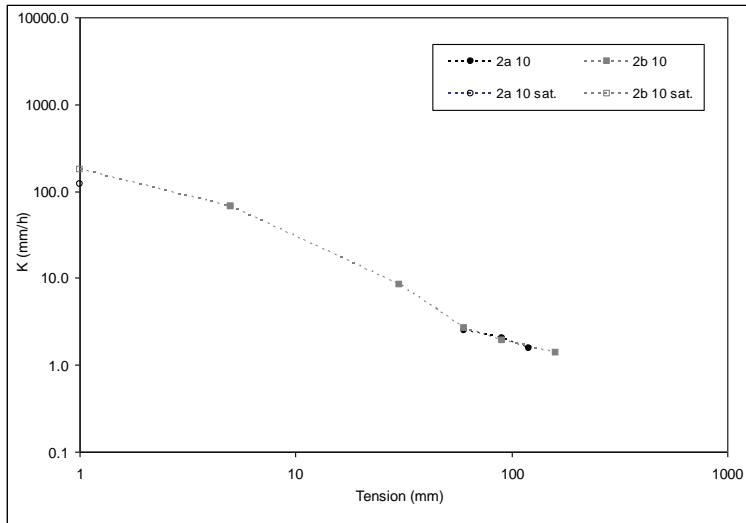


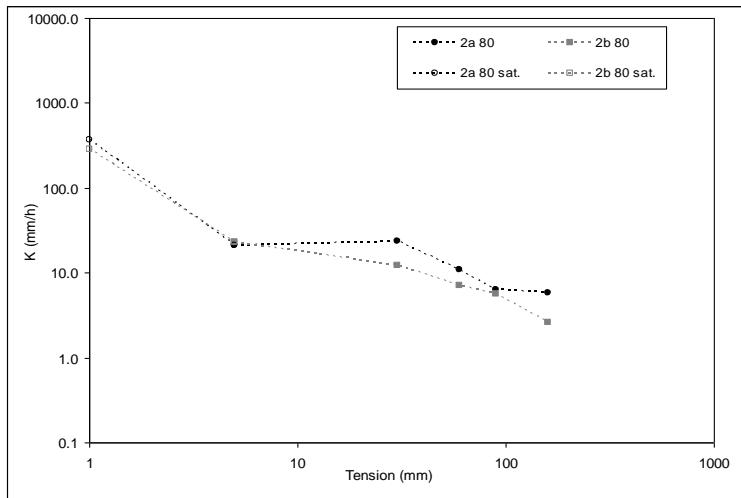
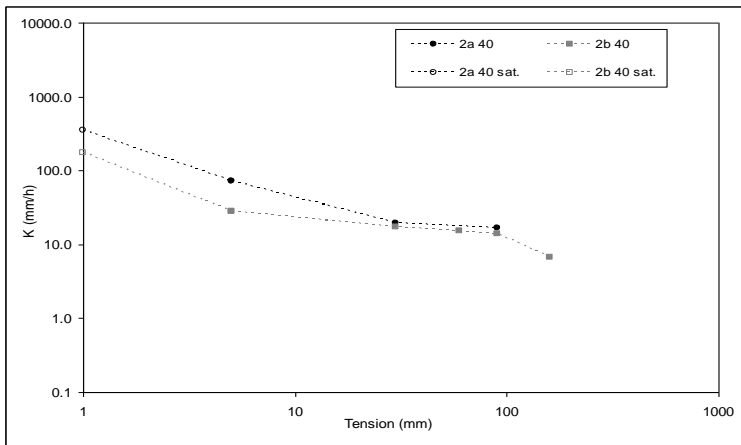
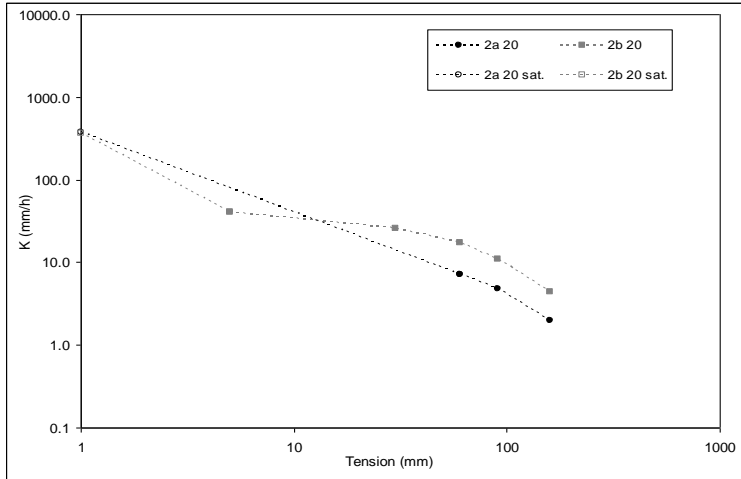
Trench 2 800mm

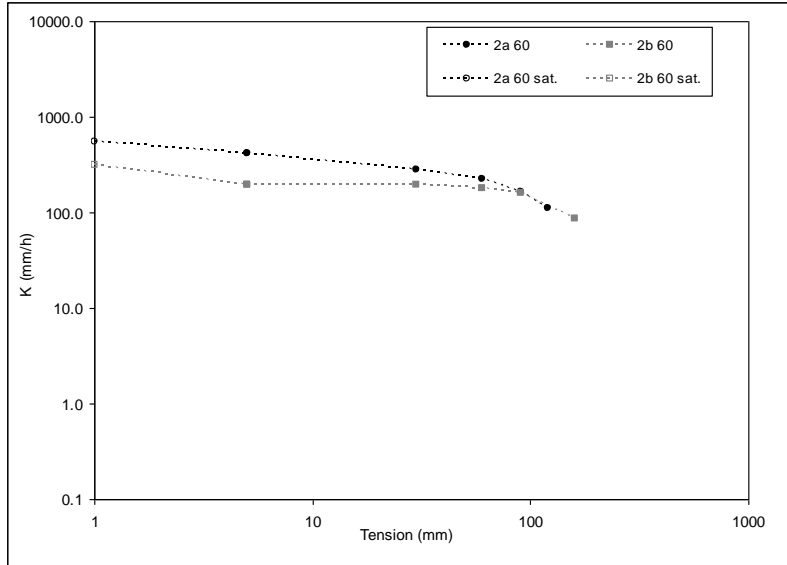
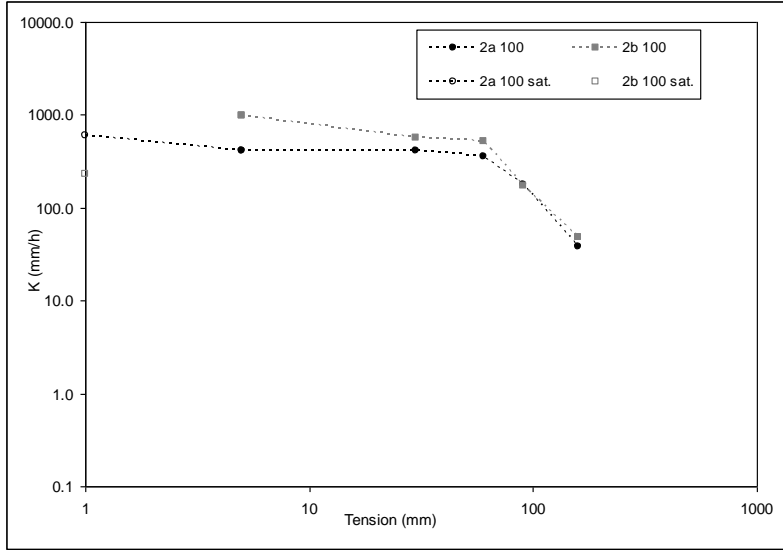


Hydraulic Conductivity Characteristics

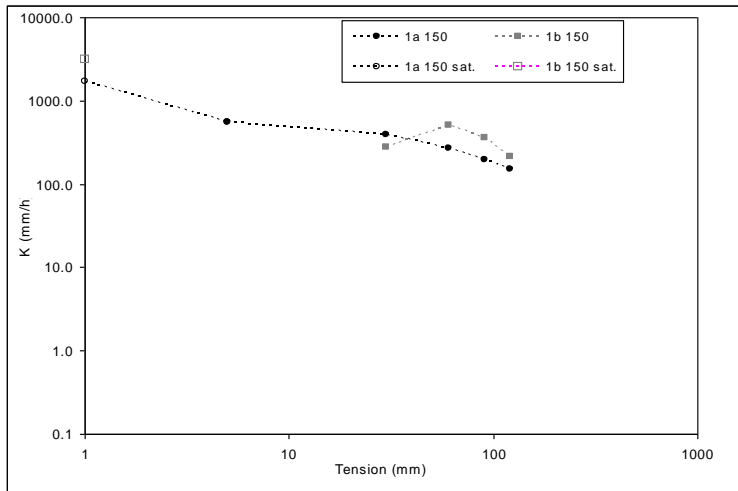
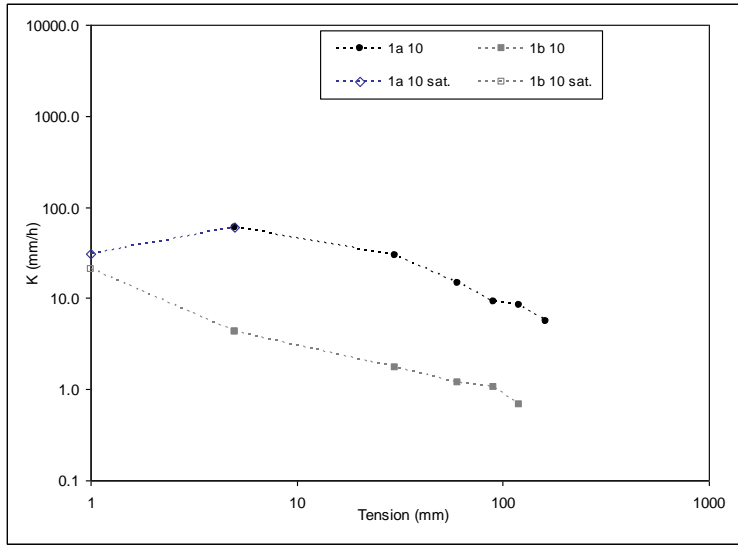
Inside Trench 2



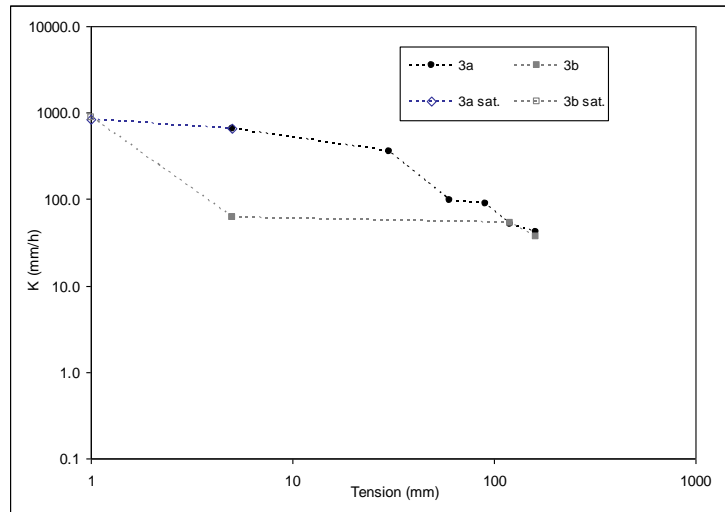
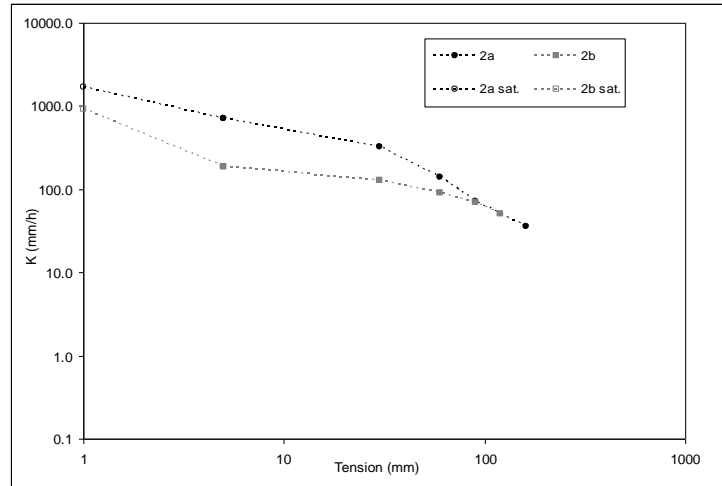
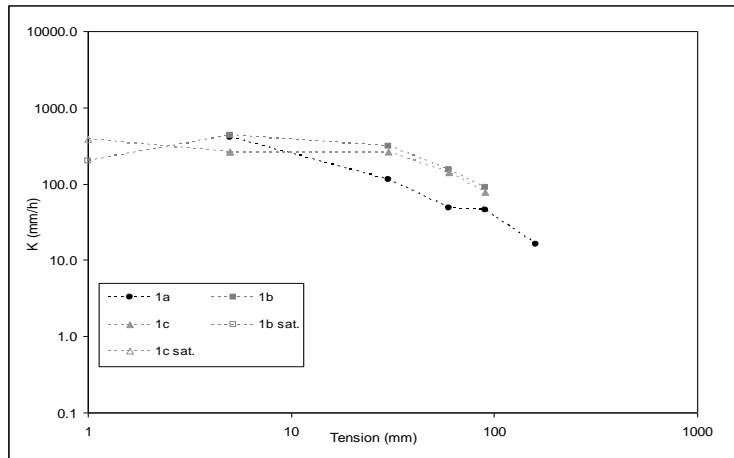


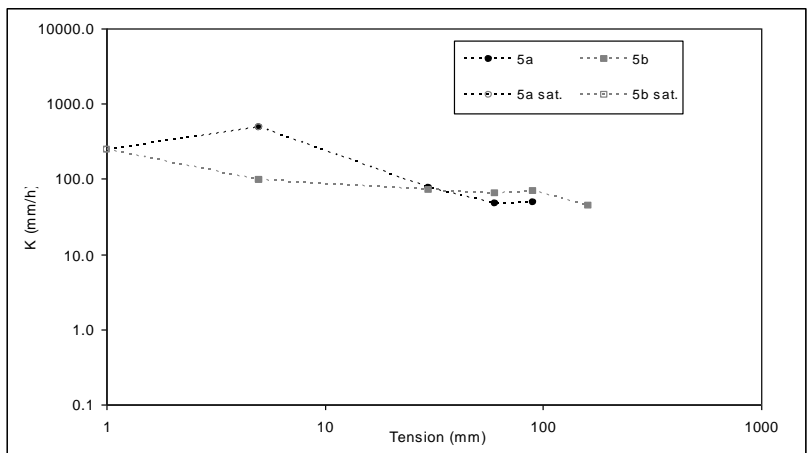
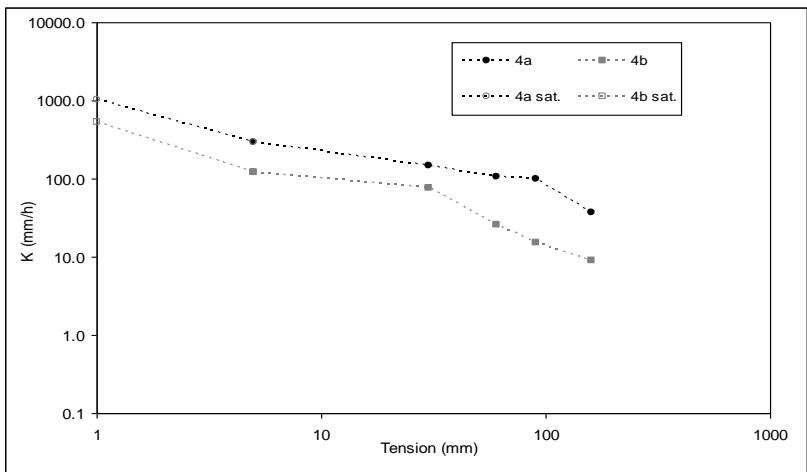


Inside Trench 1

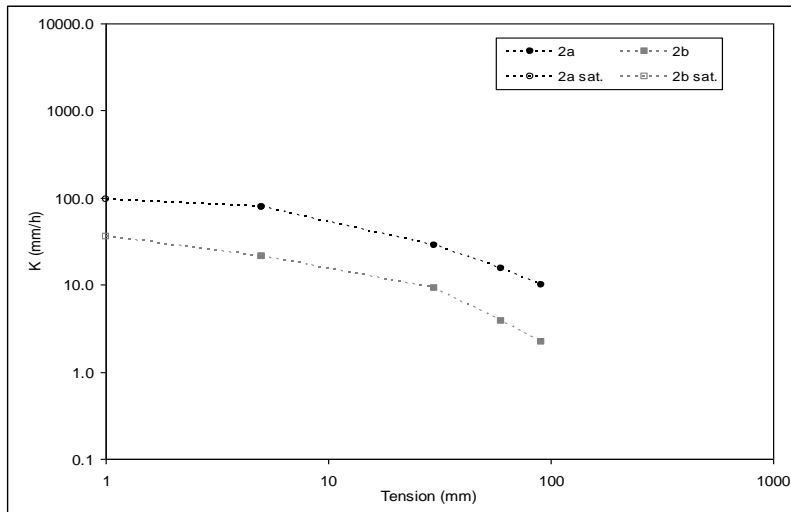
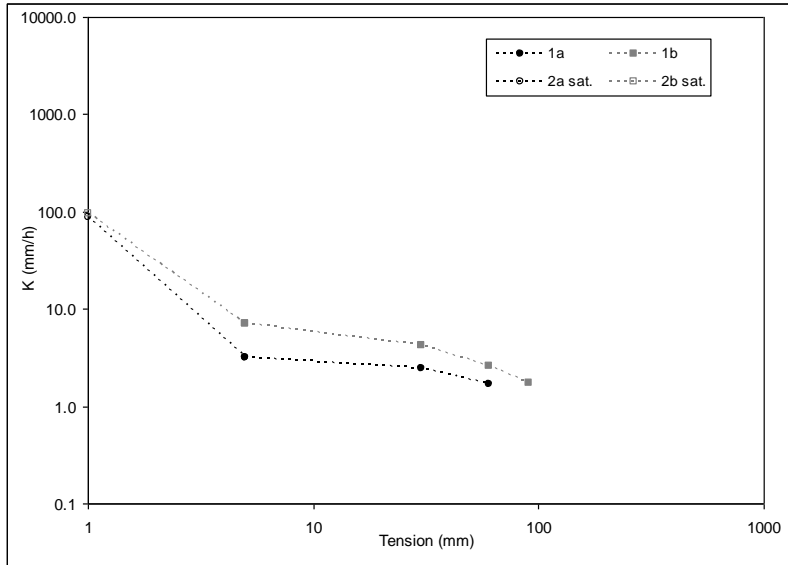


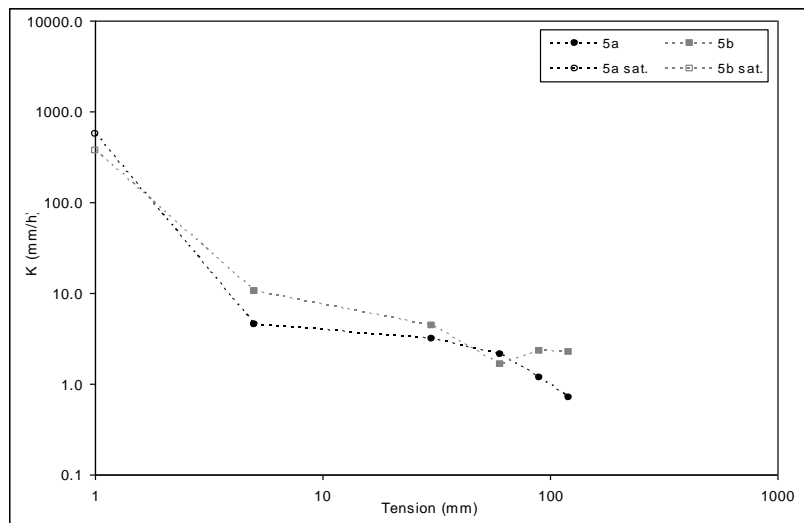
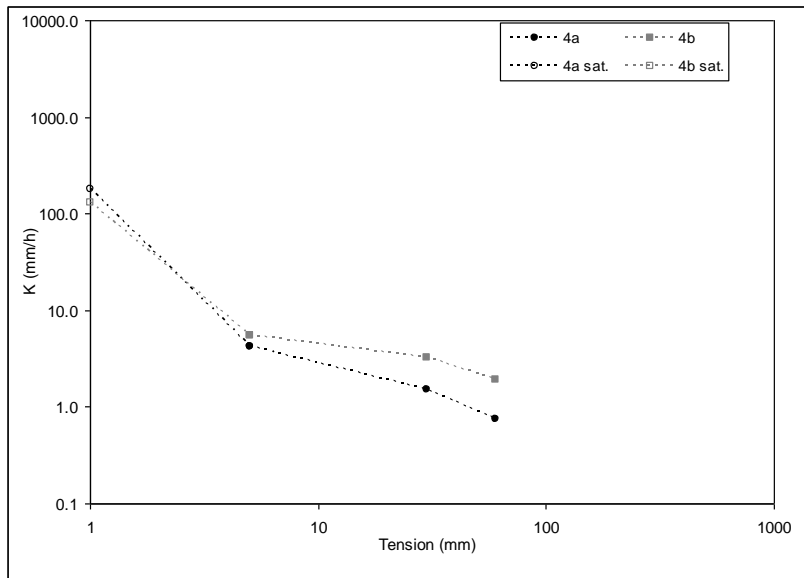
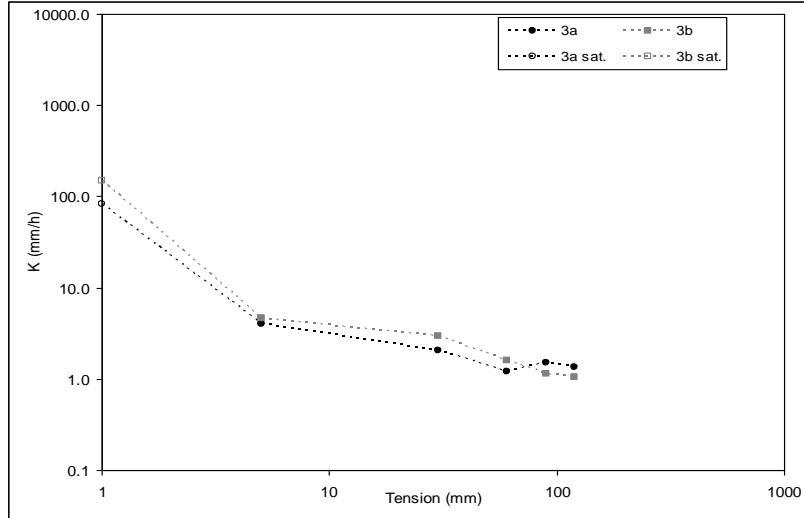
Top of Trenches



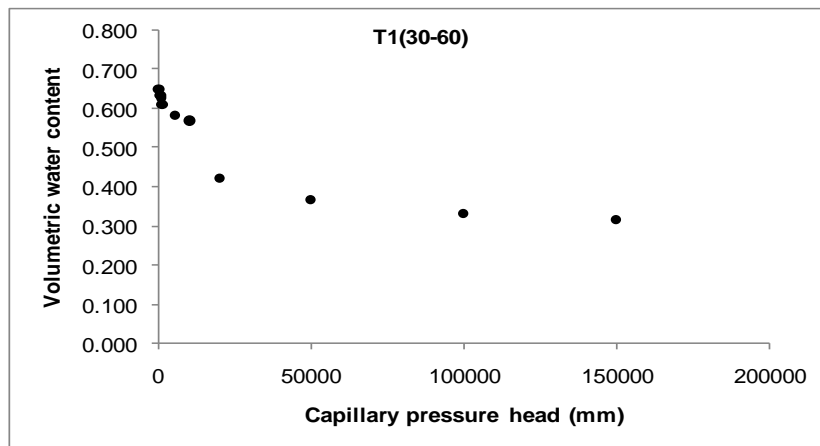
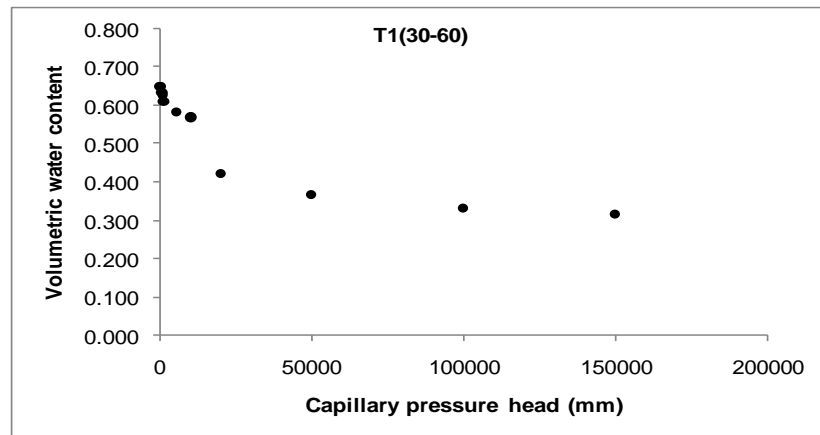
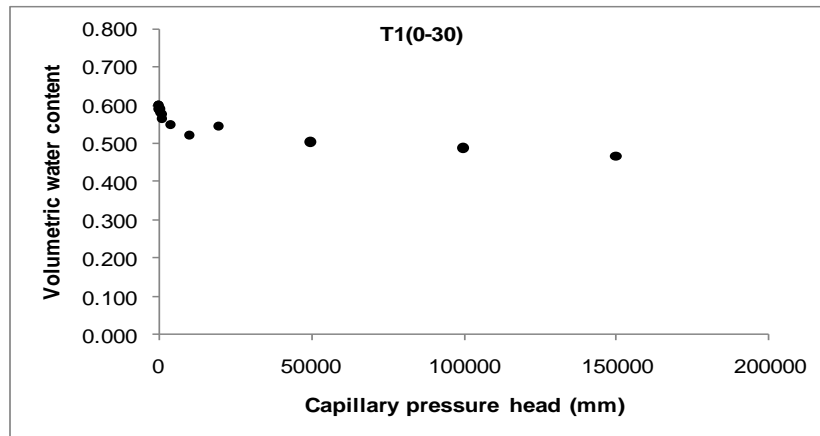


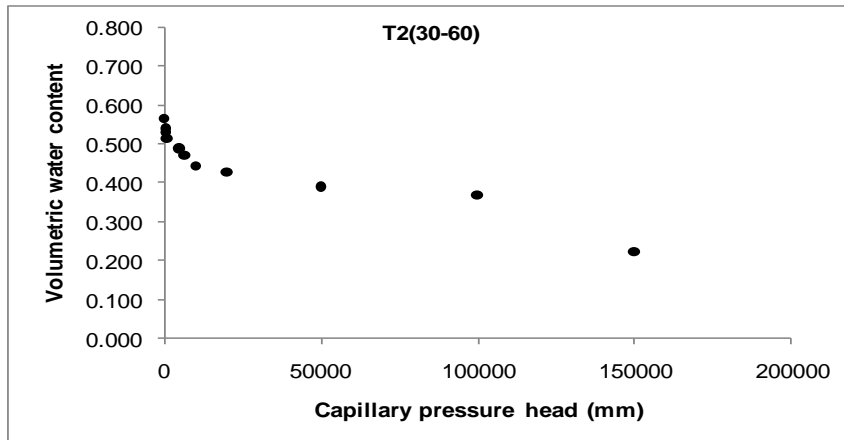
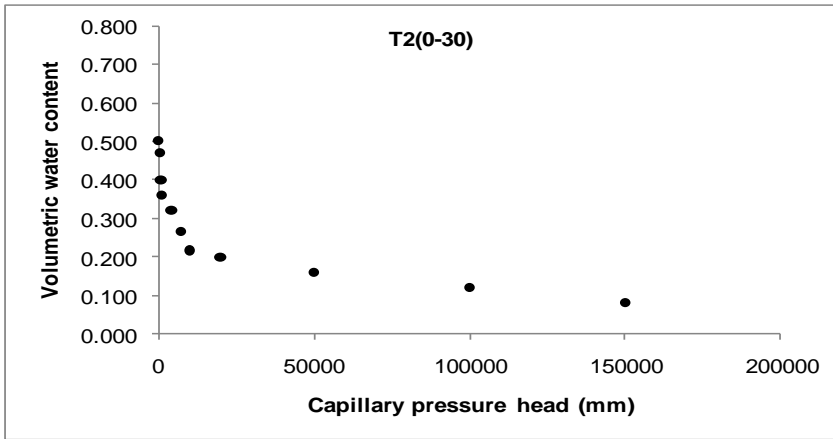
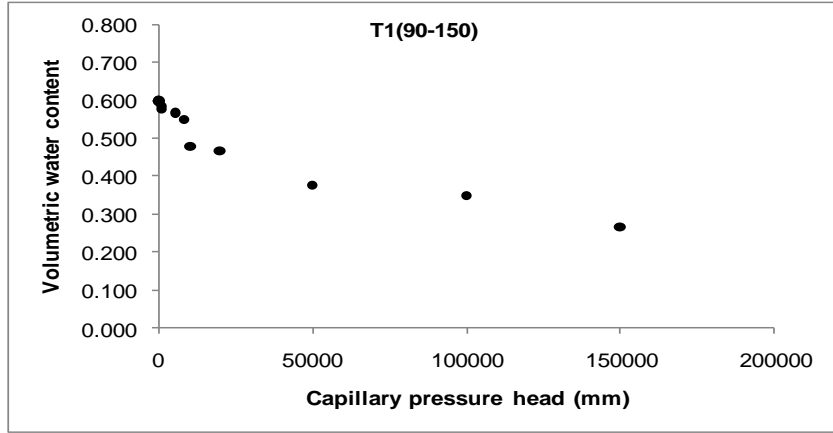
Undisturbed Surface

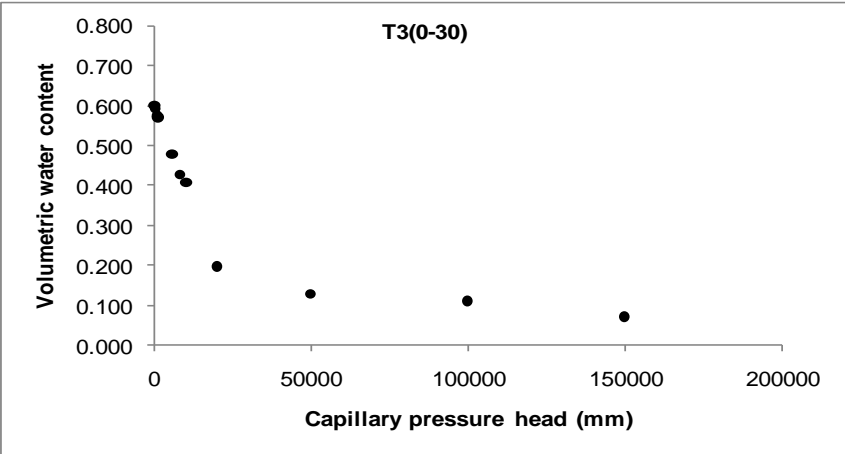
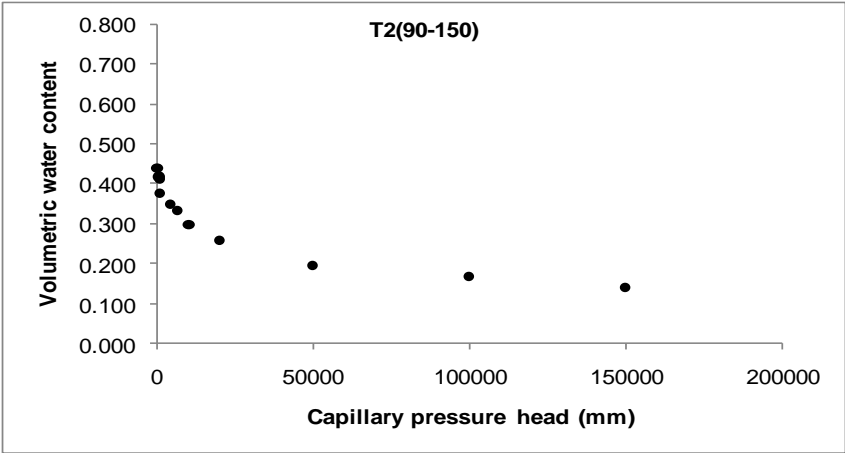
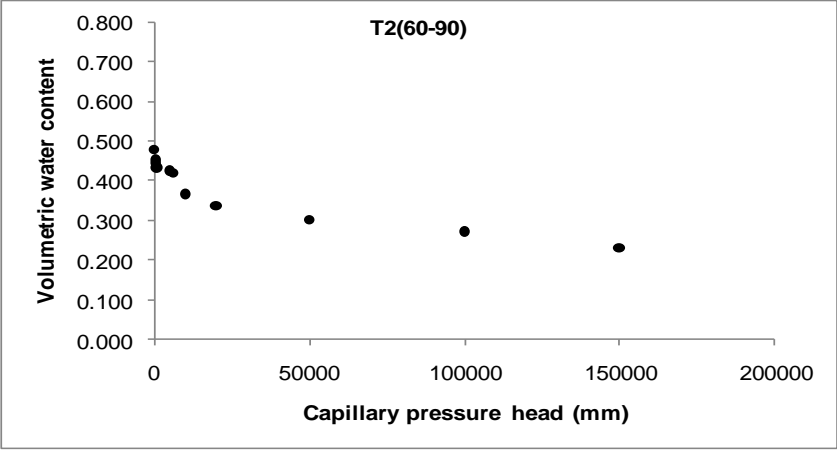


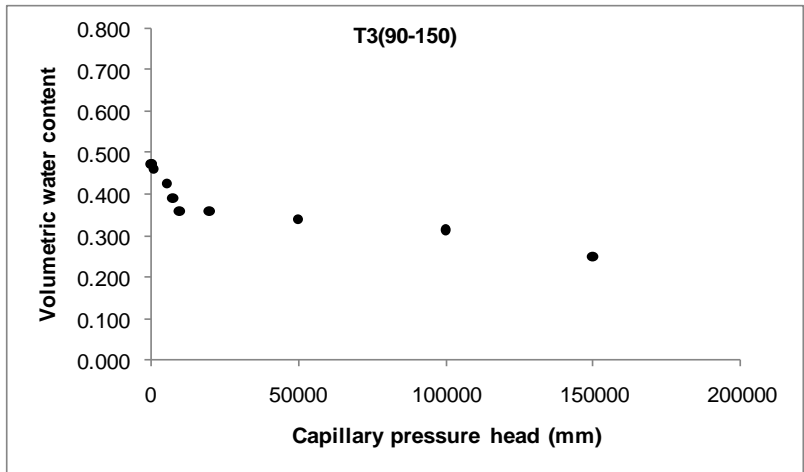
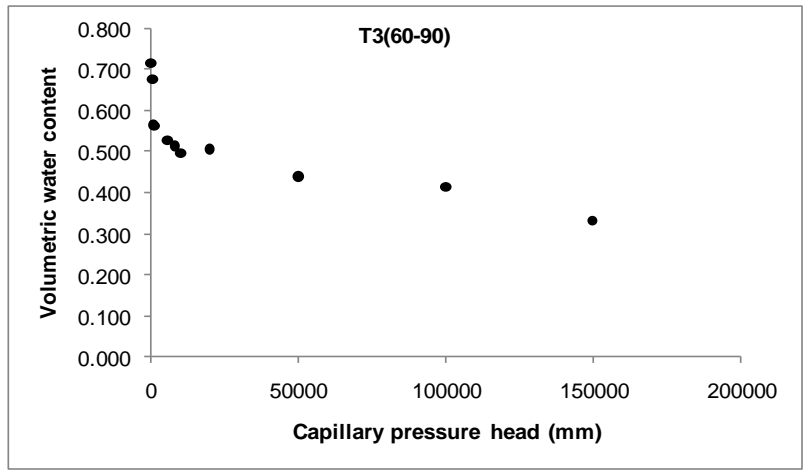
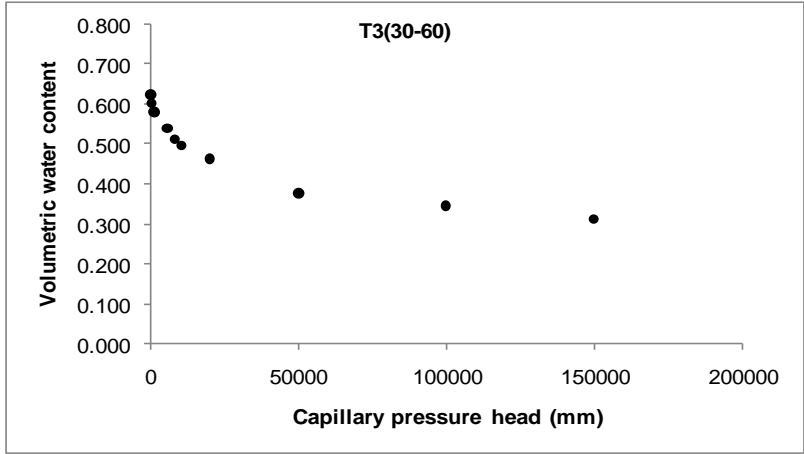


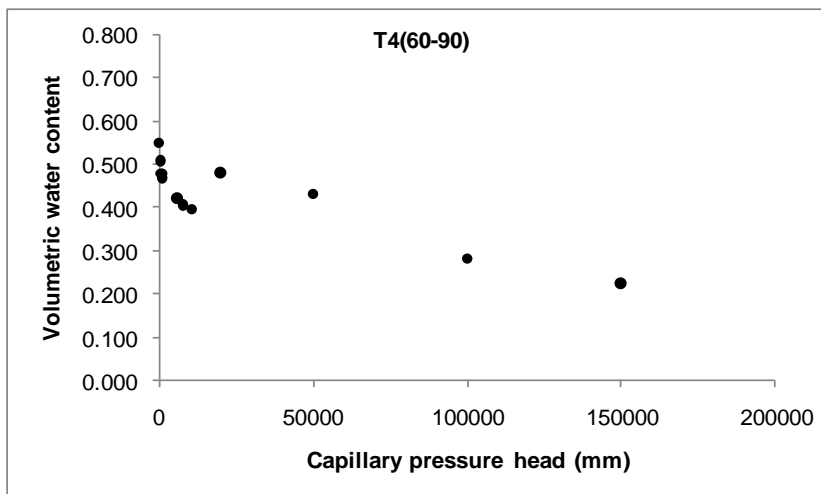
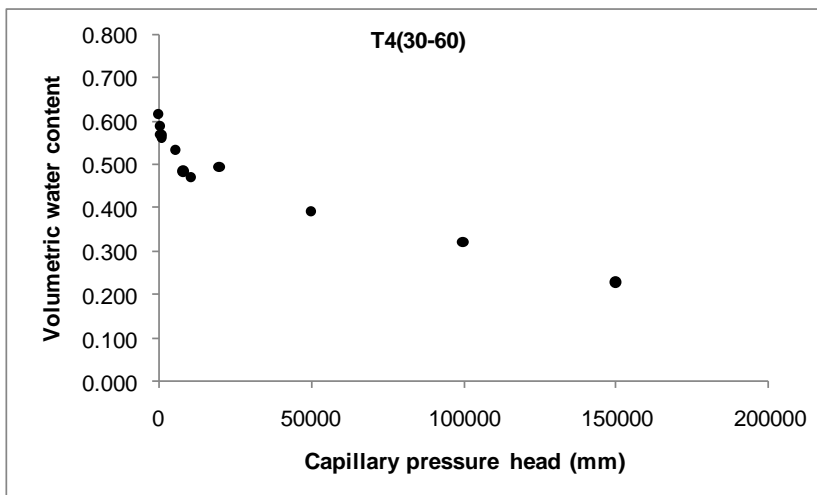
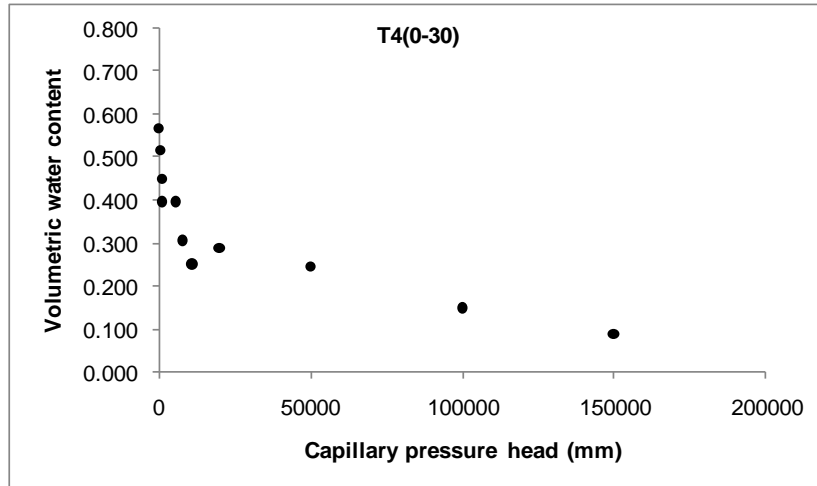
Measured water retention characteristics in treatment at SAPPI

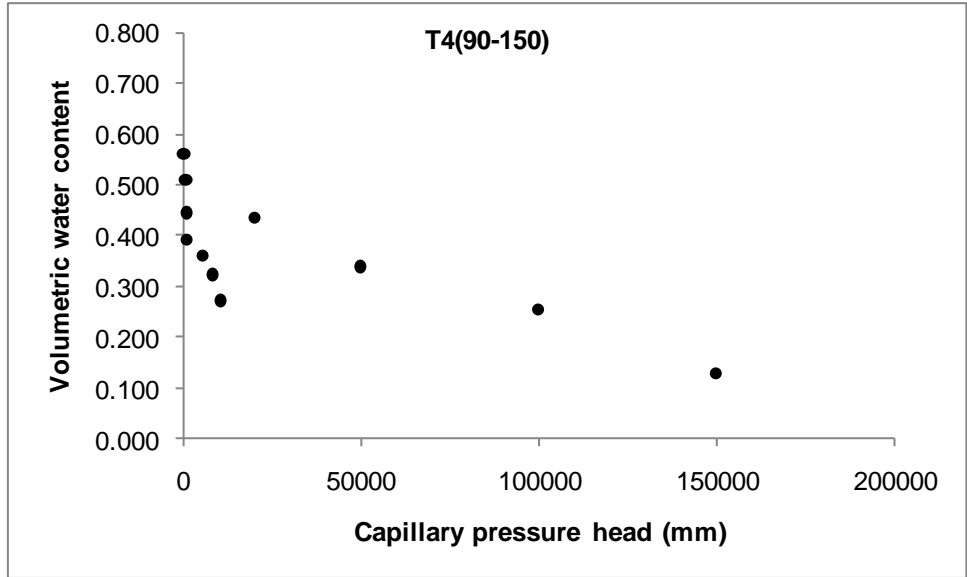




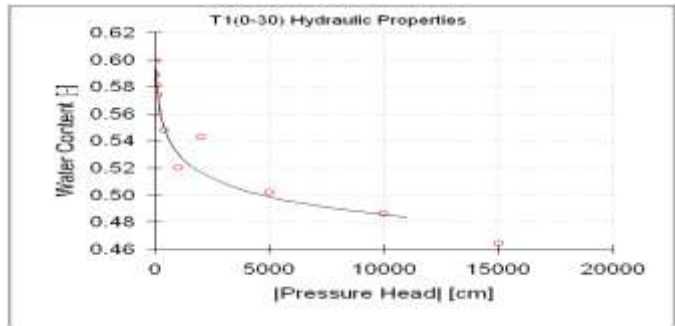




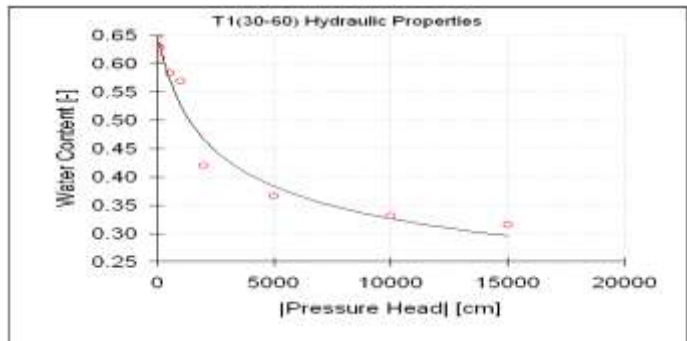




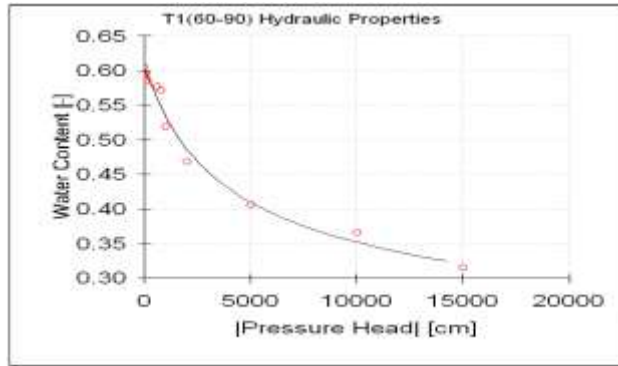
RETc Fitted Soil Water Retention Characteristics in treatments at SAPPI site



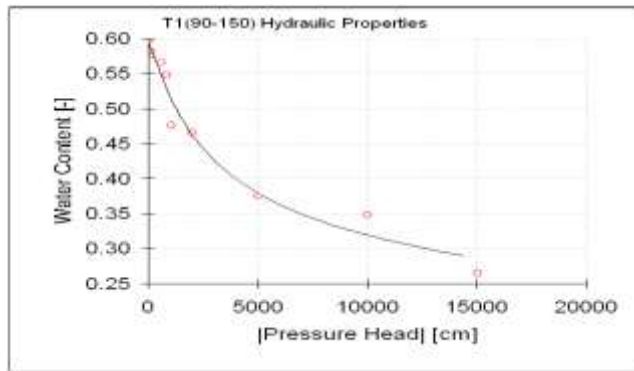
Soil-water retention curve for T1 (0-30 cm)



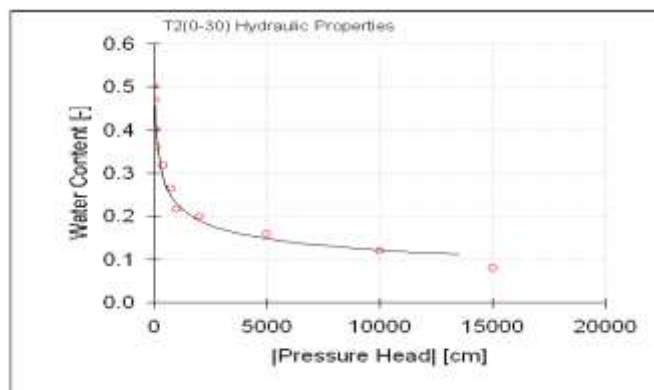
Soil-water retention curve for T1 (30-60 cm)



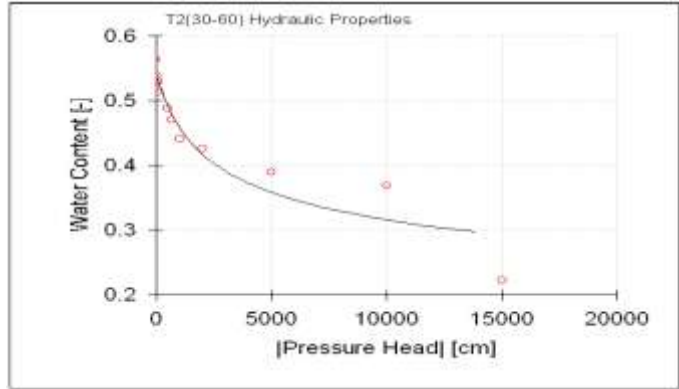
Soil-water retention curve for T1 (60-90 cm)



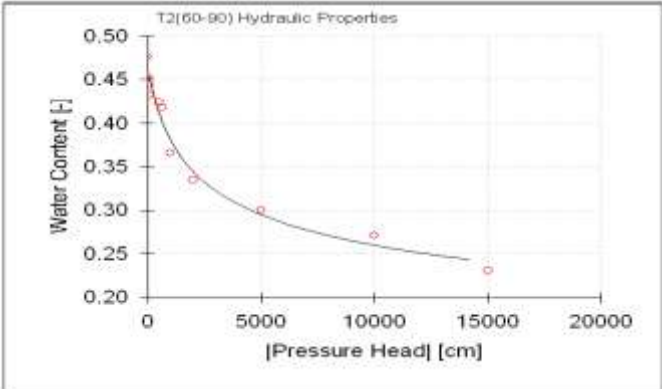
Soil-water retention curve for T1 (90-150 cm)



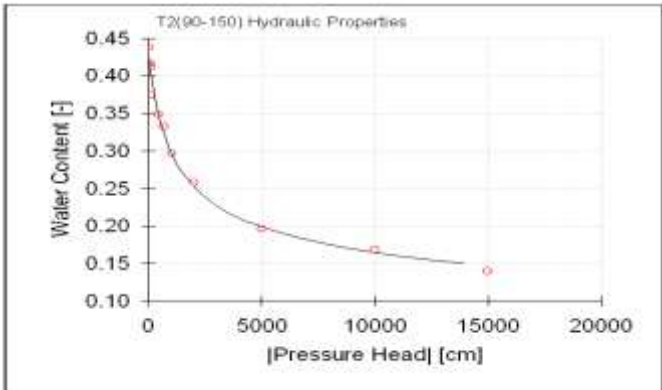
Soil-water retention curve for T2 (0-30 cm)



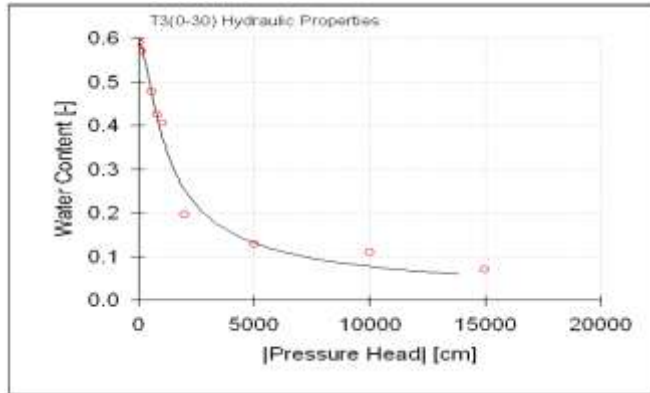
Soil-water retention curve for T2 (30-60 cm)



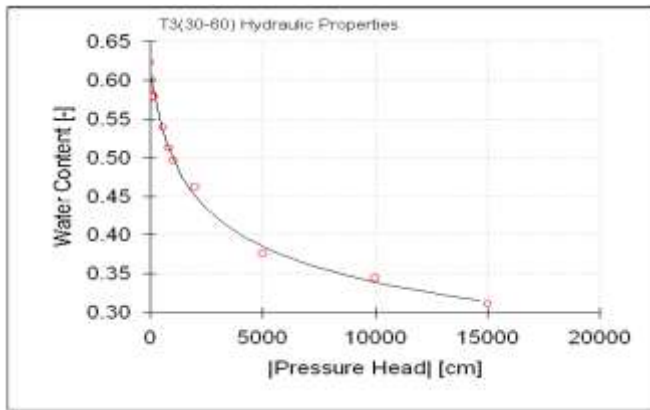
Soil-water retention curve for T2 (60-90 cm)



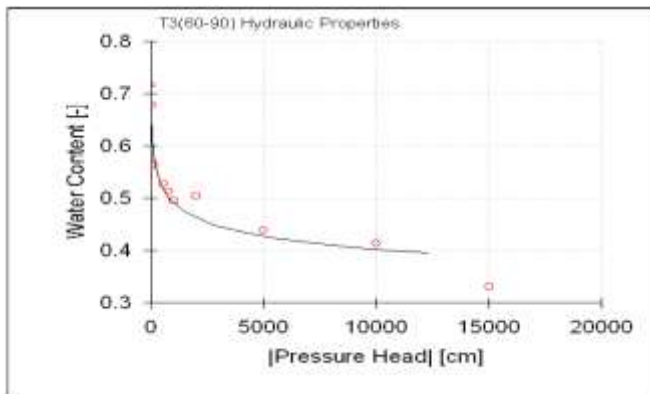
Soil-water retention curve for T2 (90-150 cm)



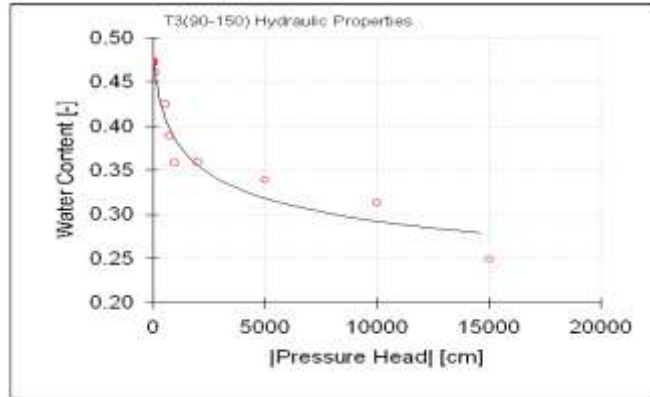
Soil-water retention curve for T3 (0-30 cm)



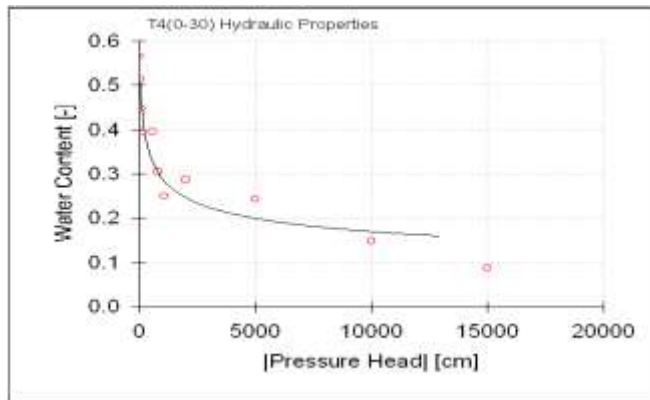
Soil-water retention curve for T3 (30-60 cm)



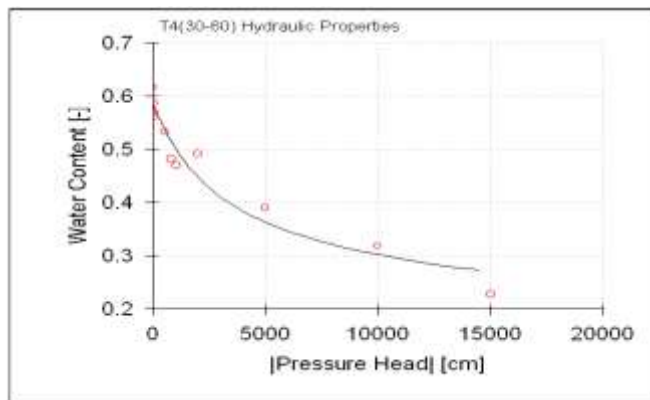
Soil-water retention curve for T3 (60-90 cm)



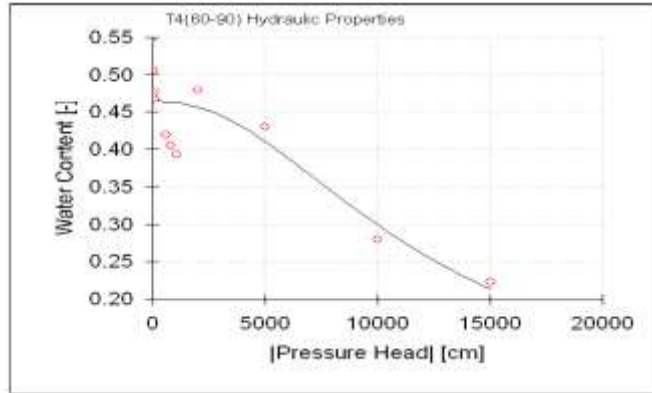
Soil-water retention curve for T3 (90-150 cm)



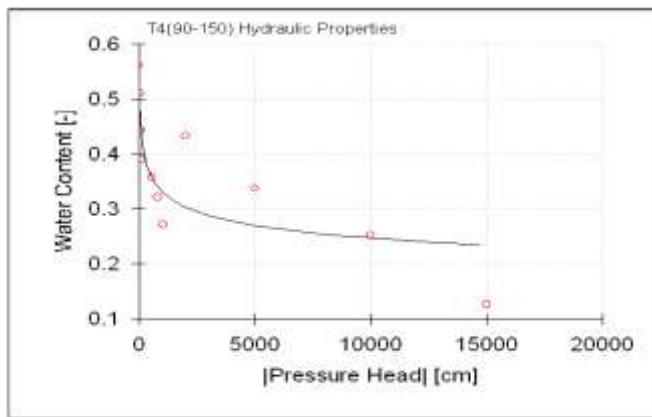
Soil-water retention curve for T4 (0-30 cm)



Soil-water retention curve for T4 (90-150 cm)

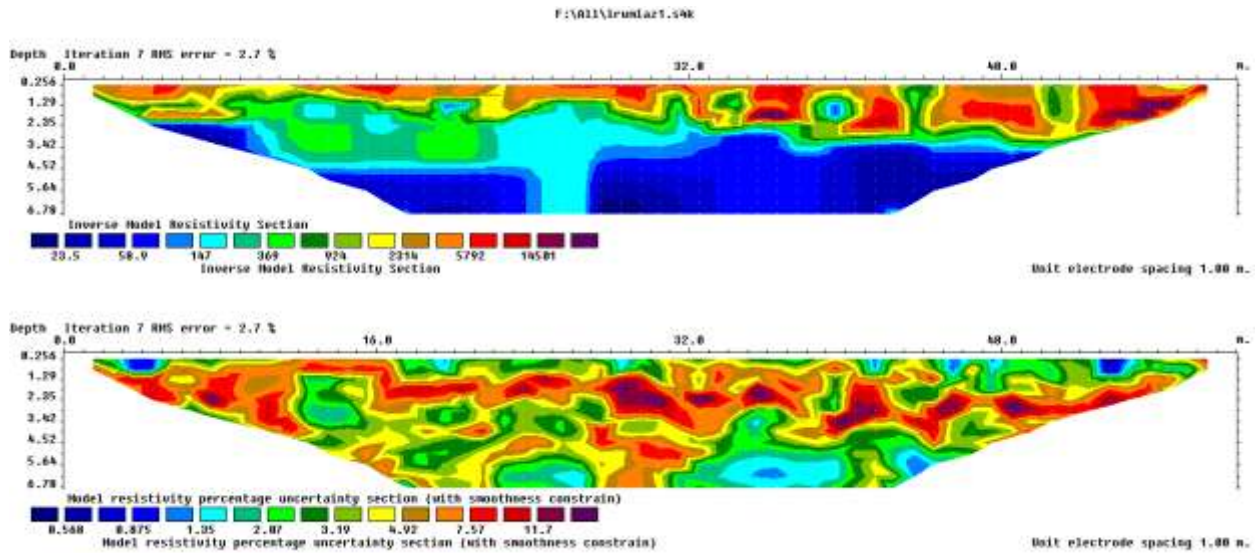


Soil-water retention curve for T4 (60-90cm)

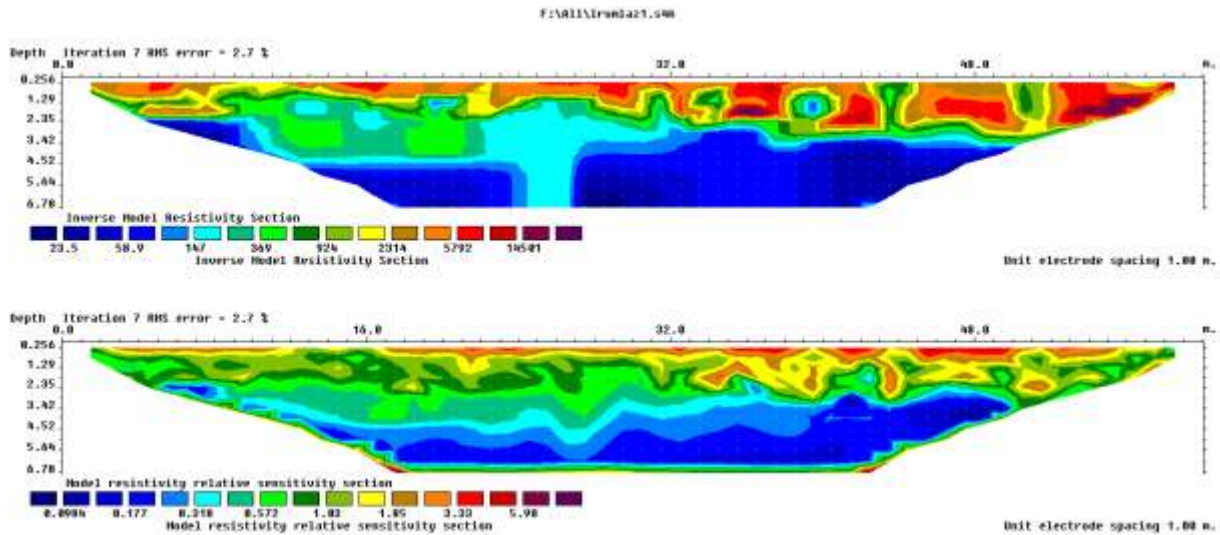


Soil-water retention curve for T4 (90-150)

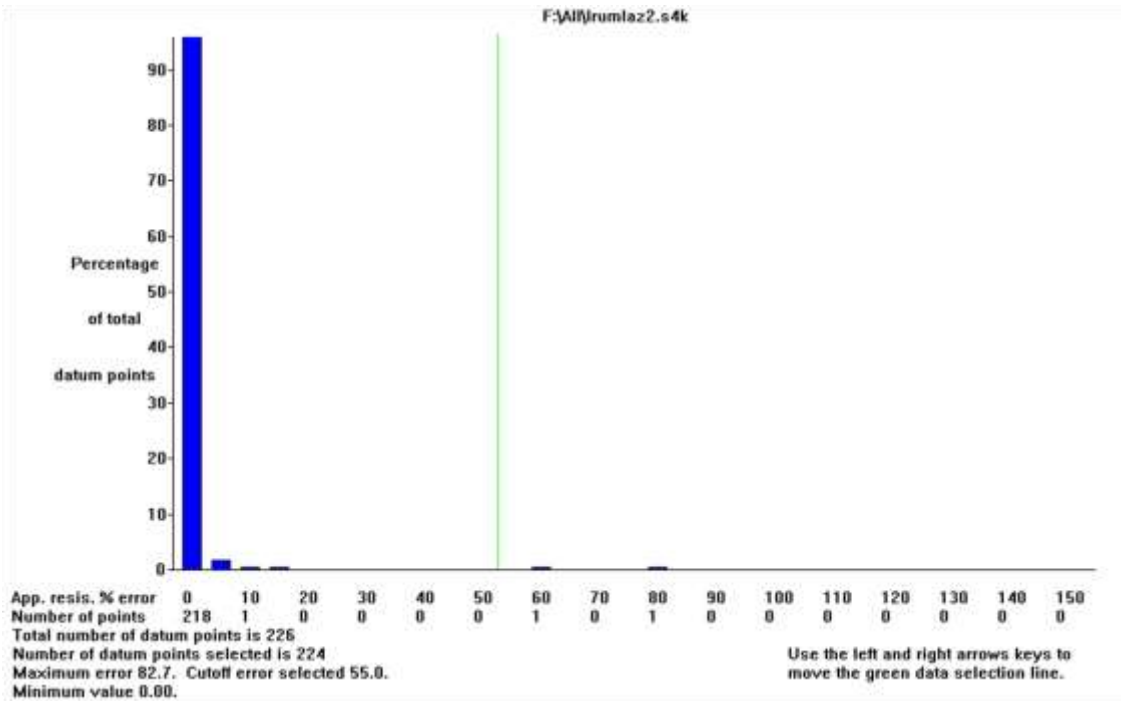
APPENDIX D



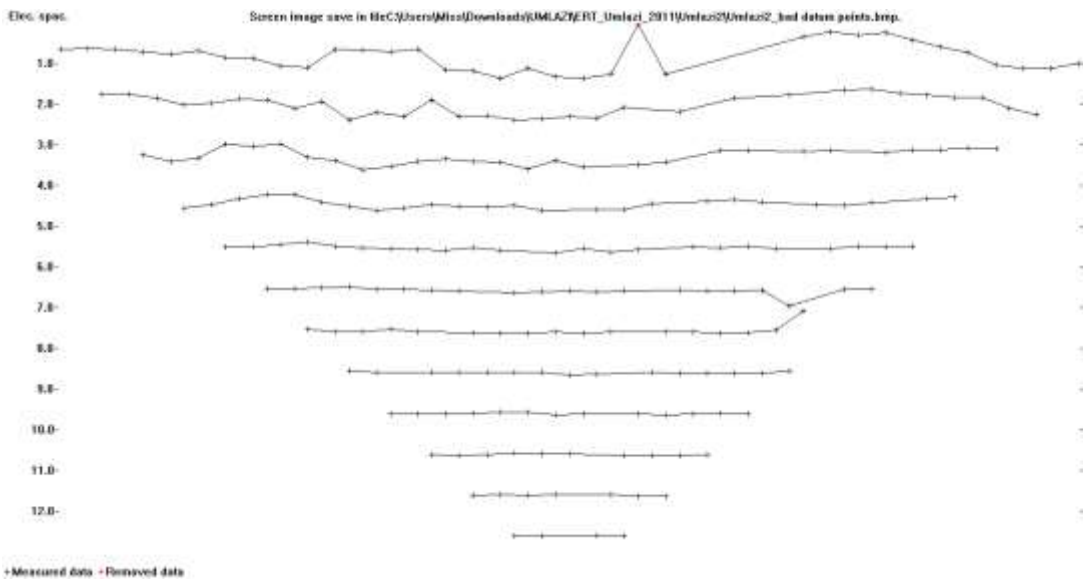
Umlaz1, Top : Inverse model resistivity section, Bottom : Model resistivity percentage uncertainty section



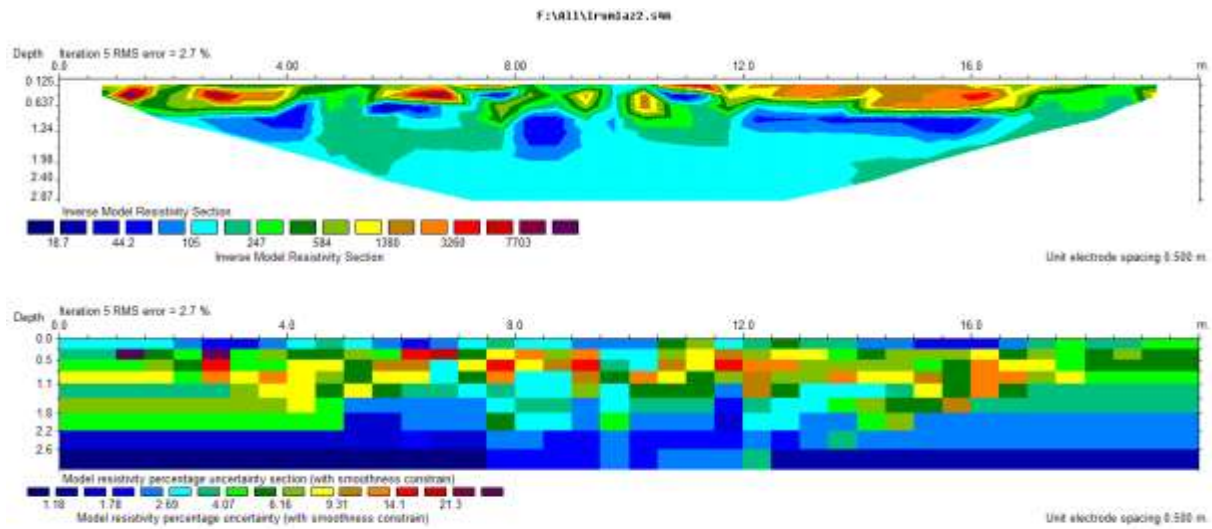
Umlaz1. Top : Inverse model resistivity section, Bottom : Model resistivity relative sensitivity section



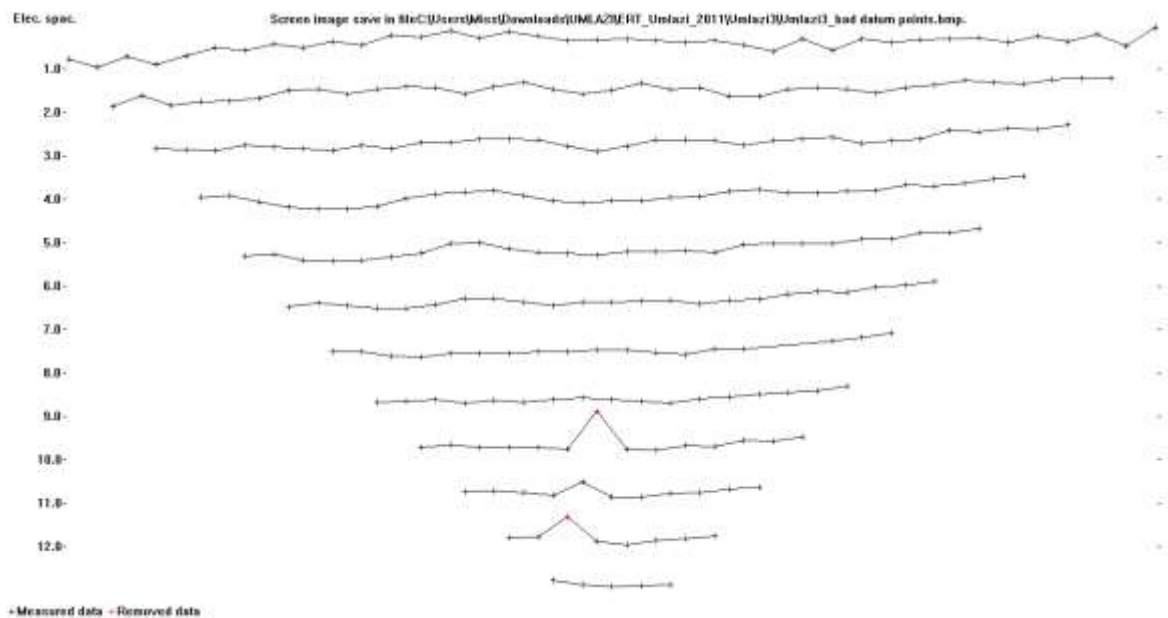
Umlaz2, Excluded points with high percentage error of apparent resistivity values



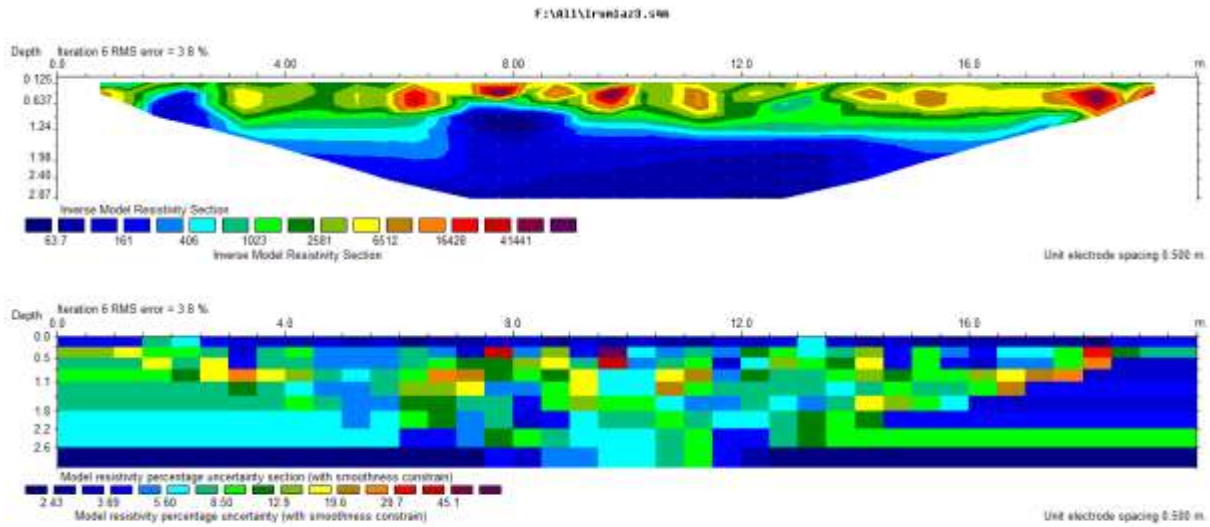
Umlaz2, Bad datum points removed in red



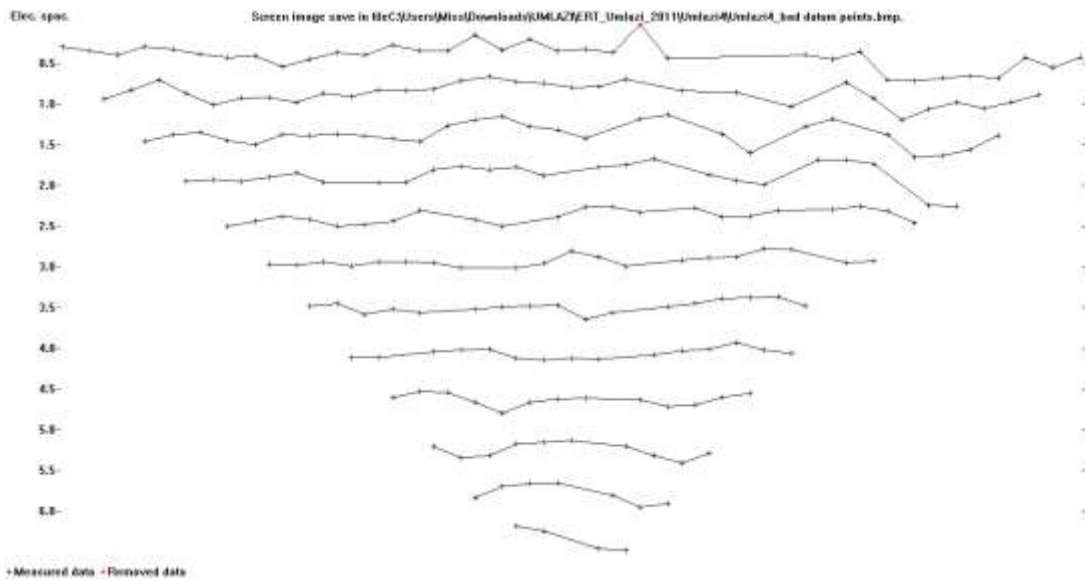
Umlaz2, Top : Inverse model resistivity section, Bottom : Model resistivity percentage uncertainty section



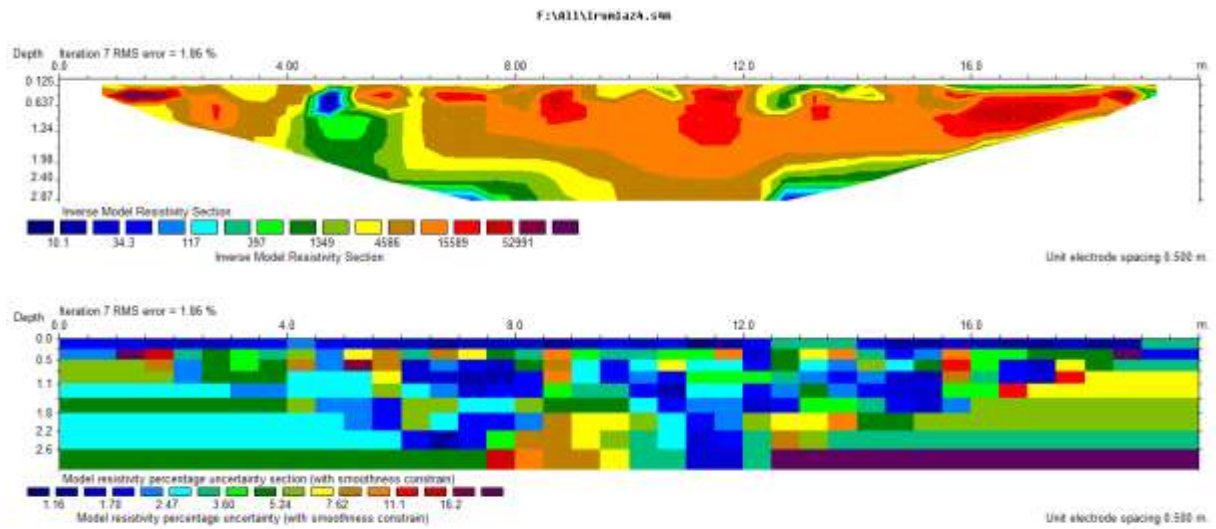
Umlaz3, Bad datum points removed in red



Umlaz3, Top : Inverse model resistivity section, Bottom : Model resistivity percentage uncertainty section



Umlaz4, Bad datum points removed in red



Umlaz4, Top : Inverse model resistivity section, Bottom : Model resistivity percentage uncertainty section